

On Demand Manufacturing of Solid Dosage Forms via Fused Deposition Modelling (FDM) 3D Printing

by

Tochukwu Chijioke Okwuosa

A thesis submitted in partial fulfilment for the requirements for the degree of
Doctor of Philosophy at the University of Central Lancashire

December 2018

DECLARATION

I declare that while registered as a candidate for the research degree, I have not been a registered candidate or enrolled student for another award of the University or other academic or professional institution. I declare that no material in the thesis has been used in any other submission or an academic award and is solely my own work.

Signature

Date

DEDICATION

To my parents, Pharm. Dr Ugo and Lady Uzo Okwuosa (Owele Ogidi)

ACKNOWLEDGEMENTS

I am forever grateful to my supervisor, Dr Mahamed Albed Alhnan for being the best at this job. I am so pleased to have worked under you and will like to thank you for giving me the opportunity. I hope to retain your creativity and goal driven attitude to research, which has contributed immensely to the success of this PhD. Thanks for your support and kind gestures both inside and outside working environment.

I will not forget Dr Abdullah Isreb, Dr Basel Arafat, Dr Sarah Dennison, Dr Julie Burrow, Dr Jane Elizabeth Alde, Dr Enoche Oga, Dr Chahinez Houacine and Dr Sakib for your support during this research.

I will also like to acknowledge some of the great researchers I was privileged to have worked with, Stefaniak Dominica, Pereira Beatriz, Cieszynska Milenna, Soares Cindy, Gollwitzer Verena, Habashy Rober, Muzna Sadia, Christopher, Filipa, Kasia, Christoph, Oliver, Cristina, Magda, Shola, Joanna, Suha, Mogan and Jean-Baptiste. You have taught me how to be a team player and how to balance work and life. Thanks for giving me reasons to smile every day.

I will also thank my siblings, Dr Nneamaka, Dr Ayodele, Dr Kenekwue, Onyeka and Ugochukwu. I will also not forget my lovely wife, Nkechi and my baby girl, Chizitalu. Family is everything and thanks for keeping me mentally and emotionally stable most of the time.

ABSTRACT

There is an increased emphasis on personalised treatment in a patient-centred health care. Personalising dosage forms are often carried out by tablet splitting, which could be inaccurate and risky. The industrial platform for tablet manufacturing is geared to mass productions, therefore, impractical and too expensive for small batch productions. Fused deposition modelling (FDM) 3D printing in solid dosage form manufacturing provides a flexible technique suitable for dose modification at a low cost. However, it was limited to non-pharmaceutical grade and extended release polymers, and often uses relatively high temperature (230 °C). Therefore, this research aims at tackling these limitations by producing 3D printed immediate and modified release tablets and liquid-filled capsules using pharmaceutical grade polymers for small and large molecule (peptides and protein) drug models.

Bridging 3D printing processes with hot melt extrusion (HME) in the presence of a thermostable filler, talc and pharmaceutical grade polymers enabled the fabrication of tablets and capsules shells using FDM 3D printing. The first example of immediate release 3D printed tablets using polyvinyl pyrrolidone (PVP)-based filaments was demonstrated, with suitability for different actives (aspirin, dipyridamole and theophylline). This was achieved at a relatively low temperature of 110 °C. Thermogravimetric analysis (TGA) demonstrated that the excipients and actives were stable within the HME and 3D printing temperatures apart from aspirin as observed from further high-pressure liquid chromatography (HPLC). The hygroscopic nature of the polymer had a major impact in the glass transition temperature (T_g) of the PVP-filament and its compatibility with FDM 3D printers.

Furthermore, for the first time, enteric release tablets were fabricated using a dual FDM 3D printer, using Eudragit L100-55-based shell and PVP-based drug loaded core filaments. This was achieved in a single process, requiring a shell layer thickness ≥ 0.52 mm to achieve adequate acid resistance. British Pharmacopoeia (BP) criteria for enteric release was met by replacing talc with tribasic phosphate (TBP). This however, resulted in the degradation of the active pharmaceutical ingredient (API), emphasising the superiority of talc (non-melting component) for filament formulations. The system also demonstrated suitability for other actives (budesonide, diclofenac and theophylline).

By coordinating FDM 3D printing and liquid dispensing, immediate and extended liquid-filled capsules were fabricated using Eudragit EPO and RL respectively. The syringe-based liquid dispenser demonstrated a linear relationship between the estimated and actual doses obtained ($R^2 = 0.9985$). The integrity of the shell was maintained during the filling process by using a multi-phase 3D printing approach, 1.6 mm shell thickness, 100 % shell infill and concentric infill pattern. This process avoided thermal exposure during the capsule filling which prompted investigations into the encapsulation of antimicrobial peptides (AMPs). Aurein 2.6 and LL-37 demonstrated a concentration and time dependent increase in anticancer activities against HT-29 and only the former against Caco-2 colon cancer cell lines. The solution structure of the peptides was maintained during encapsulation. As a proof of concept to demonstrate colon targeting, a Eudragit S100-based capsule shell and theophylline solution model core was presented.

Accelerated stability studies indicated that the PVP-based filament was only stable when stored at 5 °C. However, Eudragit L100-55 and S100 remained stable in all the investigated storage conditions. By adapting these pharmaceutical grade polymers for FDM 3D printing and the modification of the FDM 3D printer head, it was possible to fabricate immediate, enteric, extended and colonic release tablets and liquid-filled capsules. These demonstrated suitability for thermostable and thermolabile actives. In a clinical setting, health care staffs will be able to rapidly manufacture varied doses of tablets and small volume liquid-filled capsules with individualised dose contents and release pattern in response to specific patient's needs.

CONTENTS

| | |
|---|----|
| ABSTRACT..... | v |
| LIST OF FIGURES..... | 11 |
| LIST OF TABLES..... | 16 |
| LIST OF PUBLICATIONS..... | 17 |
| POSTER PRESENTATIONS..... | 17 |
| INTELLECTUAL PROPERTY..... | 17 |
| ABBREVIATIONS AND ACRONYMS..... | 18 |
| OVERVIEW..... | 19 |
| Chapter 1 : General Introduction..... | 20 |
| 1.1 Anatomy of the gastrointestinal tract..... | 21 |
| 1.1.1 Epidemiology of colorectal cancer..... | 25 |
| 1.1.2 Stages of colorectal cancer..... | 25 |
| 1.1.3 Treatment of colorectal cancer..... | 28 |
| 1.3 Oral drug delivery..... | 30 |
| 1.3.1 Oral Liquid dosage forms..... | 30 |
| 1.3.2 Oral solid dosage form..... | 30 |
| 1.4 Drug release patterns from oral drug delivery..... | 37 |
| 1.4.1 Immediate release..... | 37 |
| 1.4.2 Modified release..... | 37 |
| 1.5 Physiological changes along the GIT that affects oral delivery systems..... | 41 |
| 1.5.1 pH changes across the GIT..... | 41 |
| 1.5.2 Transit time..... | 41 |
| 1.5.3 Gut Microbiota..... | 43 |
| 1.6 Pharmacogenomics and individualised drug therapy..... | 43 |
| 1.7.1 Current approaches to dose personalisation..... | 45 |
| 1.8 3D printing and its various types..... | 47 |
| 1.8.1 Stereolithographic 3D printing (STA)..... | 47 |
| 1.8.2 Powder-bed 3D printing (PB)..... | 49 |
| 1.8.3 3D printing by semi-solid extrusion (SSE)..... | 49 |
| 1.8.4 3D printing by fused deposition modelling (FDM)..... | 49 |
| 1.9 3D printing challenges in pharmaceutical field..... | 51 |
| 1.9.1 Limitations of FDM 3D printing in pharmaceutical manufacturing..... | 51 |
| 1.9.2 Regulatory challenges..... | 52 |
| 1.10 Scope of the research..... | 53 |
| 1.11 Project aims..... | 53 |

| | |
|---|----|
| Chapter 2 : A Lower Temperature FDM 3D Printing for the Manufacture of Patient-Specific Immediate Release caplets Using Polyvinyl Pyrrolidone | 55 |
| 2.1 Introduction | 56 |
| 2.2 Aim and Objectives | 59 |
| 2.3 Materials | 60 |
| 2.3.1 Theophylline..... | 60 |
| 2.3.2 Dipyridamole..... | 60 |
| 2.3.3 Aspirin | 61 |
| 2.3.4 Polyvinyl pyrrolidone (MW, 40,000) | 61 |
| 2.3.5 Talc | 62 |
| 2.3.6 Triethyl citrate..... | 62 |
| 2.3.7 Scotch blue painter’s tape | 62 |
| 2.4 Methods..... | 62 |
| 2.4.1 Preparation of filaments using HME | 62 |
| 2.4.2 Tablet design and printing | 65 |
| 2.4.3 Differential scanning calorimetry (DSC)..... | 65 |
| 2.4.4 Thermogravimetric analysis (TGA)..... | 66 |
| 2.4.5 X-ray Powder diffractometry (XPRD) | 66 |
| 2.4.6 Characterisation of the tablets properties..... | 67 |
| 2.4.7 Determination of drug content..... | 68 |
| 2.4.8 Scanning electron microscopy (SEM)..... | 69 |
| 2.4.9 <i>In vitro</i> drug release studies..... | 70 |
| 2.4.10 Statistical analysis | 71 |
| 2.5 Results and discussions..... | 72 |
| 2.6 Conclusions | 86 |
| Chapter 3 : Fabricating a Shell-Core Delayed Release Tablet Using Dual FDM 3D Printing for Patient-Centred Therapy | 87 |
| 3.1 Introduction | 88 |
| 3.2 Aims and objectives | 90 |
| 3.3 Materials | 92 |
| 3.3.1 Eudragit L100-55 | 92 |
| 3.3.2 PEG400 | 92 |
| 3.3.3 Castor oil | 92 |
| 3.3.4 Oleic acid | 92 |
| 3.3.5 Other ingredients..... | 93 |
| 3.4 Methods..... | 94 |
| 3.4.1 Preparation of filaments using HME | 94 |
| 3.4.2 Tablet design and printing | 94 |

| | |
|---|-----|
| 3.4.3 Thermal analysis..... | 94 |
| 3.4.4 X-ray Powder diffractometry (XRPD) | 95 |
| 3.4.5 Determination of drug content..... | 95 |
| 3.4.6 Scanning electron microscopy (SEM)..... | 96 |
| 3.4.7 Raman Spectroscopy..... | 96 |
| 3.4.8 In vitro disintegration and dissolution studies..... | 97 |
| 3.4.9 Statistical analysis | 98 |
| 3.5 Results and discussions | 99 |
| 3.6 Conclusions | 116 |
| Chapter 4 : On Demand Manufacturing of Patient-specific Liquid-filled Capsules via Co-ordinated 3D Printing and Liquid Dispensing | 117 |
| 4.1 Overview | 118 |
| 4.2 Section 1: Introduction | 119 |
| 4.3 Aims..... | 121 |
| 4.5 Materials | 122 |
| 4.5.1 Eudragit EPO | 122 |
| 4.5.2 Eudragit RL 100 | 123 |
| 4.5.3 Methocel E4 | 123 |
| 4.5.4 Tween 80..... | 123 |
| 4.5.5 Citric acid..... | 123 |
| 4.5.6 Other ingredients..... | 124 |
| 4.6 Methods..... | 124 |
| 4.6.1 Preparation of shell filament | 124 |
| 4.6.2 Thermal analysis..... | 124 |
| 4.6.3 X-ray powder diffraction | 124 |
| 4.6.4 Scanning Electron Microscopy (SEM)..... | 126 |
| 4.6.5 Preparation of the liquid core..... | 126 |
| 4.6.6 Modification of dual FDM 3D printer..... | 126 |
| 4.6.7 Liquid Capsule design and printing | 127 |
| 4.6.8 Validation of the liquid dispenser using different nozzle sizes..... | 129 |
| 4.6.9 Optimising the dosing accuracy of the liquid dispenser using different syringe sizes | 129 |
| 4.6.10 Determination of drug contents | 129 |
| 4.6.11 <i>In vitro</i> dissolution test | 130 |
| 4.6.12 Statistical analysis | 130 |
| 4.7 Results and Discussion | 132 |
| 4.8 Conclusions | 148 |
| 4.9 Section 2: Introduction | 149 |

| | |
|--|-----|
| 4.10 Aims..... | 152 |
| 4.11 Materials | 153 |
| 4.11.1 Eudragit S100 | 153 |
| 4.11.2 Aurein 2.6 (MW, 1629) | 153 |
| 4.11.3 Cathelicidin LL-37 (MW, 4493.33)..... | 153 |
| 4.11.4 HT-29 colon cancer cell line (Passage number 141) | 154 |
| 4.11.5 Caco-2 colon cancer cell line (passage number 57)..... | 154 |
| 4.11.6 Other ingredients | 154 |
| 4.12 Methods..... | 154 |
| 4.12.1 Cell recovery from cell bank..... | 154 |
| 4.12.2 Cell sub-culturing / passaging | 154 |
| 4.12.3 Cell counting using haemocytometer | 155 |
| 4.12.4 Freezing down of cells..... | 156 |
| 4.12.5 Growth curve using trypan blue | 156 |
| 4.12.6 Growth curve using MTT assay | 156 |
| 4.12.7 Cell viability / cytotoxicity studies..... | 156 |
| 4.12.8 Determination of IC ₅₀ | 157 |
| 4.12.9 Preparation of shell filament | 157 |
| 4.12.10 Preparation of liquid core | 157 |
| 4.12.11 3D printing of liquid capsules..... | 157 |
| 4.12.12 Thermal analysis using thermal imaging camera..... | 158 |
| 4.12.13 Determination of the secondary structure of the peptides using circular dichroism | 158 |
| 4.12.12 Statistical analysis | 159 |
| 4.13 Results and discussions..... | 160 |
| 4.14 Conclusion..... | 175 |
| Chapter 5 : Accelerated Stability Studies for HME processed PVP and Eudragit-based Filaments for FDM 3D printing | 176 |
| 5.1 Introduction | 177 |
| 5.2 Aims..... | 182 |
| 5.3 Materials | 183 |
| 5.4 Methods..... | 183 |
| 5.4.1 Preparation of filaments | 183 |
| 5.4.2 Accelerated stability studies (storage conditions)..... | 183 |
| 5.4.3 Printability test using Makerbot 2X FDM 3D printer (Makerbot, US)..... | 183 |
| 5.4.4 Filament dimension | 185 |
| 5.4.5 X-ray powder diffractometry (XRPD) | 185 |
| 5.4.6 Differential scanning calorimetry (DSC)..... | 185 |

| | |
|---|-----|
| 5.4.7 Thermal gravimetric analysis (TGA) | 185 |
| 5.4.8 In vitro drug release studies (PVP-based filament)..... | 185 |
| 5.4.9 Determination of drug content (PVP-based filament)..... | 186 |
| 5.4.10 Statistical analysis | 186 |
| 5.5 Results and discussions..... | 187 |
| 5.6 Conclusions | 212 |
| Chapter 6 : General conclusions and future work | 213 |
| 6.1 General conclusions | 214 |
| 6.2 Future works | 218 |
| Chapter 7 : Supplementary Data | 219 |
| References | 235 |

LIST OF FIGURES

Chapter 1

| | |
|--|----|
| Figure 1.1. The gastrointestinal tract (Anatomy&Physiology, 2013)..... | 21 |
| Figure 1.2. A cross section of the alimentary canal (Anatomy&Physiology, 2014). | 22 |
| Figure 1.3. Different classifications of the Tumour (T) stage of the TNM staging system (CancerResearchUK, 2015c)..... | 26 |
| Figure 1.4. Dukes’s method of colon cancer staging (CancerResearchUK, 2015a). | 27 |
| Figure 1.5. Treatment of (A) Colon and (B) Rectal cancer (Miller et al., 2016). | 29 |
| Figure 1.6. Perforated coating pan (Evonik, 2018) (A) fluid bed coater (Microencapsulation.net, 2018) (B)..... | 33 |
| Figure 1.7. Mechanism of various 3D printing technologies: (A) Stereolithographic (SLA), (B) Powder bed and powder jetting, (C) Semi-solid extrusion (EXT) and (D) Fused deposition modelling (FDM). | 48 |
| Figure 2.1. Chemical structure of theophylline (SIGMA-ALDRICH, 2018b)..... | 60 |
| Figure 2.2. Chemical structure of dipyridamole (SIGMA-ALDRICH, 2016a)..... | 60 |
| Figure 2.3: Chemical structure of aspirin (SIGMA-ALDRICH, 2018a) | 61 |
| Figure 2.4: Chemical structure of PVP (SIGMA-ALDRICH, 2016b)..... | 61 |
| Figure 2.5. Formulation of a solid dispersion by hot melt extrusion process (ParticleScience, 2011). | 63 |
| Figure 2.6. Schematic illustration of Bragg spectrometer (Libretexts, 2017). | 67 |
| Figure 2.7. Components of HPLC (LaboratoryInfo.com, 2015). | 68 |
| Figure 2.8. The set-up of a scanning electron microscope (Technoorg-Linda, 2018)..... | 70 |
| Figure 2.9. Schematic illustration of the fabrication of immediate release 3D-printed tablet. (A) Materials mixture (API, PVP and talc) are processed through HME to produce (B) API loaded PVP filament is extruded (C) Stereolithographic file is designed via CAD software and (D) FDM 3D printer uses the filament as a feed to fabricate drug loaded immediate release tablet (E) at 110 °C. | 73 |
| Figure 2.10. TGA Thermal degradation profiles of TEC, PVP, PVP:TEC filament, API-free and API loaded filaments, and 3D printed tablets for (A) Aspirin, (B) Dipyridamole, (C) theophylline and the excipients used. | 75 |
| Figure 2.11. Reversing MTDSC thermographs of PVP, PVP:TEC filament, API-free and API- loaded filaments, and 3D printed tablets for Aspirin (A) First heat-scan and (B) second heat- scan)..... | 77 |
| Figure 2.12. Reversing MTDSC thermographs of PVP, PVP:TEC filament, API-free and API- loaded filaments, and 3D printed tablets for dipyridamole (A) First heat-scan and (B) second heat-scan). | 78 |
| Figure 2.13. Reversing MTDSC thermographs of PVP, PVP:TEC filament, API-free and API- loaded filaments, and 3D printed tablets for theophylline (A) First heat-scan and (B) second heat-scan). | 79 |
| Figure 2.14. Determination of the physical form of the actives before and after processing using HME and 3D printing for (A) aspirin, (B) dipyridamole and (C) theophylline..... | 81 |
| Figure 2.15. XRPD patterns of PVP, PVP:TEC filament, API-free and API-loaded filaments, and 3D printed tablets for aspirin (A) dipyridamole (B) and theophylline. (C)..... | 82 |
| Figure 2.16. Immediate drug release profile from PVP 3D tablets (n=3). | 85 |
| Figure 3.1. Chemical structure of Eudragit L100-55 (Hamman, 2010). | 92 |
| Figure 3.2. The components and working principles of Raman spectroscopy (Frejberg, 2013). 96 | |
| Figure 3.3. Schematic illustration of the fabrication of 3D-printed shell-core enteric tablet. (A) Two complementary stereolithographic files are designed via CAD software to create a shell- core structure (B) Dual FDM 3D printer is employed with two different filaments; i) filament for enteric shell (based on Eudragit L), and ii) filament core (based API, PVP) processed through | |

| | |
|---|-----|
| HME compounder. A lubricating station is installed for PVP to facilitate the printing of the core during nozzle alternation. (C) Image of the 30% completed FDM 3D printer Shell-core. | 100 |
| Figure 3.4. Impact of lubricants on (A) TGA thermal degradation profiles of PVP filament and (B) the in vitro release pattern of theophylline from core tablet. | 101 |
| Figure 3.5. (A and B) Rendered images (Autodesk 3DS Max) of shell-core designs with increasing shell thickness (0.17, 0.35, 0.52, 0.70 and 0.87mm), (C) Images of 30% completed shell-core designs with theophylline core and increasing Eudragit L100-55 shell thickness, (D) SEM images of the surface of the tablets (E) Impact of shell thickness of 3D printing on in vitro release pattern of theophylline from 3D printed tablet in USP II pH change dissolution test. | 102 |
| Figure 3.6. (A) Images of 3D printed enteric theophylline tablet printed with low, medium and higher resolution, (B) Impact of resolution of 3D printing on in vitro release pattern of theophylline from 3D printed tablet in USP II pH change dissolution test. (C) Impact of filler (TBP or talc) on the in vitro release pattern of theophylline from 3D printed tablets in USP II pH change dissolution test in phosphate buffer, (D1,2) SEM and Raman images (respectively) of a cross-sections of 0.52 mm thickness shell theophylline table..... | 104 |
| Figure 3.7. TGA thermal degradation profiles of the raw materials of; theophylline, PVP, TBP, TEC as well as the physical mixture, the filament and the 3D printed tablets. | 106 |
| Figure 3.8. TGA thermal degradation profiles of TEC, PVP, PVP:TEC filament, API-free and API loaded filaments, and 3D printed tablets for (A) budesonide and (B) diclofenac sodium. | 108 |
| Figure 3.9. Reversing DSC thermographs of PVP, PVP: TEC filament, API-free and API-loaded filaments, and 3D printed tablets for budesonide (A1 first heat-scan and A2 second heat-scan) and diclofenac sodium (B1 first heat-scan and B2 second heat-scan). | 109 |
| Figure 3.10. Reversing DSC thermographs of PVP, PVP: TEC filament, API-free and API-loaded filaments, and 3D printed tablets for budesonide (A1 first heat-scan and A2 second heat-scan) and diclofenac sodium (B1 first heat-scan and B2 second heat-scan). | 110 |
| Figure 3.11. XRPD patterns of PVP, PVP: TEC filament, API-free and API-loaded filaments, and 3D printed tablets for (A) budesonide, (B) diclofenac sodium and (C) theophylline..... | 112 |
| Figure 3.12. In vitro release pattern of APIs; budesonide, diclofenac sodium or theophylline from 3D printed tablets using a USP II pH change dissolution test in (A) phosphate buffer and (B) bicarbonate buffer..... | 114 |
| Figure 4.1. Chemical structure of Eudragit EPO (An Nguyen et al., 2006)..... | 122 |
| Figure 4.2. Chemical structure of Eudragit RL100 (An Nguyen et al., 2006). | 123 |
| Figure 4.3. Schematic illustration of the fabrication of 3D-printed liquid capsule using a modified dual FDM 3D printer. | 131 |
| Figure 4.4. The co-ordination of FDM nozzle and liquid syringe dispenser is achieved in two different printing modes: i) Single-phase printing: (A1) the core is located in the centre of the cavity of the shell, (A2) Shell printing and capsule filling is achieved by alternation at each layer. (A3) Image of completed shell-core designs with dipyrindamole core and Eudragit EPO shell. ii) Multi-phase printing: (B1) the core is located in a median level between the bottom shell (75%) and the top shell (25%). (B2) the shell is printed first followed by complete filling of the shell bottom, the printing is completed by printing the shell top. (B3) Image of completed shell-core designs (shell top was separated from bottom for demonstration). (See Supplementary Data Videos S1 and S2). | 133 |
| Figure 4.5. TGA analysis of polymer, polymer:TEC physical mixture, polymer:TEC:talc physical mixture, filament and 3D printed shell for Eudragit EPO (A) and RL (B) respectively. | 135 |
| Figure 4.6. DSC thermographs of polymer, polymer:TEC physical mixture, polymer:TEC:talc physical mixture, filament and 3D printed shell for Eudragit EPO (A) and RL (B) respectively. | 137 |
| Figure 4.7. XRPD patterns of polymer, talc and polymer:TEC:talc physical mixture, filament and 3D printed shell for Eudragit EPO. | 138 |

| | |
|---|-----|
| Figure 4.8. Impact of 3D printing pattern on the structure and integrity of the shell: SEM images of (A1 and B1) external surface and (A2 and B2) internal surface of the Eudragit E based shell, in rectilinear or concentric infill respectively. | 139 |
| Figure 4.9. The impact of printing pattern on the structure of the shell: SEM image of external surface of the corner and side of Eudragit E based capsule shell produced via (A1 and A2) single-phase or (B1 and B2) multi-phase 3D printing. | 140 |
| Figure 4.10. Impact of single-phase and multi-phase 3D printing modes on dispensed volume of dipyridamole suspension (1.5% w/v) from the liquid dispenser using (A) 2 mL or (B) 10 mL syringe. | 142 |
| Figure 4.11. Dose accuracy using syringe liquid dispenser of dipyridamole suspension (1.5% w/v): (A) relation of theoretical volume of the core in the software and dispensed dose using single- or multi-phase 3D printing modes, (B) correlation between theoretical and actual volume. | 144 |
| Figure 4.12. A) In vitro release pattern of dipyridamole suspension from 3D printed liquid Eudragit EPO capsule using USP II with different core volumes in gastric media (pH 1.2). B) In vitro release of theophylline from 3D printed liquid capsule filled with theophylline solution based on (B) Eudragit E or (C) Eudragit RL. All capsules were printed using multi-phase mode 3D printing and 2 mL syringe liquid dispenser. | 146 |
| Figure 4.13. Chemical structure of Eudragit S100 (Yoo et al., 2011). | 153 |
| Figure 4.14. The surface of a haemocytometer. | 155 |
| Figure 4.15. 50 % confluent Caco-2 (A) and HT-29 (B) colon cancer cell lines. | 161 |
| Figure 4.16. Growth curve of Caco-2 and HT-29 using trypan blue (A) and MTT assay (B). | 162 |
| Figure 4.17. Cytotoxicity of aurein 2.6 (A), LL-37 (B) and cisplatin (C) on HT-29 colon cancer cell line. | 164 |
| Figure 4.18. Cytotoxicity of aurein 2.6 (A), LL-37 (B) and cisplatin (C) on Caco-2 colon cancer cell line. | 165 |
| Figure 4.19. TGA (A) and DSC (B) thermographs of Eudragit S100 polymer and Eudragit S100-based filament. | 167 |
| Figure 4.20. Temperature changes during FDM 3D printing of Eudragit S100. | 168 |
| Figure 4.21. Temperature changes during FDM 3D printing of Eudragit S100. | 169 |
| Figure 4.22. Impact of temperature on the secondary structure of aurein 2.6 (A) and LL-37 (B). | 171 |
| Figure 4.23. The impact of coordinated FDM 3D printing and syringe-based liquid dispenser on the secondary structure of aurein 2.6 (A) and LL-37 (B). | 173 |
| Figure 4.24. In vitro dissolution studies of the 3D printed colon targeting liquid capsule. | 174 |
| Figure 5.1. The impact of storage at 5 °C on the XRPD of PVP-based filament (A) no vacuum (B) vacuum. | 190 |
| Figure 5.2. The impact of storage at 5 °C on the XRPD of Eudragit L 100-55-based filament (A) no vacuum (B) vacuum. | 192 |
| Figure 5.3. The impact of storage at 30 °C + 65 %RH on the XRPD of Eudragit L 100-55-based filament (A) no vacuum (B) vacuum. | 193 |
| Figure 5.4. The impact of storage at 40 °C + 75 %RH on the XRPD of Eudragit L 100-55-based filament (A) no vacuum (B) vacuum. | 194 |
| Figure 5.5. The impact of storage at 5 °C on the XRPD of Eudragit S100-filament (A) no vacuum (B) vacuum. | 195 |
| Figure 5.6. The impact of storage at 30 °C + 65 %RH on the XRPD of Eudragit S100-filament (A) no vacuum (B) vacuum. | 196 |
| Figure 5.7. The impact of storage at 40 °C + 75 %RH on the XRPD of Eudragit S100-based filament (A) no vacuum (B) vacuum. | 197 |
| Figure 5.8. The impact of different storage condition on TGA of PVP-based filament after 1 month. | 199 |

| | |
|--|-----|
| Figure 5.9. The impact of storage at 5 °C on the TGA of PVP-based filament (A) no vacuum (B) vacuum..... | 200 |
| Figure 5.10. The impact of storage at 5 °C on the TGA of Eudragit L 100-55-based filament (A) no vacuum (B) vacuum. | 202 |
| Figure 5.11. The impact of storage at 30 °C + 65 %RH on the TGA of Eudragit L 100-55-based filament (A) no vacuum (B) vacuum. | 203 |
| Figure 5.12. The impact of storage at 40 °C + 75 %RH on the TGA of Eudragit L 100-55-based filament (A) no vacuum (B) vacuum. | 204 |
| Figure 5.13. The impact of storage at 5 °C on the TGA of Eudragit S100-based filament (A) no vacuum (B) vacuum..... | 206 |
| Figure 5.14. The impact of storage at 30 °C + 65 %RH on the TGA of Eudragit S100-based filament (A) no vacuum (B) vacuum. | 207 |
| Figure 5.15. The impact of storage at 40 °C + 65 %RH on the TGA of Eudragit S100-based filament (A) no vacuum (B) vacuum. | 208 |
| Figure 5.16. In-vitro drug release profile from PVP-based filament after storage in different condition for 1 month (A) and after storage at 5 °C alone for 6 months (B)..... | 211 |
| Figure 7.1. Reversing MTDSC thermographs of Eudragit L100-55, Eudragit L100-55:TEC filament, API-free filaments, and 3D printed shell (A) First heat-scan and (B) second heat-scan. | 220 |
| Figure 7.2 Reversing DSC thermographs of PVP, PVP: TEC (12.5%) filament, as well as diclofenac-loaded filaments (first heat-scan). | 221 |
| Figure 7.3. Linear relationship theoretical volume of the software and dispensed volume using single-phase printing mode and different nozzle aperture sizes (blue, orange and grey graphs for 0.25, 0.41 or 0.84 mm nozzles respectively). | 222 |
| Figure 7.4. Linear relationship theoretical volume of the software and dispensed volume using multi-phase printing mode and different nozzle aperture sizes (blue, orange and grey graphs for 0.25, 0.41 or 0.84 mm nozzles respectively). | 223 |
| Figure 7.5. Reversible heat flow for the first (A) and second (B) MTDSC thermograph used to investigate the impact of storage at 5 oC without vacuum on the Tg of PVP-based filaments. | 224 |
| Figure 7.6. Reversible heat flow for the first (A) and second (B) MTDSC thermograph used to investigate the impact of storage at 5 oC + vacuum on the Tg of PVP-based filaments..... | 225 |
| Figure 7.7. Reversible heat flow for the first (A) and second (B) MTDSC thermograph used to investigate the impact of storage at 5 °C without vacuum on the Tg of Eudragit L100-55-based filaments. | 226 |
| Figure 7.8. Reversible heat flow for the first (A) and second (B) MTDSC thermograph used to investigate the impact of storage at 5 °C + vacuum on the Tg of Eudragit L100-55-based filaments. | 227 |
| Figure 7.9. Reversible heat flow for the first (A) and second (B) MTDSC thermograph used to investigate the impact of storage at 30 °C and 65 %RH without vacuum on the Tg of Eudragit L100-55-based filaments..... | 228 |
| Figure 7.10. Reversible heat flow for the first (A) and second (B) MTDSC thermograph used to investigate the impact of storage at 30 °C and 65 %RH + vacuum on the Tg of Eudragit L100-55-based filaments..... | 229 |
| Figure 7.11. Reversible heat flow for the first (A) and second (B) MTDSC thermograph used to investigate the impact of storage at 40 °C and 75 %RH without vacuum on the Tg of Eudragit L100-55-based filaments..... | 230 |
| Figure 7.12. Reversible heat flow for the first (A) and second (B) MTDSC thermograph used to investigate the impact of storage at 40 oC and 75 %RH + vacuum on the Tg of Eudragit L100-55-based filaments..... | 231 |

| | |
|---|-----|
| Figure 7.13. Reversible heat flow for the MTDSC thermograph used to investigate the impact of storage at 5 °C without vacuum (A) or with vacuum (B) on the Tg of Eudragit S100-based filaments. | 232 |
| Figure 7.14. Reversible heat flow for the MTDSC thermograph used to investigate the impact of storage at 30 °C and 65 %RH without vacuum (A) or with vacuum (B) on the Tg of Eudragit S100-based filaments..... | 233 |
| Figure 7.15. Reversible heat flow for the MTDSC thermograph used to investigate the impact of storage at 40 °C and 75 %RH without vacuum (A) or with vacuum (B) on the Tg of Eudragit S100-based filaments..... | 234 |

LIST OF TABLES

Chapter 1

| | |
|--|-----|
| Table 1.1. Examples of polymers employed in dosage form manufacturing and their applications. | 40 |
| Table 2.1. HME and FDM 3D printing processing parameters..... | 64 |
| Table 2.2. Physical characterisation (Weight uniformity n=20, Crushing strength n=3, Disintegration n=6). | 84 |
| Table 2.3. The dimensions of the 3D printed tablets (n=6). | 84 |
| Table 2.4. Drug content analysis using HPLC (n=3)..... | 84 |
| Table 3.1. Summary of the compositions of API loaded filament and residual drug contents following HME and dual FDM 3D printing. | 106 |
| Table 3.2. Summary of gastric resistant properties of 3D printed enteric tablets. | 115 |
| Table 4.1. The formulation and processing parameters for HME and FDM 3D printing of shell filament formulations. | 125 |
| Table 4.2. A summary of the volume, dimensions and respective volumes, estimated volume, estimated dose and actual dose for different cores in the 3D printed liquid capsules (n=4, ±SD). | 128 |
| Table 4.3. IC ₅₀ of aurein 2.6, LL-37 and cisplatin on HT-29 and Caco-2 colon cancer cell lines. | 166 |
| Table 5.1. Stability testing conditions based on climatic zones (WHO, 2009)..... | 178 |
| Table 5.2. General case of stability studies (ICH, 2003)..... | 178 |
| Table 5.3. APIs and products intended to be stored in the fridge (ICH, 2003). | 178 |
| Table 5.4. APIs and products intended for storage in freezer (ICH, 2003). | 178 |
| Table 5.5. Analytical equipment commonly used in physical characterisations and their applications (Guo et al., 2013). | 179 |
| Table 5.6. Filament formulation, HME and 3D printing parameters. | 184 |
| Table 5.7. Impact of storage conditions on filament diameter. | 188 |
| Table 5.8. Investigation of the moisture uptake of the stored filaments using TGA..... | 198 |

LIST OF PUBLICATIONS

Alhnan, M.A., Okwuosa, T.C., Sadia, M., Wan, K.W., Ahmed, W., Arafat, B., 2016, Emergence of 3D Printed Dosage Forms: Opportunities and Challenges, *Pharm Res*, 33, 1817-1832.

Okwuosa, T.C., Stefaniak, D., Arafat, B., Isreb, A., Wan, K.W., Alhnan, M.A., 2016, A Lower Temperature FDM 3D Printing for the Manufacture of Patient-Specific Immediate Release Tablets, *Pharm Res*, 33, 2704-2712.

Okwuosa, T.C., Pereira, B.C., Arafat, B., Cieszynska, M., Isreb, A., Alhnan, M.A., 2017, Fabricating a Shell-Core Delayed Release Tablet Using Dual FDM 3D Printing for Patient-Centred Therapy, *Pharm Res*, 34, 427-437.

Okwuosa, T.C., Soares, C., Golwitzer, V., Habashy, R., Timmins, T., Alhnan, M.A., 2018, On Demand Manufacturing of Patient-Specific Liquid Capsule via Co-ordinated 3D Printing and Liquid Dispensing, *Eur.J.Pharm.Sci*, 118, 134-143.

POSTER PRESENTATIONS

Okwuosa, T.C., Pereira, B.C., Arafat, B., Cieszynska, M., Isreb, A., Alhnan, M.A., 2016 November, Fabricating a Shell-Core Enteric Tablet Using Dual FDM 3D Printing, American Association of Pharmaceutical Scientists Annual Meeting and Exposition.

Okwuosa, T.C., Stefaniak, D., Arafat, B., Isreb, A., Wan, K.W., Alhnan, M.A., 2016 November, FDM Printing of Patient-Specific Immediate Release PVP Based Tablets, American Association of Pharmaceutical Scientists Annual Meeting and Exposition.

Okwuosa, T.C., Stefaniak, D., Arafat, B., Isreb, A., Wan, K.W., Alhnan, M.A., 2016 November, The Impact of Hot Melt Extrusion and Fused Deposition Modelling 3D Printing on Polyvinyl pyrrolidone-Based Matrix, American Association of Pharmaceutical Scientists Annual Meeting and Exposition.

Okwuosa, T.C., Soares, C., Golwitzer, V., Habashy, R., Timmins, T., Alhnan, M.A., 2017 November, Fully Automated Fabrication of Novel Liquid Capsules by Coordinated FDM 3D Printing and Liquid Dispensing, American Association of Pharmaceutical Scientists Annual Meeting and Exposition.

Okwuosa, T.C., Soares, C., Golwitzer, V., Habashy, R., Timmins, T., Alhnan, M.A., 2017 November, Dosing Accuracy of a Novel 3D Printed Liquid Capsule Dispenser, American Association of Pharmaceutical Scientists Annual Meeting and Exposition.

INTELLECTUAL PROPERTY

Alhnan, M.A., Okwuosa, T.C., 2018, Solid Dosage Form Production, WO 2018/020237 A1.

ABBREVIATIONS AND ACRONYMS

| | |
|----------------|---|
| ADRs | Adverse drug reactions |
| AMPs | Antimicrobial peptides |
| API | Active pharmaceutical ingredient |
| BCS | Biopharmaceutics Classification System |
| BP | British Pharmacopoeia |
| CAD | Computer aided design |
| CD | Circular dichroism |
| DMSO | Dimethyl sulphoxide |
| DSC | Differential scanning calorimetry |
| FDA | Food and Drug Administration |
| FDM | Fused Deposition Modelling |
| GIT | Gastrointestinal tract |
| HME | Hot melt extrusion |
| HCl | Hydrochloric acid |
| HPC | Hydroxypropyl cellulose |
| HPLC | High performance liquid chromatography |
| HPMC | Hydroxypropyl methylcellulose |
| MTDSC | Modulated temperature differential scanning calorimetry |
| PBS | Phosphate buffer solution |
| PLA | Polylactic acid |
| PVA | Polyvinyl alcohol |
| PVP | Polyvinyl pyrrolidone |
| RH | Relative humidity |
| SEM | Scanning electron microscopy |
| SIF | Simulated intestinal fluid |
| TEC | Triethyl citrate |
| Temp | Temperature |
| T _g | Glass transition temperature |
| T _m | Melting point |
| TGA | Thermal gravimetric analysis |
| XRPD | X-ray powder diffraction |

OVERVIEW

This research focuses on the adaptations of a benchtop FDM 3D printer to the manufacturing immediate and modified release oral dosage forms (tablets and capsules) for both large and small molecules with dose personalisation potentials. Therefore, it will be beneficial to understand how the gastrointestinal tract (GIT) functions and how they affect the oral delivery of pharmaceutical products (Chapter 1). The pathologies of the colon were discussed since colon cancer was investigated in this research. Also, different types of oral dosage forms were introduced, including different drug release patterns. Current approaches to personalised dosing was discussed and the potentials of 3D printing in providing a more flexible platform that can revolutionise drug dosing towards a more individualised approach was discussed.

Chapter 2 discusses the use of PVP-based filament in the manufacturing of immediate release dosage form. Chapter 3 discussed the use of dual FDM 3D printing in the manufacturing of enteric tablets in a single process. This was unlike the conventional approach which involves core manufacturing followed by another coating stage. Investigations into the use of this technology in the manufacturing of liquid-filled capsules were discussed in Chapter 4. This involved the replacement of one of the heads of a dual FDM 3D printer with a syringe-based liquid dispenser. This was explored for the delivery of both small and large molecules and was used to achieve both immediate and modified drug release profiles. An investigation into the stability of the adapted filaments were discussed in Chapter 5 followed by the conclusions and future work in Chapter 6.

Chapter 1 : General Introduction

1.1 Anatomy of the gastrointestinal tract

The gastrointestinal tract (GIT), also called the digestive tract or alimentary canal, is a large muscular tube which runs from the mouth to the anus. (Figure 1.1). It forms a complex system through which ingested food and oral dosage forms travel which creates a major barrier in the oral delivery of the variety of modified release dosage forms currently available in the market (Dressman and Lennernas, 2000).

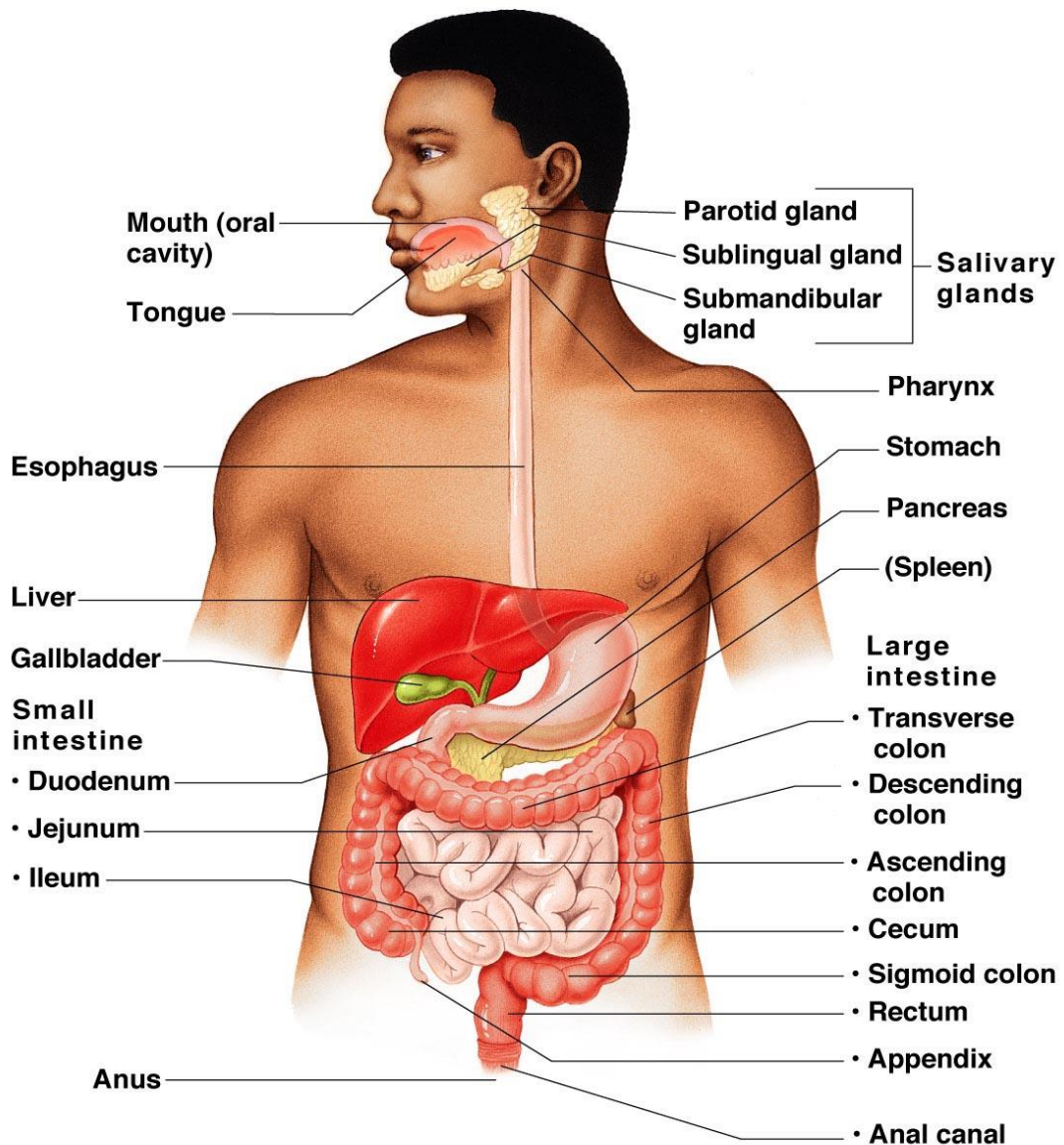


Figure 1.1. The gastrointestinal tract (Anatomy&Physiology, 2013).

A cross sectional view of the GIT reveals four tissues, the mucosa, submucosa, muscularis layer and serosa (Figure 1.2) (Anatomy&Physiology, 2014, Reinus and Simon, 2014). The mucosa layer forms the inner lining of the GIT and is the only tissue

layer in direct contact with substances passing through the GIT. It is made up of non-keratinised stratified epithelial tissues and protects the GIT from rough substances passing through it. It also protects the GIT from the harsh conditions of the stomach. The submucosa contains connective tissue and provides blood and nerve supply to the mucosa and other tissues. Surrounding the submucosa is the muscularis layer, which controls the contraction and expansion of the GIT to move substances along it (peristalsis) while the serosa forms the outer cover around the GIT and loosely attaches it to surrounding organs.

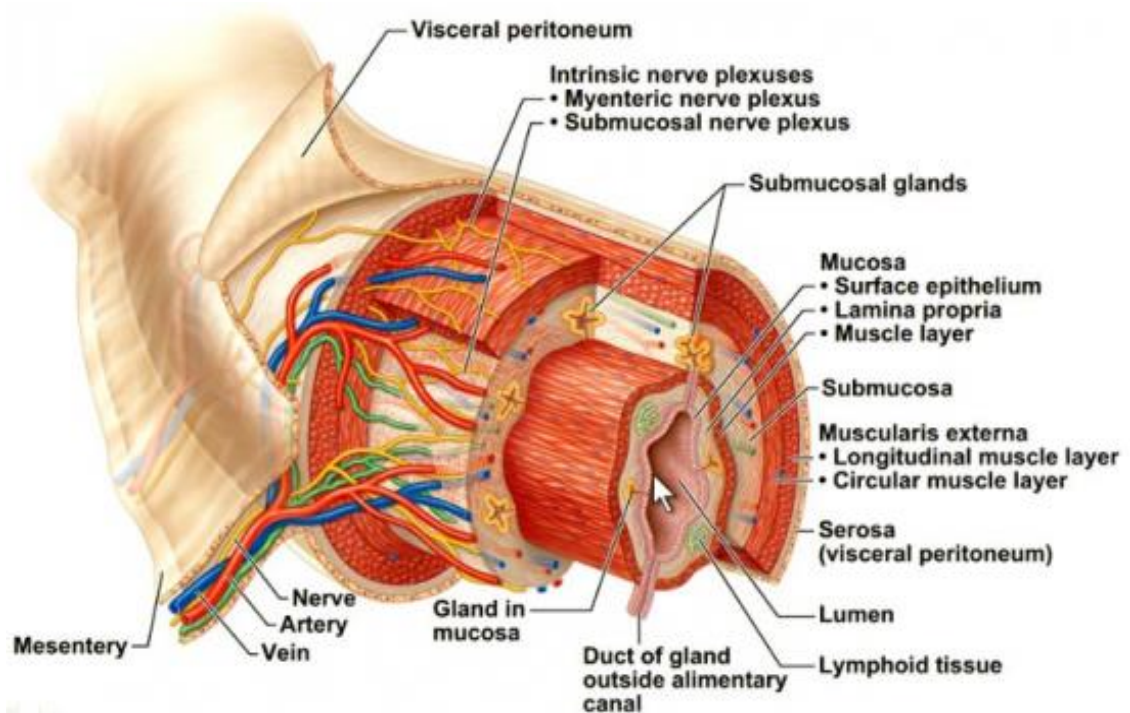


Figure 1.2. A cross section of the alimentary canal (Anatomy&Physiology, 2014).

The GIT is made up of the oesophagus, stomach and duodenum also known as the upper GIT and the small and large intestinal areas, also known as the lower GIT. The oesophagus is a 25 cm long muscular tube that runs from the laryngopharynx through the thorax and attaches to the stomach in the abdomen (Kopoor, 2016). When food is ingested into the mouth, it travels down the oesophagus down to the stomach by peristalsis under the control of the oesophageal sphincter which controls food emptying into the stomach (Peate, 2018).

In the stomach, the ingested food is mixed with water and digestive juice, producing a chyme, before being emptied into the small intestine through the pyloric sphincter. The food could be stored for about 1-2 hours during these processes as the intestine, pancreas, gallbladder and liver prepares to complete digestion. The size of the stomach

varies, but it can contain 1.5 litres of food and fluid on average (Mahadevan, 2017). In the stomach, food is being digested both mechanically and chemically. The mechanical digestion occurs due to the contraction of the smooth muscles of the stomach wall, leading to the mixing and breaking down of food boluses into smaller bits. Chemical digestion occurs while the food is being physically mixed with gastric juice (Innerbody, 2018, Peate, 2018). The enzymes in the gastric juice e.g. gastric lipase splits triglyceride fats into fatty acid and diglyceride while pepsin breaks down protein into amino acids.

Further digestion takes place in the small intestine, and it is at this stage that nutrients get absorbed into the blood stream. This long, highly convoluted tube absorbs 90% of nutrients from food and distribute them to the rest of the body. It is about 1 inch in diameter and about twice the length of the large intestine measuring up to 10 feet in length (Innerbody, 2018, Faiz et al., 2011). The first section of the small intestine is the duodenum and is approximately 10 inches in length, connecting to the pyloric sphincter of the stomach. In this part of the intestine, chime from the stomach is mixed with bile from the liver and pancreatic juice to complete digestion. Absorption of nutrients occurs at the jejunum, which is the mid-section of the small intestine (3 feet in length) (Faiz et al., 2011). The food travels into the ileum, the final section of the small intestine where absorption continues before being emptied into the large intestine through the ileocecal sphincter.

The colon or the large intestine is a long muscular tube (approximately 1.5 m) that connects the small intestine to the rectum. It is 7.6 cm in diameter and its primary function is to absorb water from wastes, creating a stool, which is stored until stimulated to empty when full. Nutrient absorption primary occurs in the small intestine although some could be absorbed in the colon as well (Faiz et al., 2011).

The colon (Figure 1.1) is made of the ascending colon, which lies vertically and occupies the lateral part of the abdominal cavity, occupying the right iliac fossa, right lumbar region and right hypochondrium (Kapoor, 2016). The colon takes a right-angled turn below the liver to form the transverse colon. This runs horizontally, occupying the right hypochondrium, epigastrium and left hypochondrium. The transverse colon also takes a right-angled turn to form the descending colon. This runs vertically and occupied the left hypochondrium, left lumbar region and left iliac fossa. The descending colon leads to the sigmoid colon, which becomes the rectum (Kapoor, 2016).

Several conditions could affect the colon, their treatment strategies depending on severity. Treatments may involve lifestyle/diet modification, use of medicine and in some cases, surgery. Some of the conditions of the colon includes:

a. Colonic polyps

Polyps are extra piece of tissues growing inside the body. Colonic polyps grow in the colon and are usually not dangerous but can also grow into cancer. They are usually asymptomatic but, in some cases, symptoms might include blood in the stool, bloodstains on underwear, constipation or diarrhoea lasting for weeks. Polyps are usually removed by surgical procedure and in most cases tested to determine if cancerous. Polyps are usually common with people over 50 years of age, people that have had it before and people with a family history of polyps or colon cancer (MedlinePlus, 2018).

b. Diverticulitis

This is the inflammation of the diverticula. They are small pouches that bulge outward through the colon. Common symptoms include abdominal pain, usually on the left side, fever, nausea, vomiting, chills, cramping and constipation. In serious cases, bleeding, tears or blockages could be experienced. The treatment of this condition could involve the use of antibiotics, pain relievers, the use of soft or liquid diet and surgical removal depending on severity. Diverticulitis was believed by Doctors to be because of low-fibre diet and is usually common with elderly people (MedlinePlus, 2018).

c. Ulcerative colitis

Ulcerative colitis (UC) is one of the diseases called inflammatory bowel disease (Fenoglio-Preiser and Ovid Technologies, 2008). It causes inflammation and sores (ulcer) in the lining of the colon and the rectum. This tends to run in families and the most common symptoms are pain in the abdomen and blood or pus in diarrhoea. Other symptoms include Anaemia, sever tiredness, weight loss, loss of appetite, bleeding from the rectum, sores on the skin, joint pain and growth failure in children. It could happen at any age and treatments could range from the use of drugs or the surgical removal of the colon (MedlinePlus, 2018).

d. Irritable bowel syndrome (IBS)

IBS is one of the problems of the colon, which results in abdominal cramping, bloating, and change in bowel habits, constipation and diarrhoea. As discomforting as this can be, it does not harm the intestine. It affects mostly women and the exact cause is unknown. This syndrome is usually managed with lifestyle/diet modification, stress management, probiotics and medicines (MedlinePlus, 2018).

e. Colorectal cancer

The colon and rectum are part of the large intestine as discussed earlier. Colorectal cancer occurs when a tumour grows in the lining of the large intestine. The symptoms includes diarrhoea or constipation, blood in the stool, weight loss, fatigue and nausea or vomiting (MedlinePlus, 2018). Colorectal cancer will be discussed in more details in the next section since its treatment and drug delivery method to this area was investigated in this research study.

1.1.1 Epidemiology of colorectal cancer

Colorectal cancer is usually associated with older people usually above 60 years (Miller et al., 2016). As of January 2016, it was estimate that there are more than 1.4 million men and women living in the US with a previous diagnosis of colorectal cancer and additional 134,490 cases yet to be diagnosed. Rectal cancer patients tend to be younger at diagnosis compared to colon cancer patients with average age of 63 and 70 respectively (Miller et al., 2016).

1.1.2 Stages of colorectal cancer

Colorectal cancer could be categorised into stages depending on progressing of the cancer, that is, whether they are still localised or spreading to other parts of the body. There are different ways of staging colorectal cancer which includes the TNM (tumour, node and metastasis), Number and Dukes' staging system.

a. TNM staging

This is a commonly used cancer-staging approach in the United Kingdom. The Tumour (T) describes the size of the tumour, which is an indication of the progression of the cancer cells and could be classified into 4 stages (T1, T2, T3 and T4) as shown in Figure 1.3. T1 indicates that the tumour is still small and is still in the inner layer of the colon wall while T2 indicates the growth of the tumour into the muscle layer of the colon wall. T3 indicates growth into the outside lining of the colon wall and T4 indicates that the tumour has grown through the outer lining of the colon wall into nearby organs or structures (CancerResearchUK, 2015c).

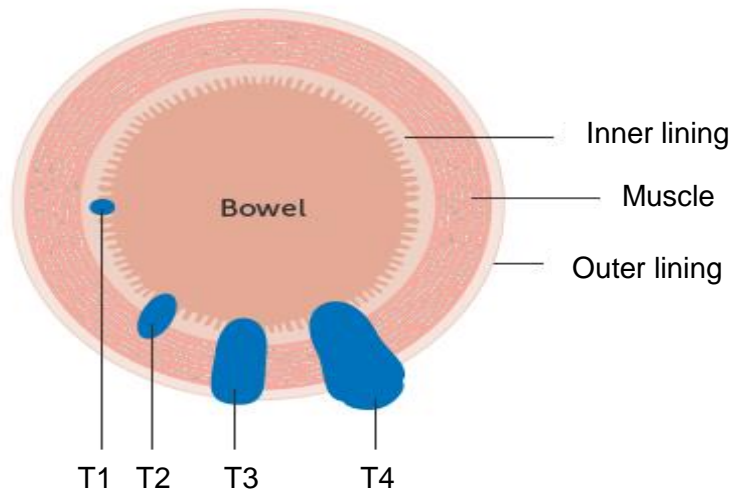


Figure 1.3. Different classifications of the Tumour (T) stage of the TNM staging system (CancerResearchUK, 2015c).

The Node (N) describes whether the lymph nodes have been affected and could be divided into 3 possible stages (N0, N1 and N2) (CancerResearchUK, 2015c). “N0” indicates that no lymph nodes have been affected by the cancer cells and therefore does not contain cancer cells. N1 indicates that 1 to 3 lymph nodes close to the colon has been affected and N2 means that 4 or more lymph nodes has been affected.

Metastasis (M) is used to describe whether the cancer has spread to different parts of the body. This has 2 possible outcomes (M0 and M1). M0 means that the cancer is still localised and has not spread to other organs and M1 means that other parts of the body have been affected by the cancer cells (CancerResearchUK, 2015c).

b. Dukes’ staging

Dukes’ staging system could be divided into Dukes’ A, B, C or D (Figure 1.4) (CancerResearchUK, 2015a). Dukes’ A indicates that the cancer is in the inner lining of the colon walls or is slightly progressing into the muscular layer. Dukes’ B indicates that the cancer has grown through the muscular layer of the colon while Dukes’ C means that at least 1 lymph node close to the colon has been affected. Duke’s D means that at this stage, the cancer cells has affected other parts of the body such as the liver, lungs or bones.

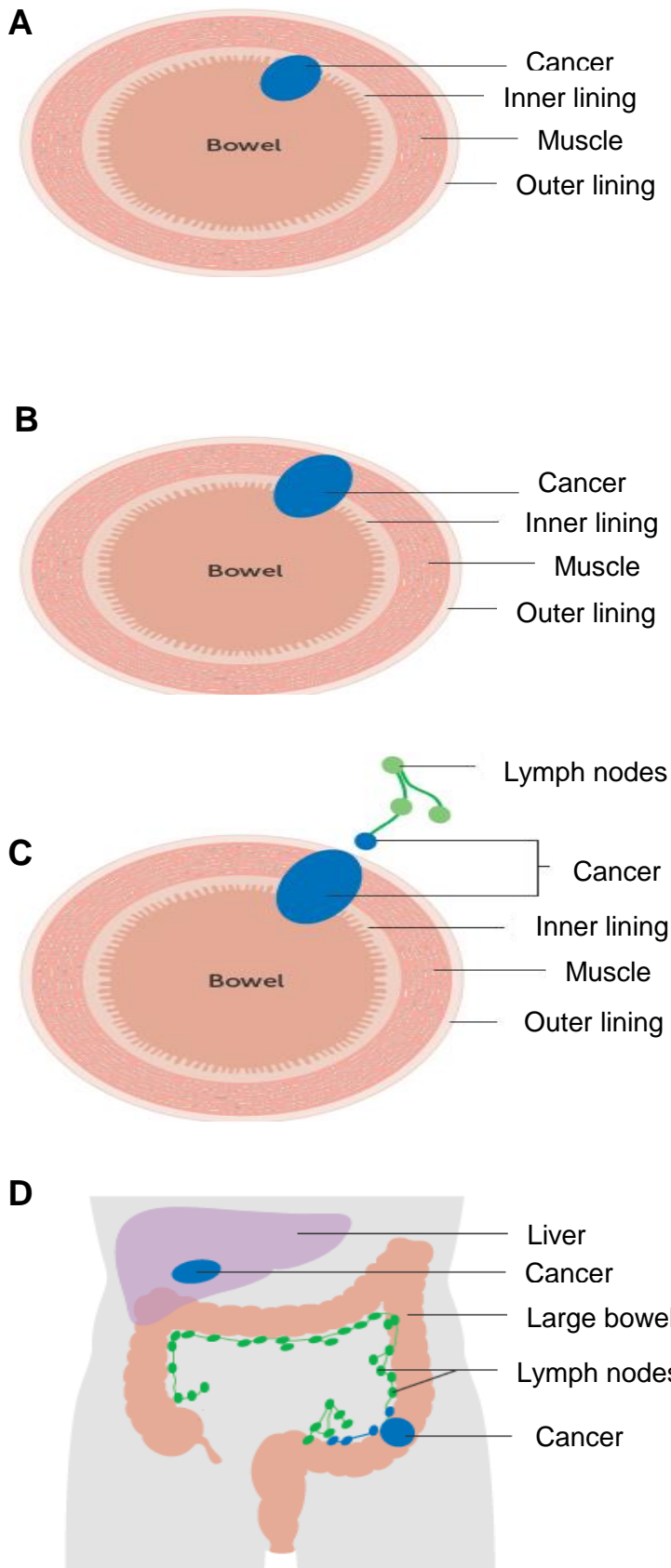


Figure 1.4. Dukes's method of colon cancer staging (CancerResearchUK, 2015a).

c. Number staging

Colorectal cancer under the number staging is classified as follows (CancerResearchUK, 2015b):

i. Stage 0 or carcinoma in situ: This is usually the early stages of colorectal cancer. There are cancer cells in the colon lining, but the risk of spreading is low at this point.

ii. Stage 1: This is equivalent to T1, N0, M0 or T2, N0, M0. The cancer cells have grown through the inner lining of the colon or has advanced into the muscular walls of the colon.

iii. Stage 2: This could be classified into 2A and 2B. At these stages, the cancer is still localised and has not spread into the lymph nodes. Stage 2A indicates the growth of the cancer cells into the outer lining of the colon and is equivalent to T3, N0 or M0 of the TNM staging system. On the other hand, Stage 2B indicates that the cancer cells have grown through the outer lining of the colon and advancing into nearby tissues or organs. This is equivalent to T4, N0 or M0 of the TNM staging system.

iv. Stage 3: This could be classified into 3A, 3B and 3C. Stage 3A indicates that the cancer cell is either still in the inner lining of the colon wall or has grown into the muscular layer. At this stage, 1 to 3 nearby lymph nodes may be affected and is equivalent to the T1, N1, M0 or T2, N1, M0 of the TNM staging system. Stage 3B indicates that the cancer cells have grown into the outer lining of the colon or into nearby organs and body tissues and 1 to 3 nearby lymph nodes may also contain cancer cells. Stage 3C indicates that the cancer could be any size but has affected 4 or more lymph nodes but however has not spread to any other part of the body. This is equivalent to Any T, N2, and M0 of the TNM staging systems.

v. Stage 4: This stage means that the cancer cells has spread to other parts of the body e.g. the liver, lungs or bones and it is the same as any T, any N, and M1 of the TNM staging system.

1.1.3 Treatment of colorectal cancer

Over the years, the treatment/management of colorectal cancer ranges from the use of chemotherapy, radiotherapy, surgery or a combined approach depending on the stage and the extent of proliferation of the cancer cells.

As estimated from a 2013 treatment pattern depending on the stage of the cancer, majority of patients (84 %) with a stage I and II colon cancer undergoes partial or full colectomy alone. Two-third of those with stage III cancer and some with the stage II

cancer receive chemotherapy alongside colectomy to reduce chances of reoccurrence (Figure 1.5A). Majority of people at stage IV undergoes colectomy and chemotherapy but, in some cases, only chemotherapy could be used depending on the extent of metastasis. For patients with rectal cancer at the stages I, II and III, proctectomy is usually done and depending on the extent of cancer growth, chemotherapy or radiotherapy could be used in combination (Figure 1.5B). Chemotherapy is the main treatment for stage IV rectal cancer patients.

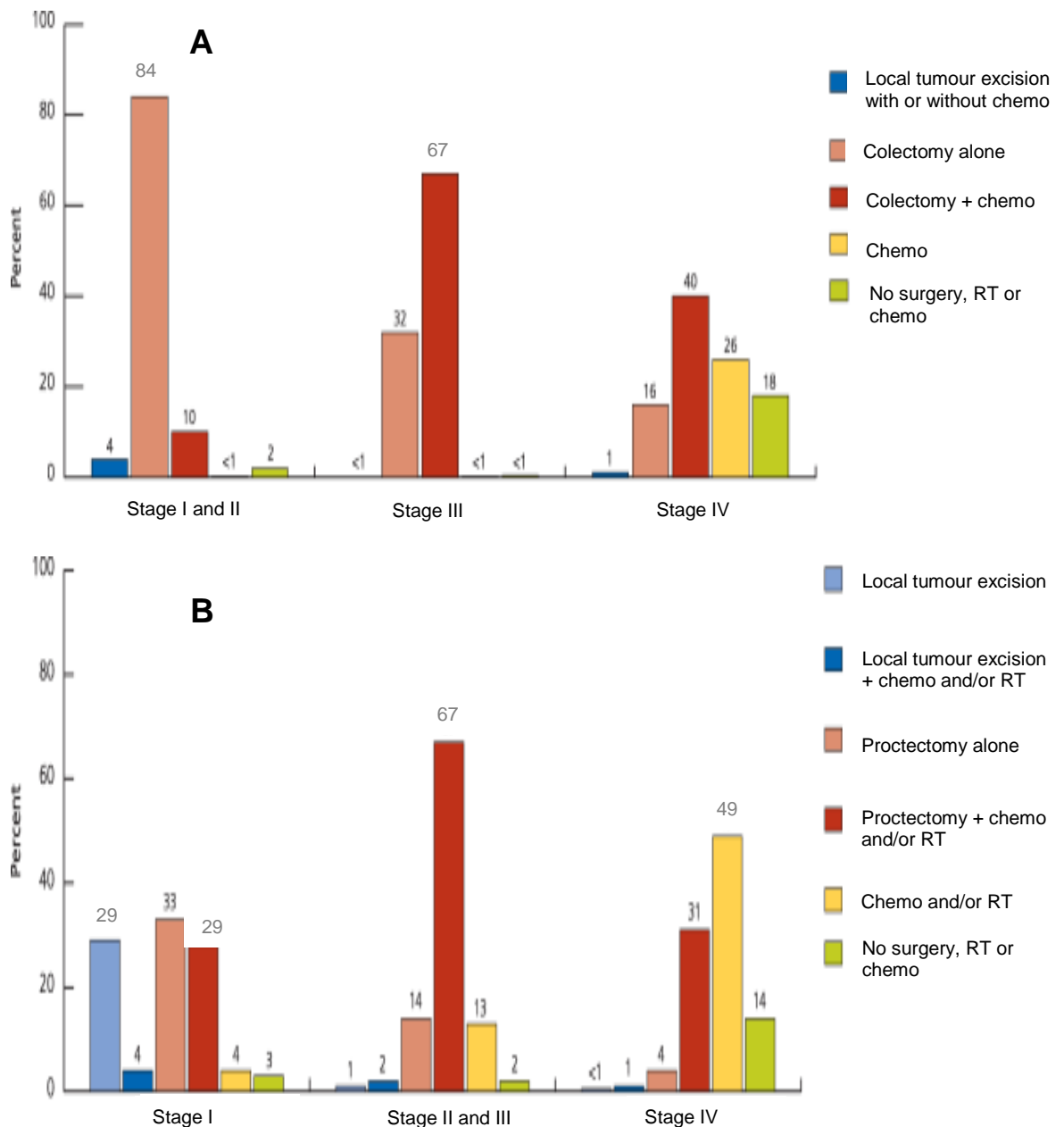


Figure 1.5. Treatment of (A) Colon and (B) Rectal cancer (Miller et al., 2016).

Commonly used drugs in the management of colorectal cancer includes fluorouracil, capecitabine, oxaliplatin and irinotecan. The sides effects of chemotherapy and radiotherapy has been the downside of the conventional approaches to colorectal cancer and the treatment of other forms of cancer. Side effects from therapy could include diarrhoea, increased risk of infection, sore mouth, sickness, hair loss and even toxicity to normal cells etc. As a result, there are many ongoing investigations on alternative cancer therapies, including the potential activities of antimicrobial peptides (AMPs) against cancer cells. This will be discussed in more details in Chapter 4 (Section 2).

1.3 Oral drug delivery

Oral drug delivery remains the dominant delivery route for most drugs, targeting various therapeutic areas. The importance of oral drug delivery manifested in a 2013 report about drug delivery technology market as it comprises 40 % of all drug delivery routes (Marketsandmarkets, 2013). It was also expected in 2010 that oral drug delivery market values will rise from \$49 billion to \$97 billion by 2017 (GBIResearch, 2012). It is the route of choice for majority of patients as it is relatively safe, convenient, affordable and easy to use. Commonly used oral dosage forms includes liquids (solutions, suspensions and emulsions) or solids (tablets and capsules).

1.3.1 Oral Liquid dosage forms

Liquids dosage forms includes solutions, suspensions and emulsions. Their use has the advantage of an early onset of action when compared to tablets due to ease of processing and absorption into the body. Dose alteration is easy using dosing aids. Despite the advantages of liquid dosage forms, they lack efficiency especially when large doses are required, and some drugs cannot be manufactured as liquids due to poor solubility of many actives. Their preparation in the form of suspensions could bring about physical, chemical and microbiological stability challenges particularly during storage. Drugs in their solid state also normally have a longer half-life (Pamudji et al., 2014), making liquids less suitable for long term storage since liquids support the growth of microorganisms. In addition, manufacturing liquid dosage forms is capital-intensive, and products are usually significantly heavier which increases the delivery and storage costs.

1.3.2 Oral solid dosage forms

Oral solid dosage forms are usually manufactured as tablets or capsules depending on the manufacturer's preferences, properties of the actives and excipients or the desired release profile.

a. Tablets

Tablets are solid oral dosage forms usually manufactured by the compression of granulated excipients and actives (Ervasti et al., 2015). This has been the method for tablet manufacturing until the discovery of the potential application of 3D for dose personalisation.

The use of tablets like most orally administered dosage forms is safe and easy to administer and has been used for decades to deliver several actives especially those that could not be formulated as liquids. Taste masking is easier using tablets and early onset of action is obtainable depending on the properties of the actives and excipients. On the other hand, friability could be one of the potential problems of tablets manufacturing. In addition, swallowing these dosage forms could be difficult for infants and adults with swallowing difficulties.

Depending on the desired release profile, release-modifying excipients could be used during the tablet formulations to modify drug release. In some cases, another stage of functional coating is utilised to either offer protection or modify drug release depending on the coating material used.

a.1 Tablet Coating

Coating is a well-established pharmaceutical technique and is one of the oldest pharmaceutical processes still in existence. It involves applying a dry outer layer of the coating material to the surface of a dosage form to offer certain advantages over uncoated dosage forms. Sugar or polymeric materials are usually used for coating and has been used for different purposes; improve the aesthetic appeal of a substrate, mask undesirable odour, colour or the taste of a bitter active/excipient, which improves patient's compliance. It could also be used to protect the dosage form from the harsh condition of the stomach or vice versa (Haastrup et al., 2015), improve the mechanical strength of dosage forms and determine areas of drug release along the GIT (Macchi et al., 2015).

i. Sugar coating

The sugar coating of tablets pioneered the development of coating. It involves the use of sugar to mask the taste of a dosage form and provide an attractive appearance (Ando et al., 2007, Ohmori et al., 2004). Tablet coating using this approach involves several steps, which is one of its downsides. Before sugar coating takes place, tablets are first sealed to protect the tablet core from moisture. Afterwards, a sub coat is applied to round their edges to allow for easy distribution of the coating material. The tablets are then covered

with the syrup coating to cover imperfections and achieve the desired tablet weight before being coloured, dried and polished. The time-consuming nature of this process led to its replacement with film coating in addition to the ability to use film coating to modify drug release.

ii. Film coating

This involved covering the dosage form with a layer(s) of polymeric material. The type of polymer used depends on the required area of drug release or required drug release profile. Functional film coating is applied to modify the release of the original uncoated tablet to achieve a delayed drug release or extend the release of active from a dosage form. This could be achieved using polymers with certain properties as will be discussed in more details in Section 1.4. On the other hand, non-functional film coating involves the use of coating materials based on factors that affect mechanical properties of the coating. The primary aim of this coating is to improve the physical appearance of the dosage form, allow for a smooth and glossy finish, and readily dissolve in the GIT.

a.2 Coating technologies/techniques

i. Pan Coating

A standard coating pan is a circular metal pan usually mounted at about 40 ° to the horizontal. The pan rotates on its horizontal axis to mix the coated tablets and the coating dispersion is supplied by ladling or spraying, usually fitted with atomiser to produce even distribution of the coating material (Kneidl et al., 2014). It also has a hot air inlet for the drying of the tablets and an exhaust for heat circulation. The drawbacks of this technology include poor mixing efficiency of the tablets and poor drying efficiency that led to the development of the perforated coating pan. It is fully perforated as the name suggests and contains a mixing blade that encouraged easy mixing of tablets, even distribution of the sprayed material and makes drying more efficient (Figure 1.6A).

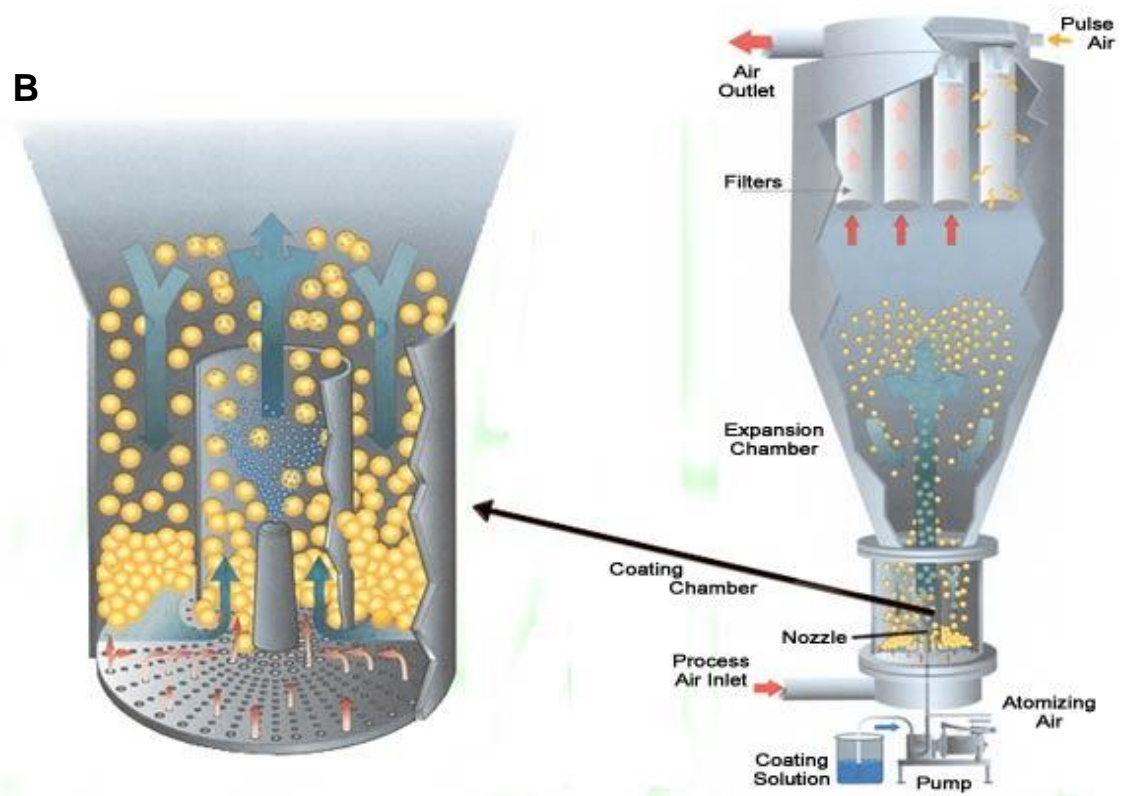
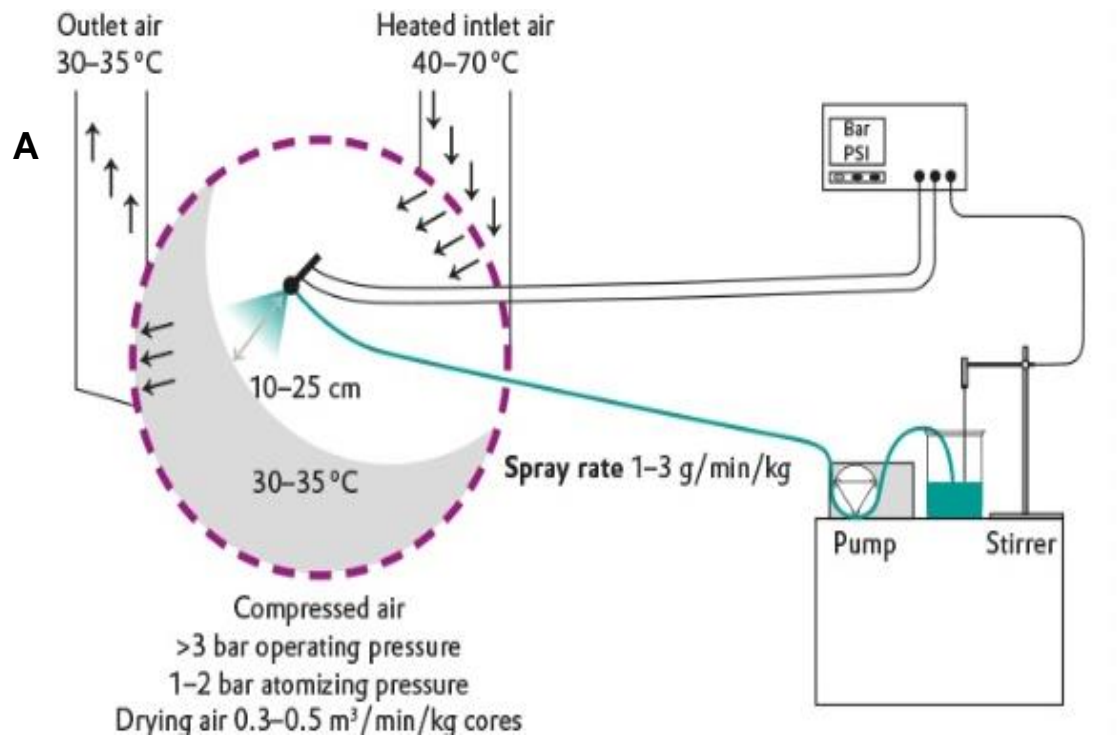


Figure 1.6. Perforated coating pan (Evonik, 2018) (A) fluid bed coater (Microencapsulation.net, 2018) (B).

ii. Fluid bed coating

The fluidised bed coater achieves fast and uniform coating using air to mix, dry and coat the substrates. This technique originated from the fluidised bed dryer used in wet powder/granule drying. The air inlet comes from the bottom, blowing the substrates up and at the same time, the coating material is sprayed onto them (Figure 1.6B).

Depending on the position of the spray nozzle, a fluidised bed coater can be classified into top spray, bottom spray and tangential spray with their advantage and disadvantages. This technique, however, was less popular due to its mechanical stress on tablets, leading to a compromised physical appearance.

iii. Compression coating

This coating approach involves the compression of the coating material around the tablet core using a conventional tablet compression machine. This is commonly used when the shell material has poor film forming properties. It involves an initial filling of the die with a layer of the coating material before placing the core tablet in the middle of this material. As the lower die moves down, more coating material fills the die surrounding the core before compression and ejection. It has the advantage of being short manufacturing process by avoiding the use of solvents, which requires drying afterward like in liquid coatings (Bose and Bogner, 2007). These aqueous or organic based polymer solutions when used could result to residual solvents in the product, which might be hazardous when not removed efficiently.

A floating tablet for the time-controlled release of an active has been produced using this coating technique, which proved to be effective. Hydroxypropyl cellulose (HPC) was combined with sodium bicarbonate (effervescent agent) to produce a dosage form that becomes buoyant over a period of 12 hours and provide a zero order drug release (Qi et al., 2015). Zero order drug release has also be achieved using only HPC to coat by compression, a glipizide core tablet (Huang et al., 2013). Colonic drug release has also be achieved using this method by coating the tablets with colon targeting polymers (Vemula, 2015a, Pachuau and Mazumder, 2013, Sinha et al., 2007b). In a study by Vemula (2015b), a double compression coated tablet using hydroxypropyl methylcellulose (HPMC) and Eudragit S100 was use to achieve a pulsatile drug release. A compression coated indomethacin tablet with polyethylene oxide was used to produce a dosage form that follows the circadian rhythms, with potential application in the treatment of rheumatoid arthritis (Songa et al., 2013). This seemed effective both *in vitro* and *in vivo*.

iv. Dry coating

This coating process is also called powder coating and involves coating of tablets with polymer powder followed by a curing process. In some processes, the powder layer is sprayed simultaneously with a plasticiser to reduce curing temperature especially for thermolabile actives. This approach was called plasticiser-dry-coating and could be achieved using pan coaters or a fluidised bed coater (Obara et al., 1999, Luo et al., 2008) which allows for the even coating of the substrates with the powder and also provides a means to spray the plasticiser. In a study by Obara et al. (1999), this technique was used to enteric coat, using hydroxypropyl methylcellulose acetate which demonstrated reasonable gastric resistance. Adhesion of the powder materials on the substrates depends on the wetting of the dosage form surface as well as the coating powders, which results in film formation with heat. Film formation could be attributed to the capillary force from the liquid plasticiser before uptake into the polymer particles which results in particle deformation (Kablitz and Urbanetz, 2007).

Another approach of dry coating involves electrostatic coating of the substrates with powder material. The powder materials become electrostatically charged when propelled from a spray gun and adheres to the earthed substrate surface to form the film layer. This was called electrostatic-dry-coating (Luo et al., 2008) and could also be used in combination with plasticiser spraying to encourage better film formation (Qiao et al., 2013, Qiao et al., 2010b, Qiao et al., 2010a)

A heat-dry-coating method has also been investigated for dry coating. The process makes use of a source of heat, which partially melts the coating powder and encourages adhesion to the substrate. This coating technique was developed by Cerea et al. (2004) and involves the use of low T_g polymers to obviate the need for plasticisers.

In a research Yang et al. (2015), the substrates were first loaded into a preheated coating pan before simultaneously spraying the plasticiser and the electrostatically charged powder to the substrates, demonstrating a combined use of different approaches. Different polymers were investigated and used to achieve different drug release patterns (Yang et al., 2015).

vi. Melt coating

This provides an alternative to the application of polymeric solutions or dispersions. It involves the use of coating materials that could be applied molten. The use of this offers the advantage of shorter processing time since the drying process of coating is reduced. The solvent free approach reduces cost and the possibility of microbial contamination

(Jannin and Cuppok, 2013). On the other hand, high temperature is used during the process and it is important to maintain the temperature of the molten polymer above the melting point during the process to ensure adequate flow and delivery to the spray nozzles and avoid blockage.

The use of a spray system was entirely avoided in a research using a conventional coating pan Sakarkar et al. (2013). Pellets with adequate surface morphology and texture was produced and release modification was achieved (Sakarkar et al., 2013, Griffin and Niebergall, 1999). This technique has also been used in combination with other forms of coating (film coating using fluidised bed) to produce a sustained-release pellet (Yang et al., 2008). In a study by Patil Arun (2011), this approach was used to mask the taste of bromhexine hydrochloride by spraying a molten wax on the pellets in a heated coating pan at a coating level above 3 %w/w.

b. Capsules

Capsules remain one of the most acceptable oral drug delivery systems, which allows for the delivery of actives in different forms. Powders, pellets, liquids and even tablets could be delivered using capsules, which breaks up in the GIT to release its content.

Capsules are commonly made from gelatine but could also be casted using HPC (Macchi et al., 2015), plant polysaccharides, carrageenan and modified forms of starch and cellulose which are water soluble and readily disintegrated in the stomach to release its content. Capsules come in different sizes, their use depending on the quantity of the content/actives to be delivered.

Capsule shells are made of physiologically inert materials, easily digested in the GIT and requires less adjuvants when compare to tablets. The use of capsules has the advantage of easy taste and odour masking. This plays a major role in its increased acceptance by patient. In addition, capsules become slippery when moist, which facilitates swallowing. They withstand handling and transportation and could be coated with polymers to target different areas of the GIT (Macchi et al., 2015) or opacified with titanium dioxide or colours to offer light protection to photosensitive actives.

1.4 Drug release patterns from oral drug delivery

Oral drug delivery could be engineered to possess different release patterns, which determines area of drug release. This could be classified into immediate and modified drug release.

1.4.1 Immediate release

According to the British Pharmacopeia, a solid dosage form is immediate release if ≥ 75 % of the active is released before 45 min in an *in vitro* release study. This implies a fast onset of action and is usually the release pattern obtained when using liquid dosage forms. To achieve this fast release using solid dosage forms, most manufacturers make use of highly soluble excipients. Excipients that aid to break down the tablet into smaller particles once in contact with the body fluid (disintegrants) are often added. This increases the surface area available for dissolution and drug release. For capsules, the soluble shell dissolves once in contact with body fluid to release its content.

Immediate release dosage forms are used when therapeutic activity is required as soon as possible. In a situation where the actives are poorly soluble in water, solubility enhancing polymers could be employed during the formulation to ensure dissolution after disintegration (Pietrzak et al., 2015, Okwuosa et al., 2016). Immediate release polymers are shown in Table 1.1.

1.4.2 Modified release

Modified release dosage forms are used to classify dosage forms that are not immediate release. This includes delayed drug release (enteric, colonic, pulsatile and bimodal drug release systems), prolonged drug release over a period (extended release) and site-specific targeting (targeted-release dosage forms). These release modifications are achieved using polymers with different properties as shown in Table 1.1.

a. Delayed drug release (DDR)

This release modification involves the application of a polymer barrier on an oral medication, therefore creating a lag time between administration and therapeutic effect. This system usually responds to increased pH that occurs at the lower end of the GIT, which allows the dissolution of the used polymer and therefore drug release (Varum et al., 2014, Fang et al., 2014, Okwuosa et al., 2017).

Enteric coating is a form of a DDR system which is done either to protect the drug from the acidic environment of the stomach or to protect the stomach walls from the harmful

effects of the drug. According to the British pharmacopoeia, a dosage form is enteric if $\leq 10\%$ of the active is released in an acidic environment (pH 1.2) after two hrs, followed by $\geq 85\%$ release in a basic media (pH 6.8) before 30 min.

Colonic drug deliveries are desirable for actives that are absorbed in that area of the GIT or to achieve a localised treatment for diseases like inflammatory bowel disease and colon cancer. The colon has also been recognised as the gateway to the systemic circulation and has been hypothesised to enhance the oral bioavailability of peptides, proteins, nucleic acid and oligonucleotides (Maroni et al., 2010). Polymers that dissolve at high pH values in comparison to those used for enteric release comes into play here since pH increases down the GIT although it has been shown to vary. The use of polymers to target the lower GIT has been well established with a wide variety of polymers engineered to dissolve at $\text{pH} \geq 5$ (Table 1.1) thereby inhibiting release in the gastric fluid, followed by polymer dissolution and drug release at higher pH values.

b. Extended drug release (XDR)

This is used to achieve a prolonged drug release in contrast to an immediate release dosage form. This release pattern maintains the level of the actives in the systemic circulation over a prolonged time and therefore reduces dose administration frequency, which improves patient compliance. Tablets could be produced in the form of a drug polymer matrix where the polymer slows down or controls the rate of drug release (Oliveira et al., 2013, Li et al., 2014). A popular technique for polymer-drug matrix formation is HME. An extended drug release could also be achieved using an osmotic system. In this technique, the tablet is placed in a semi-permeable outer membrane with one or more laser-drilled holes. Water is absorbed through the semi-permeable membrane which creates an osmotic pressure that forces the active(s) out through the holes in the tablet (e.g. OROS by ALZA Corporation) (Stevens et al., 1998). Another technique for XDR involves the use of floating systems where dosage forms are designed to be buoyant which avoids gastric emptying thereby prolonging drug release (Radwan et al., 2015, Ijaz et al., 2015).

c. Targeted drug release (TDR)

This drug delivery approach is used to achieve a site-specific delivery of active pharmaceutical ingredients (APIs). It could be done actively by modifying the surface of the carrier to have affinity for certain areas of the body or cells using bio adhesives, non-ionic surfactants, specific cells, tissue antibodies or protein. Micro- and nano-particles are used effectively in this regard, as well as carrier vesicles. The incorporation of

anisamide ligand to a doxorubicin-loaded liposome had more affinity for prostate cancer cell lines due to its overexpressed sigma receptors (Banerjee et al., 2004). In another report, oestrone ligand was used to target oestrogen receptors of breast carcinoma cells (Paliwal et al., 2010) and many other applications (Li et al., 2009, Hong et al., 2009).

A passive drug targeting relies on the circulation time of the drug carrier. This approach modifies the drug carrier to avoid phagocytosis and therefore removal by the reticuloendothelial system (RES), which enables circulation for a longer time. Polyethylene glycol has been used to render liposomes more hydrophilic which reduces rate of removal by the hydrophobic RES (Gabizon and Papahadjopoulos, 1988, Allen et al., 1991, Gabizon et al., 1994).

Targeting could also be achieved physically. This type of targeting depends on environmental changes like temperature and pH because of the pathological area in comparison to the normal tissues. For example, inflamed or neoplastic areas normally demonstrate some level of hypothermia and acidosis which could be used as an advantage in drug targeting (Torchilin, 2000). A pH sensitive liposome has been used to enhance skin penetration of both hydrophilic and hydrophobic compounds (Tokudome et al., 2015) and the potentials of thermos-sensitive liposomes has been demonstrated (Kneidl et al., 2014). This similar approach finds use in the delivery of actives using pH sensitive polymers for enteric and colon targeting as will be discussed in Chapter 4.

Table 1.1. Examples of polymers employed in dosage form manufacturing and their applications.

| Immediate release polymers | Delayed release Polymer | | Extended release polymers |
|---|---|----------------------------|---|
| Eudragit EPO (Sadia et al., 2016) | Polyvinyl acetate phthalate (Zaid, 2012) | Dissolves at pH \geq 5.0 | Eudragit RL 100 (Roy et al., 2013) |
| Eudragit E 100 (Mansing G. Patil, 2011) | Eudragit L 30 D-55 (Nair et al., 2010) | Dissolves at pH \geq 5.5 | Eudragit RL PO (Sahoo et al., 2009) |
| Eudragit E 12,5 (Evonik, 2010) | Eudragit L 100-55 (A et al., 2013) | | Eudragit RS 100 (Tiwari et al., 2014) |
| Polyvinyl pyrrolidone (Kim et al., 2016) | Cellulose acetate trimellitate (Giunchedi et al., 1995) | | Eudragit RS PO (Roni et al., 2009) |
| Polyethylene glycol (Blaesi and Saka, 2015) | Hydroxypropyl methylcellulose phthalate (Bendas and Abdelbary, 2014, Sharma et al., 2013) | | Ethocel premium ethylcellulose (Colorcon, 2018) |
| Hydroxypropyl cellulose (Mohammed et al., 2012) | Eudragit L100 (Wilson et al., 2013) | Dissolves above pH 6.0 | Methocel premium cellulose ethers CR (Colorcon, 2018) |
| Polyvinyl alcohol (De Jaeghere et al., 2015) | Eudragit L 12,5 (Evonik, 2010) | | Polyox water soluble resins (Colorcon, 2018) |
| | Hydroxypropyl methylcellulose acetate succinate (Jansen et al., 1998, Hilton and Deasy, 1993) | | Poly (caprolactone) (Kamaly et al., 2016) |
| | Cellulose acetate phthalate (Kotagale et al., 2010) | | Chitosan (Kamaly et al., 2016) |
| | Eudragit S 100 (Sun et al., 2014) | Dissolves above pH 7.0 | Poly (lactic acid) (Kamaly et al., 2016) |
| | Eudragit S 12,5 (Evonik, 2010) | | Poly (glycolic acid) (Kamaly et al., 2016) |
| | Eudragit FS 30 D (Huyghebaert et al., 2004) | | Poly (lactic-co-glycolic acid) (Kamaly et al., 2016) |

1.5 Physiological changes along the GIT that affects oral delivery systems

Drug release and absorption of oral dosage forms is strongly influenced by various factors that differ along the GIT. This includes enzymatic activities, pH values along the GIT, transit time and microbial activities. Some of these physiological changes also differ fasted or fed, therefore thorough comprehension of the GI conditions is necessary to understand the *in vivo* release and absorption of oral dosage forms.

1.5.1 pH changes across the GIT

Understanding the intraluminal pH values are highly relevant owing to the pH dependent behaviour of many actives and excipients commonly used in pharmaceutical industries. These pH changes sometimes become a challenge in drug delivery, as some actives might be sensitive to certain pH levels. The modified release properties of a dosage form could also be affected by these pH changes (Wonnemann et al., 2008). On the other hand, these pH changes could also be used to an advantage for site-specific delivery of actives utilising pH sensitive polymers.

The pH of the stomach is reported to be between pH 1-3 (Evans et al., 1988) but has also been reported to vary between pH 1-8 in a fasted state (Koziolek et al., 2015). However, the stomach is acidic in most cases because of the secretion of hydrochloric acid (HCl). pH values of the stomach become higher after being fed depending on the composition and quantity of the ingested content. The stomach buffers this increase by secreting more HCl and gastric emptying, the rate of buffering depending on the content and quantity of the ingested material.

In the intestine, there is usually an increase in pH value from pH 6.0 ± 0.2 in the duodenum to 7.7 ± 0.15 in the terminal ileum (Koziolek et al., 2015). This is usually because of the duodenal secretion of alkaline bicarbonates. The pH in the colon tends to be slightly more acidic as a result of the fermentation processes of the colon microbiota with an average pH value of 6.5 ± 0.3 (Koziolek et al., 2015).

1.5.2 Transit time

Orally administered dosage forms must travel down the GIT, get broken down and the actives released and absorbed to achieve its therapeutic effect. Therefore, understanding the factors that affect the transit time of dosage form to their site of action is important and is beneficial in use recommendations. The transit of oral dosage forms in the GIT relies on the gut motility and flow, which depends on the type of dosage form

and the type and timing of meals ingested. Because of these factors, the time spent by the dosage form in the stomach varies.

Oral dosage forms can come in different shapes and sizes and can be categorised into multiple unit or single unit devices (Bechgaard and Nielsen, 1978). The single unit devices stay intact and does not disintegrate throughout the GIT. These influence the time these dosage forms spend in the stomach area before being emptied, the size of the dosage form playing a major role.

In a fasted state (at least 8 hours without food ingestion prior to administration) the gastric emptying of oral dosage form ranges between 1 min – 185 min (Weitschies et al., 2010). In the absence of food, unless large single dosage forms are administered, the transit of dosage forms depends solely on myoelectric cycle or MMC. The primary job of the MCC is to move and empty left overs from a previous meal and occurs in four phases (Wilding et al., 2001):

Phase 1 - 60 min quiescence with no contraction.

Phase 2 - 40 min of intermittent contraction and action potentials.

Phase 3 - “House keeper waves” which completely empties the stomach and involves an intense distal and proximal gastric contractions lasting between 5 -15 min.

Phase 4 - Transition from Phase 3 to phase 1.

These cycles could take up to two hours and the ingestion of food resets the cycles with a normal meal disrupting the MMC for approximately 3-4 hours (Wilding et al., 2001). Pellets and powders tend to empty fast when administered fasted, with a shot lag phase with or after a light meal (1000-2000 KJ) (Wilding et al., 2001).

The presence of food delays the emptying of oral dosage forms as the stomach stores and attempts to break down the food into chyme before emptying into the proximal small intestine. During this process, liquids and small particles could pass through the partially constricted pylorus while the large units are retained in the stomach. The emptying of pellets from the stomach tends to be faster when compared to tablets in the presence of food. The reverse is however the case in the intestine as pellets get caught into the rough surface of the intestine due to their smaller size (Abrahamsson et al., 1996), which delays transit.

1.5.3 Gut Microbiota

A high level of bacterial activity has been observed in the distal part of the intestine compared to the rest of the GIT. The gut harbours a complex community of microorganisms (up to 100 trillion) which influences human physiology and metabolism (Enright et al., 2016). They also contribute to the low pH value obtained in the colon in comparison to the rest of the intestine. It could be argued that since most drug absorption takes place in the small intestine before reaching the colon, then the impact of the high level of microbiota in the colon should not be put into consideration. However, new insight into the small intestinal microbiota have revealed high microbial activity as well (El Aidy et al., 2015). Moreover, newly developed drug candidates tend to have low solubility or permeability, which prolongs residence time in the GIT and therefore, high probability of microbial interaction in the distal areas of the GIT.

The intestinal microbiota has been associated with several pharmacokinetic activities. They could mediate a prodrug activation which could be used to an advantage in drug targeting (Enright et al., 2016). They have also been implicated in the alteration of the absorption of certain actives e.g. probiotic bacterium, *Escherichia coli* (Nissle 1917) improved the bioavailability of amiodarone, a class III antiarrhythmic, in rats (Matuskova et al., 2014). It was believed to reduce intestinal pH and enhance ionisation of the molecules and therefore easy mucosal transit.

1.6 Pharmacogenomics and individualised drug therapy

Pharmacogenomics, which could be used interchangeably with pharmacogenetics, is a term used to describe the relationship between drug responses and genetic variations. As research and development continues to grow as well as the knowledge about pharmacogenomics, there is an increasing interest to apply them in the drug discovery and approval processes (Mooney, 2015). It was observed that patients present large interindividual differences in drug response and toxicity with most major classes of drug when administered at a standard dose. No response from a medication could be observed in some patients, partial response in others and adverse drug reactions in others. These were linked to genetic variations, which influences the pharmacodynamics and pharmacokinetics of the individual patients. Variations in dose responses could also be due to physiological or pathophysiological differences. However, in some classes of drug, genetic factors could account for up to 95 % of interindividual variations (Eichelbaum et al., 2006).

The idea that genetic factors could alter patient's response to medications evolved in the 1950s. It was observed that the inherent lack of glucose-6-phosphate dehydrogenase led to haemolytic anaemia when patients were exposed to the antimalarial drug, primaquine (Beutler, 1969). Severe adverse drug reactions (ADRs) (e.g. hepatotoxicity and drug-induced arrhythmias) becomes challenging in drug discovery and development and could be linked to several hospitalisations and deaths (Lazarou et al., 1998). Therefore, the knowledge about the roles of genetic factors will not only improve patient's outcome from drug use but also reduce ADRs drastically. This led to the term personalised medicine, which focusses on tailoring therapy towards patients need to obtain the best response and highest safety margin.

Personalised medicine allows physicians to go beyond the use of the "One Size Fits All" standard dosing approach to a more patient specific approach (Ginsburg and Willard, 2009). This is known as personalised dosing and was defined by FDA as providing "the right patient with the right drug at the right dose at the right time" (FDA, 2013). As a result of this, the demand for a unique medical approach for every individual is on the rise with more emphasis on a patient specific or tailored method of dosing and dose combinations rather than conventional mass produced dosage forms (Rajjada et al., 2013, Vogenberg et al., 2010).

In addition to dose personalisation in response to genetic variations, there is also an increased necessity to tailor doses for children, disabled patients, in geriatrics and in some certain disease conditions. The lack of personalisation has been linked to the major causes of drug adverse effects which was realised to be worse in geriatric medicines due to the number of drugs they use on a daily basis (Davies et al., 2009).

Since dose personalisation requires customising healthcare individually, the big question is "how these unique medicines for each patient can be made on a routine basis?" The manufacturing processes involved in the production of conventional oral solid dosage forms were not suitable for the degree of flexibility required. Several critical steps (e.g. mixing, granulation, drying, sieving etc.) are usually involved which makes flexibility a problem during manufacturing.

1.7.1 Current approaches to dose personalisation

To improve drug use efficiency and minimise adverse effects in drug use, several approaches have been used to achieve dose personalisation.

a. Dose personalisation using oral liquid dosage forms

Liquids are the dosage form of choice for infants, toddlers and children due to the ease of modifying the dose in addition to overcoming swallowing difficulties with solid dosage forms. Liquids are also available for adult use especially in geriatrics where swallowing difficulties commonly exist (Rosemond, 2015). In addition, where no suitable licensed liquid dosage forms are available, prescribers may need to order liquids from “Specials” manufacturers to meet the need of these patients (Schiele et al., 2013).

For decades, the use of liquid dosage forms for patient medication encouraged dose personalisation. This can be easily achieved by altering the administered volumes using various dosing aids usually included as part of the packaging of the dosage form (Brown et al., 2004). Commonly used dosing aids includes disposable medication measuring cups, plastic medicine spoons, oral syringes, Pasteur pipettes, medicine dropper, all used in different situations with the primary aim of improving dosing accuracy. However, inaccuracies in dosing could result from irregularities in the measurements from the dosing aids (Grießmann et al., 2007, Yin et al., 2010) or from the patient or carers incompetence (McMahon et al., 1997).

b. Dose personalisation using oral Solid dosage forms

Dose personalisation using solid dosage forms has been achieved by dispensing multiples of a small dose, splitting of tablets to obtain smaller doses or a combination of both approaches in some cases. However, the physical alteration of solid dosage forms could affect drug release especially for modified/controlled release formulations (Hill et al., 2009, Shah et al., 1987, Erramouspe and Jarvi, 1997). Coated tablets will be affected, as the function of the coating will be lost. In the United States, it was estimated that 3000 compounding pharmacies formulate approximately 30 million prescriptions per year in an attempt to customise drugs to individual patients (WeillCornellMedicalCollege, 2014). The majority of these prescriptions have been linked to the lack of commercially available dose or drug combinations.

c. Dose personalisation by inkjet printing

Another approach to personalized medication involves the use of inkjet printers. This idea originated from the same technique used in computer-operated inkjet printing which

recreates digital images by propelling ink droplets onto paper in a 2D format. It was adapted for pharmaceutical application by the replacement of the ink with pharmaceutical solutions containing drugs and normal paper with edible sheets known as substrates (Scoutaris et al., 2011, Meléndez et al., 2008). A list of the possible substrates that could be used in ink jet printing has been compiled in a review by Alomari et al. (2014). Manipulating the dose in inkjet printing could be achieved by changing the number of printed layers for a given area or by increasing the total printed area. The advancements in inkjet printing were based on the potential to print designed ratios of drugs and excipients as individual microdots onto an edible substrate. Two main inkjet dispensing systems have been investigated for pharmaceutical applications: thermal (Buanz et al., 2011, Meléndez et al., 2008) or piezoelectric inkjet printers (Boehm et al., 2015, Lee et al., 2012, Lorber et al., 2014, Uddin et al., 2015).

Inkjet drug printing offers a significant advantage of accurate control of dose combination and pattern of drug release. It has demonstrated that deviations as low as 1.4 % relative standard deviation can be achieved when 1 cm² is printed with about 52 µg of the model drug (Raijada et al., 2013). This however, is influenced by the nature of the substrate or printing technology (Buanz et al., 2011, Sandler et al., 2011).

Ink jet printing requires the starting materials to possess certain characteristics mainly; particle size needs to be <1 µm to avoid clogging the printer head, viscosity needs to be <20 cP and surface tension between 30-70 mN/m for efficient flow (Lee et al., 2012, Sandler et al., 2011). Ink jet printing is thus highly suitable for manufacturing drugs with low therapeutic doses, ideally in the microgram range, when printing a smaller area on the substrate is needed. Obtaining higher doses will otherwise imply numerous printings on a particular area, which could lead to longer drying time and potential instabilities. A large surface area could be covered for larger doses, but this means that a greater amount of substrate needs to be consumed thus inflating the size of the dosage form.

Inkjet printing has also been adapted for the 3D printing of solid dosage forms. One of the approaches involved the photoionisation of the pharmaceutical ink during the building processes to achieve the structure of the tablet on a poly (ethylene terephthalate) substrate (Clark et al., 2017). The use of liquid was avoided by using a heated inkjet head, loaded with a mixture of the API and beeswax. This demonstrated the flexibility and potentials of this approach in drug dosing and in the manufacturing of complex geometries and drug release pattern (Kyobula et al., 2017). The 3D printing of dosage forms will be discussed in more details in the next sections.

d. 3D printing

A promising approach towards dose personalisation is the application of 3D printers in drug manufacturing. 3D printing is a rapid prototyping technique which builds a 3D object by successive layering of 2D forms in a layer-by-layer fashion. Examples of the 3D printers are shown in Figure 1.7. The use of 3D printers is well established for the development of customised medical devices (Chung et al., 2014, Dombroski et al., 2014). It has also been extensively used in tissue engineering (Boland et al., 2006, Pati et al., 2013) and in the manufacturing of implants (Water et al., 2015). 3D printing is a fast evolving process and is currently been investigated for pharmaceutical dosage form manufacturing for dose personalisation (Goyanes et al., 2015a, Okwuosa et al., 2016, Sadia et al., 2018, Yu et al., 2009b, Katstra et al., 2000).

1.8 3D printing and its various types

Various types of 3D printers have been used over the years and are as follows:

1.8.1 Stereolithographic 3D printing (STA)

Stereolithographic 3D printing (Figure 1.7A) involves the curing of photo-sensitive material(s) (photo-polymerisation) (Melchels et al., 2010). Curing of the polymers are usually done using ultraviolet (UV) rays (Cooke et al., 2003, Lan et al., 2009) or the use of digital light projection which uses a digital mirror device (Liska et al., 2007, Lu and Chen, 2012, Melchels et al., 2009) to initiates polymerisation reaction in the photopolymer causing it to solidify in the exposed area. This process is now repeated layer after layer to build the object as the unreacted functional groups on the solidified structure in the initial layer polymerises with the illuminated resin in the next layer (McMains, 2005). Post printing processing are usually required to remove excess resin and remove supporting structures (Melchels et al., 2010).

This technique is associated with high printing accuracy (25 μm) (Formlabs, 2015) and has found use in tissue engineering (Lan et al., 2009, Melchels et al., 2009, Skoog et al., 2014) and manufacturing of implantable devices (Popov et al., 2004).

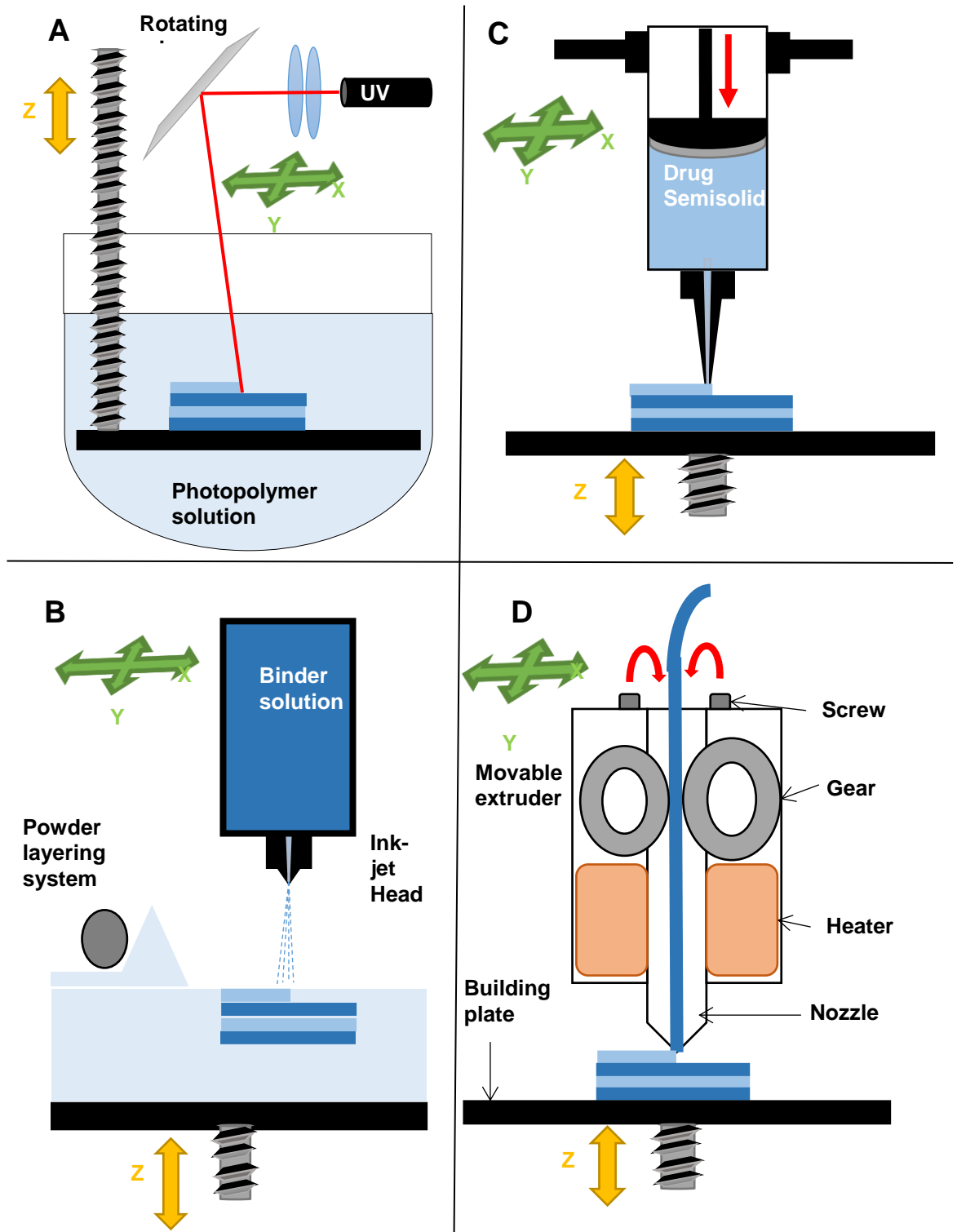


Figure 1.7. Mechanism of various 3D printing technologies: (A) Stereolithographic (SLA), (B) Powder bed and powder jetting, (C) Semi-solid extrusion (EXT) and (D) Fused deposition modelling (FDM).

1.8.2 Powder-bed 3D printing (PB)

Powder bed 3D printing (Figure 1.7B) remains one of the oldest methods of 3D printing developed at the Massachusetts Institute of Technology in the late 1980s (Aprecia, 2014). This technology involves the distribution of thin layers of powder selectively joined by drops of liquid binder deposited from an inkjet printer head (Katstra et al., 2000). It has been investigated in the manufacturing of implants (Huang et al., 2007) and oral dosage forms (Rowe et al., 2000, Katstra et al., 2000, Yu et al., 2009a, Yu et al., 2007).

The potentials of this technology was highlighted with the FDA approval of Spritam (the first FDA approved 3D printed product) an anti-epileptic drug (Aprecia, 2014). The fast product disintegration (4 sec) was attributed to the highly porous structure signature of the technique. However, the resolution is usually low and post printing processing like dusting and drying are required.

1.8.3 3D printing by semi-solid extrusion (SSE)

Another method of 3D printing involves the layer-by-layer deposition of semi-solids through a syringe-based tool-head (Figure 1.7C). The starting materials are usually in the form of gels or pastes formulated by the mixing of an optimal ratio of a polymer powder and suitable solvent to obtain viscosity suitable for printing (Khaled et al., 2014, Rattanakit et al., 2012, Khaled et al., 2018). This technique showed several potentials in personalised dosing with acceptable in batch variations. It is a non-thermal approach which creates room for a wide variety of APIs.

The use of this technique in the manufacturing of guaifenesin bilayer tablets was compared with a commercially available guaifenesin tablets (Khaled et al., 2014). Similar drug release profiles were observed, showing the versatility of this technique and also offering an easier approach to drug manufacturing, most especially in personalised dosing. The versatility of this 3D printing technique was also demonstrated in the manufacturing of “polypills” as it was successfully used to compartmentalise different drugs using different polymers to achieve complex release profiles (Khaled et al., 2015b, Khaled et al., 2015a). Up to five actives were loaded in a single dose using this approach, utilising multiple extrusion heads which was aimed at dose personalisation for cardiovascular treatment regimen (Khaled et al., 2015a).

1.8.4 3D printing by fused deposition modelling (FDM)

Fused deposition modelling (FDM) was commercialised in 1991 (Wendel et al., 2008) and till date remains one of the mostly used technique in 3D printing. It involves passing a filament based on thermoplastic polymers through a hot nozzle (Figure 1.7D), where temperature is elevated above its glass transition temperature (T_g). The extruded material is deposited layer-by-layer to form an object, with solidification occurring in less than a second.

The potential of FDM 3D printers has been explored in the incorporation of different API molecules through their loading into commercially available PVA (Goyanes et al., 2015a, Skowrya et al., 2015). This was usually achieved by immersing the PVA filament in a solution of the active for several hours, which is then dried and 3D printed. These previous attempts, however, displayed several limitations such as the use of non-pharmaceutical grade ingredients and limited drug loading (Goyanes et al., 2015a, Goyanes et al., 2015b). In addition, the process of drug loading usually involves the use of organic solvents which might not be safe when not completely removed, in addition to the time consuming nature of the technique. Due to the high T_g of this polymer, previous reports suggested the need for using high temperatures, [220 °C (Goyanes et al., 2014), 210 °C (Goyanes et al., 2015a) and 250 °C (Skowrya et al., 2015)] when PVA based dosage forms were fabricated using FDM 3D printers. Moreover, several examples of PLA printed structures employed a temperature range of 180-210 °C (Boetker et al., 2016, Rosenzweig et al., 2015, Senatov et al., 2016). The use of high temperature up to 180 °C indicated lack of suitability for sensitive actives which was demonstrated in an example by (Goyanes et al., 2015a) were 4-aminosalicylate with a melting point of 180 °C degraded during 3D printing even though the amount of time spend in the FDM 3D printing nozzle was minimal. This therefore emphasises the need to adapt new polymers that operate at lower temperatures to encourage the use of thermosensitive actives.

The use of FDM 3D printing in dose personalisation is evolving fast and seems to be the technique with the most potential considering the number of ongoing research in that area. The use of FDM was reported to produce tablets with high mechanical strength at a low cost using a low-cost unit (Pietrzak et al., 2015, Skowrya et al., 2015). Also, the discovery of the application of HME in the manufacturing of filaments in the form of solid dispersion using pharmaceutical grade polymers was promising (Pietrzak et al., 2015). In addition, FDM requires no specialised facilities or large spaces, hence could potentially be a candidate for use as a mini-dispenser, which led this 3D printing technique being the primary focus in research.

1.9 3D printing challenges in pharmaceutical field

Adopting 3D printing for pharmaceutical purposing is still at the early stages and as expected presents many challenges/limitations at these early stages of development. In addition, due to its novelty, its regulation is still not clear. These challenges will be discussed in the following sections.

1.9.1 Limitations of FDM 3D printing in pharmaceutical manufacturing

3D printing allows ease of variations of shapes and sizes whilst maintaining control over manufacturing through a software in comparison to a more rigid casting and compression approach to manufacturing. However, this flexibility is associated with some technical challenges, which were limiting its application for pharmaceutical purposes.

Primarily, the application of 3D printers in pharmaceutical manufacturing is dependent on the level of technological advancement of the 3D printer used. This made manufacturing of certain dosage forms extensively difficult and in some cases requiring individual modifications to achieve certain goals. Advancements in technologies are expected to improve the potentials of 3D printers in drug manufacturing for individualised dosing.

As already explained earlier, manufacturing using 3D printers occurs in a layer-by-layer fashion, which is one of the core identity of 3D printed objects. However, this layer-by-layer deposition of material contributes to its slow output in comparison to conventional manufacturing processes. In addition, it creates more room for errors during printing. Partial nozzle blockage could occur and create inconsistency in the final weight and shape of the final product. A total blockage in-between printing could also occur resulting to printing failure and material wastage. Once few layers are omitted during the head movement, gaps are created between the nozzle and the object leading to failure. This printing pattern also limits the final resolution of the object printed to 0.1 mm layers.

In the beginning of this research, one of the major limitations in the 3D printing of pharmaceutical dosage forms is the lack of applicable pharmaceutical grade polymers. This led to the use of non-pharmaceutical grade polymers (Skowyra et al., 2015), which were usually polymers with relatively high T_g, therefore requiring high temperature during processing. This limits applicable actives with available examples mostly using thermostable small molecules with no example of its application for large molecules like peptide and proteins.

Drug release from the polymers used were mostly extended which was determined by the properties of the polymer in a polymer-drug matrix system. This further emphasises the need to adapt more polymer for 3D printing to be able to engineer desired drug release patterns. There was little to no report of immediate release dosage form manufacturing using this approach and no report for enteric release or colon targeting. Conventional drug release modification methods require the need to apply a coating on the tablets, which will create a barrier and therefore modify release based on the properties of the polymer. However, coating using 3D printer has major challenges. To achieve coating using 3D printing, it will be necessary to create tight layers of the dose modifying polymers to prevent leakage and therefore modify release. This becomes more challenging in an attempt to fill the core of the dosage form with semisolids or liquids.

One of the main questions being asked by most pharmaceutical companies about any new manufacturing technique is whether it could be scaled up or not. Scaling up of the 3D printing process itself will not benefit dose personalisation. However, the filament manufacturing could be scaled up and stored in a ready to use form for individualised dosing. The optimisation and validation of this process possess a major challenge since variations in the diameter of the filament might result to fluctuations in the weight of the extruded filament and therefore the dosage forms. This could also lead to blockages and the inability to feed the filament into the printing head.

1.9.2 Regulatory challenges

The rapid advancement of 3D printing has made manufacturing closer to users. The expiring of the patents on 3D printers has even made acquiring one easy and affordable. With the ever-growing research in the 3D printing of pharmaceutical dosage forms for dose personalisation, the question on how its use will be regulated keeps resurfacing.

The regulatory bodies to ensure safety and efficacy before being introduced into the market must approve every pharmaceutical product or medical devices. Until date, there has been no clear or unique regulatory route for the approval of 3D printed drugs. However, there are existing and flexible pathways that could be used for new technologies like this (PharmTech, 2016). 3D printing as one of the emerging technologies has received a lot of attention from FDA and its Centre of Drug Evaluation and Research (CDER) created the Emerging Technology Program to promote the adoption of novel and innovative approaches for pharmaceutical product manufacturing and design (FDA, 2018, PharmTech, 2016). This new organisation played a key role in the approval of the first 3D printed dosage form (Spritam), a fast disintegration 3D printed

tablet by Aprelia Pharmaceutical for epilepsy (Forbes, 2016). It bridged the communication gap between innovator and regulatory bodies and most importantly caters for emerging technologies for which 3D printing manufacturing is included.

Since dose personalisation using 3D printers could be potentially done in a hospital, community pharmacy or even the patient's home, how will the use of 3D printing be controlled? Or will it be the use of the pharmaceutical ink (filament for FDM 3D printing, powders and binders for powder-based 3D printing etc.) that is monitored. The answers to these questions are still not clear. However, as the application of 3D printers in pharmaceutical manufacturing advances over the years, these questions will have to be answered eventually. Besides the FDA reserves the right to modify laws based on outcomes, especially for new techniques like 3D printing. FDA's CDER has also gone as far as launching researches on 3D printing to facilitate discoveries on its impact on active ingredients and excipients in order to determine potential quality control processes (FDA, 2017b, FDA, 2017a). This was to understand the policy framework needed to ensure the quality and safety of 3D printed products are maintained.

1.10 Scope of the research

Having identified the challenges and limitations of 3D printing of pharmaceutical dosage forms, it is obvious that having more pharmaceutical grade polymers for FDM 3D printing can reduce printing temperature, which will increase the range of applicable actives and enable ease of dose modification using pH sensitive polymers. It will also be interesting to adapt 3D printing for large molecules like peptides and proteins, which are also being investigated for therapeutic potentials in disease management. These will add to increasing the potentials of 3D printing as a pharmaceutical manufacturing process in dose personalisation.

1.11 Project aims

This research aims at manufacturing oral tablets and liquid capsules using FDM 3D printing for immediate, extended, enteric or colonic drug delivery, using pharmaceutical grade polymers. As a result, the following objectives will be carried out:

- To adapt pharmaceutical grade polymers for FDM 3D printing
- To manufacture immediate release PVP-based tablets using FDM 3D printing
- To provide the first example of an enteric tablet manufactured using dual FDM 3D printer with a drug loaded PVP-based core and a Eudragit L100-55 shell

- To manufacture liquid capsules using a modified dual FDM 3D printer for immediate and extended drug release using Eudragit EPO and RL respectively.
- To establish the colon cancer activities of AMPs (Aurein 2.6 and LL-37) and to demonstrate a proof of concept for colon targeting in the form of a liquid capsule using a Eudragit S100-based shell filament.
- To establish the stability of the PVP, Eudragit L100-55 and S100-based filament by 6 month accelerated stability studies.

**Chapter 2 : A Lower Temperature FDM
3D Printing for the Manufacture of
Patient-Specific Immediate Release
Caplets Using Polyvinyl Pyrrolidone**

2.1 Introduction

3D printing has established roots in various disciplines allowing users to be able to recreate their imaginations in a 3D format without the need for casting as used in the conventional manufacturing methods. It has changed the world of arts and seems to be exploited in all its forms from architecture to music to painting etc. In engineering especially in automobile industries, 3D printing finds use in the manufacturing of functional prototypes which aids better understanding of a project in a smaller scale (Leapfrog, 2018). It allows the manufacturing of unique parts that are hard to manufacture using conventional methods. A 3D printed part for a jet engine has been certified by the Federal Aviation Administration (FAA) (Winick, 2017) and attempts have also been made by NASA to manufacture a jet engine using this approach. For medical purposes, 3D printing is used in the manufacturing of low-cost prosthetics, customised medical implants and regenerative medicine with the prospects of being able to reproduce organs and body parts using biomaterial (Chung et al., 2014, Dombroski et al., 2014). At the start of this project, the exploitation of 3D printing for pharmaceutical applications was still at its early stages. However, with the emergence of the first FDA approved 3D printed tablet, Spritam (Aprecia, 2014), a fast disintegrating tablet manufactured by powder bed 3D printing, the momentum of this technology is on track to potentially change many means of production for oral dosage forms for individualised dosing. Individualising doses have always been based on a patient's age and body weight with a more recent consideration of genetic makes-up, due to improved knowledge in pharmogenomics.

Fulfilling individual requirements has always been challenging in drug dosing and the absence of large array of commercially available API combinations and strengths remains the most frequent problem facing compounding pharmacies today (McLean et al., 2013). As a result, most pharmacies resort to approaches like dosage splitting to enable dose individualisation. This approach proved to be unrealisable and becomes risky especially when dealing with drugs with low therapeutic index (Habib et al., 2014). Tablet splitting is often encouraged by manufactures by the scoring the tablets in attempt to reduce variations from such approach. However, research has shown otherwise (Ciavarella et al., 2016). In addition, the traditional tableting methods require multiple processing stages (mixing, granulation, drying, sieving and compressing), costly facilities and experienced personnel, thus rendering tablet manufacturing impractical when dose modification for one or small group of patients is required. By contrast, 3D printing, not only circumvent these challenges of conventional tableting, but also offers a means of fabricating medicines at the point of dispensing (Sanderson, 2015). Amongst

the different explored 3D printing technologies, fused deposition modelling (FDM) shows significant promise in low-cost dose fabrication (Goyanes et al., 2015c). This stems up from the fact that FDM printers are available today at low cost and capable of producing 3D objects at a high accuracy, without post-printing steps (Skowryra et al., 2015).

Despite the potentials of FDM 3D printing in drug manufacturing and dose personalisation, limitation to the use of PVA (Skowryra et al., 2015, Goyanes et al., 2015a) and PLA (Sandler et al., 2014b) filaments restricted drug release patterns towards being mostly extended due to the properties of the polymer. This major limitation to the use of an extended release polymer rendered the use of FDM 3D printing unsuitable for the production of immediate release tablets, which account for approximately 70% of all oral dosage forms (GBIResearch, 2012). However, immediate release dosage forms have been achieved using other 3D printing methods. A polypill system with an immediate release layer has been produced using an extrusion based 3D printer (Khaled et al., 2015a) in addition to the already mentioned FDA approved “Spritam” (Aprecia, 2014).

Unless a particular area of the body is targeted, or an extended release is required, most oral dosage forms quickly disintegrate and release their actives once in contact with the gastric fluid. This provides an early onset of action and finds use in emergency situations where immediate therapeutic effect is required. For a dosage form to be called immediate release according to the BP, it must release 75 % of the active ingredient (s) within 45 min of an *in vitro* dissolution studies in an acid media. To be able to meet this criteria for conventional manufacturing, a fast disintegration is usually required of the dosage form which increases the surface area for drug dissolution to take place (Desai et al., 2016). Disintegrants are used to aid disintegration which swells and break up the compressed tablet into smaller particles in addition to the use of highly soluble bulking agents to facilitate fast dissolution. However, the manufacturing technique for FDM 3D printing does not involve any compression but a layer-by-layer deposition of the extruded filaments, therefore presenting new challenges in the manufacturing of immediate drug release dosage forms. In a rare example, Pietrzak et al. (2015) reported the fabrication of immediate release tablets based on positively charged methacrylic polymers loaded with theophylline without the need for disintegrants. Filaments for this study were processed by HME and also the research demonstrated the possibility of dose alteration by modifying the size of the printed tablets (Pietrzak et al., 2015). The use of hot melt extrusion in filaments manufacturing (Pietrzak et al., 2015) created more opportunity to adapt many other pharmaceutical grade polymers for FDM 3D printing in addition to being a well-established technique in pharmaceutical formulations. It is a popular

technique used in the formulation of polymer matrix by using heat to soften the material before mixing is carried out under pressure created by the rotating screw. The molten mass is cooled and extruded using suitable nozzle diameters to regular the diameter of the product.

Polyvinylpyrrolidone (PVP) has demonstrated compatibility with the use of HME and finds application in the manufacturing of immediate release dosage forms using the conventional manufacturing approach. It is among the most common carriers used in amorphous solid dispersion which was first reported in 1966 (Mayersohn and Gibaldi, 1966). PVP exhibit solubility in both hydrophilic and hydrophobic media which makes them suitable for both solvent evaporation and hot melt extrusion (HME). With an increasing number of new drug candidates being poorly soluble, these polymers now play major roles in improving drug solubility (Knopp et al., 2015, Shah et al., 2008, Sharma and Jain, 2010, Ahuja et al., 2007, Knopp et al., 2016). PVP in solid dispersion with a drug inhibits crystallisation, and due to the molecular mix between the drug and the polymer, the dissolution of the dispersion is driven by the properties of the polymer (Knopp et al., 2016, Leuner and Dressman, 2000). At the beginning of this study, this polymer had not been used for FDM 3D printing. As a result, it will be of great interest to adapt this water soluble polymer for FDM 3D printing of tablets for immediate drug release.

2.2 Aim and Objectives

The aim of this research is to produce immediate release tablets via FDM 3D printing at a reduced temperature using a pharmaceutical grade polymer (PVP), the first example of its application in FDM 3D printing. To be able to achieve this goal, the objectives of this research includes:

- To investigate the application of this pharmaceutically accepted polymer in 3D printing of tablets by FDM.
- Optimisation of PVP polymer to be able to print at a lower temperature when compared with the commercially available filaments.
- Optimisation of the drug loading of the PVP-filaments both for acidic (aspirin) and basic (dipyridamole, theophylline) actives.
- Characterisation of the actives, excipients and the formulations by
 - Scanning electron microscopy (SEM)
 - Thermal analysis (DSC and TGA)
 - X-ray powder diffraction (XRPD)
 - Pharmacopoeial characterisation of 3D printed tablets (weight variation, hardness, disintegration, friability and drug content)
 - In vitro dissolution studies

2.3 Materials

The materials used for these studies includes:

2.3.1 Theophylline

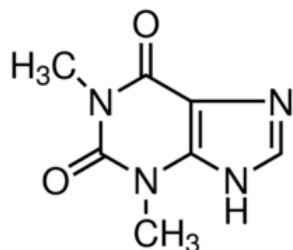


Figure 2.1. Chemical structure of theophylline (SIGMA-ALDRICH, 2018b).

Theophylline is a xanthine derivative (Figure 2.1) from tea, prepared synthetically with a melting point of 270 °C (SIGMA-ALDRICH, 2016c). It is a Biopharmaceutics Classification System (BCS) class I drug which has a diuretic, smooth muscle relaxant, bronchial dilating, cardiac and central nervous system activities. It is usually indicated for the treatment of airflow obstructions associated with chronic asthma, emphysema and chronic bronchitis. A loading dose of 5 mg/kg is usually recommended for a healthy non-smoking adult with acute asthma. This might go up to 16 mg/kg for a healthy smoking adult (Drugs.com, 2018c). Side effects from theophylline use includes chest pain or discomfort, dizziness, fainting, and light-headedness. Abdominal pain, loss of appetite, blurred vision, and dark coloured urine could be symptoms of overdose (Drugs.com, 2018c). For this research, theophylline was purchased from ACROS Organics (UK) and used as a drug model.

2.3.2 Dipyridamole

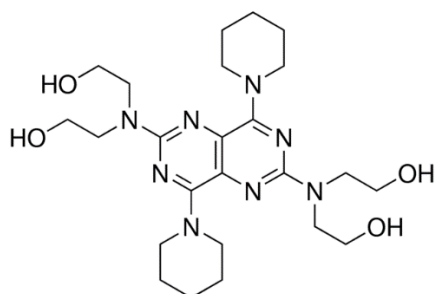


Figure 2.2. Chemical structure of dipyridamole (SIGMA-ALDRICH, 2016a).

Dipyridamole (Figure 2.2) is a phosphodiesterase inhibitor, which blocks the metabolism and uptake of adenosine. It is used as an anticoagulant, an adjunct to coumarin

anticoagulants. It is a yellow powder with a melting point of 165-166 °C (SIGMA-ALDRICH, 2016a). Common side effects include abdominal or stomach cramps, diarrhoea and dizziness. Sometimes, flushing, headache, nausea and weakness could be experienced but it is less common (Drugs.com, 2018a). For this research, dipyridamole was purchased from Sigma-Aldrich (UK) and used as a drug model.

2.3.3 Aspirin

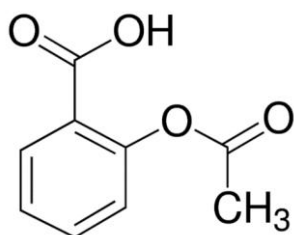


Figure 2.3: Chemical structure of aspirin (SIGMA-ALDRICH, 2018a)

Aspirin (Figure 2.3) is a white, crystalline, weakly acidic substance with a melting and boiling point of 136 °C and 140 °C respectively. It is an analgesic, antipyretic and anti-inflammatory agent which acts by irreversibly blocking the activity of both cyclooxygenase 1 and 2. This decreases the precursors of prostaglandins and thromboxanes from arachidonic acid. It is usually indicated for pain relief and inflammation associated with rheumatoid arthritis, osteoarthritis and ankylosing spondylitis (DrugBank, 2017). Side effects may include abdominal pain, constipation and bloody or cloudy urine (Drugs.com, 2017). For this research, aspirin was purchased from Sigma-Aldrich (UK) and used a drug model.

2.3.4 Polyvinyl pyrrolidone (MW, 40,000)

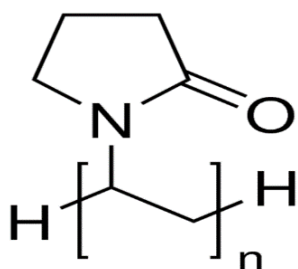


Figure 2.4: Chemical structure of PVP (SIGMA-ALDRICH, 2016b)

PVP (Figure 2.4) is a fine, white to creamy-white, odourless powder with a molecular weight ranging from 2500 – 3000000. It is hygroscopic and are freely soluble in acids, chloroform, ethanol, ketones, methanol, and water. They are practically insoluble in

ether, hydrocarbons, and mineral oil. PVP (MW, 40,000) for this research was purchased from Sigma-Aldrich (UK).

2.3.5 Talc

Talc is a clay mineral made up of hydrated magnesium silicate with the chemical formula, $Mg_3Si_4O_{10}(OH)_2$. Its colour ranges from white to grey and it is a major component of baby powder. They are insoluble in water and when applied for pharmaceutical purposes, are commonly used as lubricants and anticaking agent to improve powder flow during compression (Drugs.com, 2018b). Talc finds use in some food products and is generally recognised as safe by the FDA (FDA, 1979). For this research, talc was ordered from Fluka Analytical (UK) (350 mesh) and used as a non-melting component for filament manufacturing.

2.3.6 Triethyl citrate

Triethyl citrate (TEC), an odourless, colourless, oily liquid which finds use as a food additive and in pharmaceutical manufacturing. It is an ester of citric acid commonly used as a plasticiser to reduce the glass transition temperature of polymers especially during processes like coating and hot melt extrusion. It was purchased from Sigma-Aldrich (UK) and used as a plasticiser during the HME of the filaments.

2.3.7 Scotch blue painter's tape

Scotch blue painter's tape 50 mm was supplied by 3M (Bracknell, UK).

2.4 Methods

2.4.1 Preparation of filaments using HME

The pharmaceutical filaments were manufactured as a solid dispersion which is one of the popular techniques used to improve drug solubility. The application of polymers to this effect was first reported in 1969 by Chiou and Riegelman (Chiou and Riegelman, 1969). Other techniques include the use of solubilising agents, micronisation, nano-sizing and co-solvency.

Hot melt extrusion is one of the methods used to create solid dispersion which forms a molecular mix between a drug and a polymer. The hot melt extruder works by softening the added materials under pressure usually created by the screws. The materials are mixed and compacted together and then extruded to form the solid dispersion. An illustration on how the HME works is shown in Figure 2.5.

The preparation of the filaments were carried out using a Hot Melt Extruder (Thermo Scientific HAAKE MiniCTW, Netherland) which is a counter rotating extruder with a maximum speed and temperature of 300 rpm and 300 °C respectively (Thermoflsher, 2017). These compounders find use in research and development especially at the initial stages as small samples could be extruded (5 g). An optimised ratio of a powder mixture constituting of the polymer (PVP), plasticizer (TEC), filler (talc) and API (aspirin, dipyridamole or theophylline) was gradually added to the HME. The screw speed was set at 80 rpm and the powders were allowed to mix for 5 min in order to allow homogenous distribution of the molten mass prior to extrusion using a torque of 0.4 Nm. Table 2.1 shows the drug free and drug loaded PVP-based filament formulations and their processing conditions.

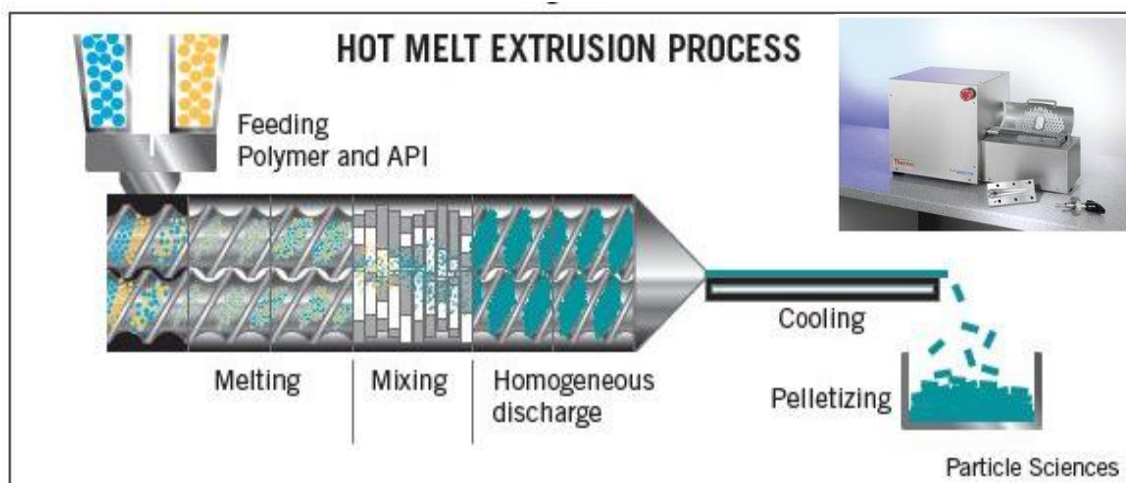


Figure 2.5. Formulation of a solid dispersion by hot melt extrusion process (ParticleScience, 2011).

Table 2.1. HME and FDM 3D printing processing parameters.

| Formulation | HME processing | | | 3D printing process | | |
|--|-----------------------|-------------------------|---------------------|----------------------------|------------------------------|---------------------|
| Weight ratio | Feeding temp. (°C) | Extruding temp. (°C) | Nozzle size (mm) | Extruding temp. (°C) | Building plate temp. (°C) | Nozzle size (mm) |
| PVP/TEC/Talc 50%/12.5%/37.5% | 100 | 90 | 1.25 | 110 | 40 | 0.4 |
| PVP/TEC/Talc/Drug 50%/12.5%/27.5%/10% | 100 | 90 | 1.25 | 110 | 40 | 0.4 |

2.4.2 Tablet design and printing

Tablets in this study were designed in a caplet shape using an Autodesk® 3ds Max® Design 2012 software version 14.0 (Autodesk, Inc., USA). The templates design was then imported to the 3D printer's software in a stereolithography (.stl) file format. For the printing of tablets, pre-prepared filaments were fed into a commercial FDM 3D printer equipped with 0.4 mm nozzle size and MakerWare software Version 2.4.0.17 (Makerbot Industries, LLC., USA). Tablets were printed using a standard printing resolution, 90 mm/s extrusion speed, at 100 % infill and 200 µm layer height as reported by (Pietrzak et al., 2015).

2.4.3 Differential scanning calorimetry (DSC)

DSC is a highly sensitive technique used to determine the thermotropic properties of excipients or actives. It is a thermoanalytical technique which measures the difference in the amount of heat required to increase the temperature of a sample and reference. This technique was first developed by E.S. Watson and M.J. O'Neil in 1962.

Basic principles of this technique is that as samples are heated and they undergo physical transformation such as phase transition, more or less heat flows to the sample when compared to the reference to maintain both at the same temperature. It is these heat changes that are picked up by the equipment, a heat gain (endothermic) or heat loss (exothermic). Heat gain by samples usually leads to softening of material (glass transition temperature) or the melting of the material due to absorption of heat to undergo the endothermic phase transition. On the other hand, heat loss usually results from crystallisation of materials and require less heat to raise the samples temperature (Chiu and Prenner, 2011).

A modulated temperature differential scanning calorimetry (MTDSC) is an advancement in the regular DSC where a sinusoidal heating program is used instead of a linear heating program. This enables the deconvolution of complex and overlapping thermal events by allowing the resolution of the obtained heat flow into a reversing and non-reversing signal (Coleman and Craig, 1996).

In this research, a MTDSC analysis was achieved using a differential scanning calorimeter (DSC) Q2000 (TA Instruments, Elstree, Hertfordshire, UK) at a heating rate of 2 °C/min. Each sample was subjected to a heat-cool-heat scan in order to measure and exclude the effect of moisture contents on filament plasticity. A modulated scan was applied using an amplitude of 0.212 °C and a period of 40 sec, scanning from -70 to 200 °C. Analysis was carried out under a purge of nitrogen (50 mL/min). The data was

analysed using a TA 2000 analysis software. TA pin-holed lid and 40 μL aluminium pans were filled with approximately 5 mg sample for the analysis. All measurements were carried out in triplicates.

2.4.4 Thermogravimetric analysis (TGA)

Thermogravimetric analysis is a thermal analysis method which measure changes in the mass/weight as a function of temperature, time and atmosphere. Results from such analysis could be used to determine the thermal and oxidation stability of materials. It also provides information about the components of a material, decomposition kinetics, moisture and volatile content of materials (Mohomed, 2016). Weight loss during analysis is usually an indication of decomposition, evaporation, reduction or desorption. On the other hand, a weight gain indicates oxidation or absorption.

For TGA analysis, printed tablets, raw materials as well as extruded filaments were measured using a TGA Q5000 (TA Instruments, Hertfordshire, UK). Samples (10 mg) were added to an aluminium pan without lid and heated from 25 $^{\circ}\text{C}$ to 500 $^{\circ}\text{C}$ at a heating rate of 10 $^{\circ}\text{C}/\text{min}$. All measurements were carried out in triplicates.

2.4.5 X-ray Powder diffractometry (XPRD)

X-ray powder diffraction is a non-destructive technique with a lot of pharmaceutical applications. It is used to determine the physical form of samples, excipient compatibility, process parameter optimisation, detection of purities, and monitoring uniformity of dosage forms and batches (Cynthia S. Randall, 2010).

In XRPD, a detector is used to measure the diffraction pattern from the atoms of the samples due to an incident X-ray. The diffraction pattern provides information about the atomic arrangement within the crystal of the sample. However, this is not the case for amorphous materials as they do not produce any diffraction pattern due to lack of periodic array with long-range order.

An X-ray diffractometer is made up of the X-ray tube, sample holder and the detector. The position of the diffraction peaks are determined by the distance between parallel planes of atom according to Bragg's Law:

$$n\lambda = 2d \sin\theta \qquad \text{Equation 2.1}$$

where n represents the positive integer, λ is the wavelength of the incident wave, d is the interplanar distance and θ is the scattering angle. The path difference between two incident waves undergoing interference from the crystal is given by $2d \sin\theta$. A schematic illustration of Bragg's spectrometer is shown in Figure 2.6

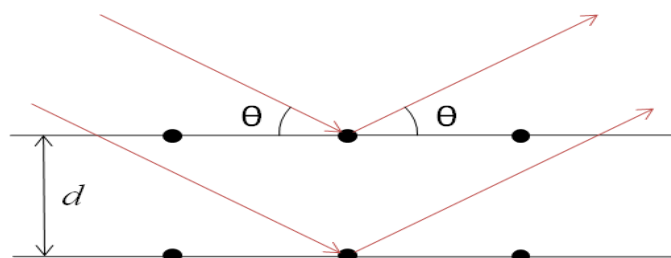


Figure 2.6. Schematic illustration of Bragg spectrometer (Libretexts, 2017).

A powder X-ray diffractometer, D2 Phaser with Lynxeye (Bruker, Germany) was used to assess the physical form of APIs in PVP, PVP:TEC filament, API-free and API-loaded filaments, and 3D printed tablets. Samples were scanned from 2Theta (2θ)= 5° to 50° using 0.01° step width and a 1 second time count. The divergence slit was 1 mm and the scatter slit was 0.6 mm. The wavelength of the X-ray was 0.154 nm using Cu source and a voltage of 30 kV. Filament emission was 10 mA using a scan type coupled with a two theta/theta scintillation counter over 30 min.

2.4.6 Characterisation of the tablets properties

Tablets in this study were characterised for; weight variation, drug content, friability, hardness and disintegration time. To determine weight uniformity, 20 tablets were randomly selected and weighed individually using a digital analytical balance Ohaus® (Discovery DV215CD). The average weights of the tablets were measured and the percentage deviation from the mean was then determined.

The crushing strength of 10 tablets was measured using a TBH 220 D (Erweka GmbH, Heusenstamm, Germany). This is a device that measure the force required to crush a tablet usually inserted in-between the jaws of the device.

The friability of the 3D printed tablets was determined using an Erweka Friability Tester TAR 10 (Erweka GmbH, Heusenstamm, Germany). Friability testers are devices used to investigate how the dosage form will withstand handling and transportation after manufacturing. It is made of a drum with an internal diameter between 283 and 291 mm and a depth between 36 to 40 mm. A curved projection inside the drum (75.5 to 85.5 mm) tumbles the tablet at each rotation. Twenty tablets were randomly selected, weighed and tested at a rotation of 25 rpm for 4 min. Tablets were then collected, dusted and reweighed. The differences in weight were calculated and displayed as a percentage of the original sample weight.

In order to determine the disintegration time for the 3D printed tablets, an Erweka ZT 220 Disintegration tester (Erweka GmbH, Heusenstamm, Germany) was utilised. It consists of a basket-rack assembly, a 1L beaker, a system for temperature regulation and movement of the device. When set up adequately, it functions by lowering the basket containing the dosage forms in and out of the immersion fluid and the disintegration time is noted when no residue remains in the screen of the test apparatus. Six tablets were randomly selected and individually placed in the 6 cylinders of the basket rack assembly. The tablets in the cylinders were then covered with discs and the basket rack was immersed into a beaker containing 750 mL of 0.1 M HCl at 37 ± 0.5 °C. The time required for all tablets to leave the mesh was then visually assessed and timed.

2.4.7 Determination of drug content

Drug contents for pharmaceutical purposes are analysed using HPLC. It has the mobile phase reservoir, injection system, the column and the detector as the major components (Figure 2.7). It is an equipment used to separate, identify and quantify every component in a mixture. This technique relies on forcing a pressurised liquid and the samples through a column containing solid absorbent materials. The components of the mixtures interact differently with these materials resulting in the separation of the components of the mixture and therefore being detected separately. The mobile phase and the flow rate used during analysis also affects the time of detection.

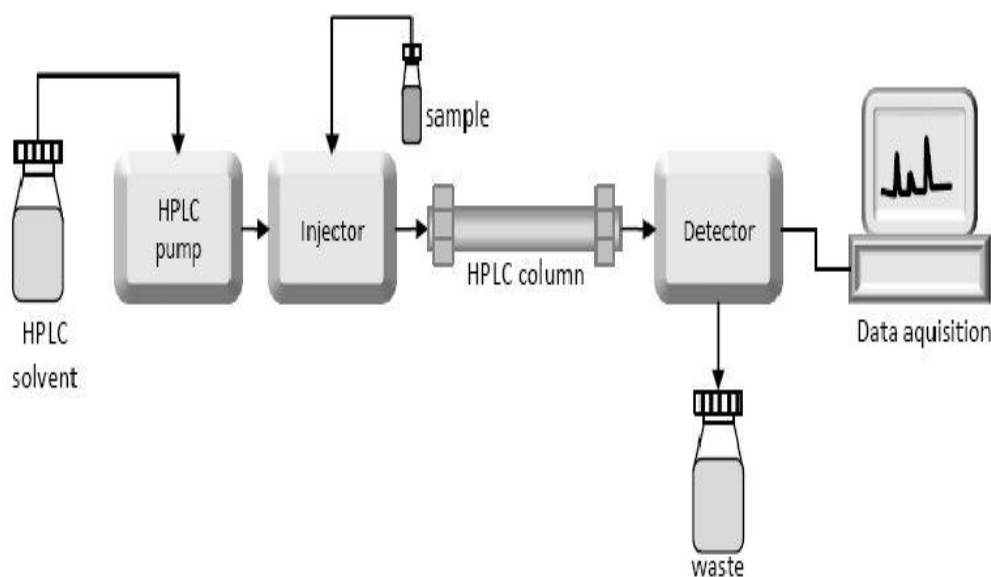


Figure 2.7. Components of HPLC (LaboratoryInfo.com, 2015).

To investigate the effect of HME and FDM 3D printing on the integrity of the drugs, API-loaded filaments and 3D printed tablets were analysed for drug content prior and following HME as well as in the 3D printed tablets. The drug content of the aspirin filament and 3D printed aspirin tablets were analysed using HPLC system (Agilent technologies 1200 series, Germany). Tablets were selected randomly and placed in 500 ml of HPLC water in a volumetric flask. This was sonicated for 1 hr, cooled and filtered before the analysis. HPLC system consists of Agilent ZORBAX Eclipse XDB-C8 3.0 x 150 mm, 5 µm column (made in USA) heated to 40 °C. The mobile phase was HPLC water and acetonitrile (90:10) at a flow rate of 1 mL/min. The injection volume was 5 µL and the maximum run time was 5 min. The assay was carried out at 230 nm wavelength.

Dipyridamole and theophylline loaded filaments or 3D printed tablets were accurately weighed and placed in a 500 mL of 1:1 water:acetonitrile mixture for 2 h under sonication. The solutions were filtered through 0.22 µm Millex-GP syringe filters (Merck Millipore, USA) and prepared for HPLC analysis.

Dipyridamole content in relevant samples were assessed using an Agilent UV-HPLC 1260 series (Agilent Technologies, Inc., Germany) equipped with XTerra RP 18 column (150 x 4.6 mm, 5µm particle size) (Waters, Ireland) at temperature 40°C. The mobile phase (60:40, phosphate buffer pH 6.8:acetonitrile) was employed at a flow rate of 1 mL/min and dipyridamole was detected at a wavelength of 282 nm. The injection volume was 10 µL and a stop time was 10 min per sample.

For theophylline, the same UV-HPLC system and column were used as detailed above for dipyridamole. The mobile phase constituted of 10 mM solution of ammonium acetate buffer, methanol and acetonitrile (86:7:7). Analysis was carried out at a wavelength of 272 nm, temperature of 40 °C, flow rate of 1 mL/min, injection volume was 5 µL and a run time of 7 min.

2.4.8 Scanning electron microscopy (SEM)

This is a type of electron microscope which produces images by scanning the surface of the material with a beam of electrons which interacts with the atoms on the surface of the sample to produce signals about its surface topography. The components of an SEM is shown in Figure 2.8

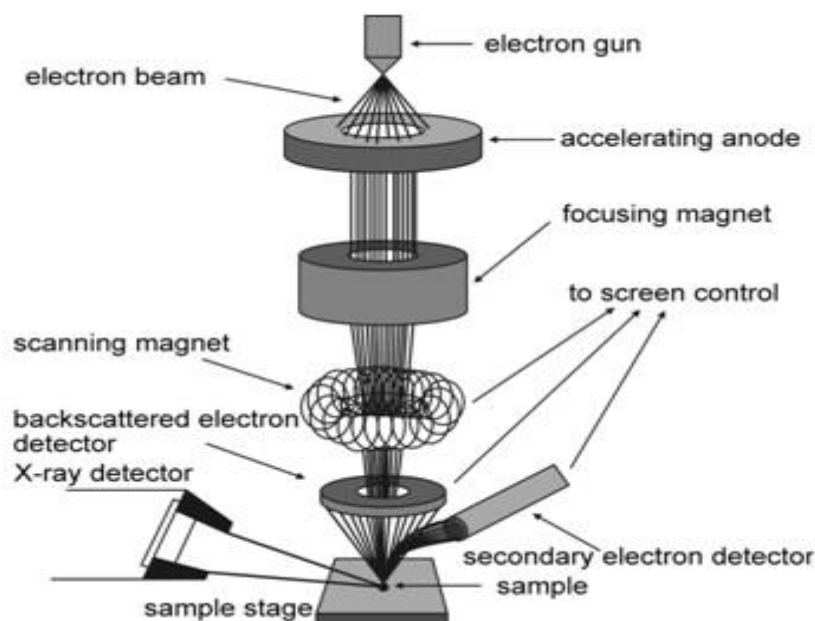


Figure 2.8. The set-up of a scanning electron microscope (Technoorg-Linda, 2018).

The surface morphology of the filaments and the printed tablets was examined using Quanta-200 SEM microscope at 20 kV. Samples were placed on a metallic stub and gold coated under vacuum using JFC-1200 Fine Coater (Jeol, Tokyo, Japan). Photographs of the tablets were also taken with a Canon EOS-1D Mark IV (Canon Ltd, Japan).

2.4.9 *In vitro* drug release studies

In vitro dissolution test is usually carried out on pharmaceutical products in order to correlate *in vivo* activities of the drug. This is done to determine the drug release pattern of the dosage form and usually involves a transparent inert vessel for the dissolution media, a motor or drive shaft for the cylindrical basket (USP I) or paddle (USP II). The vessel is usually immersed in a temperature regulated water bath used to simulate the temperature of the human body. Sampling could be done automatically or manually and analysed by UV or HPLC.

In vitro drug release studies were investigated using an Erweka DT 600 dissolution tester (USP II). Three tablets were randomly selected and individually placed in the dissolution vessels each containing 900 mL of 0.1M HCl and stirred at 50 rpm and 37 ± 0.5 °C. Four mL aliquots were manually collected using 5 mL Leur-Lok syringes at (0, 5, 10, 15, 20, 25, 30, 40, 50, 60 and 70 min) time intervals and filtered through a Millex-HA 0.45- μ m filter. Each aliquot withdrawn was replaced with 4 mL of 0.1M HCl. The absorbance of the samples was finally measured using a UV spectrophotometer (Bibby Scientific Ltd, UK) at 230, 282 and 272 nm for aspirin, dipyridamole and theophylline respectively.

2.4.10 Statistical analysis

One-way ANOVA was employed using SPSS Software (22.0.0.2) to analyse the results. Differences in results above probability level ($p > 0.05$) were considered not significant whilst; ($p < 0.001$) were considered very significant and between $p = 0.01$ and 0.05 were considered significant.

2.5 Results and discussions

PVP is a well-known pharmaceutical excipient generally recognised as safe by the Food and Drug Administration (FDA). It is highly water soluble and finds use as a solubility enhancer amongst other uses in the pharmaceutical industries. These properties of this polymer in addition to a well-established HME processing technique in the preparation of solid dispersion, made it a suitable candidate for FDM 3D printing drug manufacturing. In this research, TEC was used as a plasticiser to lower the HME processing temperature of this polymer which reflected on the 3D printing temperature of the PVP-based filament which was less than the temperature used for the commercially available PVA polymer. To the author's knowledge, this is the first report of the use of PVP in the 3D printing of tablets using FDM 3D printing at such a low temperature. It was observed that as a result of this low T_g of the resultant filaments, it was difficult to obtain a 3D structure from the filaments as the building layer tended to collapse during the process. Talc was introduced into the filament formulation to prevent this. Talc being a thermostable substance with a melting point of 1500 °C, its primary function in the formulation was to support the structure of the product and encourage the formation of 3D structures during the layer depositions. This provided a blank filament formulation which could then be loaded with drugs by replacing some percentage of the talc with the actives as demonstrated with aspirin, dipyridamole and theophylline. The use of a thermostable substance with such high melting point was not carried out in the study by Pietrzak et al. (2015). However, it was believed that the high concentration of the actives aids the formation of the 3D structure since printing was done at temperatures below the melting point of the drug which might restrict the system to drugs with high melting points. Figure 2.9 reveals the stages from filament production using HME to FDM 3D printing of the tablets using the parameters in Table 2.1. A 1.25 mm HME nozzle was used to produce filaments compatible with the FDM 3D printer head which was observed to expand during extrusion to achieve filaments of approximately 1.5 mm, which is close to the size of the commercially available PVA filament (1.75 mm). It was also observed that the presence of talc reduced the polymer expansion during extrusion which is important as large filament cannot pass through the metal channel that leads to the nozzle. 3D printing was carried out at 110 °C with the temperature of the building plate maintained at 40 °C to enable fast cooling during 3D printing and at the same time aid tablet adhesion to its surface. Tablet adhesion was also enhanced by using Scotch blue painter's tape on the surface of the building plate.

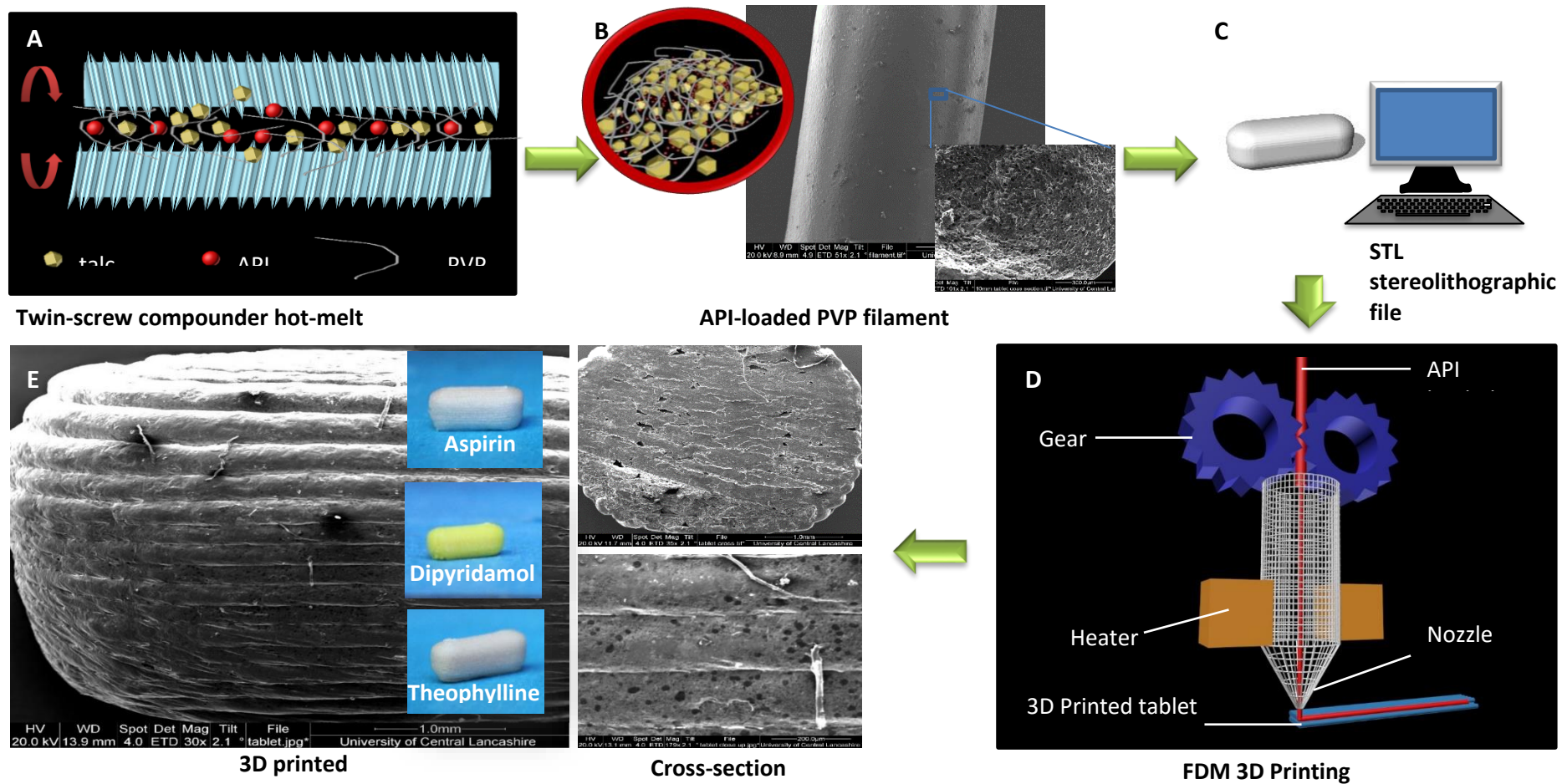


Figure 2.9. Schematic illustration of the fabrication of immediate release 3D-printed tablet. (A) Materials mixture (API, PVP and talc) are processed through HME to produce (B) API loaded PVP filament is extruded (C) Stereolithographic file is designed via CAD software and (D) FDM 3D printer uses the filament as a feed to fabricate drug loaded immediate release tablet (E) at 110 °C.

The SEM images of the 3D printed tablets revealed the layer-by-layer signature structure of forms produced using 3D printers (Figure 2.9). This was also seen from a cross section image of the tablet. The filament before 3D printing was mostly smooth with few rough areas in comparison to the 3D printed structure. The cross-section view of the filament revealed the presence of void or air pockets which might be as a result of moisture loss during heating in the HME.

Thermogravimetric analysis (Figures 2.10A, B and C) revealed initial mass loss from PVP alone (approx. 8%) and when in the formulation (approx. 4%) before 100 °C. This was attributed to polymer dehydration as PVP is known to be hygroscopic with the ability of taking up moisture up to 40% of its weight. This also revealed the stability of the polymer, with weight loss occurring above 380 °C. TEC alone demonstrated weight loss at approx. 115 °C. However, when in combination with PVP, weight loss was observed above 250 °C. This stabilising effect was also noticed when PVP was formulated with aspirin. Weight loss on aspirin occurs in two stages as demonstrated in Figure 2.10A, the first occurring above 150 °C as a result of the elimination of acetic acid and the evaporation of salicylic and acetylsalicylic acid (Ribeiro et al., 1996). This was however prevented with the addition of PVP with the second weight loss starting at approximately 300 °C as a result of the elimination of residual acetic acid and salicylic acid with the thermal decomposition of 2,2- bis (acetate) diphenyl ester (Ribeiro et al., 1996). These stabilising properties further strengthens the use of PVP in the formulation. This stabilising effect was however not noticed in a PVP-dipyridamole and theophylline solid dispersions. The TGA of dipyridamole alone revealed an initial 35 % mass loss which could be as a result of the dissociation of two piperidine substituent groups attached to carbon C4 and C8 of pyrimido-pyrimidine ring (Silva Oliveira et al., 2006). The second mass loss (approx. 35%) could be as a result of the dissociation of two diethanolic groups attached to the substituents at positions C2 and 6 of the central ring (Silva Oliveira et al., 2006). Talc was stable up to 500 °C confirming its role as the structure forming agent without which the structure of the tablets cannot be maintained.

In conclusion, the excipients and the actives used in the filament fabrication demonstrated thermal stability at the HME (100 °C) and 3D printing (110 °C) processing temperatures which was necessary to maintain their integrity throughout the process.

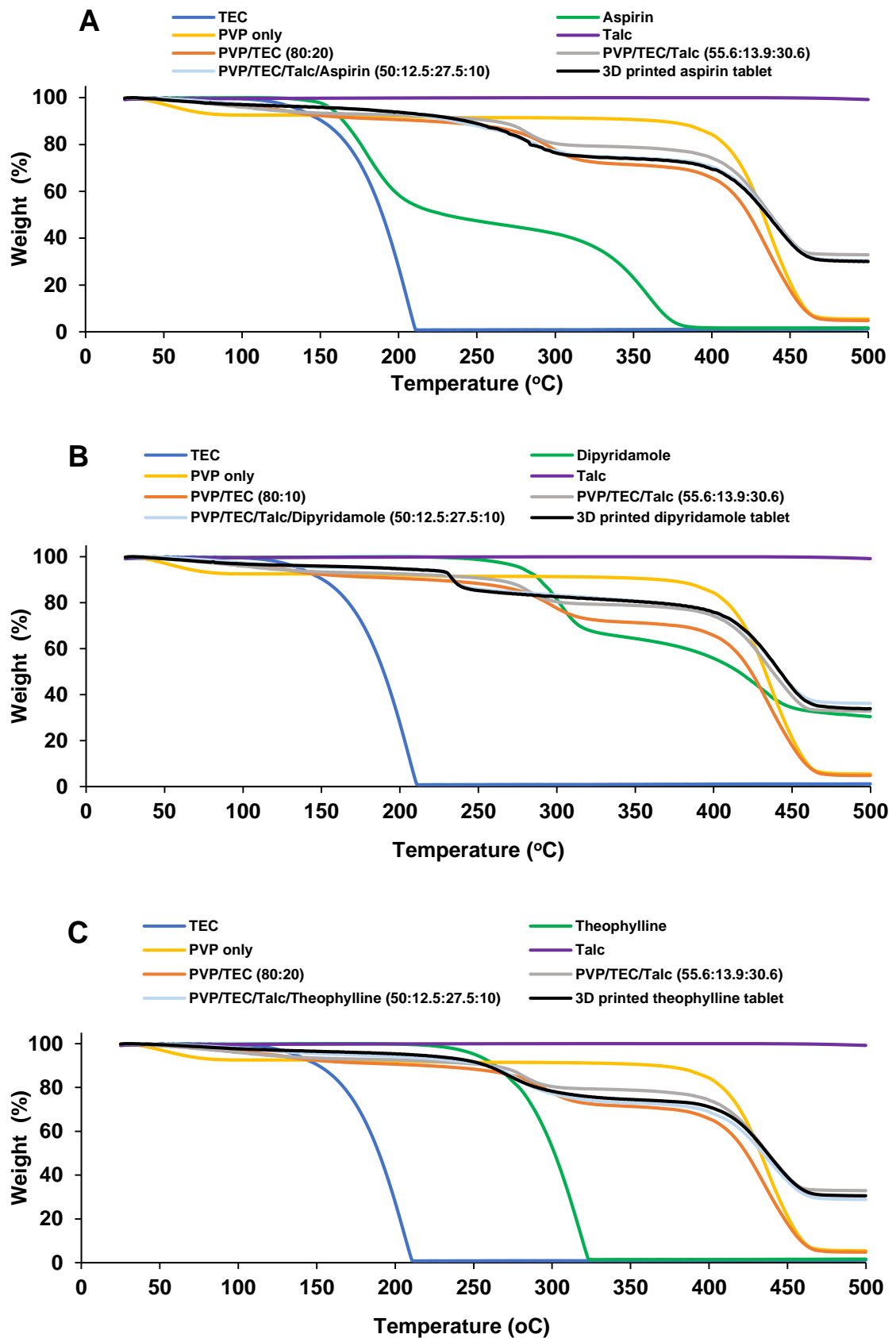


Figure 2.10. TGA Thermal degradation profiles of TEC, PVP, PVP:TEC filament, API-free and API loaded filaments, and 3D printed tablets for (A) Aspirin, (B) Dipyridamole, (C) theophylline and the excipients used.

The DSC thermographs of the first heat-scans all displayed a large endothermic event between 50-110 °C due to polymer dehydration (Figures 2.11A, 2.12A and 2.13A). This might be related to the hygroscopic nature of PVP, where electronegative groups of the carbonyl group in the pyrrolidone structure are able to form hydrogen bonds with water (Verdonck et al., 1999). Therefore, a modulated heat-scan was utilized to assess this event-complex. In order to investigate the impact of water on glass transition temperature (T_g), a heat-cool-heat scan was employed.

The reversing heat flow of the first heat-scan indicated that the T_g of PVP filament (plasticised with TEC) to be in the range of 19-35 °C. This T_g was significantly lower than expected from Gordon-Taylor equation (T_g = 82.3 °C) and was related to the plasticising effect of water. On the other hand, the second heat-scan indicated a significantly higher T_g value of 93 °C (in comparison to the T_g of first heat-scan, p < 0.05), confirming that moisture has an impact on the plasticity of PVP. Such a plasticizing effect of moisture on PVP was previously reported (Szakonyi and Zelkó, 2012, Lai et al., 1999).

The addition of talc did not show any significant effect on the thermal behaviour of PVP as noted in the first and second heat-scans (Figures 2.11B, 2.12B and 2.13B). The addition of aspirin, dipyridamole and theophylline shifted the T_g of the filament in the second scan from 93 °C to 62, 78 and 70 °C respectively. Such depression in the T_g indicates a plasticizing effect of the actives used. Similar findings have been reported earlier for other API-PVP blends (Nair et al., 2001).

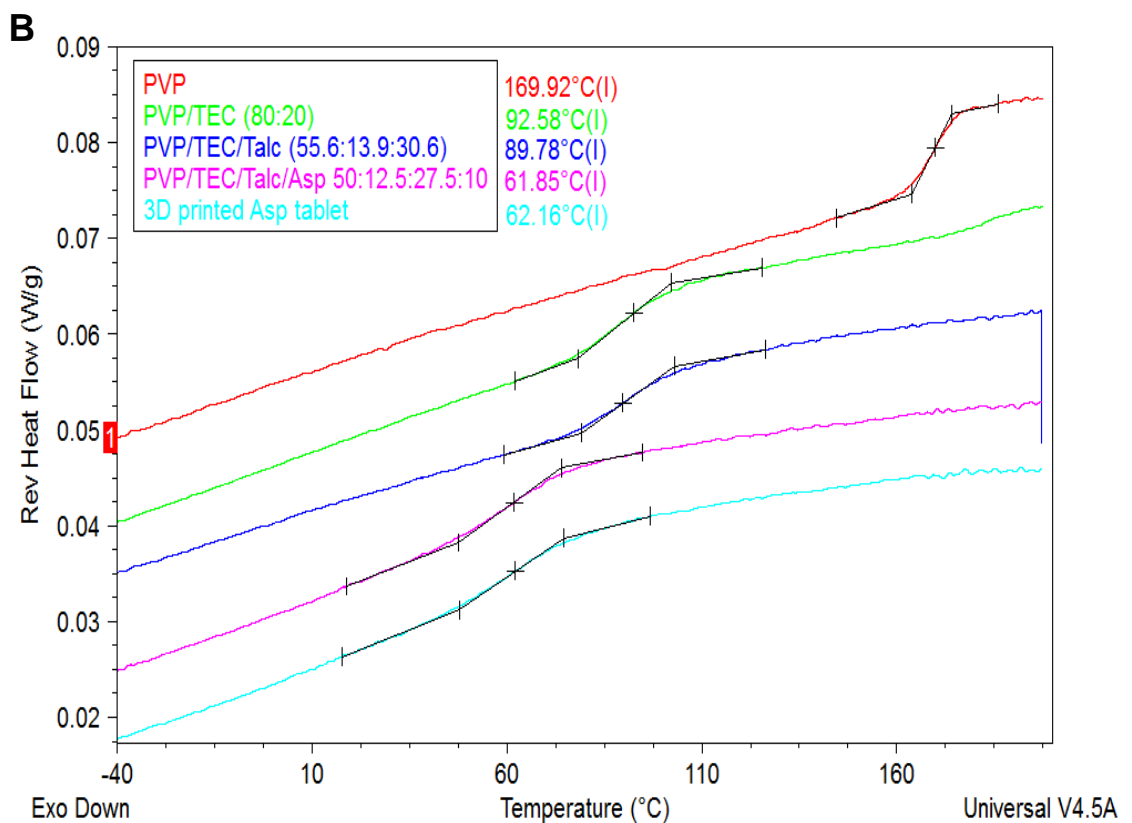
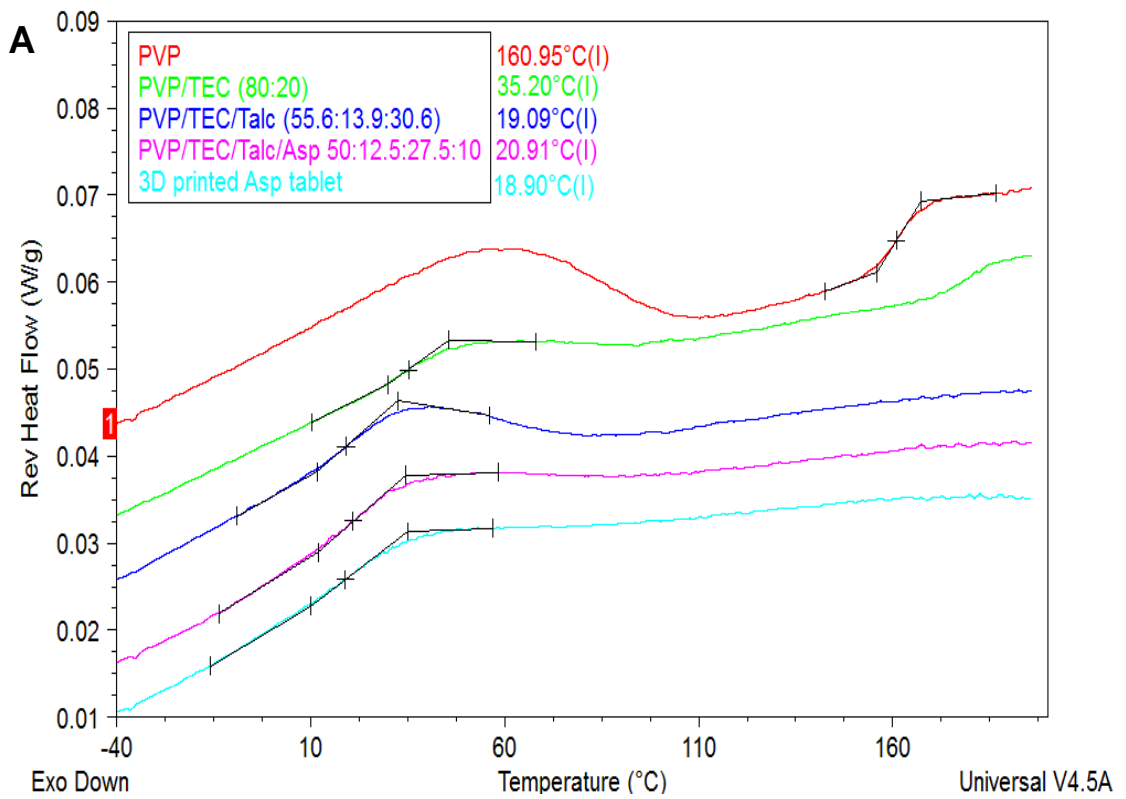


Figure 2.11. Reversing MTDSC thermographs of PVP, PVP:TEC filament, API-free and API-loaded filaments, and 3D printed tablets for Aspirin (A) First heat-scan and (B) second heat-scan).

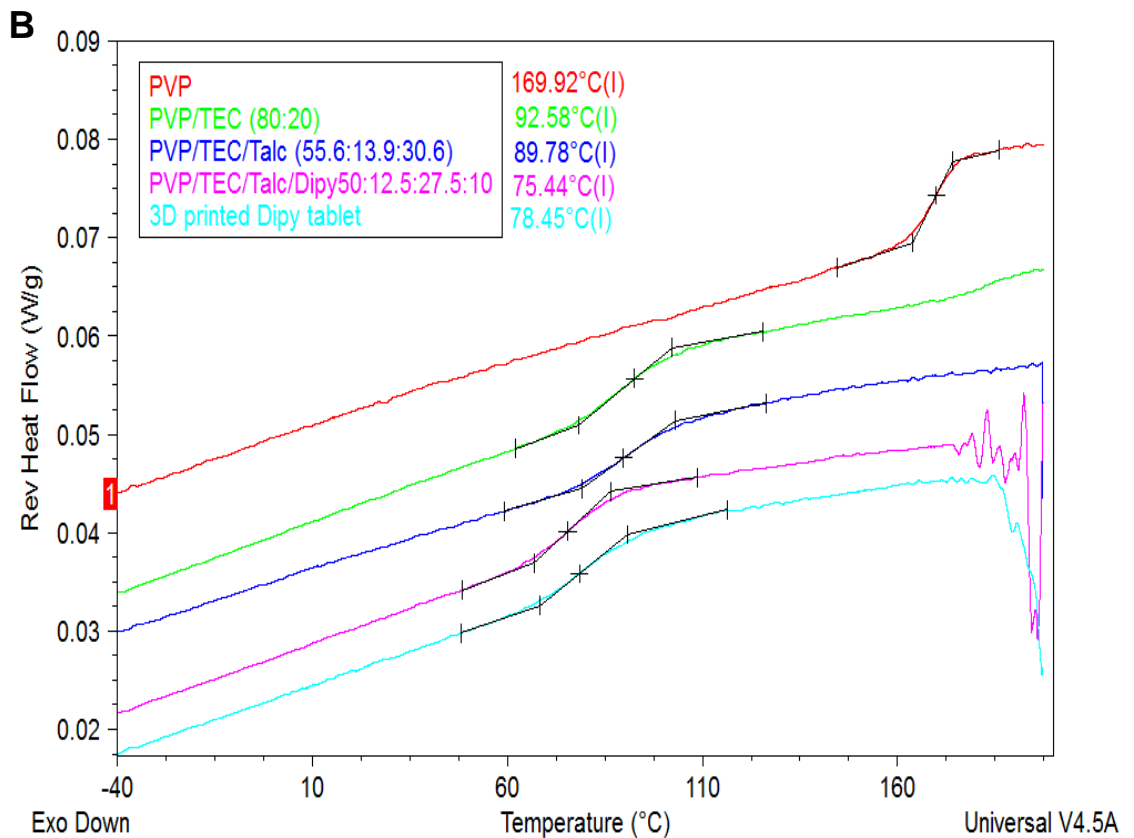
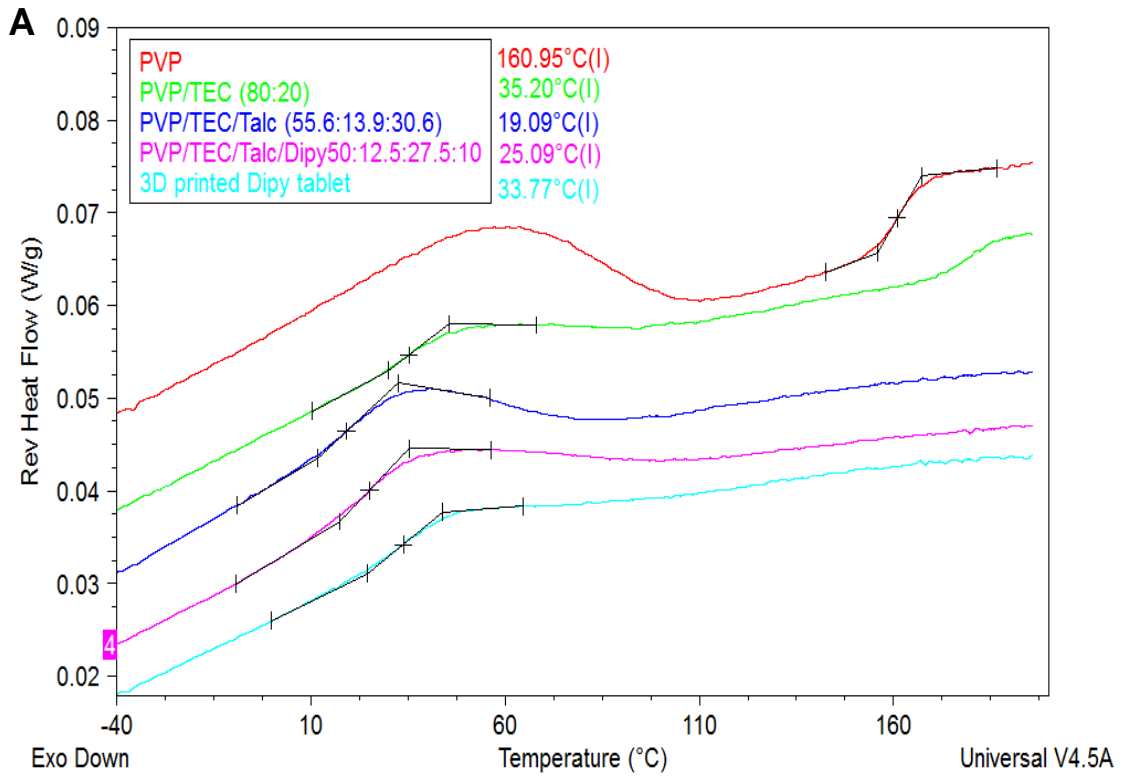


Figure 2.12. Reversing MTDSC thermographs of PVP, PVP:TEC filament, API-free and API-loaded filaments, and 3D printed tablets for dipyrindamole (A) First heat-scan and (B) second heat-scan).

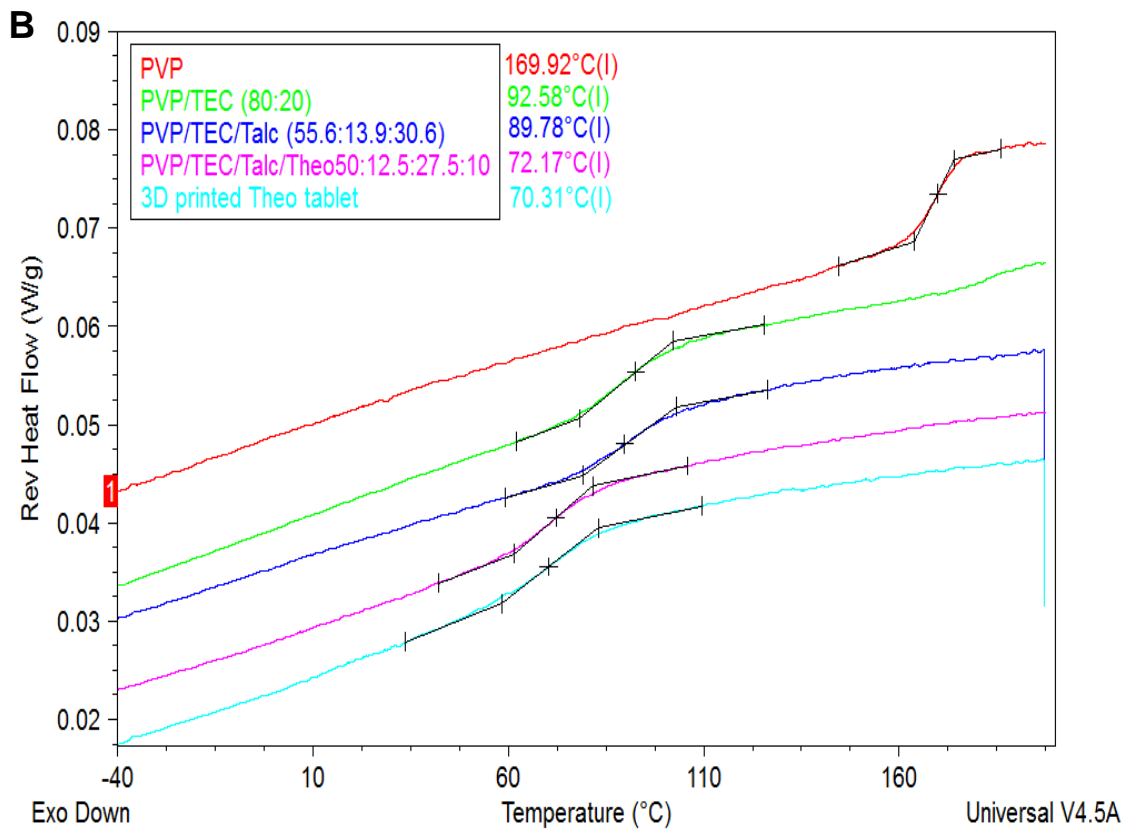
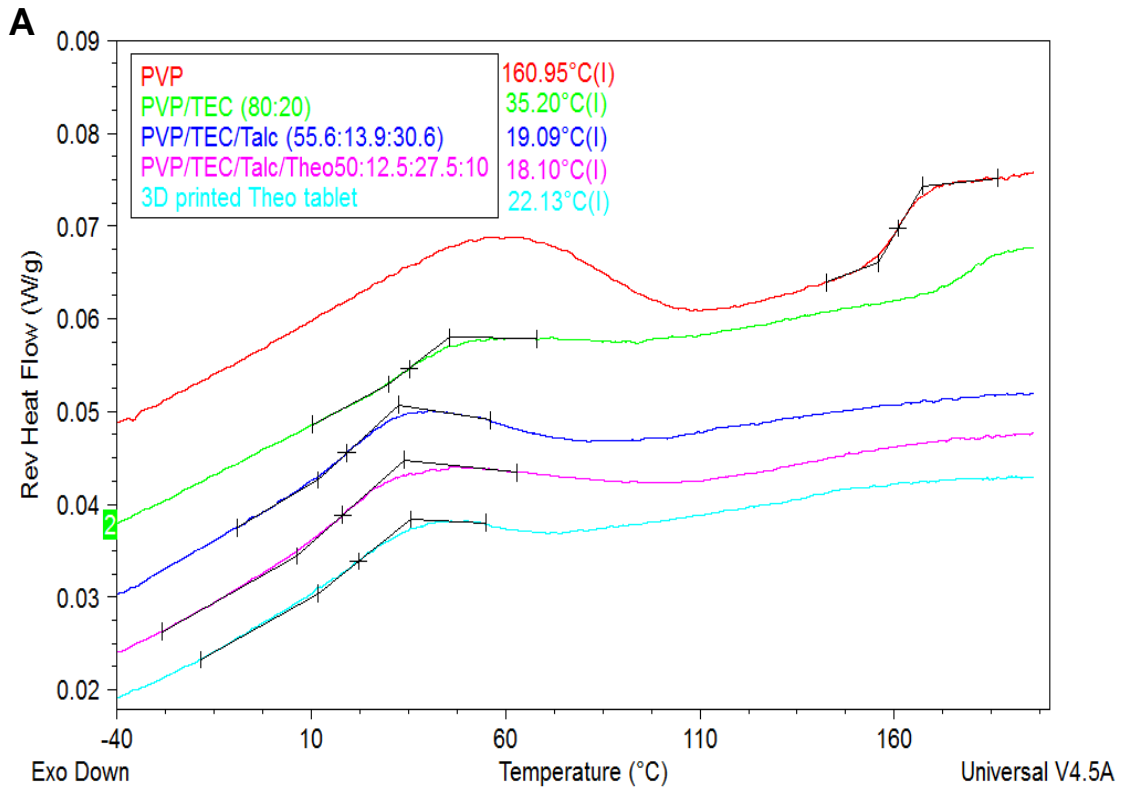


Figure 2.13. Reversing MTDSC thermographs of PVP, PVP:TEC filament, API-free and API-loaded filaments, and 3D printed tablets for theophylline (A) First heat-scan and (B) second heat-scan).

Initial investigation into the physical forms of the drug in the filaments after processing by HME and 3D printing was carried out using MTDSC, where the presence of a drug peak due to its melting point indicates crystallinity and a shift in baseline (T_g) or the absence of peaks indicates an amorphous formulation. The non-reversible heat flow from the MTDSC result of the actives alone demonstrated peaks due to the melting point of aspirin, dipyridamole and theophylline at approx. 137, 165 and 271 °C respectively (Figure 2.14A, B, C). However, processing these actives with the polymer and the other excipients resulted in the absence of these drug peaks for the three actives which was also observed after the 3D printing processes. This was expected as when actives are dispersed at the molecular level in a polymer matrix, the system therefore exhibits the properties of the polymer due to its crystalline inhibition properties.

To further confirm this observation, an X-ray powder diffraction analysis technique was used. The XRPD pattern for aspirin alone showed peaks at $(2\theta) = 7.98, 15.80, 22.85, 23.39, 27.05^\circ$ (Figure 2.15A). However, this was absent in the aspirin loaded filament and tablets indicating no crystalline presence in the PVP matrix. This was also the case for dipyridamole loaded filament and tablets (Figure 2.15B) which showed the absence of peaks at $(2\theta) = 10.13, 17.89, 18.91, 20.42, 20.98, 23.65, 26.12, 28.49, 30.45^\circ$. XRD spectra for theophylline alone elucidated diffraction peaks at $(2\theta) = 7, 12, 14$ and 24° analogous to previous findings (Räsänen et al., 2001). However, the presence of some peaks at $(2\theta) = 12$ and 7° (Figure 2.15C) indicated that a percentage of theophylline remained in the crystalline form. This contradicted the initial finding about the physical form of theophylline using DSC technique. In another research, a polymer matrix with PVP remained amorphous at up to 20 % drug loading (LaFontaine et al., 2016). However the investigated active was a micronised greseofulvin and the nature of the active and its interaction with the polymers plays a key role in the type of solid dispersion formed. In addition to these findings, it was observed that talc remained in its crystalline form in all the formulations with peaks at $(2\theta) = 9.44, 19.03$ and 28.66° from talc alone remaining present after processing by HME and 3D printing. The application of XRPD in the determination of physical forms of actives and excipients seems to be a more reliable technique since it is non-invasive and relies on x-ray diffractions from crystal patterns in a sample. This is unlike DSC which involves the use of thermal energy which might change the behaviour of the polymer matrix. In this regard, it was concluded that some portion of theophylline remained in their crystalline form after these processes. Drugs are more soluble when in their amorphous forms, therefore it will be interesting to determine how this affects the solubility of the theophylline loaded caplets in comparison to the other actives.

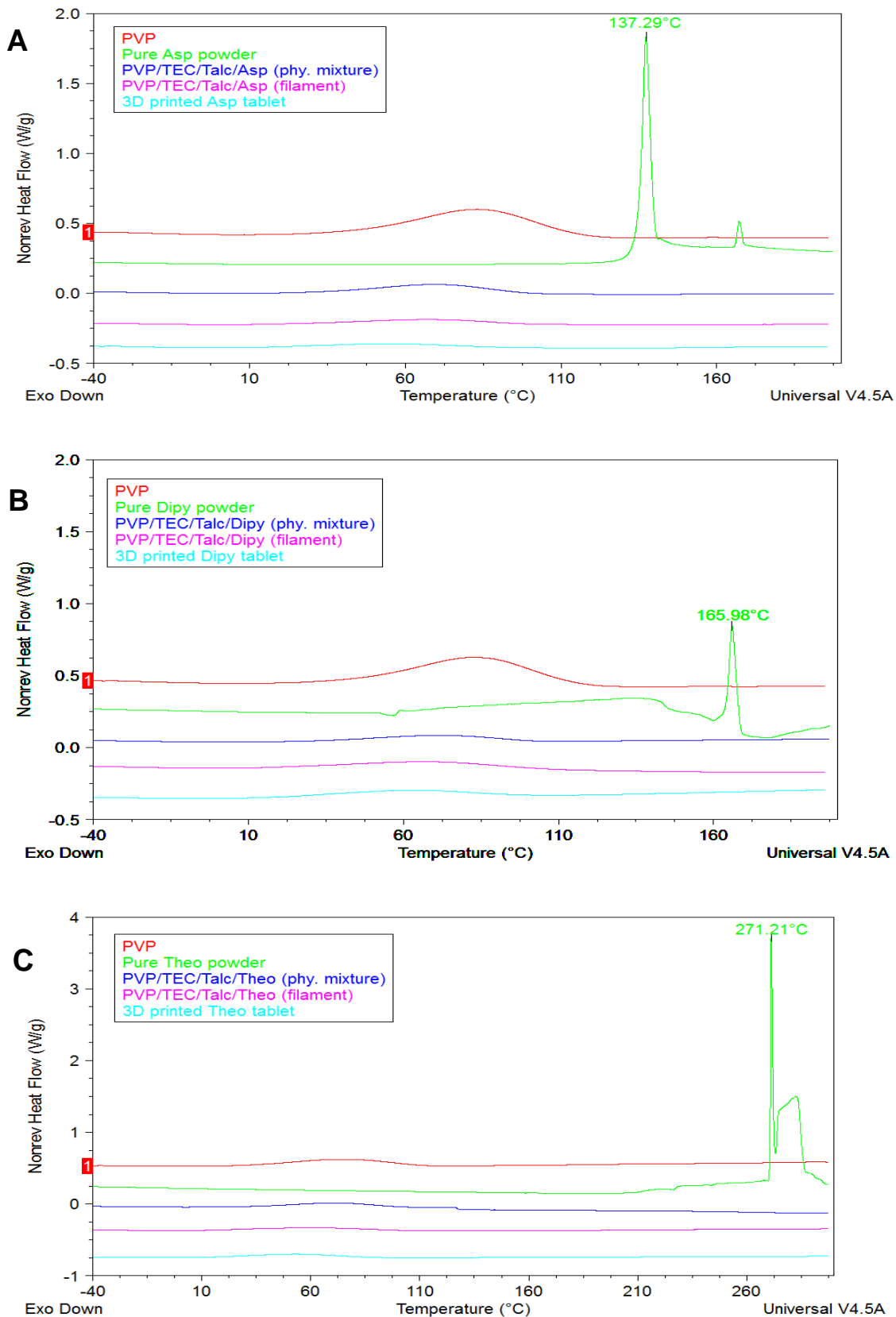


Figure 2.14. Determination of the physical form of the actives before and after processing using HME and 3D printing for (A) aspirin, (B) dipyrnidamole and (C) theophylline.

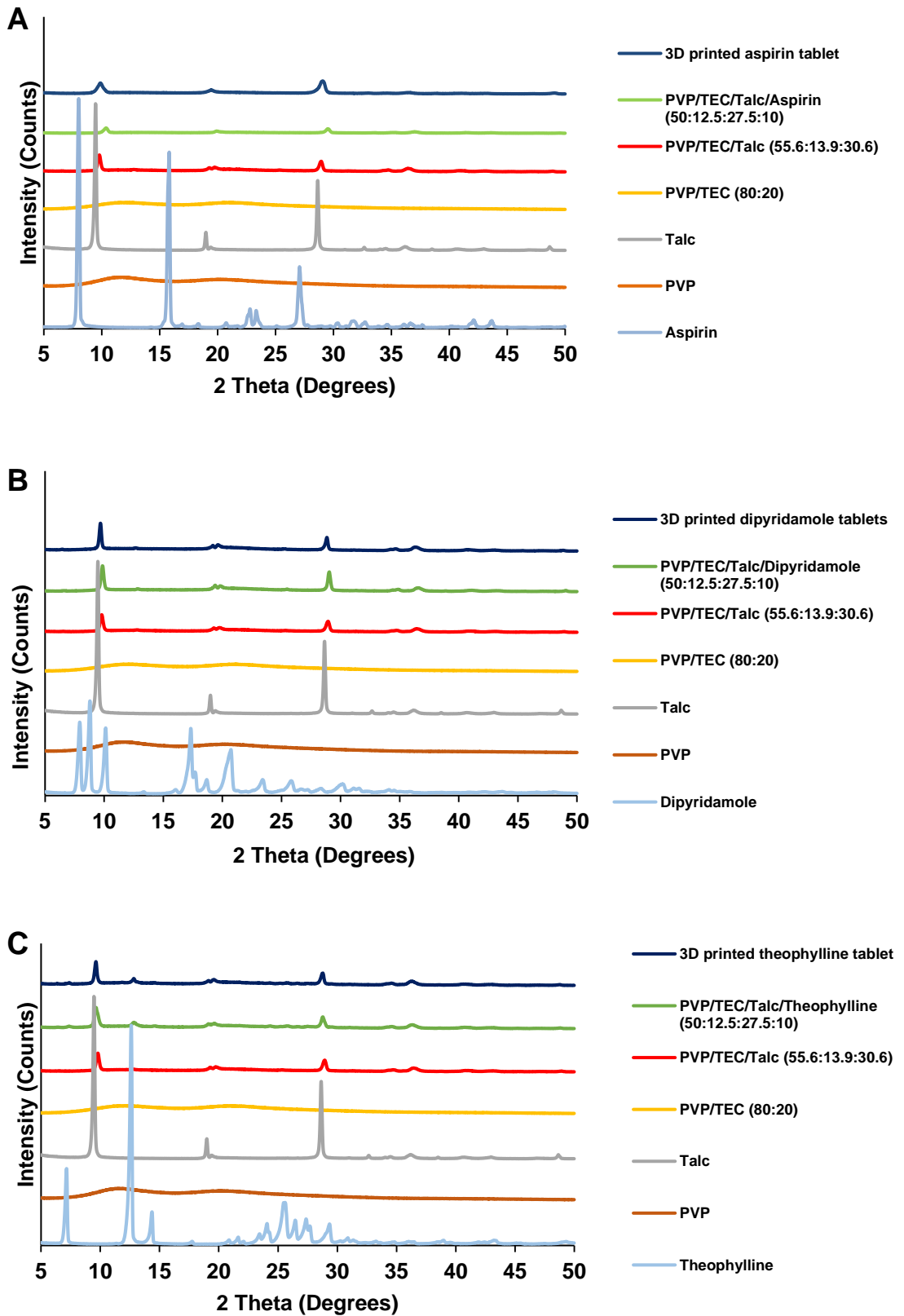


Figure 2.15. XRPD patterns of PVP, PVP:TEC filament, API-free and API-loaded filaments, and 3D printed tablets for aspirin (A) dipyridamole (B) and theophylline. (C).

The 3D printed tablets demonstrated adequate mechanical properties, demonstrating a high crushing strength with 0 % friability. This high crushing strength was attributed to the tablet manufacturing mechanism which involves a layer-by-layer deposition of material fused as a result of heat in addition to the plasticity of the polymer. For conventional tablet, crushing strength depends on compaction pressure during tableting and the quantity of binder used during the formulation. Although this is an unofficial test, it could affect the rate of tablet disintegration which could be improved using super disintegrants for conventional tablets. The 3D printed caplets were able to disintegrate before 15 min (Table 2.2) which was the required criteria for immediate release dosage forms irrespective of the high crushing strength without the need for disintegrants. Weight variations were observed for the 3D caplets which could be as a result of irregularity in the filament diameter or as a result of accumulation of particles in the 3D printer nozzle especially from the insoluble and non-melting component of the formulation (talc). However, these weight variations did not reflect in the dimensions of the tablets of the same formulation (deviation was ≤ 0.15) (Table 2.3), which might be related to materials distributions in the filament which result in layers of similar dimension having different weight. Variations in weight and dimensions were noticed between the different formulations. Moreover, the theoretical dimension of the caplets was higher than the actual dimensions obtained after 3D printing demonstrating the need to optimise the technology for pharmaceutical purposes to ensure more accurate dispensing.

To determine the effect of the processes on the model drugs, HPLC analysis was carried out on the produced filaments to check for the effect of the HME, and on the drugs and the 3D printed tablets to check for the effect of the FDM. Drug contents of $102.60 \pm 0.59\%$ and $101.18 \pm 3.9\%$ ($p > 0.05$), 100 ± 0.09 and 99.56 ± 0.48 ($p > 0.05$) of the actives was recovered for dipyridamole and theophylline respectively from the filament (after HME) and 3D printed tablets (Table 2.4). This level of drug recovery after these processes was attributed to the low operating temperature of the optimised PVP polymer ($110\text{ }^{\circ}\text{C}$) on the FDM. This might not be the case for the commercially available PVA or PLA filaments usually printing above $220\text{ }^{\circ}\text{C}$ since dipyridamole and theophylline starts degrading at approx. $230\text{ }^{\circ}\text{C}$. Drug degradation was observed for the hot melt extruded aspirin-PVP formulation and 3D tablets ($p < 0.05$). However, these findings are not conclusive. Aspirin is a sensitive molecule and could be easily hydrolysed into salicylic acid and acetate. Therefore, this degradation could be during the extraction of the drug from the filament and the 3D tablets since water was used. Besides the TGA analysis revealed no mass loss at the processing temperatures, therefore it was concluded that optimising the extraction of aspirin will avoid this degradation.

Table 2.2. Physical characterisation (Weight uniformity n=20, Crushing strength n=3, Disintegration n=6).

| Drug | Weight Uniformity ±SD (mg) | SD% | Friability (%) | Crushing strength (N) | Disintegration time (min) |
|---------------------|---------------------------------------|------------|-----------------------|------------------------------|----------------------------------|
| Aspirin | 112.05 ± 4.58 | 4.09 | 0 | 411.33 ±15 | 8 |
| Dipyridamole | 121.68 ± 9.28 | 7.63 | 0 | 432.67 ±24 | 10 |
| Theophylline | 111.01 ± 5.30 | 4.78 | 0 | 353.00 ±22 | 13 |

Table 2.3. The dimensions of the 3D printed tablets (n=6).

| 3D printed tablets | X ±SD (mm) | Y ±SD (mm) | Z ±SD (mm) |
|---------------------------|-------------------|-------------------|-------------------|
| Theoretical values | 10 | 3.96 | 3.64 |
| Aspirin | 9.41 ±0.05 | 3.74 ±0.13 | 3.53 ±0.11 |
| Dipyridamole | 9.23 ±0.15 | 3.86 ±0.09 | 3.80 ±0.12 |
| Theophylline | 9.43 ±0.07 | 3.65 ±0.02 | 3.54 ±0.08 |

Table 2.4. Drug content analysis using HPLC (n=3).

| Active ingredient | Drug content before HME | Drug content after HME (%) ±SD | Drug content After 3D printing (%) ±SD |
|--------------------------|--------------------------------|---------------------------------------|---|
| Aspirin | 100 | 83.65 ±0.96 | 89.07 ±2.04 |
| Dipyridamole | 100 | 102.60 ±0.59 | 101.18 ±3.91 |
| Theophylline | 100 | 100.23 ±0.09 | 99.56 ±0.48 |

The immediate release properties of the PVP loaded drug was demonstrated using an *in vitro* dissolution studies. It was observed that more than 85% of the actives were dissolved within 30min for the three drugs (Figure 2.16), therefore compliant with the British pharmacopeia standards. However, dipyridamole and theophylline had a faster drug release percentage at 30 min, with aspirin formulation being significantly slower ($p < 0.05$). This might be as a result of the effect of the acidic media on the degree of ionisation of aspirin. The fast dissolution of the formulations was attributed to the amorphous nature of the polymer and hence the amorphous nature of the drug after been dispersed in the polymer, leaving the drug with the fast dissolving properties of the polymer (PVP). Theophylline is also highly soluble in an acidic pH and therefore some portion of it being in the crystalline form as observed from the XRD results might not affect its rate of dissolution. In this study, it seems to demonstrate the fastest dissolution rate.

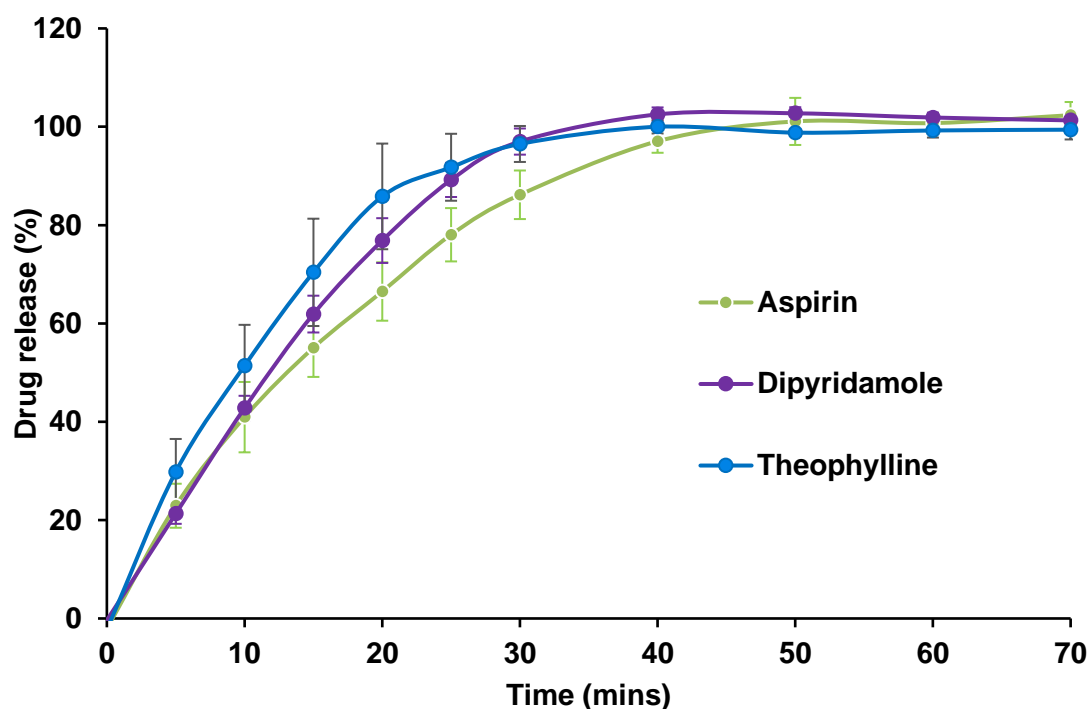


Figure 2.16. Immediate drug release profile from PVP 3D tablets (n=3).

2.6 Conclusions

By combining FDM with HME, it was possible to fabricate 3D printed caplets with immediate release properties based on PVP and talc as a matrix former and a thermostable filler. The PVP-based filament was suitable for three model drugs (aspirin, dipyridamole and theophylline) which was successfully 3D printed into caplets and characterised. These loaded actives with the exception of theophylline became amorphous in the extruded filament and 3D printed caplets. The excipients and APIs were stable within the HME and 3D printing processing temperature with the exception of aspirin which degraded during this process. This was however attributed to the method used in the extraction of aspirin for HPLC analysis since there was no weight loss at the processing temperatures when analysed using TGA. This could be as a result of the high sensitivity of the molecule to hydrolysis which could break it down into salicylic acid and acetate.

The manufactured tablets showed excellent mechanical properties and was still able to disintegrate before 15 min falling into the BP criteria for immediate release dosage forms. To the authors' knowledge, this is the first report of employing PVP in FDM 3D printing and a rare example of employing the process to produce immediate release caplets. The reported approach can be employed to fabricate patient-tailored caplets at relatively lower temperature (110 °C), using pharmaceutically approved and solubility enhancing polymer. This work confirms the possibility of expanding the use of FDM 3D printing to a wider range of APIs for on-demand fabrication of immediate release products. It also opens doors for the use of other pharmaceutical grades polymers with various release profile to encouraging the fabrication of more complex release profiles as will be discussed in the next chapter.

Chapter 3 : Fabricating a Shell-Core Delayed Release Tablet Using Dual FDM 3D Printing for Patient-Centred Therapy

3.1 Introduction

Latest advances in pharmacogenomics and clinical trials have put more emphasis on individualizing treatment in a patient-centred health care (Raijada et al., 2013). One important aspect of personalizing treatment is having the ability to individualise dosage forms to every patient's need. This has been carried out over the years with no consideration to the genetic makeup of the patients, rather the age and weight of the patients are considered during dosing, especially for infants and children. Splitting of tablets to personalise doses has been associated with dose variation (Habib et al., 2014, Peek et al., 2002) as the method of splitting and patient's/caregiver's competence plays a key role in the dosing accuracy. Moreover, the splitting of coated tablets physically compromises the barrier function of the coating, rendering dose adjustment impractical for delayed and other modified release tablets (Noviasky et al., 2006).

One potential solution in the dose personalising of tablets is the on-demand manufacturing using a benchtop 3D printer (Skowyra et al., 2015) especially the use of FDM 3D printing. This approach offers several advantages to both healthcare workers and patients, which includes flexibility in modifying the dose, shape and size of the dosage form in response to patient's or healthcare staff's needs (Alhnan et al., 2016) and also offers the potential of being able to do so at the point of care. At the point of this research, there has been no report of an enteric drug release dosage form produced using an FDM 3D printer. It will be of great benefit to be able to achieve personalisation of dosage forms with such release properties and bring the use of 3D printers closer to being a universal personalised dosing equipment.

Enteric coated dosage forms are usually achieved by film coating in conventional manufacturing and involves two main steps; i) production of an API-loaded core, and ii) coating the core with synthesized or semi-synthesized polymers (Nollenberger and Albers, 2013, Sakae and Hiroyasu, 2008). This makes the process time consuming and therefore difficult to apply for personalised dosing. Coating could be carried out using the coating techniques explained in chapter 1, Section 1.3.2, with the primary aim of creating a thin polymeric film on the drug loaded core/substrate. Enteric coating is a functional film coating system designed to protect actives from the acidic environment of the stomach and prevent drug release which occurs only at the high pH environment of the small intestine. In addition, enteric coating also avoids side effects such as nausea or bleeding by protecting the stomach walls from the irritating effect of some actives.

Tablet coating is typically performed in large batches, with coating efficiency relying on the tablet mixing dynamics, tablet size and shape and the coating method used. Coating

is usually monitored by substrate weight gains during the process as the coating material is applied. Over the years, this was deemed not efficient and research is now turning to more specific approaches to monitor coating efficiency to ensure that the function of the coating is achieved. This includes the use of terahertz in-line sensing (Lin et al., 2015) which is a non-destructive approach and was able to pick up alterations in coating thickness due to experimental changes during the research. Other techniques include the use of near-infrared frequencies and Raman spectroscopy (Romero-Torres et al., 2005). Insufficient coating or the presence of imperfection in the coating could result in ineffective gastric resistance, while too much of the coating material could result in a longer lag time before the drug is released in the intestinal area. The ionic strength, buffer capacity and the pH of the media used during the *in vitro* studies also affects the rate of polymer dissolution and drug release. In an example, bicarbonate buffer was demonstrated to provide a better *in vitro-in vivo* correlation in comparison to the use of the compendia phosphate buffer. Enteric release using several enteric polymers achieved a fast release after a pH change in the phosphate buffer which was not the case when carried out in the bicarbonate buffer media (Liu et al., 2011). Obvious release delays were noticed which seemed to correspond to the results obtained *in vivo*. These observations demonstrate the complex nature of obtaining such drug release profile.

Moreover, the chemistry of the polymer plays a major role in obtaining enteric drug release. A list of commonly used enteric polymers are shown in Chapter 1, Table 1.1. For this chapter, more emphasis will be laid on the applications of Eudragit L100-55 which is a methacrylic acid copolymer that is only soluble at $\text{pH} \geq 5.5$. Because of this property of the polymer, it finds use in enteric release and other forms of delayed release formulations in combination with other polymers. The application of a Eudragit L100 55-based polymeric film on tablets or pellets has been successful using conventional coating approaches (Qiao et al., 2013, Sauer and McGinity, 2009). In an example, a dry coating approach at 4 % coating level achieved 70 ± 4 % coating efficiency and was stable over 12 months. Drug release modification has also been demonstrated by compression coating which demonstrated adequate acid resistance and release at high pH values (Rujivipat and Bodmeier, 2010). It has also demonstrated compatibility with HME and has been used in the manufacturing of a drug polymer matrix for enteric release. This demonstrated acid resistance without the need for coating, which could be time consuming because of the nature of the process (Andrews et al., 2008).

According to the US Pharmacopeia, enteric products require a paradoxical criteria of no or limited drug release in the acid media (<10 %) followed by the release of 80 % of the actives in the intestinal phase within a certain time limit (Revision, 2007). These criteria

are usually met by applying a 30-100 µm thick polymeric film to a substrate. However, achieving such a demanding criterion via 3D printing technologies creates major technical challenges such as i) grafting a consistent protective shell within the resolution of 3D printers, ii) achieving adhesion and compatibility between the shell and core materials, and iii) coordinating simultaneous applications of the shell and core materials. Recent technological advances have made 3D printers available with multiple nozzles. Such advances paved its way in artistic designs (Hergel and Lefebvre, 2014, Reiner et al., 2014), for the manufacturing of composite elements (Dudek, 2013), as well as pharmaceutical applications. This also increases the chances of nozzle blockage during printing and creates more room for error when printing high resolution 3D objects even with the use of the commercial PVA filaments.

These challenges were reflected by the absence of literature reports utilising 3D printing technologies for the fabrication of delayed release shell-core tablets. Although a powder-based 3D printing technology have been reported for immediate and controlled release (Yu et al., 2007, Rowe et al., 2000, Katstra et al., 2000), no examples of delayed release tablets meeting the pharmacopeia criteria have been reported. One relevant attempt was the use of TheriForm technology (powder-based 3D printing) to manufacture a dual pulsatile release system composed of 3 chambers (Rowe et al., 2000). In the enteric chamber, an ethanolic solution of the enteric polymer was sprayed onto a mixture of lactose and MMC, resulting in a pH dependent behaviour and a drug release over 4 hrs in the intestinal phase.

With increased interest in FDM 3D printing of oral tablets for extended (Sandler et al., 2014a, Skowryra et al., 2015, Goyanes et al., 2015a) and immediate drug release (Sadia et al., 2016, Okwuosa et al., 2016, Pietrzak et al., 2015), few attempts have been reported utilising the technology for enteric tablets. For instance, FDM 3D printed PVA based tablets were coated with methacrylic polymer to target the colon using a conventional fluidized bed coater (Goyanes et al., 2015b). More recently, a double disc containing an enteric layer was fabricated by FDM 3D printing and the drug release from the disc was assessed using a test cell assembly (Melocchi et al., 2016). As far as the author knows, there have been no previous examples of complete production of delayed release tablets through 3D printing at the point of this research.

3.2 Aims and objectives

This research therefore aims at fabricating an enteric-coated tablet using a dual-nozzle single step FDM 3D printing process. To be able to achieve this, the following objectives will be carried out:

- Develop a Eudragit L100-55-based filament for FDM 3D printing
- Produce gastric-resistant tablets by employing a range of shell-core designs using polyvinyl pyrrolidone (PVP) and methacrylic acid co-polymer for core and shell structures respectively.
- To use theophylline as an initially model drug for its thermal stability, small molecular weight in addition to a high water solubility, rendering it an ideal model drug to test the efficiency of controlling drug release from the enteric system. Later, other model drugs commonly available as gastric-resistant products (budesonide and diclofenac sodium) were employed in this system.
- Characterise the actives, excipients and the formulations
 - Scanning electron microscopy (SEM)
 - Thermal analysis (DSC, TGA)
 - X-ray powder diffraction
 - Raman spectroscopy
 - Drug content
 - *In vitro* dissolution studies

3.3 Materials

3.3.1 Eudragit L100-55

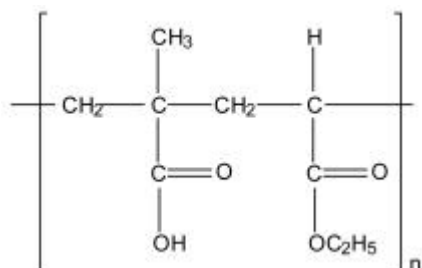


Figure 3.1. Chemical structure of Eudragit L100-55 (Hamman, 2010).

This is a methacrylic acid copolymer (Figure 3.1) with gastric resistance properties, dissolving only at pH ≥ 5.5 . This makes the polymer a perfect candidate for enteric drug delivery of actives that are acid-sensitive or mucosa aggressive. Evonik Industries (Darmstadt, Germany) donated Eudragit L100-55 for this research.

3.3.2 PEG400

This is a low molecular weight grade of polyethylene. It is a clear, colourless and viscous liquid with low toxicity leading to its various pharmaceutical applications. It has been used as a solvent, surfactant, plasticiser (Khan et al., 2015), suppository base and tablet (Fujimori et al., 2002) and capsule formulations. For this research, PEG400 was purchased from Sigma-Aldrich (UK)

3.3.3 Castor oil

Castor oil is a pale-yellow vegetable oil extracted from castor oil plants (*Ricinus communis*) with a boiling point of 313 °C. It is generally recognised as safe and finds use in the food industry as well as pharmaceutical formulations (Amaral et al., 2001). For this research, castor oil was purchased from Sigma-Aldrich (UK).

3.3.4 Oleic acid

This is a colourless and odourless oil occurring naturally in animal and vegetable fats and oil. It has a boiling point of 286 °C and finds use in the food industries and as an emulsifying or solubilising agent in the pharmaceutical industries. For this research, oleic acid was purchased from Sigma-Aldrich (UK).

3.3.5 Other ingredients

Theophylline was purchased from ACROS Organics (UK). Polyvinyl pyrrolidone (PVP, MW 40,000), triethyl citrate, tribasic phosphate (TBP) and dipyridamole were purchased from Sigma-Aldrich (UK). Talc was ordered from Fluka Analytical (UK). Scotch blue painter's tape 50 mm was supplied by 3M (Bracknell, UK).

3.4 Methods

3.4.1 Preparation of filaments using HME

For the preparation of the core filaments, a Thermo Scientific HAAKE MiniCTW hot melt extruder (Karlsruhe, Germany) was utilised. An optimised ratio of a powder mixture constituting of the polymer (PVP), plasticizer (TEC), filler [talc or tribasic phosphate sodium (TBP)] and API (Table 3.1) was adapted from previous study (Chapter 2) (Okwuosa et al., 2016). The mixture was gradually added to the HME and allowed to mix for 5 min at 100 °C to allow homogenous distribution of the molten mass. Afterwards, extrusion took place at 90 °C at a torque of 0.4 Nm and 1.25 mm nozzle size. Optimised filaments were also modified to include another two model drugs, budesonide (2.3 %wt) and diclofenac sodium (20 %wt). The change in drug concentration allowed achieving a representative dose for budesonide (3 mg) and diclofenac sodium (25 mg) from the model core. For the preparation of the shell, Eudragit L100-55, TEC and talc (50, 16.67 and 33.33%wt) were mixed at 135 °C for 5 min in a HME and extruded at 125 °C using 1 mm nozzle size.

3.4.2 Tablet design and printing

The core-shell tablets were designed in a caplet shape as described in Section 2.4.2 (Chapter 2). To assess the impact of shell thickness, several designs with increasing shell thicknesses (0.17, 0.35, 0.52, 0.70 or 0.87mm) were constructed. All the shell designs were complementary to the same core. Shell-core tablets were printed using modified settings of the software: Shell and core printing temperatures were 185 °C and 110 °C respectively and the platform was heated to 40 °C. The first layer, infill, inset and outline layers were printed at 12 mm/s extrusion speed and 50 mm/s travelling speed. The resolution was set as standard (200 µm layer thickness). In a separate experiment, to assess the impact of 3D printing resolution, the resolution of core-shell theophylline tablet with 0.52mm shell were printed at low, standard and high resolutions.

3.4.3 Thermal analysis

For modulated temperature differential scanning calorimetry (MTDSC) analysis, a differential scanning calorimeter (DSC) Q2000 (TA Instruments, Elstree, Hertfordshire, UK) was employed, using methods as previously reported in Section 2.4.3 (chapter 2).

To assess the impact of different lubricant on thermal stability of the PVP filament, TGA analysis was employed. Printed tablets, raw materials as well as extruded filaments were also measured using a TGA Q5000 (TA Instruments, Hertfordshire, UK). Approximately

10 mg of the samples were added to an aluminium pan without lid and heated from 25 °C to 500 °C at a heating rate of 10 °C/min. All measurements were carried out in triplicates.

3.4.4 X-ray Powder diffractometry (XRPD)

The physical form of model APIs in PVP, PVP: TEC filament, API-free and API-loaded filaments, and 3D printed tablets were assessed using a powder X-ray diffractometer, D2 Phaser with Lynxeye (Bruker, Germany). Samples were scanned from 2Theta (2θ) = 5° to 50° using the parameters as previously reported in Section 2.4.5 (chapter 2).

3.4.5 Determination of drug content

To examine the effect of HME and FDM 3D printing on the integrity of API, API-loaded filaments and 3D printed tablets, they were analysed for drug content prior and following HME as well as in the 3D printed tablets. Samples (API loaded filaments or tablets) were accurately weighed and placed in a 500 mL of 0.1M HCl, 1:1 water: acetonitrile mixture or phosphate buffer 6.8 for 2 hr under sonication for theophylline, budesonide and diclofenac sodium respectively. The solutions were filtered through 0.22 µm Millex-GP syringe filters (Merck Millipore, USA) and prepared for HPLC analysis.

Theophylline content in relevant samples was assessed using an Agilent UV-HPLC 1260 series (Agilent Technologies, Inc., Germany) equipped with XTerra RP C18 column (150 × 4.6 mm, 5 µm particle size) (Waters, Ireland) at a temperature of 40°C. The mobile phase consists of a 10 mM solution of ammonium acetate buffer, methanol and acetonitrile (86:7:7). Analysis was carried out at a wavelength of 272 nm, flow rate of 1 mL/min, injection volume was 5 µL and a run time of 7 min.

Budesonide content was assessed using an Agilent UV-HPLC 1260 series (Agilent Technologies, Inc., Germany) equipped with synergy max column at 30°C. A mixture of acetonitrile and pH 3 water (55:45) was used as a mobile phase. Analysis was carried out at a wavelength of 244 nm, flow rate of 1.5 mL/min, injection volume was 50 µL and a run time of 10 min.

For diclofenac sodium, samples were assessed using an Agilent UV-HPLC 1200 series (Agilent Technologies, Inc., Germany) equipped with synergy fusion column at temperature 30°C. The mobile phase was made up of methanol and pH 2 water (80: 20). Analysis was carried out at a wavelength of 280 nm, flow rate of 1 mL/min, injection volume was 10 µL and a run time of 10 min.

3.4.6 Scanning electron microscopy (SEM)

Quanta-200 SEM microscope at 20 kV was used to examine the surface morphology of the printed shell-core structures. Samples were placed on a metallic stub and then gold coated under vacuum using JFC-1200 Fine Coater (Jeol, Tokyo, Japan). Images of the tablets were also taken using a Canon EOS-1D Mark IV (Canon Ltd, Japan).

3.4.7 Raman Spectroscopy

Raman spectroscopy is a qualitative and quantitative analytical technique, which was named in the honour of the inventor, C.V. Raman (Raman and Krishnan, 1928). It consists of a light source, lenses, filters, prism and a sensitive detector all controlled by a computer system to enable analysis (Figure 3.2). Samples are illuminated with monochromatic laser beam which interacts with the molecules of the samples to produce a scattered light. A small part of the scattered light produces a frequency different from the incident light which is detected and used to construct the Raman spectrum (Bumbrah and Sharma, 2016).

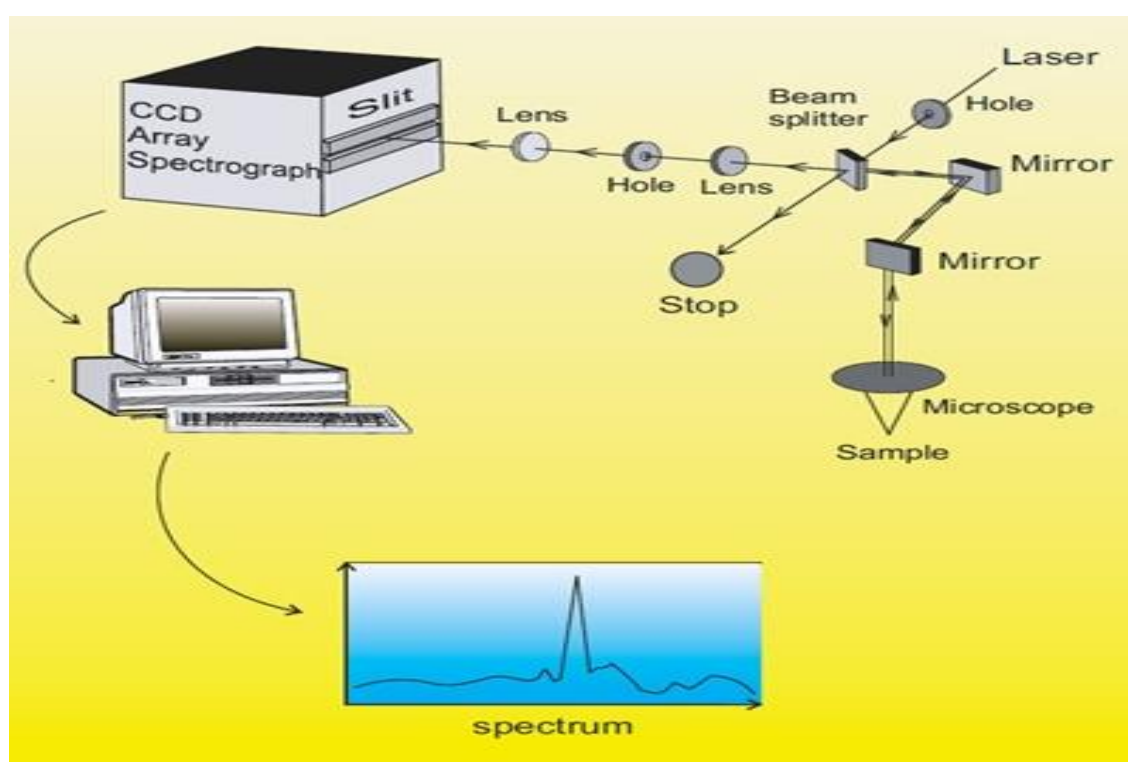


Figure 3.2. The components and working principles of Raman spectroscopy (Frejberg, 2013).

Raman spectroscopy (Horiba HR800, UK) was used to analyse and map the flat surface of the content of a 50% printed tablet. A green laser was used (532 nm) with 25 % filter and 600 grating. The slit and hole were set to 100 and 300 μm respectively. An

acquisition time of 2 sec was used with an accumulation of 5 scans per point. Samples were scanned from 1200 nm to 1800 nm with a step size of 150 nm. The band for theophylline was assigned a green colour, whilst a red colour was assigned to Eudragit L100-55. Labspec 6 spectroscopy software suite (Horiba Scientific, Japan) was used to process the data.

3.4.8 In vitro disintegration and dissolution studies

a. Disintegration tests. Disintegration studies were conducted following United States Pharmacopeia 30 standards (Revision, 2007). Six tablets were placed in the baskets of DT700 disintegration apparatus (Erweka, Germany) and were shaken for an hour in 0.1 M HCl. The gastric medium was then replaced with phosphate buffer pH 6.8. The experiment was continued and the time for complete disintegration of all tablets was recorded.

b. Acid uptake tests. To assess the ability of the 3D printed enteric shell to protect the core, three coated tablets were weighed individually prior to 2-hours exposure to 0.1 M HCl at 37 °C. The tablets were then drained off the acidic medium, dried with filter paper and weighted again. The acid uptake was calculated as follows:

$$\text{Weight gain (\%)} = [(\text{wet mass} - \text{dry mass})/\text{dry mass}] \times 100 \quad \text{Equation 3.1}$$

c. pH change dissolution test (phosphate buffer). *In vitro* drug release studies for all gastro-resistant tablets used in this study were conducted using an AT 7 Smart dissolution USP II apparatus (Sotax, Switzerland). Each experiment was carried out in triplicate in dissolution medium at 37 ±0.5 °C with a paddle speed of 50 rpm. The tablets were tested in 750 mL of a stimulated gastric fluid (0.1 M HCl, pH 1.2) for 2 h, followed by 4 hrs exposure to pH 6.8 phosphate buffer.

Within all the experiments the amount of released theophylline was determined at 5 min intervals by UV/VIS spectrophotometer (PG Instruments Limited, UK) at a wavelength of 272 nm and path length of 1 mm. Data was analysed using IDISis software (Automated Lab, 2012). For budesonide and diclofenac sodium, samples (2 mL) were manually collected at 15, 30, 60, 90, 120, 150, 165, 180, 210, 240, 300, 360, 420 and 480 min. They were then assessed using the HPLC methods outlined in the HPLC method described in Section 3.4.5.

d. pH change dissolution test (bicarbonate buffer). To assess the drug release pattern in a more physiologically relevant medium, an additional evaluation of drug

release was performed in pH 7.4 modified Krebs bicarbonate buffer. The latter better simulates the buffer capacity, pH and ionic composition of human gastric fluids (Fadda and Basit, 2005).

The dissolution test was carried out following the same protocol specified in Section 3.4.8c. For the first 2 hrs, tablets were exposed to 900 mL of 0.1 HCl (pH 1.2). Tablets were then retrieved from the acidic medium and introduced into 900 mL of modified Krebs buffer for an additional 4 hrs (1.18 mM KH_2PO_4 , 24 mM NaHCO_3 , 118.07 mM NaCl, 4.69 mM KCl, 2.52 mM CaCl_2 , and 1.18 mM $\text{MgSO}_4 \cdot 7\text{H}_2\text{O}$).

3.4.9 Statistical analysis

One-way ANOVA was employed using SPSS Software (22.0.0.2) to analyse the results. Differences in results of $p < 0.05$ were considered to be significant.

3.5 Results and discussions

Figure 3.3 provides a schematic illustration of the fabrication of 3D-printed shell-core enteric tablets. CAD software was utilized to design two complementary stereolithographic files to form a shell-core structure. Dual FDM 3D printer was employed with two different filaments; i) filament for enteric shell (Eudragit L100-55), and ii) filament for the core (API, PVP) processed through a HME compounder. Theophylline was used as a model drug to develop the enteric core structure due to its high solubility in acidic medium and small molecular weight, rendering it a major challenge for an enteric system (Alhnan et al., 2010).

Unlike single FDM 3D printing of theophylline (Okwuosa et al., 2016), frequent blocking of PVP filament (core) was encountered in dual FDM 3D printing. It is possible that whilst the first nozzle is printing, the filament in the second head remains at elevated temperature leading to material adherence to the inner wall of the nozzle head. To overcome the blocking of the nozzle, several additives were initially incorporated in the PVP filament composition. However, it led to the softening of the filament and rendered it incompatible with the gear of the 3D printer as they become easily compressed and flattened which results in the inability of the gears to pull down the filaments into the hot nozzle. An alternative solution was the use of lubricants with high boiling points (castor oil, oleic acid or PEG 400) to coat the surface of the filaments during 3D printing. All three liquids allowed successful printing of tablets without affecting the TGA patterns of the polymer (Figure 3.4A) or the dissolution rate of theophylline from the filaments (Figure 3.4B). It is likely that these liquids exhibit a lubricating rather than a protective effect and physically prevents the sticking of the filament to the internal wall of the nozzle, hence allowing smooth alternation between nozzles. Based on these findings it was decided to choose one lubricant, oleic acid to facilitate dual 3D printing.

Following the optimisation of the core matrix, it was possible to graft a shell material based on developing a filament comprising of Eudragit L100-55, TEC and talc at a ratio of 50, 16.67 and 33.33 %wt, respectively. Eudragit L100-55 is a methacrylic acid-ethyl acrylate copolymer (1:1) commonly used for the preparation of enteric solid dosage forms. Its unique structure gives it an enteric pH-dependent character, being soluble above pH 5.5 medium (Hao et al., 2013).

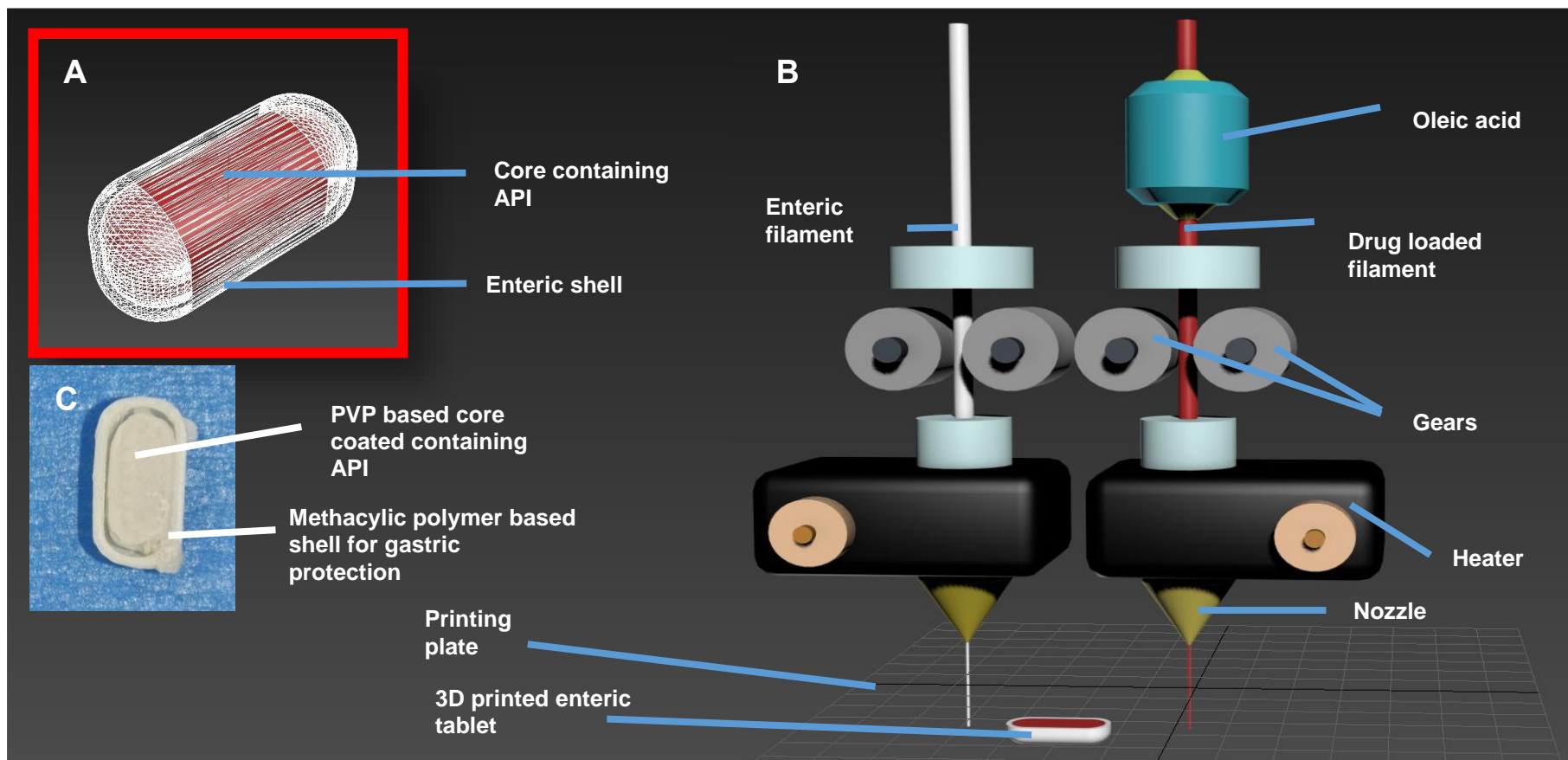


Figure 3.3. Schematic illustration of the fabrication of 3D-printed shell-core enteric tablet. (A) Two complementary stereolithographic files are designed via CAD software to create a shell-core structure (B) Dual FDM 3D printer is employed with two different filaments; i) filament for enteric shell (based on Eudragit L), and ii) filament core (based API, PVP) processed through HME compounder. A lubricating station is installed for PVP to facilitate the printing of the core during nozzle alternation. (C) Image of the 30% completed FDM 3D printer Shell-core.

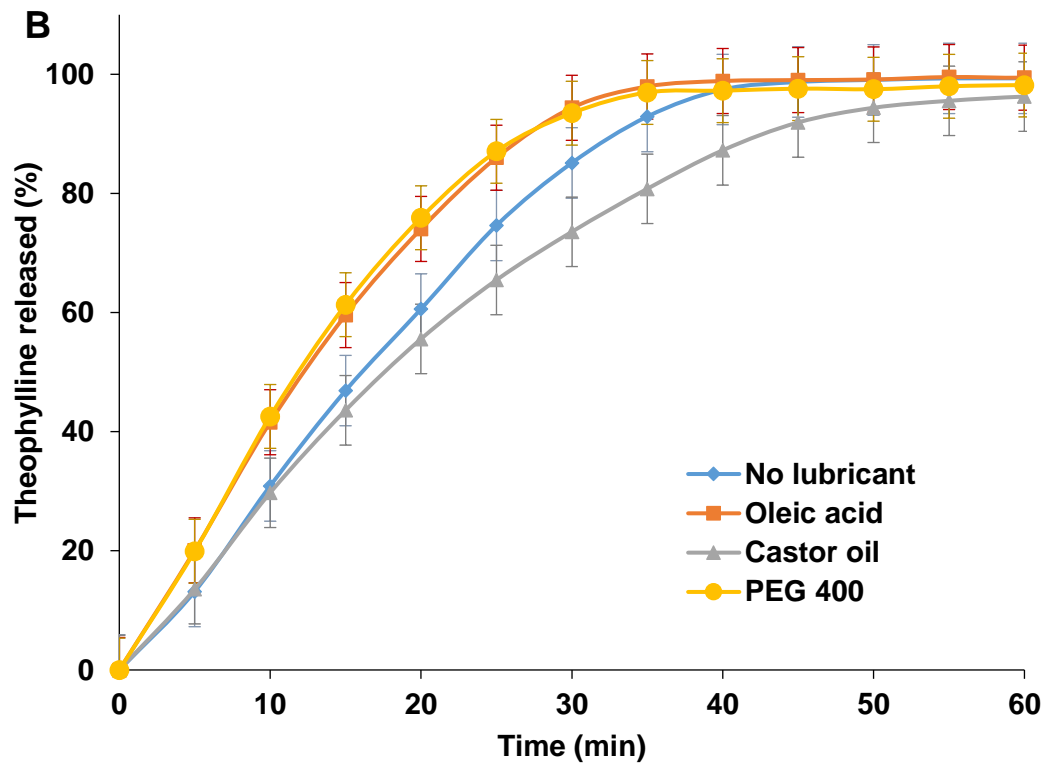
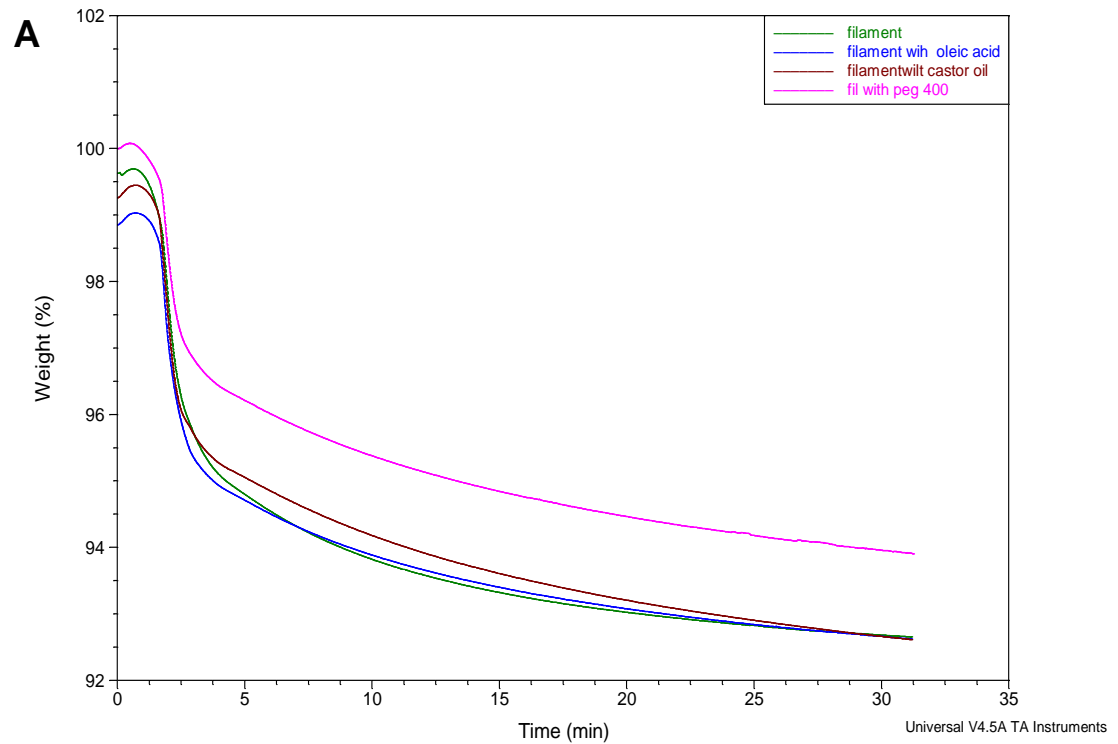


Figure 3.4. Impact of lubricants on (A) TGA thermal degradation profiles of PVP filament and (B) the in vitro release pattern of theophylline from core tablet.

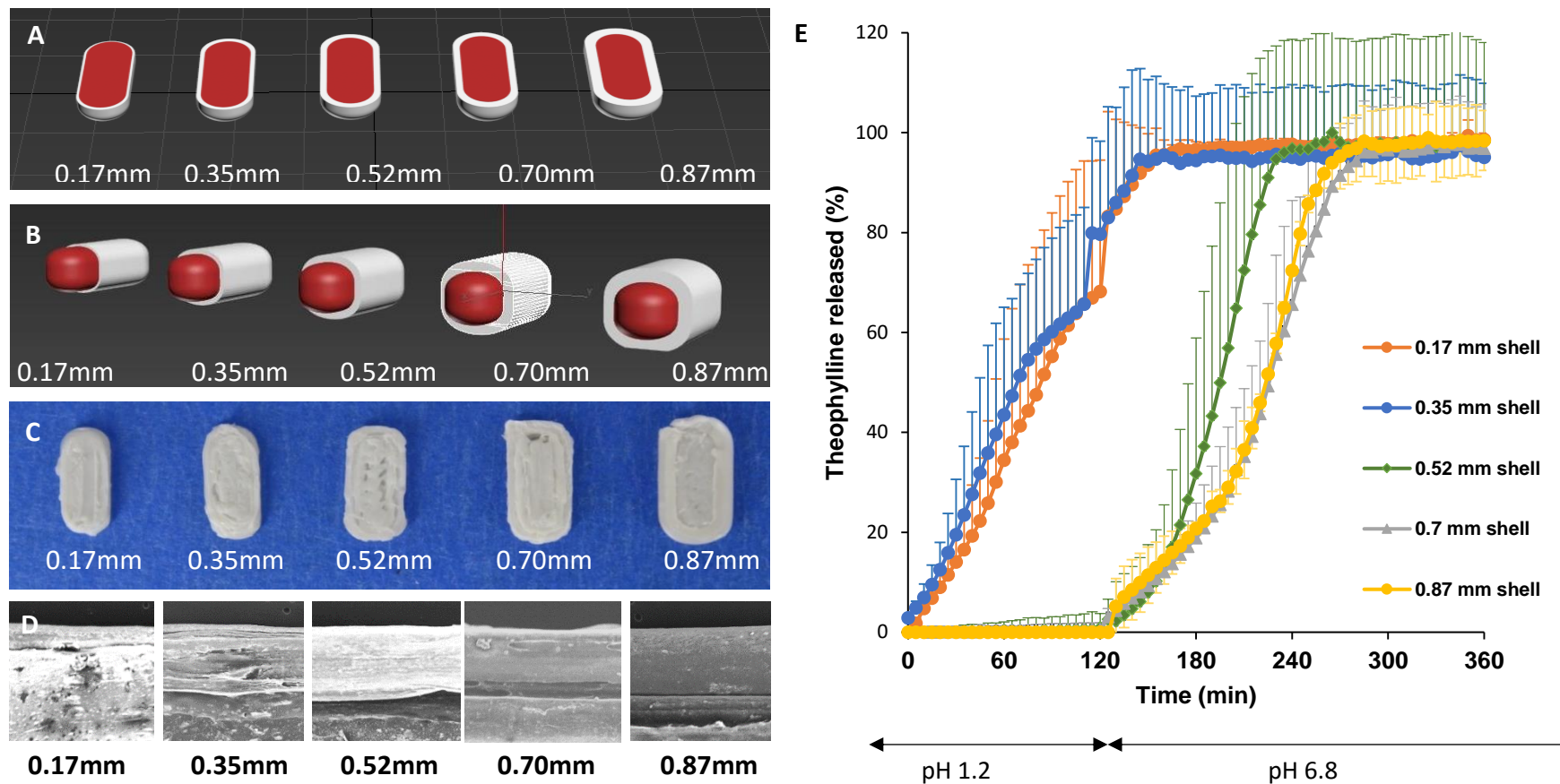


Figure 3.5. (A and B) Rendered images (Autodesk 3DS Max) of shell-core designs with increasing shell thickness (0.17, 0.35, 0.52, 0.70 and 0.87mm), (C) Images of 30% completed shell-core designs with theophylline core and increasing Eudragit L100-55 shell thickness, (D) SEM images of the surface of the tablets (E) Impact of shell thickness of 3D printing on in vitro release pattern of theophylline from 3D printed tablet in USP II pH change dissolution test.

The used ratio was deemed necessary to significantly lower the Tg of Eudragit L100-55 to 34.74 °C as obtained from the second scan of the MTDSC study, which was used to eliminate the impact of water loss on the Tg of the filament (Chapter 7: Supplementary Data, Figure 7.1) to allow continuous flow from FDM 3D printer's nozzle, whilst solidifying quickly to permit the formation of a well-defined structure. To adjust the pH response release pattern of core-shell structures, tablets with identical cores comprising of theophylline as a model drug were fabricated with increasing thicknesses of the Eudragit L100-55 shell (Figures 3.5A-D). *In vitro* dissolution tests indicated that thickness levels 0.17 and 0.35 mm led to a premature release of the drug in the acidic medium (Figure 3.5E). It is possible that these thicknesses only allowed the printing of 1-2 layers in the shell structure since the FDM 3D printer was operated at a standard resolution (0.2 mm). This was insufficient to provide a better protection in the acid media to prevent drug release. When a thicker shell design was applied (0.52, 0.7 or 0.87 mm), a superior control of drug release was achieved (<3 % of drug released after 120 min in gastric medium) in the acid media. This could be as a result of the formation of larger number of layers (3-5 layers), which is essential to construct a gastric-resistant barrier in the acidic medium. It is notable that the drug release in the intestinal phase (pH 6.8) followed a bi-phase pattern; a relatively slow drug release in the initial 45 min after pH change followed by a faster release after 45 min. It is possible that the first phase reflects the diffusion of the model drug through the eroding enteric shell layers, whilst a faster release takes place following the complete dissolution of the shell, where a water-soluble PVP-based core starts to dissolve. Such a pattern has been seen in shell-core structures (Goyanes et al., 2015d), where erosion of the external layer preceded the dissolution of the core.

The impact of FDM 3D printing resolution on the dissolution of shell-core structures was also investigated using 0.52 mm shell (Figure 3.6A) which was chosen as it was the smallest shell thickness required to provide acid resistance. The makeware software used to control the MakerBot FDM 3D printer provides the options of using high, standard or low printing resolutions corresponding to 0.1, 0.2 and 0.3 mm layer thicknesses respectively. Adjusting to a low resolution 3D printing, thereby reducing the number of layers to fabricate the shell due to a bigger extrudate resulted in a relatively slower response to pH change in comparison to high resolution (Figure 3.6B). This could be as a result of the creation of more gaps for drug release once the pH is changed since more layers were involved in the wall formation for the high resolution shell, unlike when fewer layers were used to create the same wall thickness as for the standard and low resolution 3D printing approach.

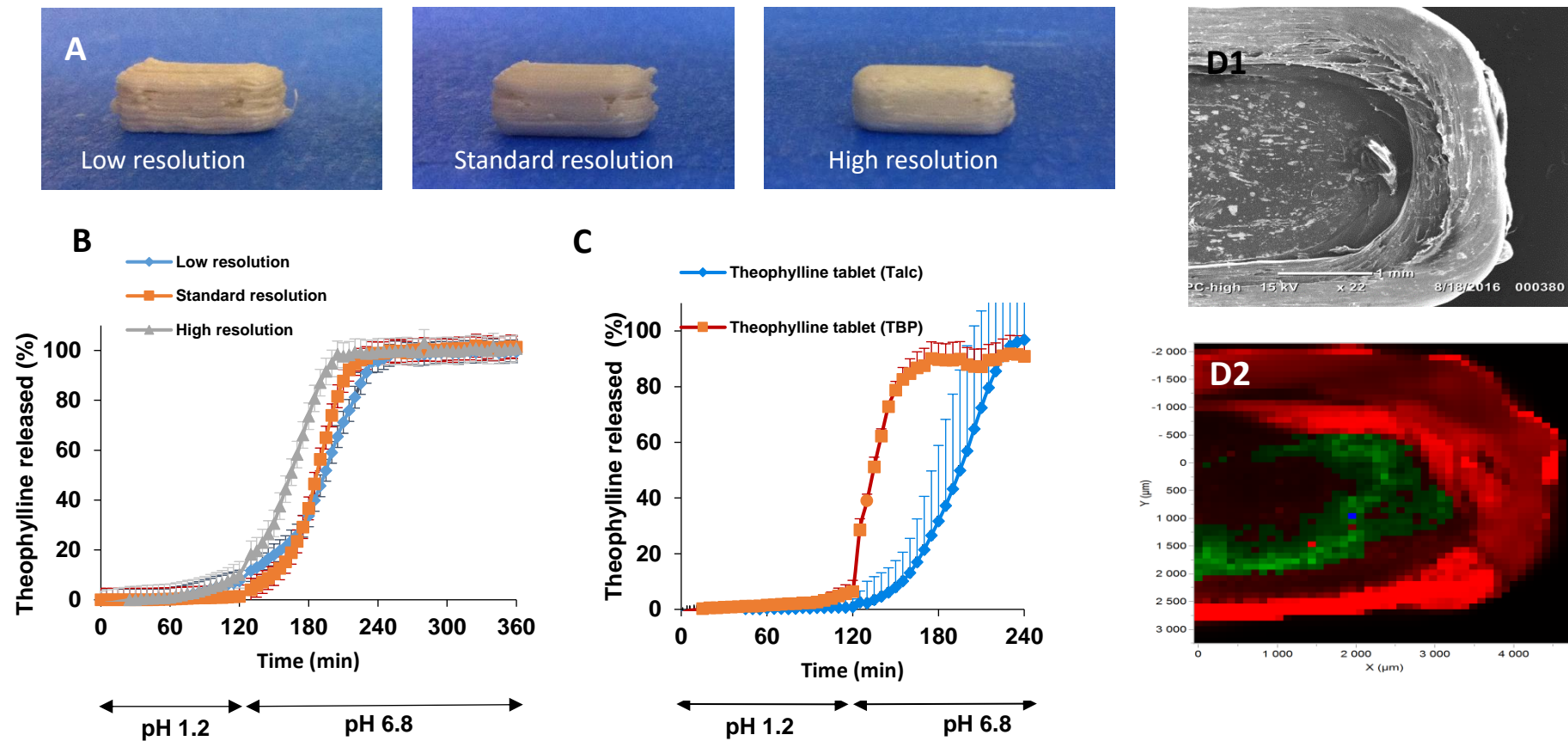


Figure 3.6. (A) Images of 3D printed enteric theophylline tablet printed with low, medium and higher resolution, (B) Impact of resolution of 3D printing on in vitro release pattern of theophylline from 3D printed tablet in USP II pH change dissolution test. (C) Impact of filler (TBP or talc) on the in vitro release pattern of theophylline from 3D printed tablets in USP II pH change dissolution test in phosphate buffer, (D1,2) SEM and Raman images (respectively) of a cross-sections of 0.52 mm thickness shell theophylline table.

However, the use of high resolution did not produce a release profile that fell within the pharmacopoeia standards. It is worthy to note that using FDM 3D printing, a much thicker shell layer was needed to achieve sufficient gastric resistant pattern in comparison to conventionally coated tablets with fluid-bed or pan coater (30-100 μm) (Thoma and Bechtold, 1999) which reflects the difficulty of producing a complete protective layer with a single layer of filament. Adjusting the printing resolution as expected influenced the overall appearance of the printed tablets as seen in Figure 3.6A with a higher resolution seeming to provide a better finish.

To accelerate drug release in the intestinal phase, an alkalinising agent, tribasic phosphate sodium (TBP), was examined as a filler to replace talc. The strategy allowed a much faster dissolution pattern in the intestinal phase (Figure 3.6C). It is likely that TBP in the core would dissolve with water imbibition upon pH change, leading to a rise in the local pH, resulting in acceleration of dissolution of Eudragit L100-55 shell and hence faster release of the API (Liu et al., 2009). A similar concept was used to reduce the lag time before drug release by using an inner layer coating neutralised to a high pH in addition to a buffer agent before the actual polymer coating (Liu et al., 2010). This demonstrated a potential method to improve drug release using polymers for lower GIT targeting. The use of TBP in this study for the core filament formulation was associated with a weight loss as revealed by its TGA analysis around the core processing temperature (Figure 3.7). To further confirm the compatibility of the system to the active, a HPLC analysis was carried out on the filaments and the 3D printed tablets which confirmed a significant drop in drug content (86%) (Table 3.1). These findings suggest that unlike talc which acts as an inert filler, TBP tends to react with theophylline at an elevated temperature leading to a significant drug degradation. Although the use of TBP produced a faster drug release that met the criteria of the BP, talc was considered as the filler of choice for this study. The investigation of other alkalinising agents that will be inert at an elevated temperature will be beneficial in a future work.

Raman spectral mapping was utilised to generate a detailed chemical image of the flat surface of a 50% complete 3D printed tablet (Figure 3.6D1). Integration of individual spectra to produce false colour representations of distribution for theophylline (green) and Eudragit L100-55 (red) elucidated a definitive separation between the core and the shell (Figure 3.6D2), suggesting the presence of theophylline in the core of the tablet with no signs of it diffusing into the Eudragit L100-55 shell.

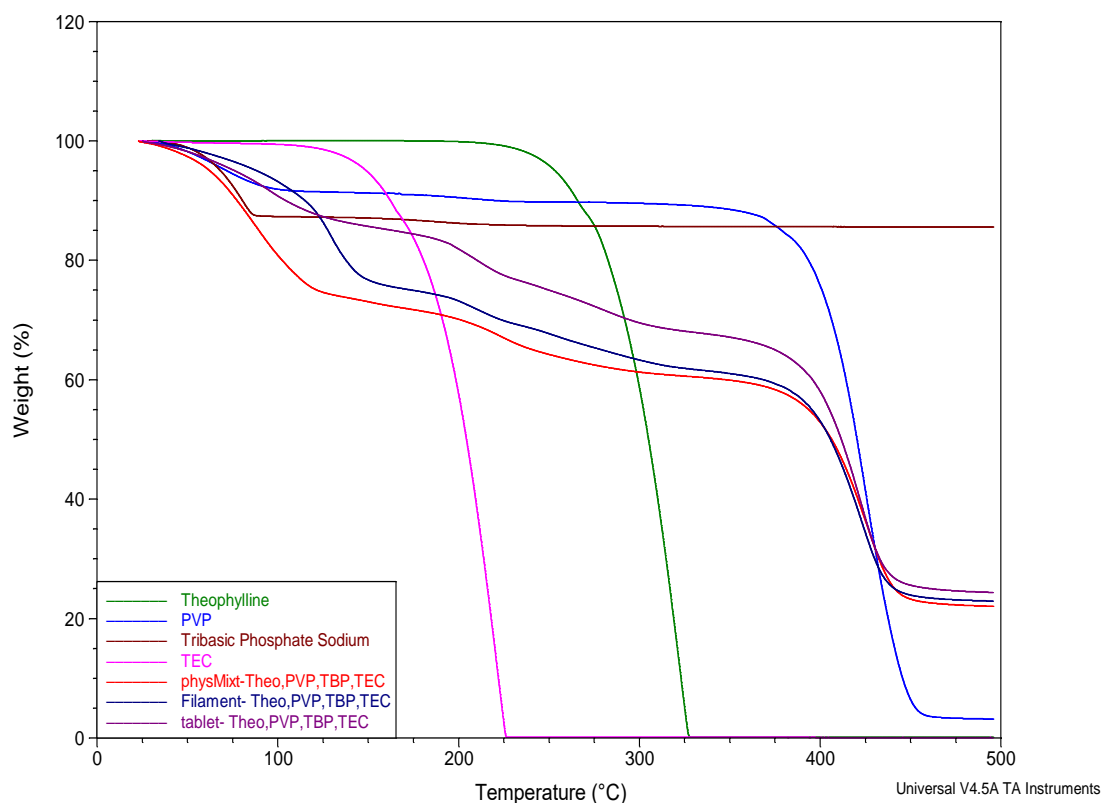


Figure 3.7. TGA thermal degradation profiles of the raw materials of; theophylline, PVP, TBP, TEC as well as the physical mixture, the filament and the 3D printed tablets.

Table 3.1. Summary of the compositions of API loaded filament and residual drug contents following HME and dual FDM 3D printing.

| Active ingredient | Contents (PVP, TEC, filler and drug) | Drug content after HME (%) \pm SD | Drug content after 3D printing (%) \pm SD |
|---------------------------------|--------------------------------------|-------------------------------------|---|
| Theophylline (Talc) | (50,12.5, 27.5 and 10%wt) | 100.23 \pm 0.09 | 99.56 \pm 0.48 |
| Theophylline (TBP) | (50,12.5, 27.5 and 10%wt) | 80.04 \pm 0.82 | 84.68 \pm 2.10 |
| Budesonide (Talc) | (50, 12.5, 35.2 and 2.3%wt) | 97.24 \pm 4.02 | 96.41 \pm 4.42 |
| Diclofenac sodium (Talc) | (45.5, 17.5, 17 and 20%wt) | 91.98 \pm 1.03 | 90.47 \pm 2.31 |

To prove the suitability of the system to different APIs, two other model drugs, budesonide or diclofenac sodium, were also examined by including them individually in the PVP-based filament. This further confirms the suitability of this filament for different actives as discussed in chapter 2. TGA thermographs (Figures 3.8A and B) showed a mass drop of PVP filaments around 100 °C due to water loss whilst a second major mass drop was also apparent at 400 °C due to the degradation of PVP. The thermal stability of both model APIs, similar to earlier studies, showed no further weight loss at temperatures <200 °C for budesonide (Goyanes et al., 2015b) and diclofenac sodium (Tudja et al., 2001).

Analogous to TGA results, DSC thermographs of PVP displayed a large endothermal event in the range of 50-110 °C due to water loss as established in Chapter 2 (Okwuosa et al., 2016). This was attributed to the hygroscopic nature of PVP (Verdonck et al., 1999). Our previous investigation using modulated heat-scan and heat-cool-heat scan indicated that water content plays a major role as a plasticiser for PVP filament (Okwuosa et al., 2016). The Tg of PVP filament (plasticised with TEC) were in much lower range (19-35 °C) than expected from Gordon-Taylor equation ($T_g = 82.3$ °C). However, the Tg obtained in the second heat flow was 93 °C.

The addition of budesonide appeared to have a limited effect on the Tg of the filament and the tablet (Figure 3.9). This might be due to the limited concentration of budesonide in the product (2.3%). In case of diclofenac sodium, when same level of plasticization was initially investigated (12.5%), a brittle filament was produced with a higher Tg (44.89 °C) (Chapter 7: Supplementary Data, Figure 7.2). In fact, a high level of plasticization (TEC 17.5%) was deemed necessary to produce a compatible filament, this was reflected with a shift of Tg upon the addition of diclofenac sodium to 16.27°C (Figure 3.10A). The addition of theophylline on the other hand as reported in our earlier work led to a depression in the Tg of the filament (Okwuosa et al., 2016). Such a shift can be attributed to the plasticising effect of theophylline (Nair et al., 2001).

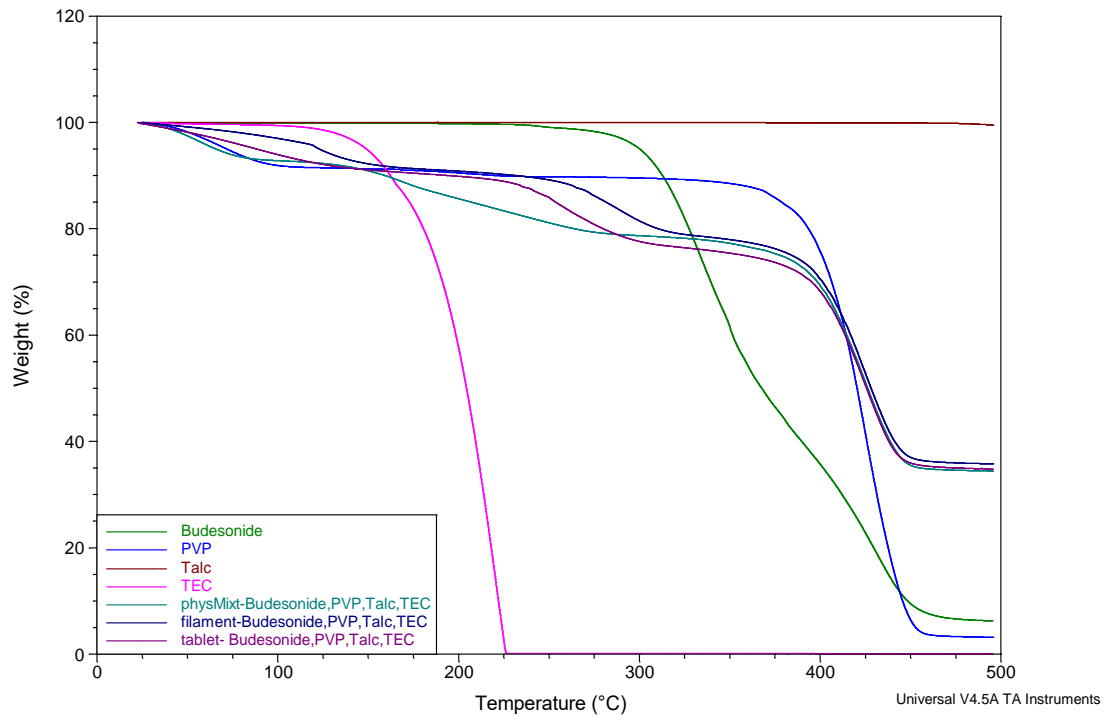
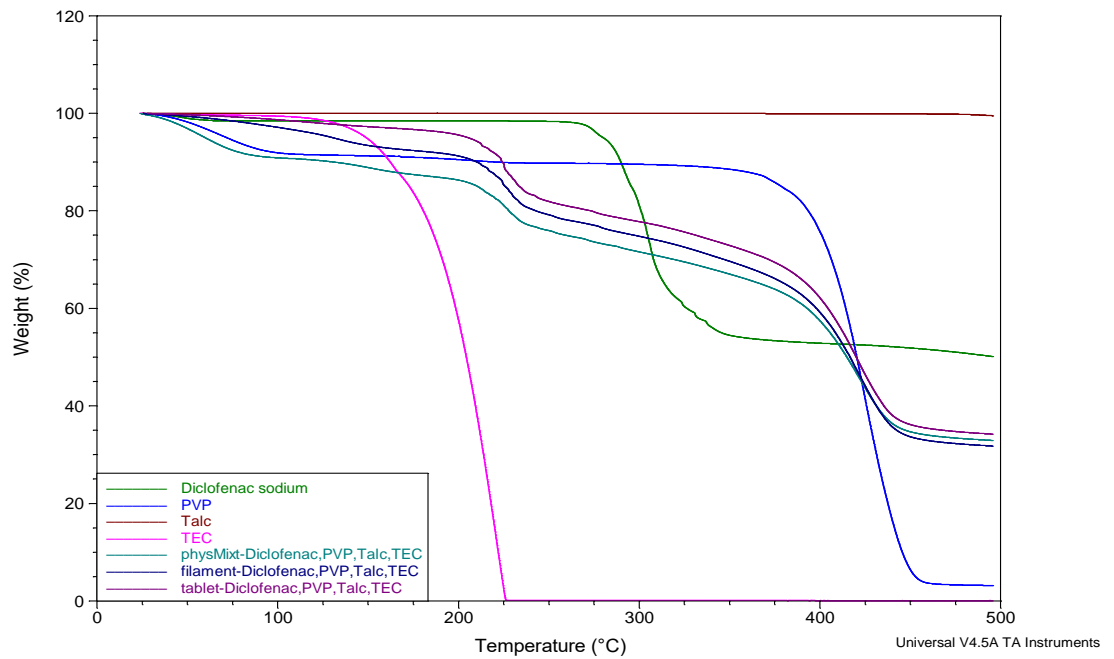
A**B**

Figure 3.8. TGA thermal degradation profiles of TEC, PVP, PVP:TEC filament, API-free and API loaded filaments, and 3D printed tablets for (A) budesonide and (B) diclofenac sodium.

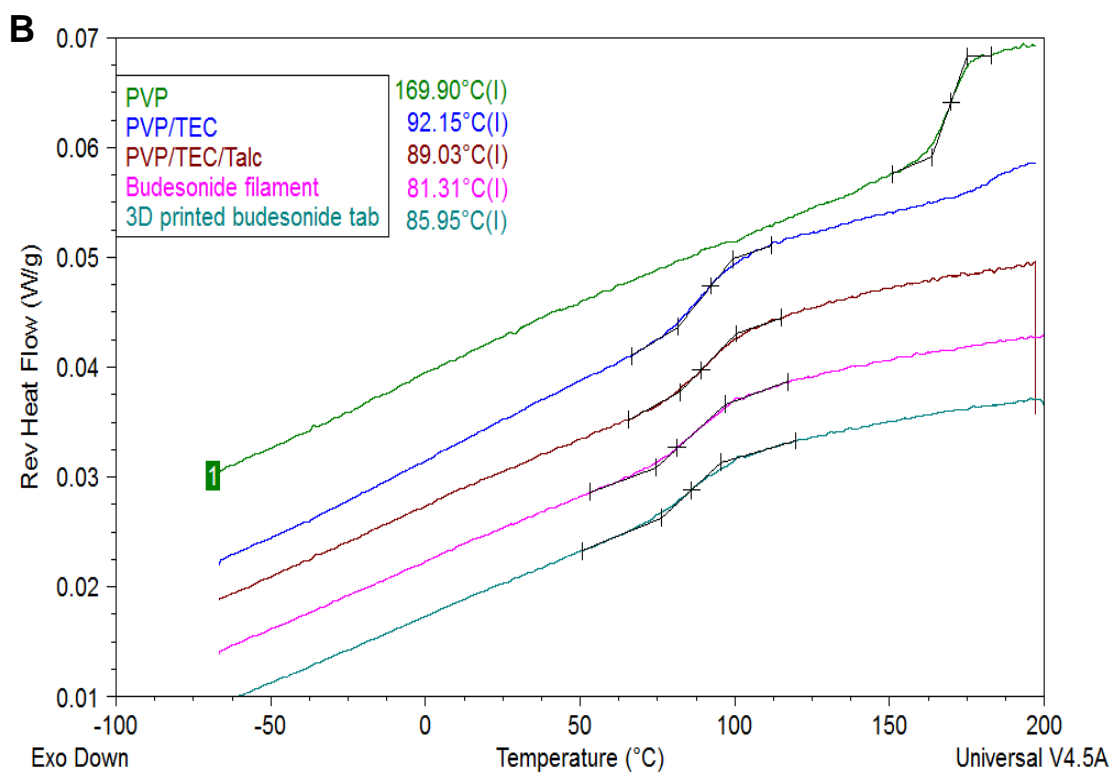
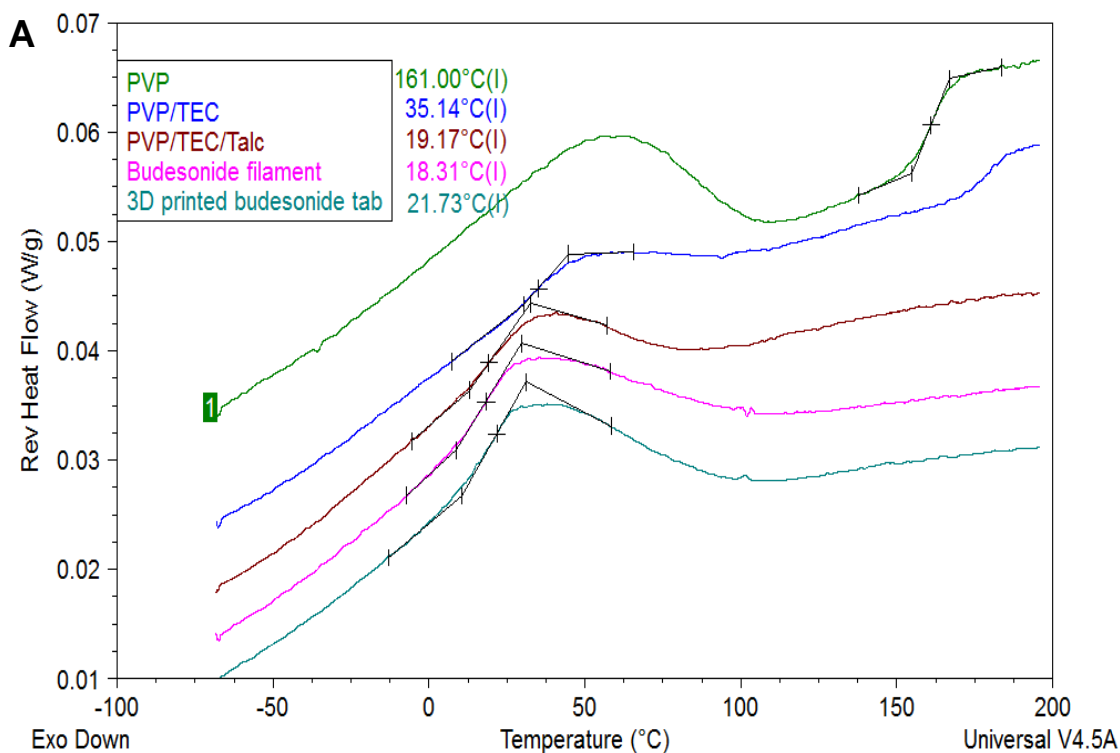


Figure 3.9. Reversing DSC thermographs of PVP, PVP: TEC filament, API-free and API-loaded filaments, and 3D printed tablets for budesonide (A1 first heat-scan and A2 second heat-scan) and diclofenac sodium (B1 first heat-scan and B2 second heat-scan).

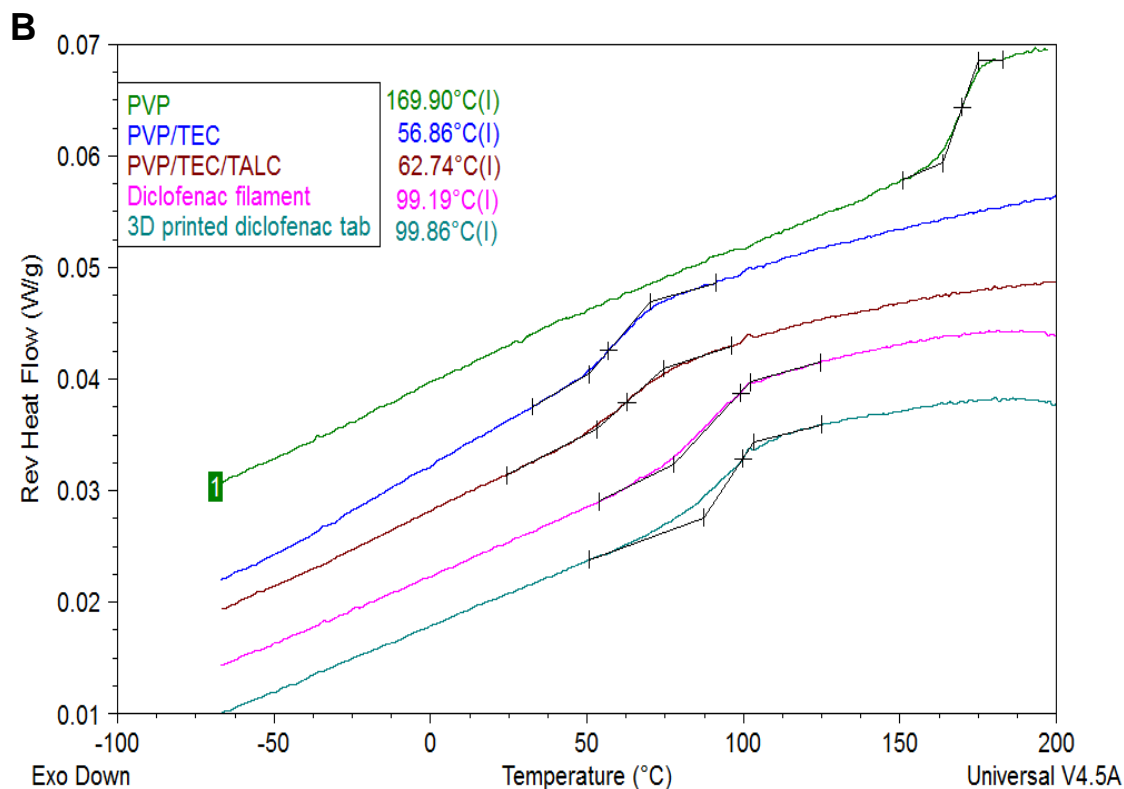
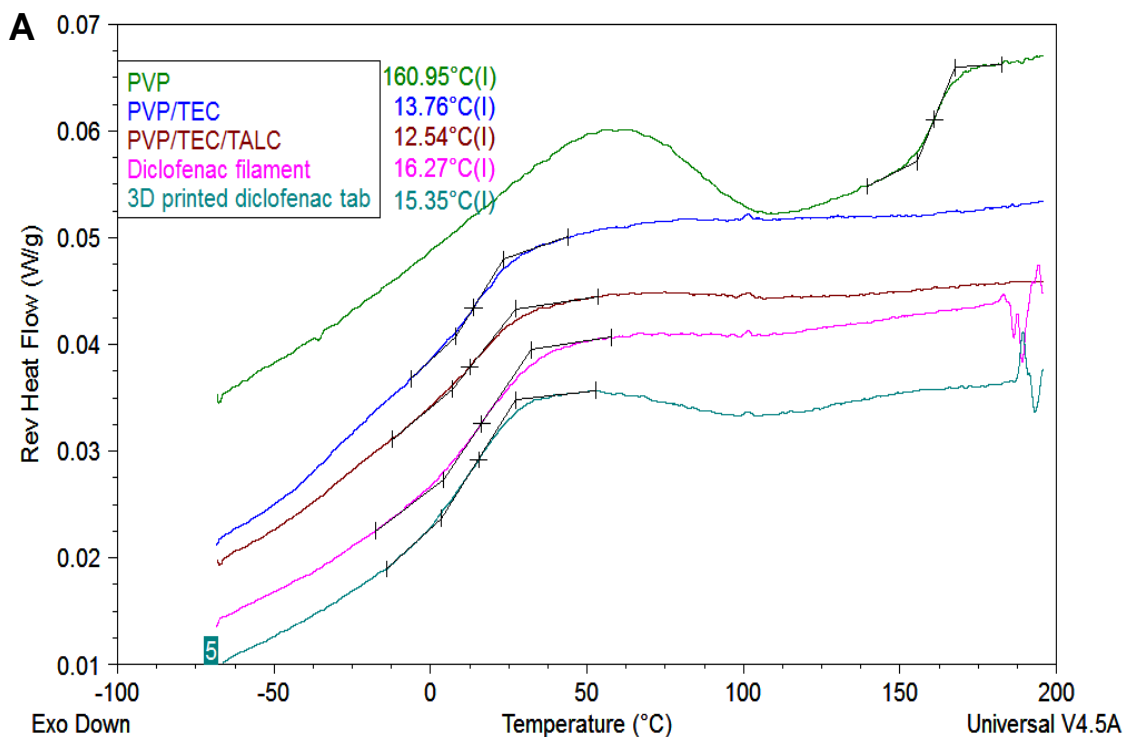


Figure 3.10. Reversing DSC thermographs of PVP, PVP: TEC filament, API-free and API-loaded filaments, and 3D printed tablets for budesonide (A1 first heat-scan and A2 second heat-scan) and diclofenac sodium (B1 first heat-scan and B2 second heat-scan).

The XRPD patterns of budesonide loaded filament and tablets (Figure 3.11A) showed the absence of peaks at $(2\theta) = 6.2, 12.1, 15.5, 16.1, 22.9$ indicating no crystalline presence in the PVP matrices (Kim et al., 2014, Toropainen et al., 2006). For diclofenac sodium, XRPD spectra (Figure 3.11B) demonstrated several diffraction peaks at $(2\theta) = 11.3, 15.3, 23.5$ (Korkiatithaweechai et al., 2011). However, the absence of such peaks in the XRPD of the API loaded filament matrix and tablet suggests that the majority of diclofenac sodium remained in the amorphous form. On the other hand, as reported in our earlier study (Okwuosa et al., 2016) (Section 2.5), theophylline remained in a crystalline form in the PVP-talc based matrix and also seemed to be the case for the PVP-TBP based matrix with peaks from theophylline still seen after HME and 3D printing processes (Figure 3.11C). The concentration of a drug, the nature of the polymer and the drug-polymer interaction plays a key role in the physical form of a drug in a polymer matrix, with a high drug concentration usually resulting in some degree of crystallinity. This also results in faster recrystallisation during storage. The diclofenac loaded filament remained amorphous even though it was twice the concentration of the used theophylline which could be due to one of the aforementioned reasons. Theophylline (10 %) solid dispersion has been also shown to remain crystalline in a drug polymer matrix (Fini et al., 2011, Asada et al., 2004).

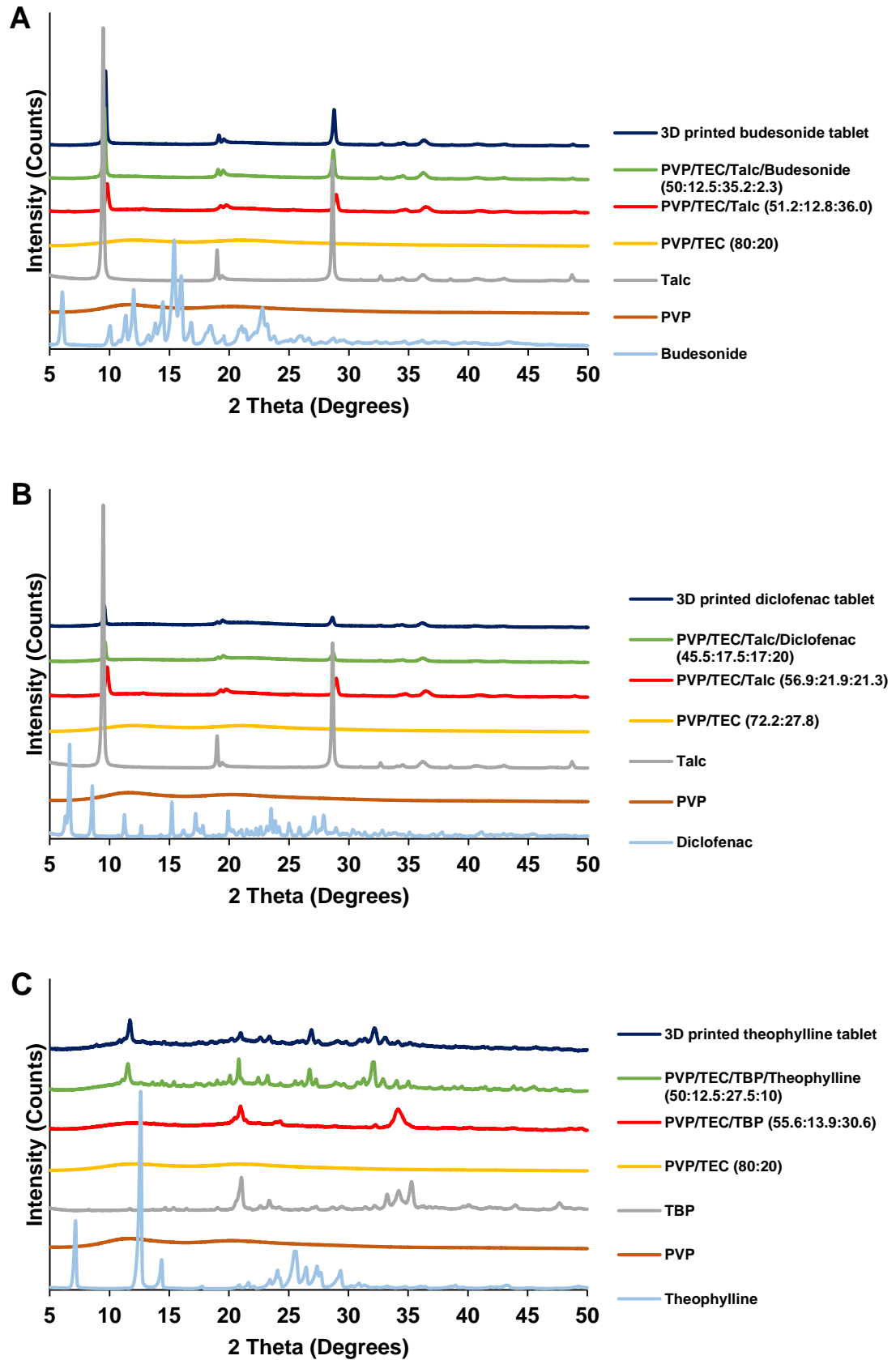


Figure 3.11. XRPD patterns of PVP, PVP: TEC filament, API-free and API-loaded filaments, and 3D printed tablets for (A) budesonide, (B) diclofenac sodium and (C) theophylline.

In vitro dissolution test was carried out on the 3D printed enteric tablets using a USP II apparatus. The dissolution pattern of all tested APIs indicated a pH-dependant drug release (Figure 3.12A) with adequate acid resistance demonstrated by <10 % drug release in the acid media. This was followed by a slow release of the actives over 4 hrs period. When these tablets were assessed in a more physiologically relevant dissolution medium (Fadda and Basit, 2005), a slower dissolution pattern was noted (Figure 3.12B). Such effect might be related to the lower buffer capacity of bicarbonate buffers in comparison to phosphate based ones (Liu et al., 2011). The faster drug release of diclofenac sodium in comparison with budesonide might be related to its higher drug loading as well as solubility (26 mg/mL) (Ming-Thau et al., 1992) in comparison to budesonide (0.0429 mg/mL) (Bhatt et al., 2014).

The disintegration test indicated that all tablets remained intact after 1 hr in the disintegration medium (Table 3.2). However, upon pH change the disintegration time was significantly longer than the Pharmacopeia standards (Revision, 2007). Such behaviour is related to the nature of core, where polymeric matrices erode slowly upon exposure to media rather than the exploding of the core as obtained in tablets produced by powder compression. The acid uptake behaviour indicated a relatively high acid uptake (Table 3.2). However, these results should be interpreted with caution when compared to coated tablets, where weight gain of 3-7% is usually applied for enteric coating to achieve protection. In the presented example, the shell represents approximately 50% of the tablet total weight which resulted in the high uptake.

In summary, by adapting FDM 3D printing to two polymeric matrices and coordinating the construction of core and shell structures, the potential of 3D printing technology in fabricating patient-specific pH-responsive tablets has been demonstrated.

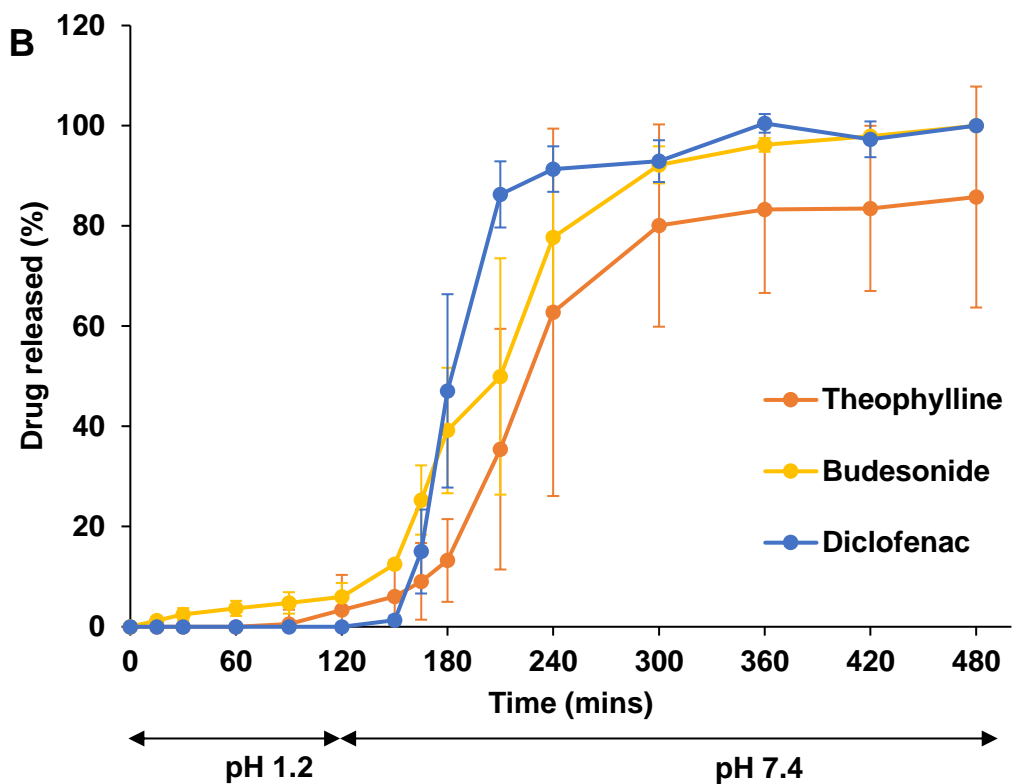
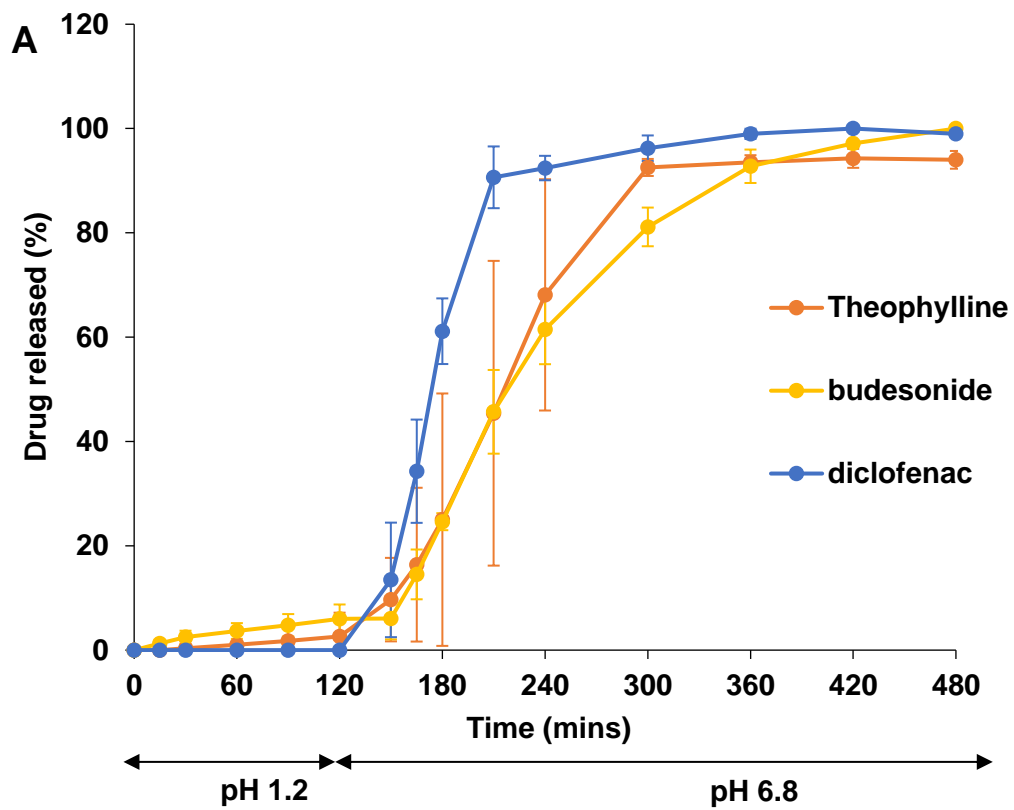


Figure 3.12. In vitro release pattern of APIs; budesonide, diclofenac sodium or theophylline from 3D printed tablets using a USP II pH change dissolution test in (A) phosphate buffer and (B) bicarbonate buffer.

Table 3.2. Summary of gastric resistant properties of 3D printed enteric tablets.

| | Theophylline (talc) | Theophylline (TBP) | Budesonide (talc) | Diclofenac sodium (talc) |
|--|----------------------------|---------------------------|--------------------------|---------------------------------|
| Disintegration test* | | | | |
| Acid medium resistance | Resistant | Resistant | Resistant | Resistant |
| Disintegration time of all tablets in SIF (min) | 33.08±2.55 | 26.96±9.18 | 39.87±9.32 | 42.28±7.92 |
| Acid uptake tests* | | | | |
| Weight gained (%) | 16.51±3.05 | 9.16±0.04 | 23.16±1.80 | 22.41±4.63 |

3.6 Conclusions

It was possible to fabricate tablets based on shell-core structure with increasing shell thicknesses using dual FDM 3D printing. The use of oleic acid reduced nozzle blockage and therefore a successfully interchanging between the nozzles during the shell and core printing. Following pH change dissolution test, it was necessary to obtain a shell thickness ≥ 0.52 mm to achieve sufficient core protection in the acid medium. The use of TBP as a non-melting component in the core filament formulation achieved a faster drug release after pH change and was able to fall within the criteria set by the BP for enteric dosage forms. This however resulted in the degradation of the loaded active indicating the superiority of the use of talc as the inert non-melting component in the formulation. The drug release from the delayed release 3D printed tablets containing theophylline, budesonide and diclofenac in the PVP-talc filament-based system demonstrated a slower release profile in a more biorelevant pH 7.4 bicarbonate buffer media. Theophylline remained in its crystalline form in both the filament and 3D printed tablets unlike budesonide and diclofenac which became amorphous in the polymer matrix.

This process presents a single step production method for gastric-resistant products with no need for a time wasting additional coating step, in addition to dose personalisation potentials. This work illustrates the potential of employing dual FDM 3D printing to overcome the rigidity of traditional techniques of manufacturing delayed release solid dosage forms in response to demands from clinical and industrial sectors.

The ability to produce a shell-core system using 3D printing increased the potential of this approach in drug manufacturing since the core of the table could be replaced with liquids or powders if the shell is able to maintain its integrity during the process. The use of powders or liquids will completely avoid the use of heat which is one of the major problems in 3D printing by FDM. The researches carried out to investigate the possibility to load the shell filament with liquids and therefore, the manufacturing of 3D printed liquid-filled capsules will be discussed in the next chapter.

Chapter 4 : On Demand Manufacturing of Patient-specific Liquid-filled Capsules via Co-ordinated 3D Printing and Liquid Dispensing

4.1 Overview

The use of capsules in drug delivery has proven to be very efficient and has been used for decades by pharmaceutical industries to target different areas of the body. In comparison to tablets, they could be filled with powders, pellets or liquids, this flexibility being one of its major benefits. It also involves fewer manufacturing steps, which encourages faster development, resulting in their use during early clinical trials.

The ever-growing research in the FDM 3D printing of pharmaceutical dosage forms has shown potential in personalised drug manufacturing and dosing. However, they were mostly used in the 3D printing of tablets of different forms with little research in their use in capsule manufacturing. This chapter will therefore demonstrate the potentials of 3D printing in the manufacturing of liquid-filled capsules by the modification of a MakerBot dual FDM 3D printer to enable the coordination of FDM 3D printing and liquid dispensing.

The first section of this chapter will show the application of 3D printing in the manufacturing of immediate and extended release liquid-filled capsules using Eudragit EPO and RL-based filaments respectively. It also demonstrates the ability to fill the capsules with either a solution or suspension of different actives, in addition to being able to control dosing and rate of drug release.

The second section focuses on demonstrating the potential of the liquid dispenser head in the delivery of large molecules to the colon. The colon cancer activity of two AMPs (Aurein 2.6 and LL-37) were determined on Caco-2 and HT-29 colon cancer cell lines which was successfully loaded into capsules using the proposed approach without altering their solution structure. Eudragit S100-based filament (pH threshold 7) was used as the colon-targeting polymer while theophylline solution was used as a proof of concept for colon targeting.

4.2 Section 1: Introduction

Personalised dosing is an upcoming and promising approach in drug therapy that ensures doses are tailored to an individual patient's needs and preferences (McDougall et al., 2016). This can reduce the incidence of side effects and risk of overdose as pharmacodynamics and pharmacokinetic factors are able to be considered along with the age and weight of the patient (Al-Metwali and Mulla, 2017). Over the years, individualising liquid oral dosage forms e.g. solutions and suspensions has been carried out using a variety of simple dosing aids e.g. calibrated spoons, droppers or syringes. Although these methods provided a low-cost solution, they were however associated with human errors during dosing (Ryu and Lee, 2012, Sobhani et al., 2008).

Another approach in the dosing of liquids involves the use of Liquid capsules which has been shown to enhance the absorption of poorly soluble drugs (Cole et al., 2008, Deepthi and Murthy, 2015, Hussein et al., 2012) since the actives are already dispersed in a liquid and becomes available for absorption once the shell dissolves. This is however not the case when capsules are filled with powders or compressed tablet since they need to disintegrate and dissolve before being absorbed by the body. Liquids capsules are usually manufactured as soft gelatine capsules which involves four steps: i) Preparation of the gelatine ii) Preparation of the fill material iii) The encapsulation process using suitable equipment iv) further processing of the filled soft capsule which includes drying, quality control, polishing and packaging.

The use of hard gelatine capsules offered significant advantages over soft gel capsules for encapsulation of liquids and semisolids. There is a reduced incidence of drug migration (Armstrong et al., 1984) and an improvement in product stability by lowering moisture and oxygen permeability, rendering it more suitable for sensitive active molecules (Hom et al., 1975, Lucas et al., 1987). Hard shell capsules also provide better taste and odour masking, and hence can improve patient's compliance. Unlike the manufacturing of a soft gel capsule, hard shells are casted separately before filling and sealing in another separate step. Their wall thicknesses ranges from 0.086 to 0.890 mm depended on the size of the chosen capsule shell (Capsulesupplies, 2018). These wall thicknesses allow fast dissolution and release of the capsule contents once in contact with the body fluid unless coated with dose modifying materials.

The applications of capsules in medical treatments are already well established; however, dose personalisation using this oral delivery system seem very complicated and impracticable. It is impossible to split these capsules as carried out on tablets because of its nature which will lead of the loss of the shell function in addition to the loss

of its content especially for liquid capsules. Besides encapsulation is carried out on a large scale using equipment that are not suitable for on demand personalisation on a small scale.

The pharmaceutical applications of 3D printers in drug manufacturing have demonstrated great potential as an alternative production technique for personalising dosage forms at a peripheral level. 3D printing has been used in the manufacturing of immediate (Okwuosa et al., 2016, Pietrzak et al., 2015, Sadia et al., 2016), extended (Chai et al., 2017, Clark et al., 2017, Goyanes et al., 2015b, Kyobula et al., 2017, Park, 2015, Skowrya et al., 2015), as well as enteric release (Okwuosa et al., 2017, Goyanes et al., 2017) dosage forms using pharmaceutical grade polymers. In FDM 3D printing, filaments are heated above the glass transition temperature (T_g) of the matrix polymer, passed down a nozzle by gears and deposited in a layer-by-layer fashion to fabricate an object without the need for post-printing processing (Alhnan et al., 2016).

In a previous attempt, FDM 3D printing was used in the fabrication of capsule by interrupting the printing of the shell and filling in the core manually before completing the shell (Markl et al., 2017). In another example, the capsule cap and bottom were 3D printed separately and then filled manually with powder (Melocchi et al., 2015). To the authors' knowledge, at the point of this research, there have been no previous reports around a fully integrated, automated 3D printing of liquid-filled capsules. This could be a reflection of major challenges associated with attempts to achieve this goal. Unlike manufacturing capsules by casting, the additive manufacturing of capsules imposes a major difficulty of sealing the spaces between the printed layers and maintaining the barrier function of the shell. In fact, a fully automated 3D printing of liquid capsules requires the coordination of a liquid dispenser with the shell manufacturing. The design of the shells, its additive manufacturing and liquid filling should be carefully organised to ensure that the resultant shell structure are compatible with the liquid core.

4.3 Aims

This research aims at demonstrating the first example of a fully automated additive manufacturing process for a liquid-filled capsule with the capability to control the dispensed dose for immediate and extended drug release. The objectives of this research include:

- Modification of a dual FDM 3D printer to include a syringe-based liquid dispenser, which was used to fabricate a capsule shell through FDM 3D printing and instantaneously dispense either a suspension or a solution formulation of model drugs.
- Optimisation of the dosing accuracy of the liquid dispenser, which was used in the manufacturing of immediate or extended release liquid-filled capsules employing two methacrylate polymers (Eudragit EPO and RL).
- Characterisation of the actives, excipients and the formulations
 - Scanning electron microscopy (SEM)
 - Thermal analysis (DSC, TGA)
 - X-ray powder diffraction
 - Drug content analysis
 - In vitro Dissolution studies

4.5 Materials

To carry out this study, the following materials were used.

4.5.1 Eudragit EPO

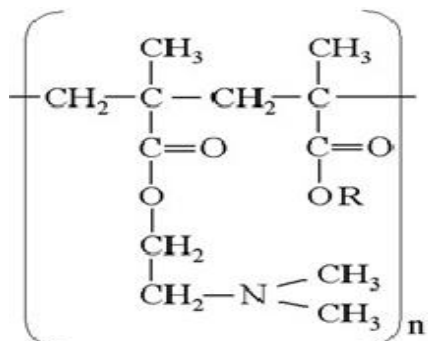


Figure 4.1. Chemical structure of Eudragit EPO (An Nguyen et al., 2006).

This is an amino alkyl methacrylate copolymer (Figure 4.1) which has immediate release properties. It is soluble at lower pH levels up to pH 5 but becomes swellable and permeable above that pH value. It is good for taste masking (Taki et al., 2017) and provides a glossy and slippery easy-to-swallow finishing. Its use is well established for pharmaceutical purposes as a solubility enhancer (Saal et al., 2018, Saal et al., 2017, Higashi et al., 2016), stability enhancer (Ochi et al., 2016) and in the manufacturing of immediate release dosage forms (Qiao et al., 2010b, Sadia et al., 2016, Yang et al., 2015). Its compatibility with hot melt extrusion has also been previously demonstrated (Ashour et al., 2016, Li et al., 2016a, Li et al., 2016b). It was donated by Evonik Industries (Darmstadt, Germany) for this research study.

4.5.2 Eudragit RL 100

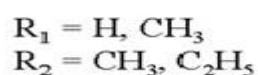
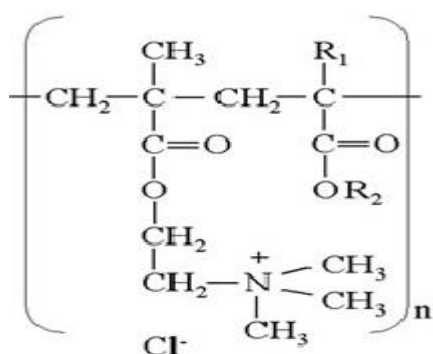


Figure 4.2. Chemical structure of Eudragit RL100 (An Nguyen et al., 2006).

This is an insoluble methacrylic ester copolymer (Figure 4.2) which becomes permeable in the digestive fluids. They are cationic polymers which enables time-controlled drug release of actives by a pH-independent swelling (Dave et al., 2015, Elzayat et al., 2017, Ozguney et al., 2007). It also provides a glossy and slippery finish which makes swallowing less difficult. They are usually supplied as granules and was donated by Evonik Industries (Darmstadt, Germany) for this study.

4.5.3 Methocel E4

Methocel E4, donated by Colorcon limited (UK) is a well-established polymer in pharmaceutical industry. It a methylcellulose-based polymer which finds use in creams, ointments, suspensions, and ophthalmic preparations as a thicker or suspending agent.

4.5.4 Tween 80

Tween 80 also called polysorbate 80 is a non-ionic surfactant and an emulsifier which find use in food, cosmetic and pharmaceutical industries. It is viscous and very water soluble and is usually yellow in colour. For this study, tween 80 was purchased from Sigma-Aldrich (UK).

4.5.5 Citric acid

This is a weak organic acid with the chemical formula C₆H₈O₇. It is GRAS and commonly used to adjust the pH of solvents and to add sour flavour to food. It was purchased from Sigma-Aldrich (UK) for this study.

4.5.6 Other ingredients

Theophylline (>99%, anhydrous) was purchased from ACROS Organics (UK). Triethyl citrate (TEC) and dipyrnidamole ($\geq 98\%$) were purchased from Sigma-Aldrich (UK). Talc (350 mesh) was purchased from Fluka Analytical (UK).

4.6 Methods

4.6.1 Preparation of shell filament

For the preparation of the capsule shell, drug-free Eudragit EPO or RL filaments were produced by a HAAKE MiniCTW hot melt compounder (Thermo Scientific, Karlsruhe, Germany). An optimised ratio of a powder mixture constituting of the polymer, plasticizer (TEC) and filler (talc) was gradually added to the HME and allowed to mix for 5 min at 80 rpm to allow homogenous distribution of the molten mass. Afterwards, the filament was extruded at 20 rpm. The processing parameters for the hot melt extrusion are shown in Table 4.1.

4.6.2 Thermal analysis

For differential scanning calorimetry (DSC) analysis of Eudragit EPO and RL, a differential scanning calorimeter (DSC) Q2000 (TA Instruments, Elstree, Hertfordshire, UK) with a heating rate of 10°C/min was employed. A standard scan was carried out from -70 to 200 °C or to 150 °C for Eudragit EPO and RL respectively. Analysis was carried out under a purge of nitrogen (50 mL/min). The data was analysed using a TA 2000 analysis software. Each sample (approximately 5 mg) was accurately weighed and placed in a 40 μ L aluminium pan and covered with pin-holed lid (TA Instruments, Elstree, Hertfordshire, UK). All measurements were carried out in triplicate.

For TGA analysis, 3D-printed capsule shells, raw materials as well as extruded filaments were investigated using a TGA Q5000 (TA Instruments, Hertfordshire, UK). Analysis was carried out from 25 °C to 500 °C as described in a in Chapter 2, Section 2.4.4 (Okwuosa et al., 2016).

4.6.3 X-ray powder diffraction

An X-ray powder diffractometer, D2 Phaser with Lynxeye (Bruker, Germany) was used to assess the physical properties of the shell filaments using parameters as reported in Chapter 2, Section 2.4.5.

Table 4.1. The formulation and processing parameters for HME and FDM 3D printing of shell filament formulations.

| Polymer name | Polymer (%) | TEC (%) | Talc (%) | Processing temp. (°C) | Extrusion temp. (°C) | Nozzle size (mm) | 3D printing temp. (°C) | Platform temp. (°C) |
|---------------------|--------------------|----------------|-----------------|------------------------------|-----------------------------|-------------------------|-------------------------------|----------------------------|
| Eudragit EPO | 45 | 5 | 50 | 100 | 90 | 1.7 | 135 | 40 |
| Eudragit RL | 45 | 5 | 50 | 130 | 120 | 1.7 | 170 | 20 |

4.6.4 Scanning Electron Microscopy (SEM)

A JOEL JCM-6000PLUS benchtop SEM microscope (Joel LTD, Tokyo, Japan) was used to examine the surface morphology of the printed shell-core structures. Images of the capsules were also taken using a Canon EOS-1D Mark IV (Canon Ltd, Japan).

4.6.5 Preparation of the liquid core

Two model liquid cores (aqueous active suspension or solution) were prepared for use in the syringe-based liquid dispenser:

a. Dipyridamole suspension was initially prepared by subjecting aqueous dipyridamole suspension (1.5 g/ 30 mL) to size reduction via application to T8.01 Ultra Turrax Homogeniser (IKA, Germany) at 25,000 rpm. This was carried out for 1 h at 15 min interval with 5 min cooling time between the intervals. Methocel E4 was added to the suspension to reach a polymer concentration 0.5% w/v before probe sonicating using Sonics Vira cell (USA) at 15 min interval in an ice bath for additional 4 hrs using an amplitude of 70%. The final suspension was diluted with Methocel E4 (0.5 % w/v in water) to achieve a drug concentration of 1.5 % w/v. The size distribution of dipyridamole particles in the suspension was confirmed by a Mastersizer 2000 laser diffraction particle size analyser (Malvern Instruments, UK).

b. Theophylline solution was prepared by adding 15 g of citric acid and 1.5 g of Tween 80 to a 4 % w/v theophylline aqueous suspension (50 mL). This was heated to 65 °C and stirred until a complete solution is formed. Methocel E4 was then added to achieve a cellulosic solution concentration of 0.25 % w/v before cooling in an ice bath.

4.6.6 Modification of dual FDM 3D printer

To devise a fully automated manufacturing of the liquid capsule, a Makerbot Replicator Experimental 2X dual FDM 3D printer (MakerBot Industries, New York, USA) was modified. The printer has two FDM nozzle heads. The right extruder/head of the dual 3D printer was replaced by a syringe-based liquid dispenser as shown in Figure 4.3. The design for the dispenser was obtained from an open source website (Thingiverse, 2017) and the different parts were produced by 3D printing using an M2 MakerGear FDM 3D printer and ABS filaments (MakerGear LLC, Ohio, USA). The dispenser head was assembled and equipped with either a 2 or 10 mL syringe. A Nema17 1.5A 4-lead stepper motor (MakerBot Industries, New York, USA) was connected to the motherboard using the default housing connectors.

4.6.7 Liquid Capsule design and printing

The shells of the capsules were designed as a 1.6 mm thick capsule shell with a capsule-shaped cavity and different dimensions (Table 4.2). Regardless of the digital design of the core, the core will be dispensed as a liquid and will fill the cavity of the capsule shell. A simple geometry (cube) was chosen as the digital design for the core to simplify the calculation of core volumes and to confine the movement of the liquid dispenser head within the cavity space. This proved to be a more suitable approach than using capsule-shaped digital design for the core. The contents of the core were manipulated by modifying the dimensions of the digital design of the core as specified in Section 4.6.8 and 4.6.9.

For the fabrication of liquid capsule, two different printing modes were employed (Figure 4.4):

a. Single-phase printing: Within the Makerbot Desktop software version 3.10.0.1364 (MakerBot Industries, New York, USA), the core was placed in the centre of the cavity of its corresponding shell and was printed by the interchanging printing of the shell filament and core liquid.

b. Multi-phase printing: A simplified 3D software version 3.1.1 (Simplify 3D LLC, Ohio, USA) was used in this printing mode. The shell was designed to comprise a complementary bottom and a cap. This liquid capsule printing was carried out in 3 phases: i) printing of the shell bottom, ii) filling of liquid core, and iii) sealing of the shell in a separate 3D printing stage.

The liquid capsules for both modes were printed with cube dimensions corresponding to 80, 160, 240 or 320 μL (Table 4.2). The settings of the software were modified, and the shells were printed using the 3D printing parameters as shown in Table 4.1. The resolution was set at medium (200 μm layer thickness), the infill was 100 % and the internal and external infill pattern were set at grid and concentric respectively. The rest of the settings were left as default. As priming was not necessary for liquids, the script of the software was also modified to omit the priming step of the liquid dispenser.

Table 4.2. A summary of the volume, dimensions and respective volumes, estimated volume, estimated dose and actual dose for different cores in the 3D printed liquid capsules (n=4, ±SD).

| Sample | Theoretical Volume (µL) | Core's Dimensions (mm) | | | Shell's Dimensions (mm) | | | Core weight (mg) | Estimated dispensed volume* (µL) | Estimated Dose** (mg) | Actual dose † (mg) | Dosing efficiency ‡ (%) |
|---------------|-------------------------|------------------------|------|------|-------------------------|-------|------|------------------|----------------------------------|-----------------------|--------------------|-------------------------|
| | | X | y | z | x | y | z | | | | | |
| Core 1 | 80 | 4.32 | 4.32 | 4.32 | 23 | 10.35 | 6.74 | 82.3 ± 6.95 | 82.7 ± 7.0 | 1.4 ± 0.1 | 1.51 ± 0.2 | 91.1 ± 7.5 |
| Core 2 | 160 | 5.43 | 5.43 | 5.43 | 23 | 10.35 | 6.74 | 185.8 ± 23.75 | 186.8 ± 23.9 | 3.1 ± 0.4 | 3.11 ± 0.2 | 99.4 ± 13.7 |
| Core 3 | 240 | 6.22 | 6.22 | 6.22 | 23 | 10.35 | 7.74 | 284.6 ± 1.48 | 286.1 ± 1.5 | 4.7 ± 0.02 | 4.99 ± 0.5 | 95.6 ± 9.8 |
| Core 4 | 320 | 6.84 | 6.84 | 6.84 | 23 | 10.35 | 9.74 | 385.7 ± 30.57 | 387.8 ± 30.7 | 6.4 ± 0.5 | 6.60 ± 0.9 | 99.0 ± 11.5 |

*The estimated dispensed volume was calculated based on the density of the dispensed dipyridamole suspension. **The estimated dose was calculated based on the concentration of the suspension and the estimated dispensed volume. †Actual dose was measured using HPLC, and ‡dosing efficiency was calculated as efficiency (%) = (estimated dose/ actual dose) x 100.

4.6.8 Validation of the liquid dispenser using different nozzle sizes

The impact of different nozzle sizes on liquid volumes from the liquid dispenser was investigated using digital design of core with cubes of edge dimensions: 2.15, 2.71, 3.42, 4.31, 4.93, 5.43, 5.85, and 6.21 mm as the printed object. These dimensions corresponded to theoretical volumes of 10, 20, 40, 80, 120, 160, 200 and 240 μL . A 10 mL syringe was then used for drug dispensing using 0.25, 0.41 or 0.84 mm nozzle sizes. The dispensed liquid was collected, weighed and the volume determined based on the density of the liquid at the operating temperature. The relationship between the theoretical volumes and the actual dispensed liquid volumes were determined. The effect of different 3D printing modes (single-phase or multi-phase) on the accuracy of the dispensed volume was also investigated.

4.6.9 Optimising the dosing accuracy of the liquid dispenser using different syringe sizes

The dosing accuracy of the liquid dispenser was investigated using dispensed liquids corresponding to digital design of the core (cube volume of 80, 160, 240 or 320 μL). The nozzle size was 0.41 mm and the effect of syringe sizes (2 or 10 mL) (Nipro Luer Lock) was investigated ($n=4$). The dispensed liquid was collected into a tared 5 mL polystyrene diamond-shaped weighing-boat (Fisher scientific, UK) and weighed. The estimated dispensed volumes were calculated based on the density of the dispensed volume. The estimated doses were calculated based on the concentration of the suspension and the estimated dispensed volume. The actual dispensed dose was determined using HPLC methods shown in Section 4.6.10. The dosing efficiency was used to compare the estimated doses versus actual doses and was calculated using Equation 4.1.

$$\text{Efficiency (\%)} = (\text{estimated dose/actual dose}) \times 100 \quad \text{Equation 4.1}$$

The relationship between the estimated and actual doses was determined using both printing modes. Due to higher accuracy of 2 mL syringe and the superior quality products produced via multi-phase mode, they were considered as a default and used for the 3D printing of all capsules reported for dissolution tests.

4.6.10 Determination of drug contents

Liquid capsules and their contents were placed in a 500 mL 1:1 acetonitrile and water in a volumetric flask and then sonicated for 2 h. The solution was filtered through 0.22 μm Millex-GP syringe filters (Merck Millipore, USA) and prepared for HPLC analysis.

Dipyridamole and theophylline contents in relevant samples were assessed using an Agilent UV-HPLC 1260 series (Agilent Technologies Inc., Germany) equipped with XTerra RP 18 column (150 × 4.6 mm, 5 µm particle size) (Waters, Ireland) as previously reported in Chapter 2 (Section 2.4.7).

4.6.11 *In vitro* dissolution test

In vitro drug release studies for all liquid-filled capsules used in this study were carried out in triplicates in 900 mL of 0.1 M HCl at 37 ± 0.5 °C in USP II apparatus (AT7, Sotax, city, Switzerland) with a paddle speed of 50 rpm. The capsules were placed in sinkers to ensure immersion in dissolution medium.

a. For the Eudragit EPO-dipyridamole liquid capsule release studies, four mL aliquots of release medium were manually collected using 5 mL Leur-Lock syringes at 0, 5, 10, 15, 20, 25, 30, 40 and 60 min time intervals and filtered through a Millex-HA 0.45-µm filter. Each aliquot withdrawn was replaced with 4 mL of 0.1 M HCl. Analysis of dipyridamole content of samples was undertaken using HPLC methods reported in Section 4.6.10.

b. Eudragit EPO-theophylline liquid capsule release studies were conducted using an in-line UV/VIS spectrophotometer (PG Instruments Limited, UK). The amount of released theophylline was determined at 5 min intervals at a wavelength of 272 nm and path length of 1 mm. Data was analysed using IDISis software 2012 (Automated Lab, UK).

c. For Eudragit RL-Theophylline extended release liquid capsules, the test was carried out using 750 mL of a stimulated gastric fluid (0.1 M HCl, pH 1.2) for 2 hrs followed by 12 hrs exposure to pH 6.8 phosphate buffer.

4.6.12 Statistical analysis

One-way ANOVA was employed using SPSS Software (22.0.0.2) to analyse the results. Differences in results above probability level ($p > 0.05$) was considered not significant whilst differences ($p < 0.05$) were considered significant.

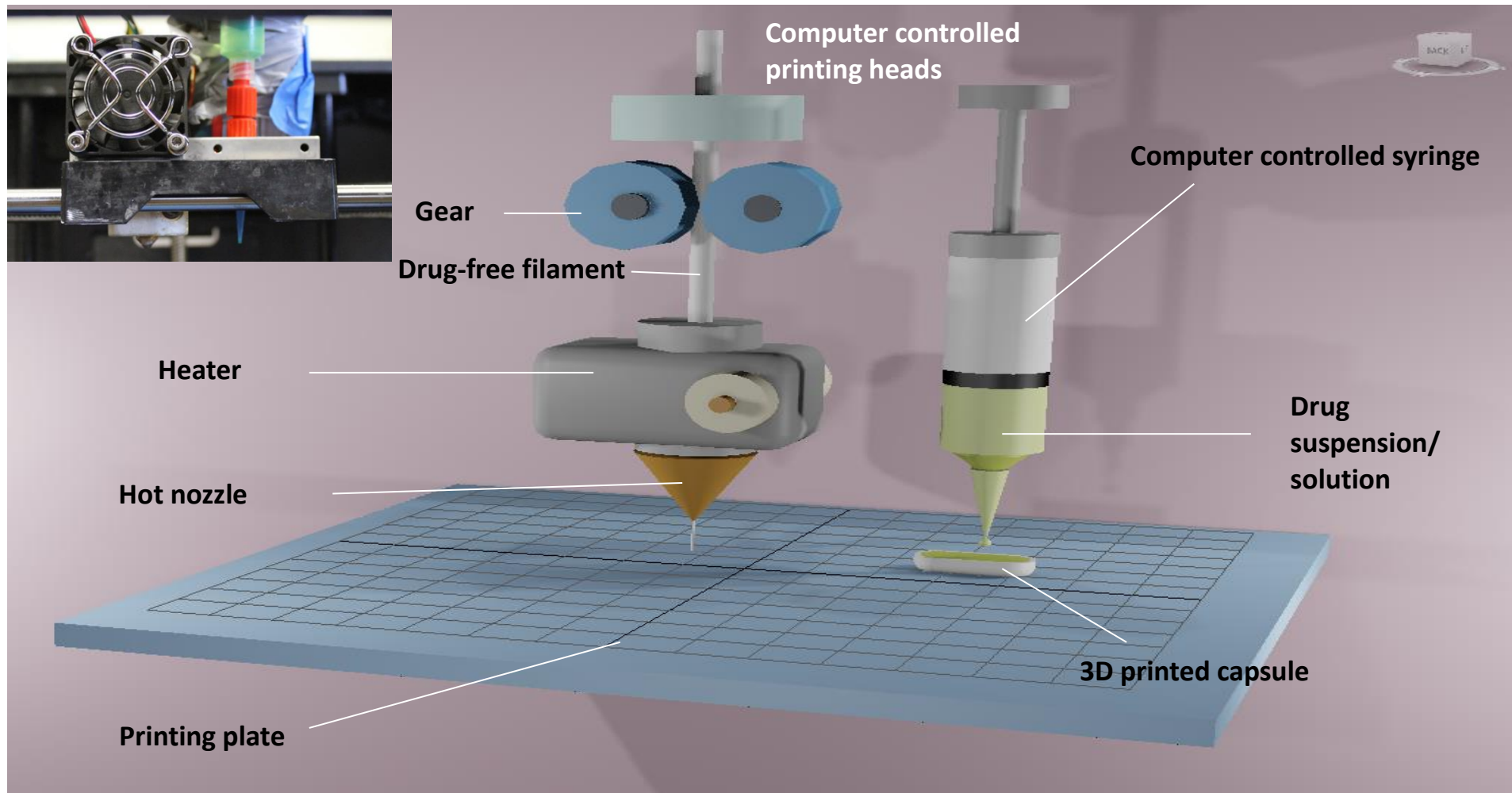


Figure 4.3. Schematic illustration of the fabrication of 3D-printed liquid capsule using a modified dual FDM 3D printer.

4.7 Results and Discussion

The co-ordination of FDM 3D printing with a liquid dispenser enabled the manufacturing of liquid capsules in a fully automated process (Figure 4.3). The proposed configuration allowed the synchronisation of two processes: i) capsule shell fabrication, and ii) capsule filling whilst maintaining control over both through 3D printing software. To orchestrate these processes, two modes of capsule shell printing and filling have been adapted. The single-phase 3D printing involves the simultaneous construction of the shell and dispensing of the liquid core into its cavity (Figure 4.4A). However, this mode implicates a constant switching between the two printing heads after building each layer, leading to frequent disruptions of the shell 3D printing process. It is possible that core liquids can interfere with the layer-by-layer deposition of filaments during shell manufacturing by the deposition of liquid on the growing layers, hence preventing the casted layers from fusing and in effect compromising the barrier function of the shell walls. This was avoided when a multi-phase printing mode was adopted. In multi-phase printing, the printing of 75% of the bottom side of the shell is first completed, followed by the core liquid filling before sealing the shell in another separate 3D printing stage (Figure 4.4B). Although both approaches were successfully used in the fabrication of liquid capsule, the later was chosen for this research due to its advantages.

The design and the printing patterns of the shell plays a key role to successfully print liquid-filled capsules. The capsule shell was hollow in the middle with a 1.6 mm thick wall to be able to accommodate the liquid core (Figure 4.4) which is by far, thicker than conventional hard shell capsules (Capsulesupplies, 2018). However, this thickness was required due to the layer-by-layer manufacturing approach used by 3D printers, thereby requiring the deposition of more layers to create a sealed shell wall and avoid linkages. When thinner wall thicknesses were initially assessed, it led to leakage of the liquid core during or following the printing process and were deemed insufficient to control liquid contents within the shell. The excipients in the liquid core could also affect the integrity of the shell as materials with a high plasticising effect on the shell polymer will lead to deformation and leakage.

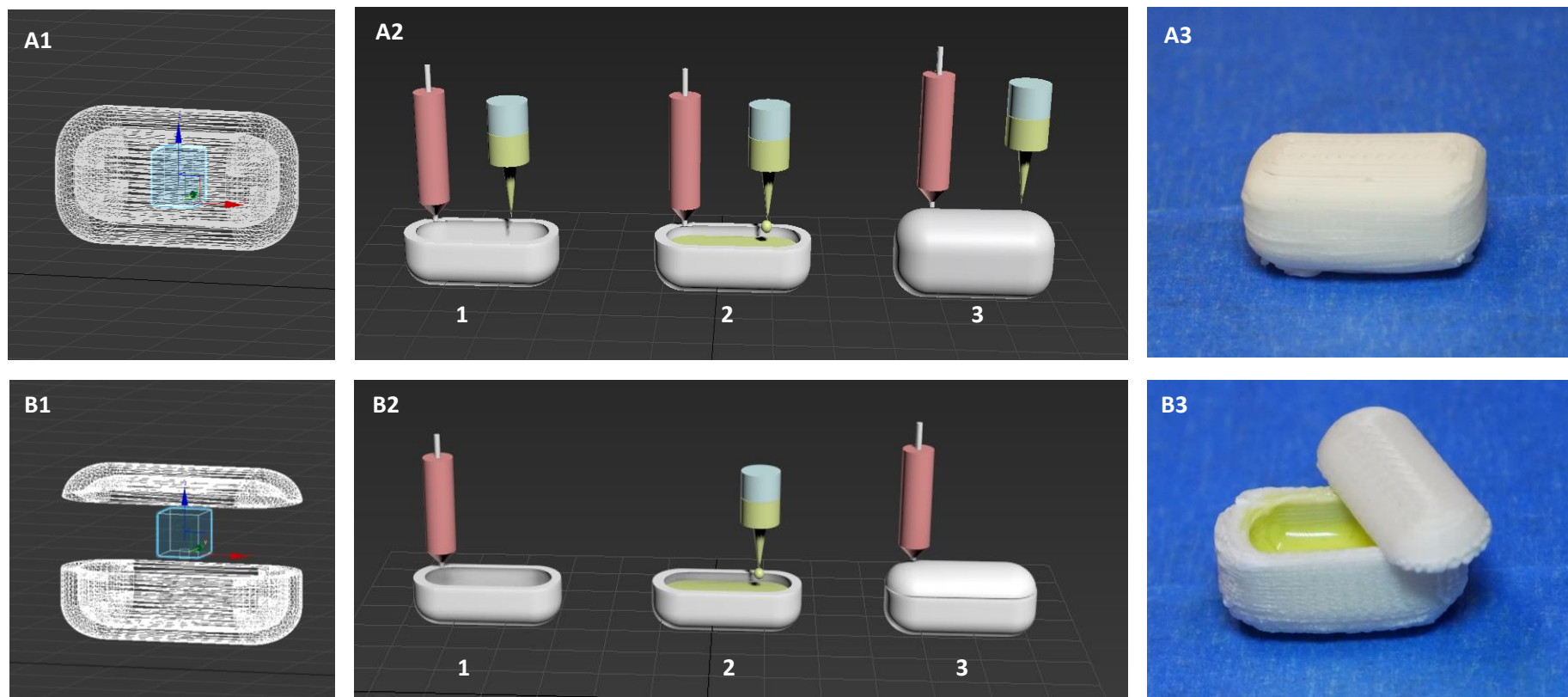


Figure 4.4. The co-ordination of FDM nozzle and liquid syringe dispenser is achieved in two different printing modes: i) **Single-phase printing:** (A1) the core is located in the centre of the cavity of the shell, (A2) Shell printing and capsule filling is achieved by alternation at each layer. (A3) Image of completed shell-core designs with dipyridamole core and Eudragit EPO shell. ii) **Multi-phase printing:** (B1) the core is located in a median level between the bottom shell (75%) and the top shell (25%). (B2) the shell is printed first followed by complete filling of the shell bottom, the printing is completed by printing the shell top. (B3) Image of completed shell-core designs (shell top was separated from bottom for demonstration). (See Supplementary Data Videos S1 and S2).

The thermogravimetric analysis of the Eudragit EPO and RL polymer powder on its own demonstrated two stages of weight losses from approx. 250 °C and 200 °C respectively (Figures 4.5A and B). A physical mixture of the polymer with TEC with or without the addition of talc showed an early weight loss due to TEC starting at approx. 115 °C. Their formulation as filaments demonstrated degradations at the same temperatures as the polymer alone. This remained the same after 3D printing with TEC seeming to become more stable in a polymer matrix, degrading with the polymer as observed in Chapter 2. Talc remained stable throughout the analysis. These filaments were not subjected to a significant weight loss at the HME and 3D printing processing temperatures (Figures 4.5A and B). This suggested the stability of these shells at the exposed temperatures and therefore suitable for shell fabricating.

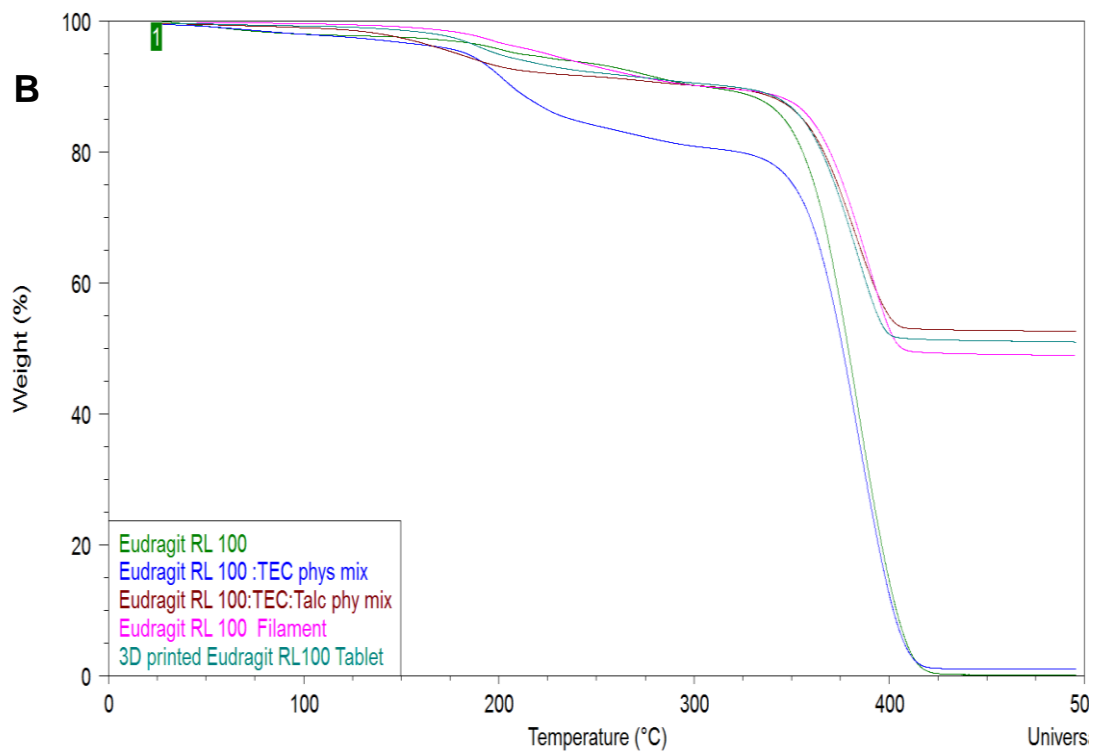
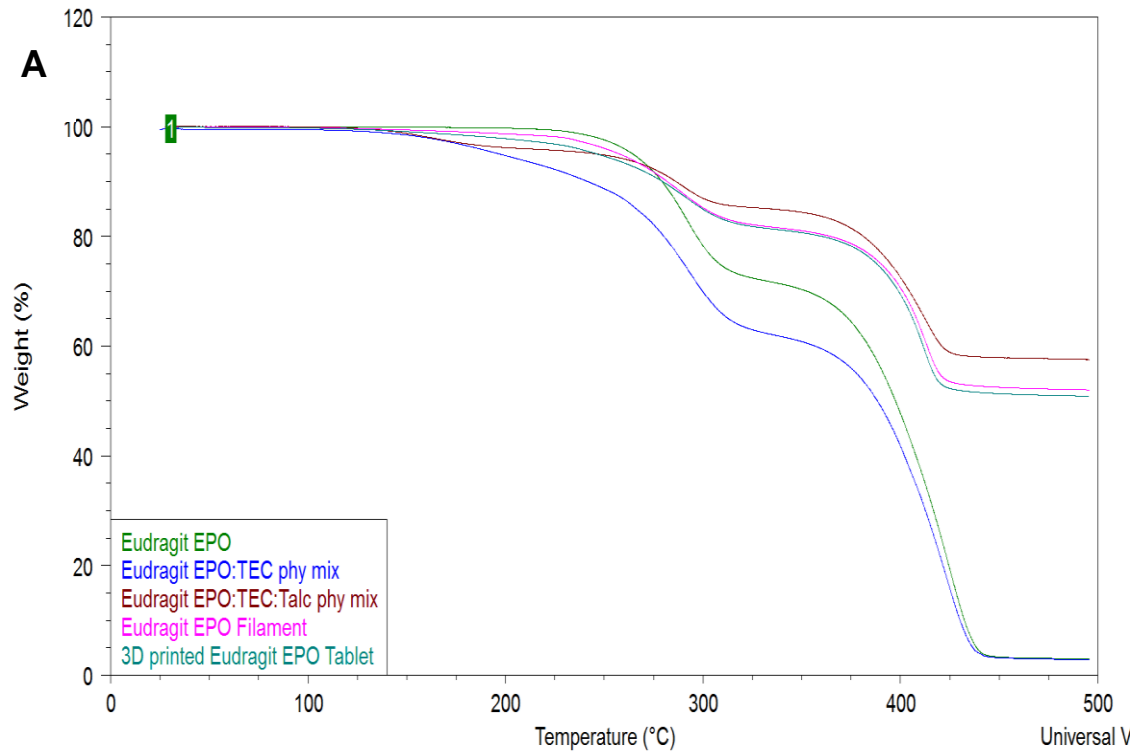


Figure 4.5. TGA analysis of polymer, polymer:TEC physical mixture, polymer:TEC:talc physical mixture, filament and 3D printed shell for Eudragit EPO (A) and RL (B) respectively.

The DSC analysis of the filaments indicated that the addition of TEC to the methacrylate polymeric matrix in filament manufacturing effectively plasticised the polymers and lowered their T_g from 43.7 to 18.9 °C and from 74.7 to 47.9 °C for Eudragit EPO and RL respectively (Figures 4.6A and B). The resultant filaments were thus compatible with FDM 3D printer head. The addition of the structure former, talc, was essential to permit the 3D printing by regulating the filament diameter, retaining the filament integrity following going through nozzles and allowing rapid solidification after extrusion from the nozzle (Okwuosa et al., 2016). With these adaptations, it was possible to carry out FDM 3D printing at 135 and 170 °C for Eudragit EPO and RL respectively.

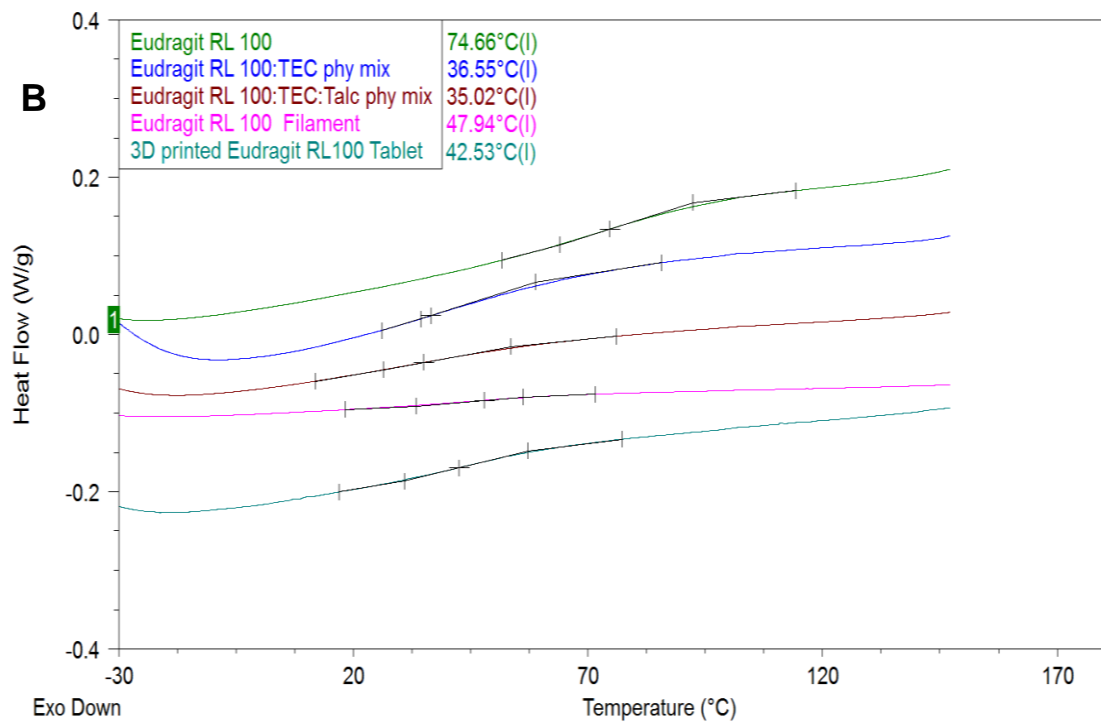
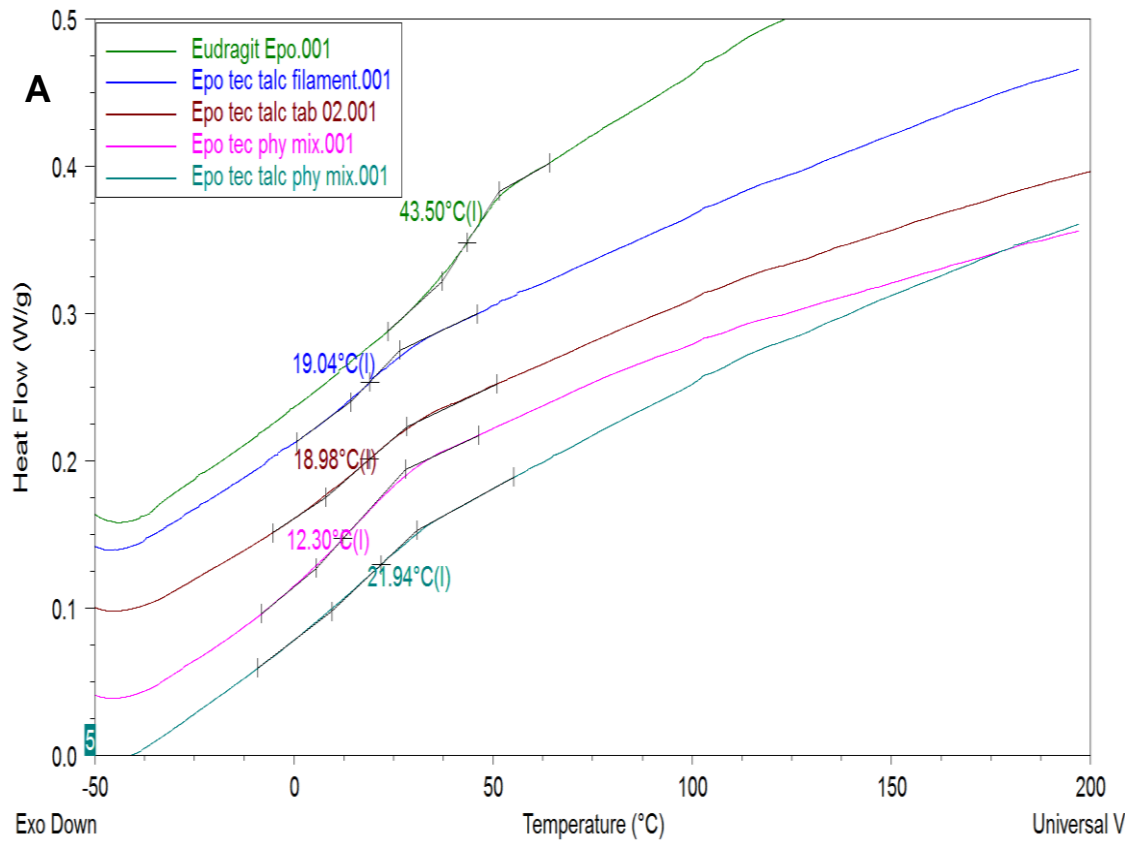


Figure 4.6. DSC thermographs of polymer, polymer:TEC physical mixture, polymer:TEC:talc physical mixture, filament and 3D printed shell for Eudragit EPO (A) and RL (B) respectively.

The XRPD patterns for the filaments and 3D printed capsule shell based on both Eudragit EPO and RL demonstrated the presence of peaks at (2θ) = 9.5, 19.0, 28.6, 36.5 and 48.9° (Figure 4.7). These peaks could be attributed to the talc used in the formulation and confirmed that talc remained in a crystalline form. Previous research also indicated that in filled polymeric systems, the addition of a non-melting component to methacrylic polymer enhanced the viscoelastic behaviour of the melt in a monotonic fashion and decreased the critical strain amplitude for strain thinning (Sadia et al., 2016).

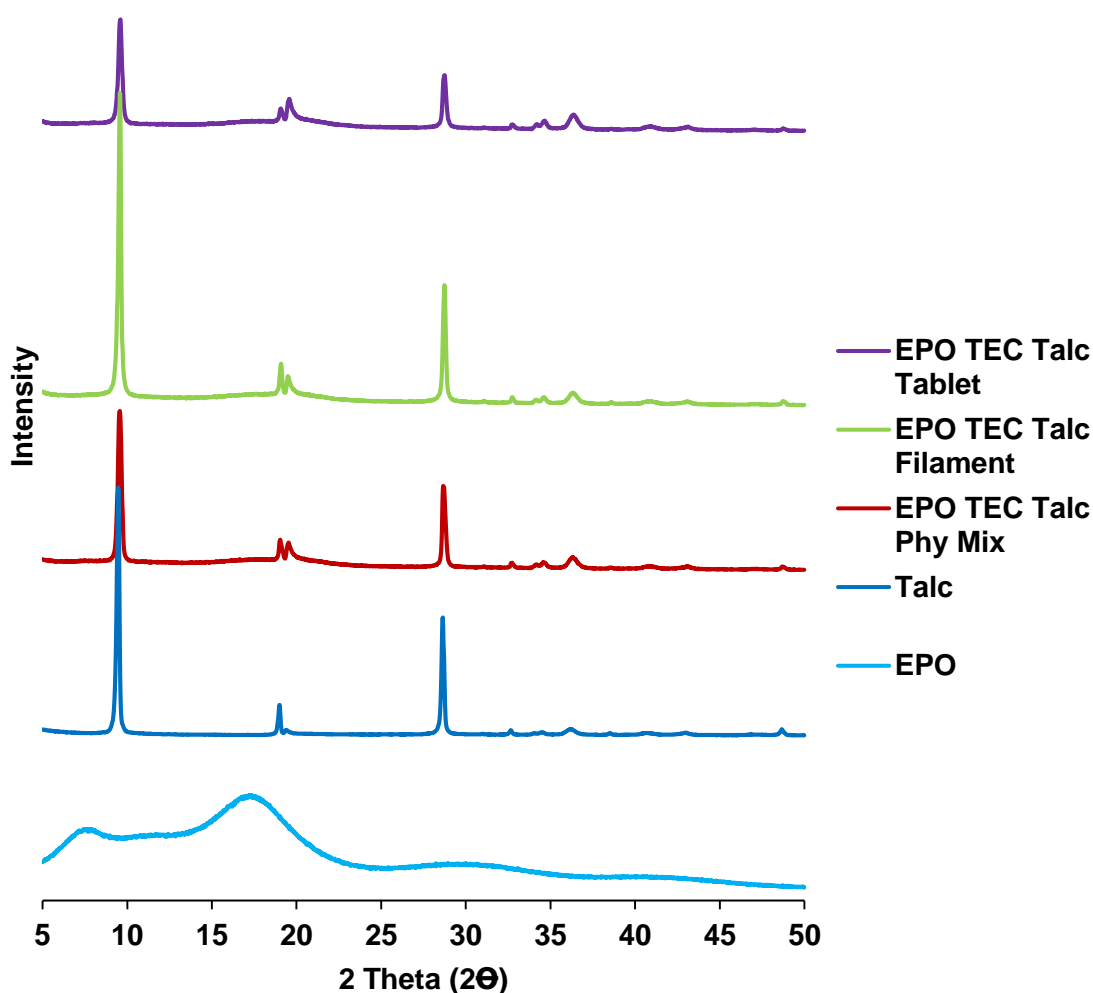


Figure 4.7. XRPD patterns of polymer, talc and polymer:TEC:talc physical mixture, filament and 3D printed shell for Eudragit EPO.

In conventional capsule filling, most gelatine capsules are designed at thicknesses of usually ≤ 0.240 mm, which could differ depending on the size and the manufacturer of the capsules (Capsugel, 2012, Limited, 2014). The body and the cap of gelatine capsules are manufactured separately, typically by casting before being filled and sealed. In this research, the shell and the core of a 3D printed liquid capsule were created simultaneously by stacking polymeric layers and filling the printed cavity with liquid. Therefore, the barrier function of the 3D printed capsule shell was maintained by increasing shell thickness to 1.6 mm and applying a 100 % infill in the shell structure using the operating software. Moreover, the pattern of shell printing also seemed to influence the integrity of the shell. While rectilinear pattern resulted in gaps of approximately $100\ \mu\text{m}$ (Figures 4.8A1 and A2), concentric capsule filling provided tighter alignment of the fused filament and resulted in more stable shell structure (Figures 4.8B1 and B2).

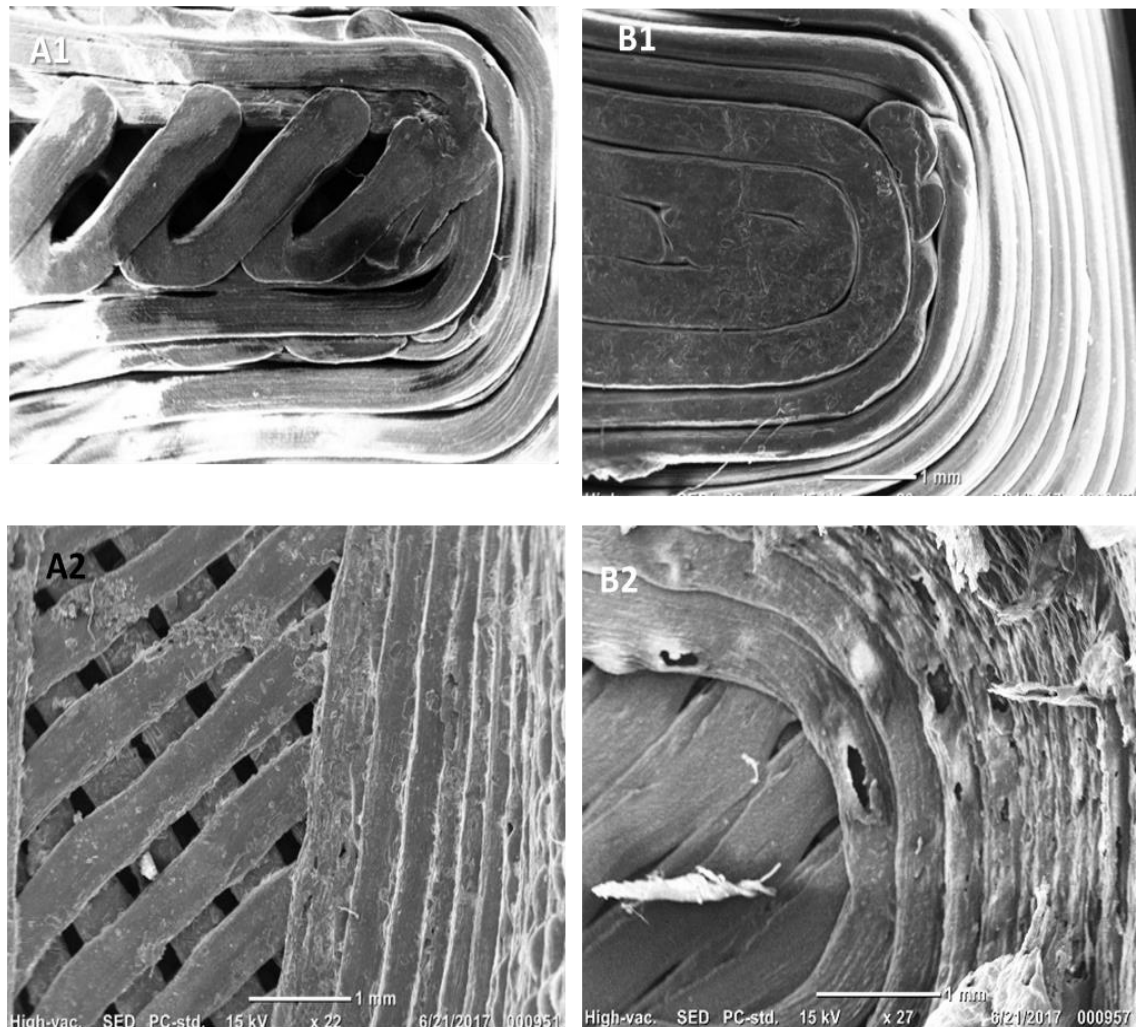


Figure 4.8. Impact of 3D printing pattern on the structure and integrity of the shell: SEM images of (A1 and B1) external surface and (A2 and B2) internal surface of the Eudragit E based shell, in rectilinear or concentric infill respectively.

The printing mode also appeared to influence the architecture and the finishing of the capsule. In multi-phase printing mode, the wall of the shell appeared tighter in comparison to single-phase printing (Figures 4.9A1 and B1). In single-phase mode, following the deposition of each layer, the FDM 3D printer's nozzle moves away from the shell to allow the liquid dispenser to fill the capsule. To add the next layer, the nozzle head returns to the same x-y spot at a higher level (200 μm , thickness of the one layer). However, the lag in the stoppage and commencement of material flow from the printer's nozzle during head movements and alternation results in the formation of a gap at each layer starting point (Figure 4.9A2). By employing multi-phase 3D printing, it was possible to minimize imperfection (Figure 4.9B2) as the 3D printing of the shell is only interrupted once. It is expected that the precision of the printing will improve with the development of highly precise 3D printers (Gross et al., 2014).

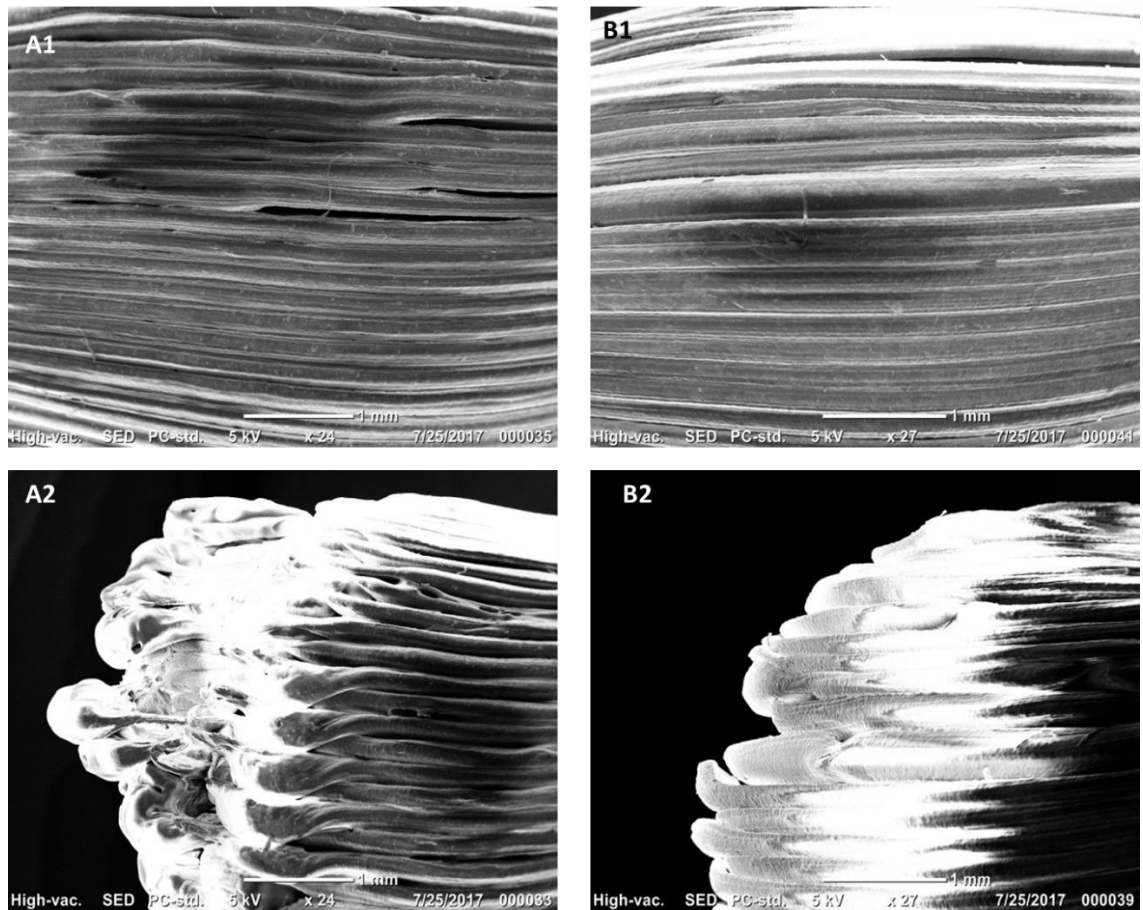


Figure 4.9. The impact of printing pattern on the structure of the shell: SEM image of external surface of the corner and side of Eudragit E based capsule shell produced via (A1 and A2) single-phase or (B1 and B2) multi-phase 3D printing.

These different modes of 3D printing appear to also affect the volume of dispensed liquid ($p < 0.05$) (Figures 4.10A and B). The lower dispensed volume from the single-phase mode compared to multi-phase printing could be attributed to the continuous stoppage and retraction of the liquid dispenser at each layer of printing (as a part of switching between FDM printing nozzle and liquid dispenser). This creates a gap between dispensed volumes leading to a lower overall volume. Therefore, the multi-phase mode was employed as a default printing method.

As accurate dose dispensing is of paramount importance for personalised dosing, it was necessary to confirm the accuracy and reproducibility of the dispenser. Initial investigation on the accuracy of the dispensed volume was demonstrated using the dipyridamole suspension (density= 1.008 g/cm³). A linear relationship was established between the theoretical volumes and the actual dispensed volumes from the liquid dispenser across the different sizes of nozzle used with R² values ≥ 0.9971 (Chapter 7: Supplementary Data, Figures 7.3 and 7.4), while a smaller aperture nozzle provided a better accuracy, the smallest aperture nozzle frequently blocked, and a nozzle diameter of 0.41 mm was used as a default.

The impact of different syringe sizes on the dispensed volumes and dosing accuracy of the liquid dispenser was also investigated (Figures 4.10A and B). Reducing the size of the syringe used on the liquid dispenser influences both the volume of dispensed liquid and its accuracy. The 2 mL syringe produced a narrower deviation and was used as a default syringe for further studies. This could be directly related to the mechanism of liquid discharge from the syringe dispenser. During liquid dispensing, although the distance travelled by the piston of the liquid dispenser motor remained identical for both 2 and 10 mL syringes, however the dispensed volume is significantly reduced by a syringe of smaller diameter. The control of liquid dispensing could also be achieved through the use of pneumatic liquid dispensers (Xie et al., 2010).

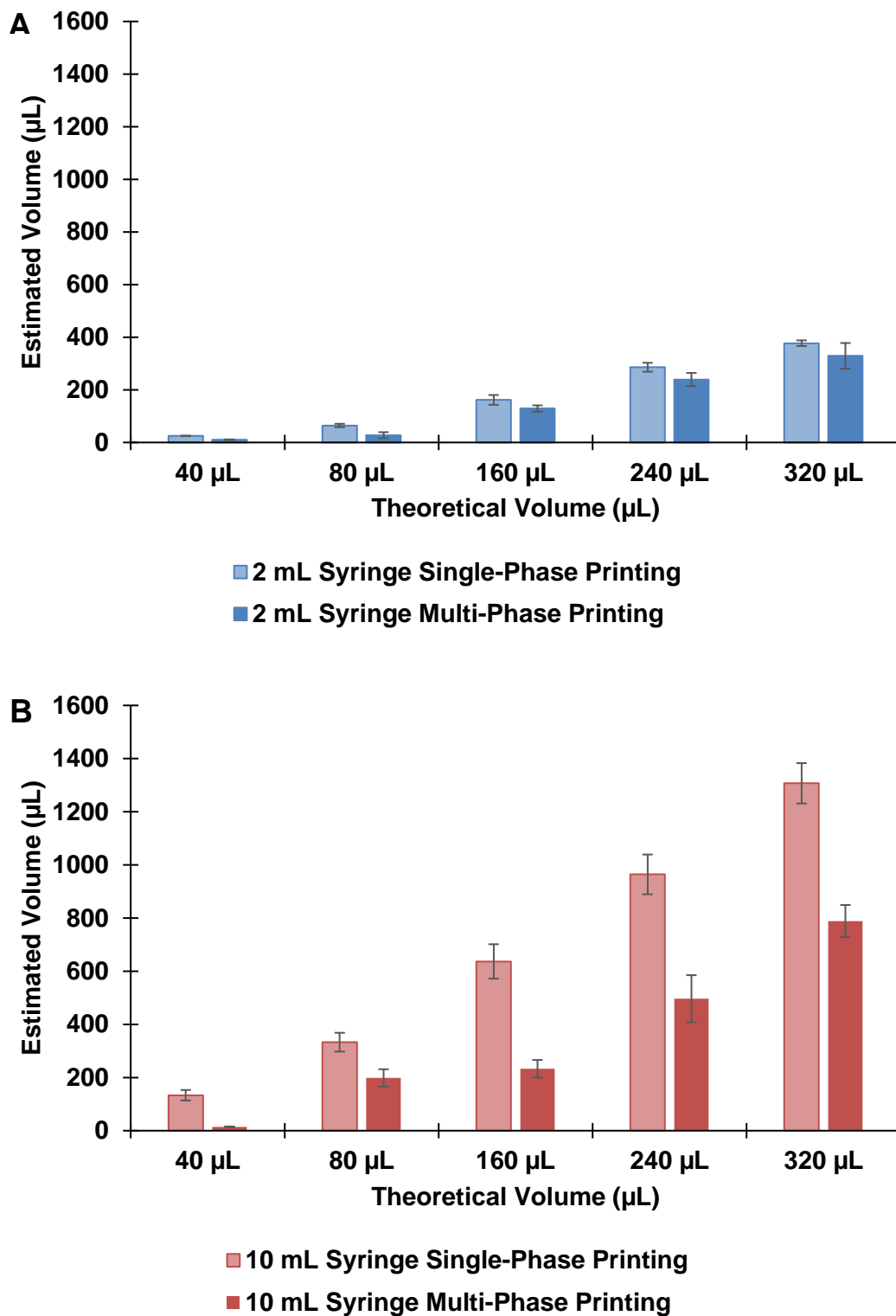


Figure 4.10. Impact of single-phase and multi-phase 3D printing modes on dispensed volume of dipyridamole suspension (1.5% w/v) from the liquid dispenser using (A) 2 mL or (B) 10 mL syringe.

Different liquid volumes (80, 160, 240 or 320 μL) of dipyridamole suspension (median particles size $5.08\pm 0.68 \mu\text{m}$) were dispensed and analysed for dosing accuracy by HPLC. It was possible to dictate the dispensed volume and hence corresponding doses by the software modification of the digital core's volume (Figure 4.11A, Table 4.2). The linearity between the estimated and the actual dose ($R^2 = 0.9985$) (Figure 4.11B) demonstrated the promising potential of this dispenser for on demand drug dosing. The accuracy of dosing was affected by surface tension related phenomena such as foam forming and droplet hanging. These were noted in both printing modes and potentially could be mitigated in commercial manufacturing via adjustments to the programme for the dispenser motor.

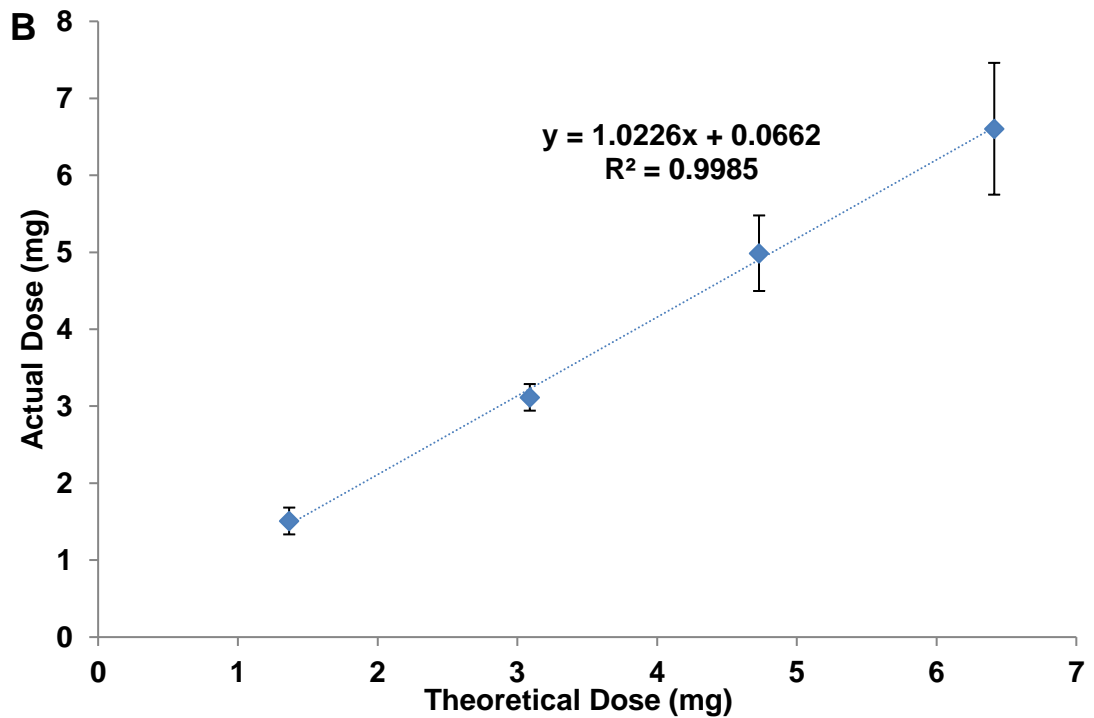
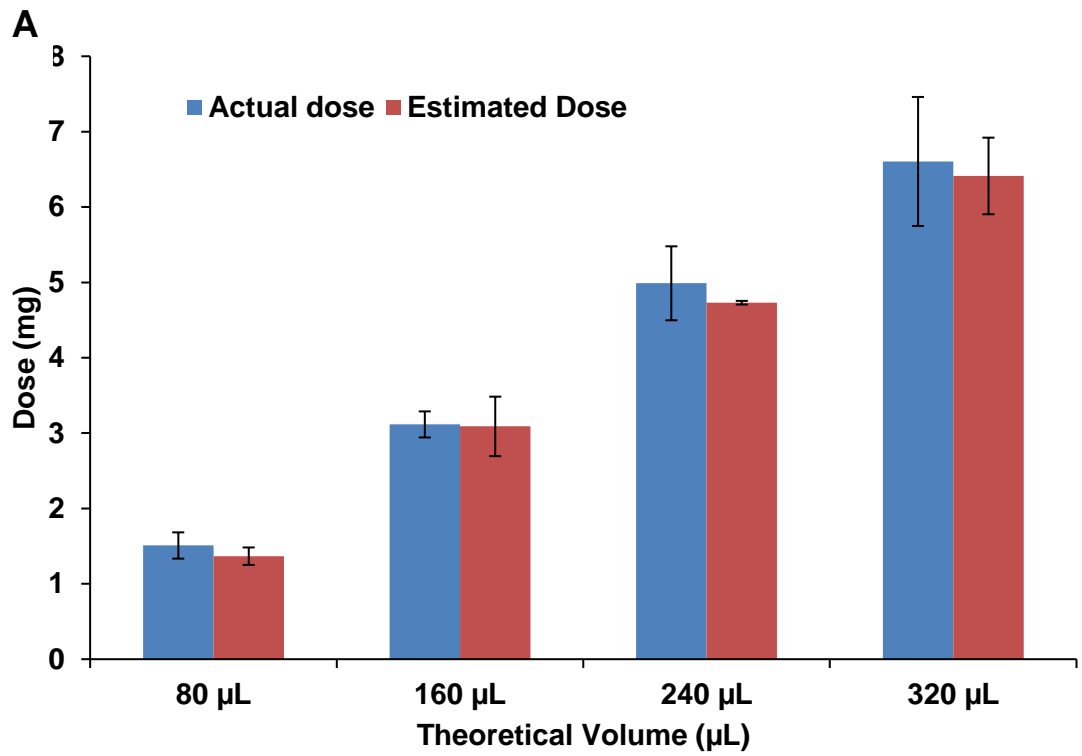


Figure 4.11. Dose accuracy using syringe liquid dispenser of dipyridamole suspension (1.5% w/v): (A) relation of theoretical volume of the core in the software and dispensed dose using single- or multi-phase 3D printing modes, (B) correlation between theoretical and actual volume.

To determine the release profile of the 3D printed liquid capsule, a USP II dissolution apparatus was used. Initially, an optimised suspension of dipyridamole was dispensed in a Eudragit EPO shell at different doses. An immediate drug release profile was obtained as >85 % of the active was released before 30 min (Figure 4.12A), and complied with USP criteria for oral dipyridamole products. (Convention, 2007) This might be attributed to rapid ionization of cationic chains of the methacrylate polymer in gastric medium (Sadia et al., 2016) as well as high solubility of dipyridamole in this medium (Alhnan et al., 2010, Paprskarova et al., 2016).

To prove the suitability of this capsule system to drug solution, the model core of drug suspension was substituted by a theophylline solution. The shell system was also effective in containing the liquid drug payload without compromising the integrity of the shell, with the absence of leakage during or after printing. *In vitro*, the capsules demonstrated their ability to dissolve quickly leading to a complete release of theophylline before 30 min (Figure 4.12B). This also demonstrated the versatility of the presented approach in the delivery of potentially a wide range of actives in different forms, and potentially holds the promise to be used where thermal processing must be avoided to minimize aggregation and potency loss.

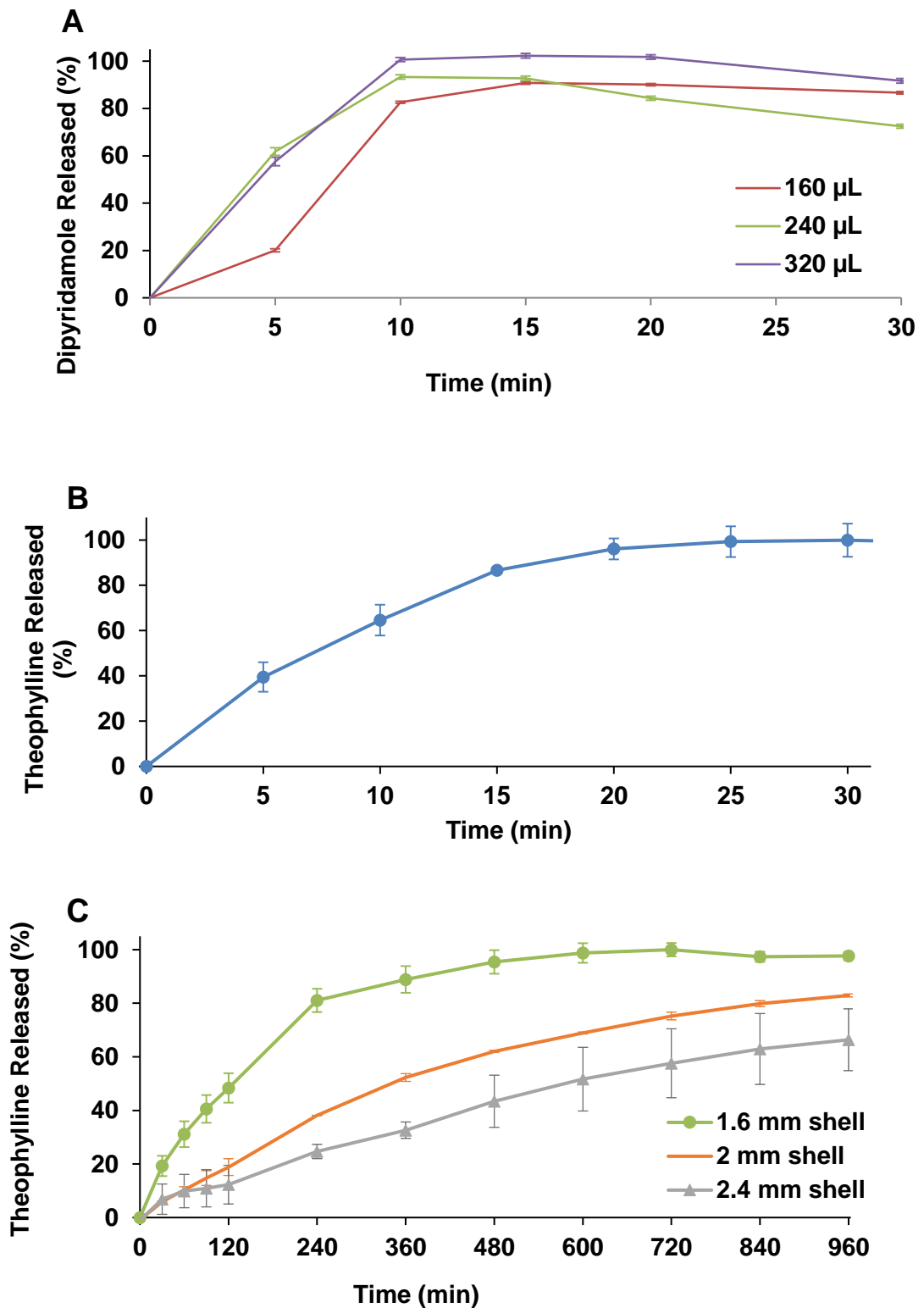


Figure 4.12. A) In vitro release pattern of dipyridamole suspension from 3D printed liquid Eudragit EPO capsule using USP II with different core volumes in gastric media (pH 1.2). B) In vitro release of theophylline from 3D printed liquid capsule filled with theophylline solution based on (B) Eudragit E or (C) Eudragit RL. All capsules were printed using multi-phase mode 3D printing and 2 mL syringe liquid dispenser.

The capacity of this shell system to extend drug release has also been subject to preliminary investigation, employing a water insoluble permeable polymer, Eudragit RL in the filament used to fabricate the shell (Figure 4.12C). This is essentially a reservoir-based controlled release system where amongst other factors, formulation of reservoir vehicle, drug loading, drug solubility, drug diffusivity through shell, plasticiser or pore formers in shell can all impact drug release rate (Ahmed and Naini, 2010).

By altering the shell thickness (1.6, 2 or 2.4 mm), it was possible to control drug release simply through a digital order, without the need to change the formulation composition. It is likely that soluble drug permeates through the insoluble acrylate layer through diffusion mechanism (Evonik, 2010). As the shell thickness increases, the travelled distance of drug will increase too thereby further prolonging drug release. It is worth noting here that the thickness of coating far exceeds typical Eudragit coating systems for pellets (Akhgari and Tavakol, 2016), this might be attributed to the porous nature of 3D printed shell due to voids between fused layers as well as the pores within the filament structure (Tsuda et al., 2015). It is worth noting that conventional coating system can provide a tighter control in comparison to the proposed 3D printed system (Emami and Kazemali, 2016, Siddique et al., 2010). However, this is the first report to achieve such control of drug release from a 3D printed capsule. With on-going advances in additive manufacturing in general, we expect that many of such limitations will be overcome in the future attempts.

In summary, we have reported a dynamic capsule-dispensing platform based on the orchestration of FDM 3D printing and liquid dispensing. Such platform is of high value when providing a small volume of liquid drug payload in a capsule is desirable. It could be potentially developed to include thermolabile substrate in the core, where hot melt extrusion (Patil et al., 2016) and FDM 3D printing (Okwuosa et al., 2016) are usually avoided. Other complex release profiles could also be feasible since the interior of the capsule shell could be compartmentalised with different wall thicknesses, which could be potentially filled with different actives for multiple active administration.

4.8 Conclusions

This is the first report of a fully automated process for the 3D printing of a liquid capsule. Both immediate and extended drug release profiles based on polymethacrylate polymer shells were fabricated with the immediate release from the Eudragit EPO polymer falling within the BP criteria. This could only be possible by using a modified dual FDM 3D printer where one of the heads was replaced with a syringe-based liquid dispenser, thereby allowing the coordination of FDM 3D printing of the shell followed by a liquid filling step.

Although the capsule shell was constructed in layer-by-layer fashion, it was possible to construct a capsule shell that maintains its integrity and instantly contains the loaded liquid doses without any curing step. This was made possible by using a concentric shell filling pattern which resulted in a tight shell structure. It was also necessary to use a wall thickness of up to 1.6 mm to avoid leakages post printing which is far thicker than the wall of a conventional capsule. The use of the multi-phase printing approach also produced a superior shell structure in comparison to the single-phase printing due to the limited need to switch between the FDM head and the syringe-based liquid dispenser head. This goes a long way to avoid creating gaps between layers during the shell printing which usually results in leakages.

The use of this modified setup also proved to be suitable for two APIs (dipyridamole and theophylline) and for suspensions or solutions as core materials, demonstrating the flexibility of the system in handling different actives in different forms. Above all, this technique demonstrated the ability to control doses as well as drug release by manipulating the dispensed volume and shell thickness simply via software. It was also observed that the use of a smaller syringe for the liquid dispenser produced a smaller and more accurate liquid dispensing. In a clinical setting, this will empower healthcare staff with capability to provide specific dosing and drug release patterns in individualised liquid-filled capsules without the need to change formulation.

The modified FDM heat completely avoided the use of temperature for the core processing, therefore creating more opportunities to employ thermosensitive actives including the use of large molecules like peptides and proteins. The application of peptides and protein in disease management and treatment is getting a lot of recognition, therefore having a 3D printing approach toward the delivery of such molecules will be an important addition to dose personalisation in the pharmaceutical industries. This will be discussed in more details in the next section.

4.9 Section 2: Introduction

The discovery of antimicrobial peptides (AMPs) dates back to 1939 with the extraction of antimicrobial agent from soil *Bacillus* strain (Dubos, 1939b, Dubos, 1939a) which was later fractionated and called tyrocidine and gramicidin (Van Epps, 2006). AMPs are small polypeptides produced by a constitutive or inducible expression in organisms and form an integral component of the host innate immune system. They are widely distributed in invertebrates, plants and higher animals, including humans and are usually less than 10 kDa (Liu et al., 2017). They are involved in the body's first line of defence with a broad spectrum of activity against various microorganisms. The Antimicrobial Peptide Database (APD) contains about 2828 AMPs, 300 of these AMPs derived from bacteria, 4 from archaea, 8 from protists, 13 from fungi, 343 from plants and 2160 from animals (UNMC, 2018). The activities of these peptides were suggested to include antibacterial, antiviral, antifungal, antiparasitic, antiprotist, antioxidant, chemotactic, insecticidal, protease inhibitor, spermicidal, surface immobilized and wound healing properties (UNMC, 2018).

Studies have shown the effect of AMPs against drug resistant bacteria (*E. coli*) both *in vitro* and *in vivo* using a novel cathelicidin peptide extracted from a king cobra (Li et al., 2012). Synthetic cationic AMPs were also found to have some activity against bacterial species associated with wound healing and therefore demonstrating potentials in the treatment of skin infection (O'Driscoll et al., 2013).

AMPs have also been identified to possess anticancer properties, demonstrating activities against breast cancer cell lines (Wong and Ng, 2005), cervical cancer (Kong et al., 2004), human adenocarcinoma and lymphoma cells (Li et al., 2002, Svargard et al., 2007, Yeshak et al., 2011). Their mechanism of action is still not clear. However research suggested that the anticancer activities of some AMPs could be due to tumour angiogenesis, tumour apoptosis, tumour necrosis, inhibition of kinases or proteases activities or interference with functional proteins (Wu et al., 2014).

Thirteen of the aurein peptide family derived from the granular dorsal glands of the Green and Golden Bell Frog (*Litoria aurea*) and the related Southern Bell Frog (*Litoria raniformis*) have been identified to possess anticancer activity. Aurein 1.2, 2.2 and 3.1 were identified as the most active (Rozek et al., 2000). Most studies on the anticancer activities of aurein were centred around aurein 1.2, which was active against cancer cell lines including colon cancer (Rozek et al., 2000) by invading the negatively charged cancer cell membrane due to their positive surface charge (Dennison et al., 2007). To

the authors understanding, the anticancer properties of aurein 2.6, which is also an active member of the aurein family, on colorectal cancer, has little information available.

LL-37, the only human cathelicidin AMP has also been investigated for anticancer activities especially for colon cancer. They are cationic which enables them to interact selective with the negatively charge cancer cell wall (membranolytic) (Hoskin and Ramamoorthy, 2008). The anticancer activity of LL-37 was improved in a DLD-1 and HT-29 colon cancer cell line when attached to the surface of a magnetic nanoparticle (Niemirowicz et al., 2015) and was able to induce cell death by apoptosis. A derivative of LL-37 (FK-16) not only demonstrated cell death by apoptosis but also by autophagic cell death due to the activation of protein p53 (Ren et al., 2013).

The use of peptides in disease management is gradually gaining recognition and as of 2016, polymyxin and enfuvirtide AMPs produced by RXGeneric and Trimeris respectively have been introduced to the United States market (Xia et al., 2017). Endogenous AMP inducers like vitamin D3, isoleucine and sodium butyrate have also been tested in a phase II clinical trials (Xia et al., 2017). However, one of its major limitation is the poor oral bioavailability of these macromolecular drugs due to pre-enzymatic degradation and poor transport across the intestinal membrane (Renukuntla et al., 2013). This resulted in the intramuscular, subcutaneous or intravenous injection of these peptides remaining the most common means of administration. The oral administration of drugs presents several advantages, including the ease of administration, patient compliance, safety and its less invasive approach, therefore the unrelenting investigation in the oral delivery of peptides and proteins. This however entails adequate understanding of the physicochemical properties (molecular weight, ionisation constant, pH stability, molecular size and hydrophobicity) and biological barriers (variable pH, poor permeability, membrane efflux and proteolysis in the stomach) that influence GIT absorption of these molecules (Renukuntla et al., 2013).

One of the approaches to improve the oral delivery of such actives include the use of absorption enhancers, which are compounds that allow actives to permeate across biological membrane more effectively (Aungst, 2012). Several absorption enhancers have been investigated, their efficiency depending on the physicochemical properties of the peptides and proteins, the vehicles used and area of absorption along the GIT. These enhancers could be classified into bile salts (sodium deoxycholate, sodium taurocholate), chelators (citric acid, salicylates), surfactants (sodium lauryl sulphate, sodium dodecyl sulphate), fatty acids (oleic acid, linoleic acid), cationic polymers (chitosan and its derivatives), anionic polymers (carbopol, n-acetyl cysteine) and

acylcarnitines (lauroyl-L-carnitine chloride, palmitoylcarnitine chloride) (Maroni et al., 2012). Their mechanisms of action may include temporarily disrupting the structural integrity of the intestinal barrier, opening the tight junctions, decreasing the viscosity of the mucus or by increasing membrane fluidity (Renukuntla et al., 2013, Maroni et al., 2012).

Another approach involves the use of enzyme inhibitors to suppress the enzymatic degradation of peptides and proteins, thereby facilitating absorption in the GIT (Yamamoto et al., 1994). These enzymes (trypsin, chymotrypsin, elastase, pepsin) are produced down the GIT to breakdown ingested food into simpler molecules before absorption. The use of enzyme inhibitors, which includes aprotinin, soyabean trypsin inhibitors, camostat mesilate, chromostatin, showed potential in improving peptide and protein activity (Yamamoto et al., 1994, Renukuntla et al., 2013). This could also be used in combination with absorption enhancers to enhance oral bioavailability (Sinha et al., 2007a).

Peptides and proteins could also be encapsulated with mucoadhesive substances to increase drug concentration gradient in the attached area, in addition to offering protection to the molecules (Muheem et al., 2016). Mucoadhesives such as chitosan (Mathiowitz et al., 1997), poly[lactic-co-glycolic acid] and thiolated polymers have been investigated in the oral delivery of peptides (Muheem et al., 2016). However, better results were obtained when used in combination with other approaches.

Colonic drug delivery avoids the acidity of the stomach and the proteolytic enzymes in the intestine, which play a key role in the reduced oral bioavailability of peptides and protein. It also offers longer transit time compared to the small intestine and may have a better responsiveness to permeation enhancers (Patel, 2011). Colonic delivery could be achieved by a microflora dependent approach (Saffran et al., 1986) where the molecules are coated with substances that are only broken down by the colon (Brøndsted and Kopeček, 1991). A time dependent colonic delivery on the other hand depends on the use of swellable/erodible polymers which delays the time of drug release to produce colon targeting. In an example, an insulin loaded core was coated with HPMC to achieve colonic delivery (Maroni et al., 2009). Colon targeting can also be achieved using polymers that dissolve at high pH levels. Eudragit S100 was used in the delivery of myovirus, *Clostridium difficile* specific bacteriophages to the colon (Vinner et al., 2017). This approach has been researched for the delivery of insulin in the colon alone or in combination with other approaches (Touitou and Rubinstein, 1986, Gwinup et al., 1991).

The site-specific approach in the delivery of peptides and proteins provides the opportunity to potentially localise drug effects in the colon. This will be beneficial in the treatment of diseases associated with the colon, including colon cancer which was discussed in Chapter 1 (Section 1.1.1). However, these drug delivery systems have been achieved using conventional tablet manufacturing approaches and, in some cases, the use of carrier vesicles (Bayat et al., 2008, Cheng and Lim, 2004).

The use of FDM 3D printers in drug manufacturing is gaining popularity, demonstrating potential in dose personalisation as shown in previous chapters. However, they have been utilised mostly for small molecules with no examples for its adaptation for large molecules like peptides and proteins. Achieving this goal using this novel approach will showcase the versatility of 3D printing in pharmaceutical manufacturing and also provide a means to tailor such molecules to individual needs. Peptides and proteins are thermosensitive and therefore could not be loaded into filaments due to the heat processing involved in HME and FDM use. This therefore calls for modifications and adaptations of the FDM head. The set up and modifications used in the printing of the liquid capsule as described in section one was investigated for its potential in the manufacturing of peptide-loaded liquid-filled capsules in this study.

4.10 Aims

This research aims at demonstrating a fully automated additive manufacturing process for a liquid-filled capsule with the potential of achieving colon targeting of anticancer AMPs. To achieve this goal, the objectives of this research includes:

- Determinations of the anticancer activities of aurein 2.6 and LL-37 using HT-29 and Caco-2 cancer cell lines as models.
- To modify a dual FDM 3D printer to include a syringe-based liquid dispenser, which was used to fabricate a capsule shell through FDM 3D printing and instantaneously dispense a solution of model drugs.
- To demonstrate the first example of a fully automated additive manufacturing process for a liquid-filled capsule containing a thermosensitive active.
- To determine the effect of the 3D process on the peptide's secondary structure
- To initially characterise colon drug delivery and release profiles by encapsulating theophylline solution into 3D printed Eudragit S100-based hard shell liquid-filled capsules.

4.11 Materials

The following materials were used in this research.

4.11.1 Eudragit S100

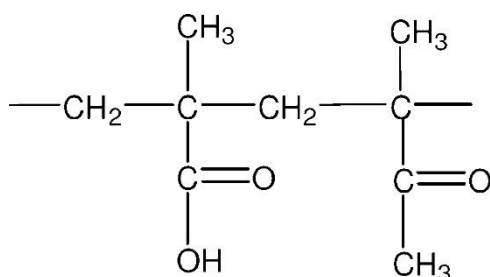


Figure 4.13. Chemical structure of Eudragit S100 (Yoo et al., 2011).

This is a methacrylic acid copolymer (Figure 4.13), which is gastric resistant and stable at low pH level. It however dissolves at $\text{pH} \geq 7$ which makes it very useful in colon delivery and other forms of delayed release products. Evonik Industries (Darmstadt, Germany) donated this polymer for this research.

4.11.2 Aurein 2.6 (MW, 1629)

Aurein 2.6 is one of the 16 antimicrobial peptides derived from the skin of *Litoria raniformis* (Southern bell frog) with the amino acid sequence GLFDIAKKVIGVIGSL-NH₂. It has been observed to demonstrate a random coil structure in an aqueous media which changes depending on the dissolution solvent used, amidation resulting to a helical structure (Mura et al., 2016). It has a wide spectrum of activity against bacteria and fungi and has been investigated for anticancer properties. This AMP was purchased from Pepceuticals, UK for this research.

4.11.3 Cathelicidin LL-37 (MW, 4493.33)

Cathelicidin LL-37 is the only AMPs under the cathelicidin family derived from humans with the amino acid sequence LLGDFFRKSKEKIGKEFKRIVQRIKDFLRNLPRTES. The solution structure of this peptides depends on the media used, its ion composition, salt type and pH (Xhindoli et al., 2014). It has been shown to demonstrate a helical structure in an aqueous buffer solution (Thennarasu et al., 2010) and a random structure in pure water (Zhang et al., 2010). It is amphipathic and serves a critical role in mammalian innate immune defence against infections (Dürr et al., 2006). It is expressed in several parts of the human body including the epithelial cells of the testis, skin, GIT, respiratory tract and in leukocytes such as monocytes, neutrophils, T cells, NK cells and B cells. They are well established to have a broad spectrum of antimicrobial activity

(Johansson et al., 1998) and have also been investigated for cytotoxic activities. This AMP was purchased from Pepceuticals, UK at 80% purity for this research.

4.11.4 HT-29 colon cancer cell line (Passage number 141)

HT-29 was derived from 44 years old human and it is a colorectal adenocarcinoma. It originated in 1964 and has been used in studies relating to colorectal cancer. This was purchased from Sigma-Aldrich (UK).

4.11.5 Caco-2 colon cancer cell line (passage number 57)

Derived from a 72 years old male Caucasian, this cell line is a colorectal adenocarcinoma which finds use in cancer studies. For this study the cell line was purchased from Public health, England.

4.11.6 Other ingredients

Theophylline (>99%, anhydrous) was purchased from ACROS Organics (UK). Triethyl citrate (TEC), Tween 80, citric acid, MTT assay, dimethyl sulphoxide (DMSO) EMEM and McCoy's 5A medium was purchased from Sigma-Aldrich (UK). Phosphate buffer tablets were from Fisher Scientific (UK). Trypsin was purchased from Lonza (Switzerland). Talc was purchased from Fluka Analytical (UK).

4.12 Methods

4.12.1 Cell recovery from cell bank

Frozen cells were received in a cryogenic vial (1 mL) and were preserved in liquid nitrogen before defrosting. Defrosting was carried out by placing the vial in a 37 °C water bath for approx. 2 min. The thawed cell suspension was added into 20 mL media (EMEM for Caco-2 and McCoy's 5A for HT-29) in a T25 flask to further dilute DMSO usually used as cryoprotectant during freezing down. The flask was incubated at 37 °C under 5 % CO₂ and the cells monitored. Once attached to the flask, which usually occurs within 24 hrs, the media was replaced with a fresh one.

4.12.2 Cell sub-culturing / passaging

Cells were grown until 80-90 % confluency as observed using a light microscope. Cells were passaged by aspirating the media from the flask and washing the cells with PBS as the media dilutes the effect of the trypsin. A 0.25 % trypsin-PBS (1 in 10 dilution) was added into the flask (2 mL in 75 cm³ flask or 1 mL in 25 cm³ flask) and incubated for 3-5 min at 37 °C. This detaches the cells from the flasks and in some cases a gentle tapping

is required to aid detaching. The effect of the trypsin was stopped by diluting with an equal volume of media. The cell suspension was centrifuged at 1000 rpm for 5 min and the supernatant removed. The cell pellet was re-suspended in fresh media and cell splitting carried out depending on the number of cells (as specified by ECACC) determined using haemocytometer.

4.12.3 Cell counting using haemocytometer

The preparation of the haemocytometer for cell counting requires cleaning the glass haemocytometer and cover slip with alcohol. The haemocytometer was moistened by breathing on it before fixing the coverslip by gently sliding it across using the two thumbs. The presence of Newton's refraction rings under the coverslip indicates proper adhesion. A haemocytometer has two counting chambers and each chamber has 9 squares that are 1 mm in length (Figure 4.14).

The cell suspension was evenly distributed before taking 100 μL of the suspension into an Eppendorf. Trypan blue (100 μL) was added to the collected cell suspension (1:1). Trypan blue is commonly used during cell counting to distinguish between live and dead cells as they can get into dead cells with ruptured membranes. This makes them appear blue under the light microscope unlike live ones with intact cell membrane. Using a pipette, 100 μL of the trypan blue-treated cell suspension was applied to the haemocytometer at the chamber underneath the coverslip, allowing the cell suspension to be taken up by capillary action. Using a hand tally counter, the live cells were counted for five different regions (Figure 4.14) and the average was multiplied by 2 (the dilution factor from the trypan blue added) and multiplied by 10^4 [(Average \times 2) $\times 10^4$].

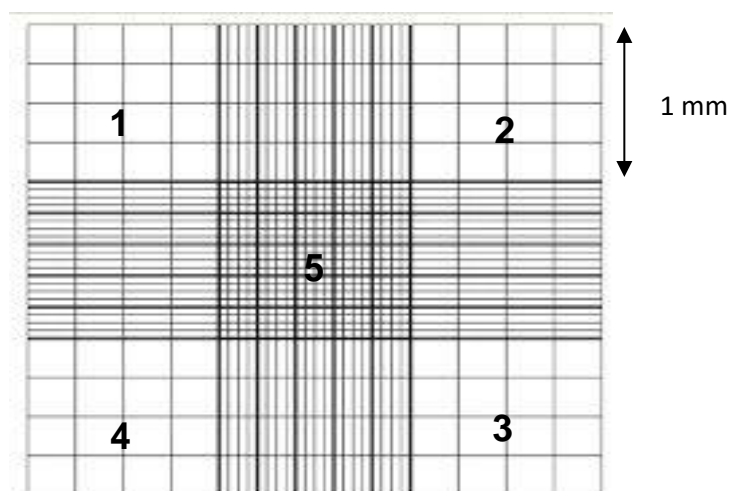


Figure 4.14. The surface of a haemocytometer.

4.12.4 Freezing down of cells

To ensure sufficient cell stocks are available for experiments, it was necessary to freeze down cells. Once the cells have been passaged into a few flasks as explained earlier (Section 4.12.2), cell counting was carried out and the cell suspension centrifuged. The supernatant was removed, and the cells were re-suspended in a freezing media, which is the culture media (EMEM for Caco-2 and McCoy's 5A for HT-29) with 10 % DMSO at a cell density as specified by ECACC. The cell suspension was transferred into cryogenic vials (1 mL) and placed into freezing container (Mr Frosty™) which was designed to achieve a cooling rate of 1 °C/min. This was placed in a -80 °C freezer and left for 24 hrs before transferring into a liquid nitrogen (-192 °C) for long term storage.

4.12.5 Growth curve using trypan blue

Cell growth for HT-29 and Caco-2 was carried out by seeding 2×10^4 cells into 6-well plates. This was incubated at 37 °C for 7 days and the cell count was checked every 24 hrs. To determine cell growth using trypan blue, after every 24 hrs, the media was aspirated, and 0.5 mL of trypsin was added to the cells to detach them from the plate. The trypsin was neutralised by adding an equal volume of the media and then centrifuged and replaced with a fresh media. Cell counting was carried out as explained in Section 4.12.3 above.

4.12.6 Growth curve using MTT assay

MTT (3-(4,5-dimethylthiazolyl-2)-2,5-diphenyltetrazolium bromide) assay is a reliable and sensitive indicator of cell metabolic activity. The assay relies on the reduction of MTT, a yellow water-soluble tetrazolium dye to a purple coloured formazan crystal, primarily by mitochondrial dehydrogenase.

Cell growth for HT-29 and Caco-2 was carried out by seeding 5×10^3 cells in 96-well plate in a total volume of 100 µL. This was incubated at 37 °C for 7 days. Every 24 hrs, 20 µL of the MTT assay reagent (5 mg/mL) was added the 100 µL cell suspension and incubated for 3 hrs. At the end of the incubation, the supernatant was careful aspirated to avoid disturbing the formazan salt. This was dissolved using 100 µL of DMSO and was incubated for another 30 min. Absorbance was taken using Tecan microtitre plate reader (Australia) at 595 nm.

4.12.7 Cell viability / cytotoxicity studies

To determine cell cytotoxicity of the actives (aurein 2.6 and LL-37) on the cells (HT-29 and Caco-2), 5×10^3 of the cells were seeded in 96-well plates. This was allowed 24 hrs

to attach to the bottom of the well plate before treating. Treatment was carried out by dissolving the actives in the cell media at concentrations of 1000, 300, 100, 30 and 10 µg/mL and used to replace the media in the well plates. This was monitored for 24, 48 and 72 hrs. The viable cells were determined by MTT assay as explained in Section 4.12.6 above. A graph of the percentage viability based on the absorbances obtained were plotted against the drug concentration. This experiment was also carried out using cisplatin as the positive control.

4.12.8 Determination of IC₅₀

IC₅₀ stands for the inhibitory concentration where the response is reduced to half. It is a measure of the potency of a substance against a biochemical or biological function (Sebaugh, 2011). The IC₅₀ of the peptides were determined using Microsoft excel software. The percentage viability was plotted against the concentrations of the peptides used in µM. the equation from the polynomial order 2 was used to determine the IC₅₀ of the actives by solving for “x”.

4.12.9 Preparation of shell filament

For the preparation of the shell, drug-free Eudragit S100 filaments were produced by a HAAKE MiniCTW hot melt compounder (Thermo Scientific, Karlsruhe, Germany). An optimised ratio of a powder mixture constituting of the polymer (52.5 %), TEC (22.5 %) and talc (25 %) was gradually added to the HME at 130 °C and allowed to mix for 5 min at 80 rpm to allow homogenous distribution of the molten mass. Afterwards, the filament was extruded at 20 rpm after cooling the HME down to 120 °C.

4.12.10 Preparation of liquid core

a. Peptide solutions were prepared by dissolving the peptides in phosphate buffer solution (PBS), pH 5.9 at 0.01 mg/mL. The PBS was prepared by mixing 92 : 8 mL of 0.1 M sodium phosphate monobasic (M.W. 138,13.8g/L) and 0.1 M sodium phosphate dibasic (M.W. 268, 26.8g/L) respectively.

b. Theophylline solution was prepared as described in Section 4.6.5b

4.12.11 3D printing of liquid capsules

A modified FDM 3D printer as described in Section 4.6.6 was used in this study. A Multi-phase printing mode using simplified 3D software version 3.1.1 (Simplify 3D LLC, Ohio, USA) was used in 3D printing of the liquid capsule. The shell was designed to comprise a complementary bottom and a cap. This liquid capsule printing was carried out in 3

phases: i) printing of the shell bottom, ii) filling of liquid core, and iii) sealing of the shell in a separate 3D printing stage.

The liquid capsules were printed with cube dimensions corresponding to 240 μL . The settings of the software were modified, and the parameters of 3D printing of the shell was carried out at 190 $^{\circ}\text{C}$ with the building plate at 20 $^{\circ}\text{C}$. The resolution was set at medium (200 μm layer thickness), the infill was 100 % and the internal and external infill pattern were set at grid and concentric respectively. The rest of the settings were left as default. As priming was not necessary for liquids, the script of the software was also modified to omit the priming step of the liquid dispenser.

4.12.12 Thermal analysis using thermal imaging camera

Thermal images were taken at different points of shell printing using FLIR B400 IR camera. The camera was positioned 30 cm from the printing stage and images were taken after every 10 secs. The printing temperature was plotted against time.

4.12.13 Determination of the secondary structure of the peptides using circular dichroism

Circular dichroism (CD) is a result of the difference in the absorption of left-handed circularly polarised light (L-CPL) and right-handed circularly polarised light (R-CPL) from a chiral molecule. In a circular dichroism spectrophotometer, a monochromatic linearly polarised light is altered by a photo-elastic modulator (PEM) which creates a left or right-circularly polarised light as it oscillates at its resonance frequency. The samples are exposed to these light and if chiral, the detectors record the light intensity due to the L-CPL and the R-CPL.

$$\text{CD} = (\nu_{\text{AC}}/\nu_{\text{DC}}) G$$

Equation 4.2

ν_{AC} = Difference in the intensity between the two circularly polarised light

ν_{DC} = The average total light intensity across many PEM oscillations

G = Calibrating-scaling factor.

This find use in assessing the secondary structure of large molecules like peptides and proteins which could be sensitive to changes due to environmental conditions.

The impact of temperature and the 3D printing processes on the integrity of the AMPs were determined using circular dichroism. This was carried out using J-815 spectropolarimeter (JASCO, UK) equipped with a peltier temperature control unit. All the experiments were carried out using a 10 mm path-length cell cover over a 260-180 nm wavelength range at a scanning speed of 50 nm/min. Scanning was carried out in

triplicate and was prepared by dissolving the peptides in phosphate buffer saline (pH 5.9) at a concentration of 0.01 mg/mL. Secondary structure analysis was carried out using Dichroweb (on-line analysis of protein circular dichroism spectra).

4.12.12 Statistical analysis

One-way ANOVA was employed using SPSS Software (22.0.0.2) to analyse the results. Differences in results of $p < 0.05$ were considered to be significant.

4.13 Results and discussions

Figures 4.15A and B. shows the images of approximately 50 % confluent Caco-2 and HT-29 colon cancer cells used in this research, respectively. These cells were cultured and monitored for 7 days to understand the growth pattern of the colon cancer cells. This was very crucial to determine the time of natural cell death and therefore the time for cell treatment to avoid obtaining false positive results. Initial investigation on the growth curve of the cells were carried out using trypan blue dye in a 6 well plate with a seeding density of 20×10^4 . This was based on the principle that only dead cells will absorb the dye due to cell wall penetration. It was observed that Caco-2 cells doubled after 24 hrs ($49.2 \times 10^4 \pm 11.4$) and the cell growth peaked after 72 hrs ($90.5 \times 10^4 \pm 11.4$) after which cell death started occurring (Figure 4.16A). On the other hand, the HT-29 cell line doubled after 48hrs ($62.3 \times 10^4 \pm 4.2$) and the time for the highest point of growth was after 120 hrs ($328.2 \times 10^4 \pm 51.2$) before cell death started occurring. The HT-29 cell population was noticed to be 3.5 times greater than that of Caco-2 cells at the highest point of growth even though the doubling time was much slower, demonstrating the rapid proliferation of HT-29 cells.

This initial understanding on the doubling time of the cells and the points of cell death gave an idea of the behaviour of the cells but however does not represent the conditions at which the cytotoxicity of the actives (AMPs) on the cell lines will be tested. As a result, another growth curve was carried out using a 96-well plate at a seeding density of 5×10^3 using MTT assay to determine only the viable cells. This seeding density was chosen based on the area of the wells of the 96-well plate in relation to that of the 6 well plates used initially. This was believed to be a better representation of the growth pattern of the cells. The seeded cells were allowed to attach to the plate after 24 hrs before growth curve determination. It was observed that both cell lines doubled 48 hrs after attachment (Figure 4.16B). A 62 hrs doubling time has been reported by American Type Culture Collection (ATCC, 2016) however factor like the culture conditions and the passage number of the cell line could play a major role in this disparity (Corrêa et al., 2016). The absorbance obtained from the MTT assay increased from 0.3701 ± 0.0018 to 0.6679 ± 0.0267 and 0.4932 ± 0.0133 to 0.8554 ± 0.0210 for Caco-2 and HT-29 cell lines respectively. The growth of both cells peaked after 96 hrs after which cell death started occurring as observed from the decrease in the absorbance obtained from the assay. It was believed that cell death for both assays were as a result of the lack of space and nutrients since no media change was conducted during this process.

As a result of these initial observations, 24, 48 and 72 hrs after cell seeding were considered as the periods of cell proliferation and therefore will be the points of consideration during treatment. Cell growth inhibition at any of these stages will indicate the influence of an external factor and in this case the administered actives.

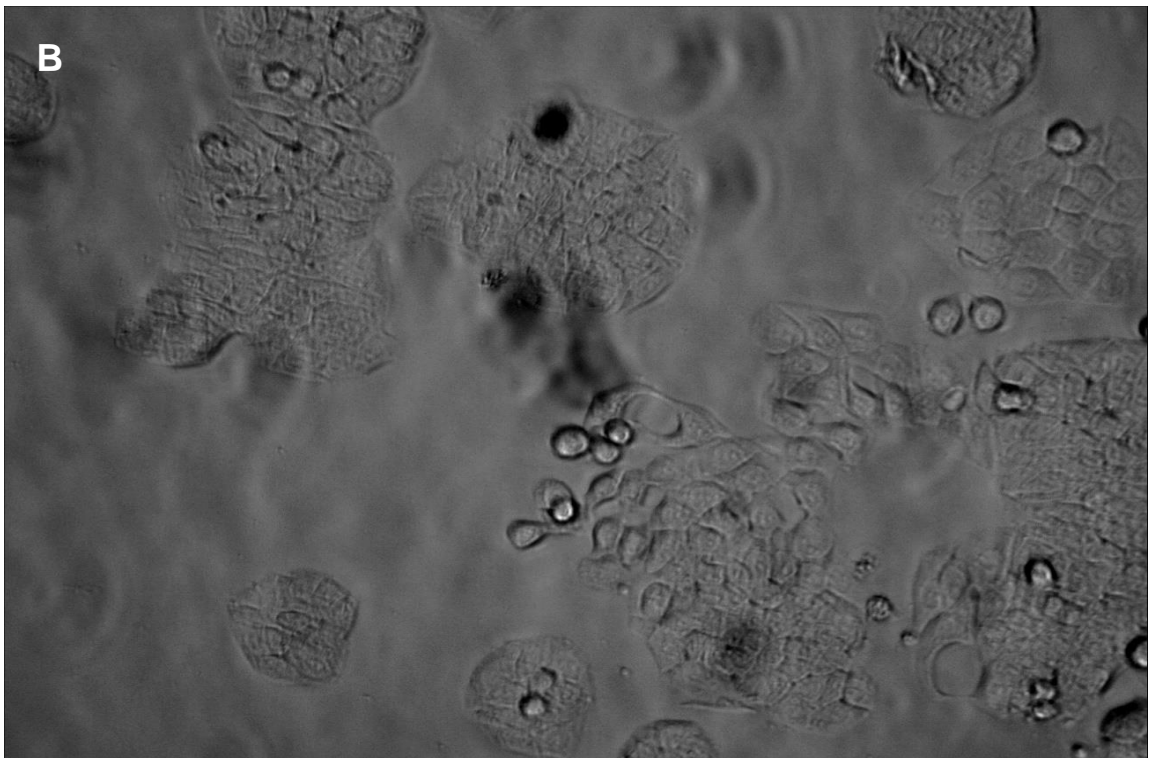
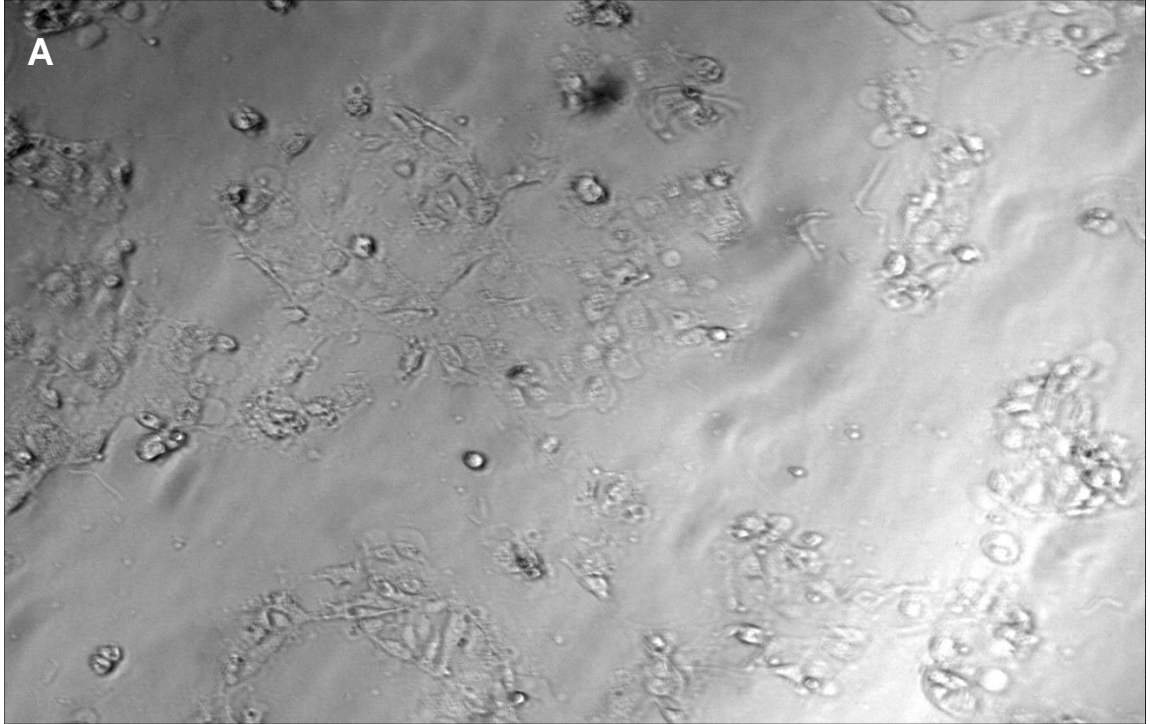


Figure 4.15. 50 % confluent Caco-2 (A) and HT-29 (B) colon cancer cell lines.

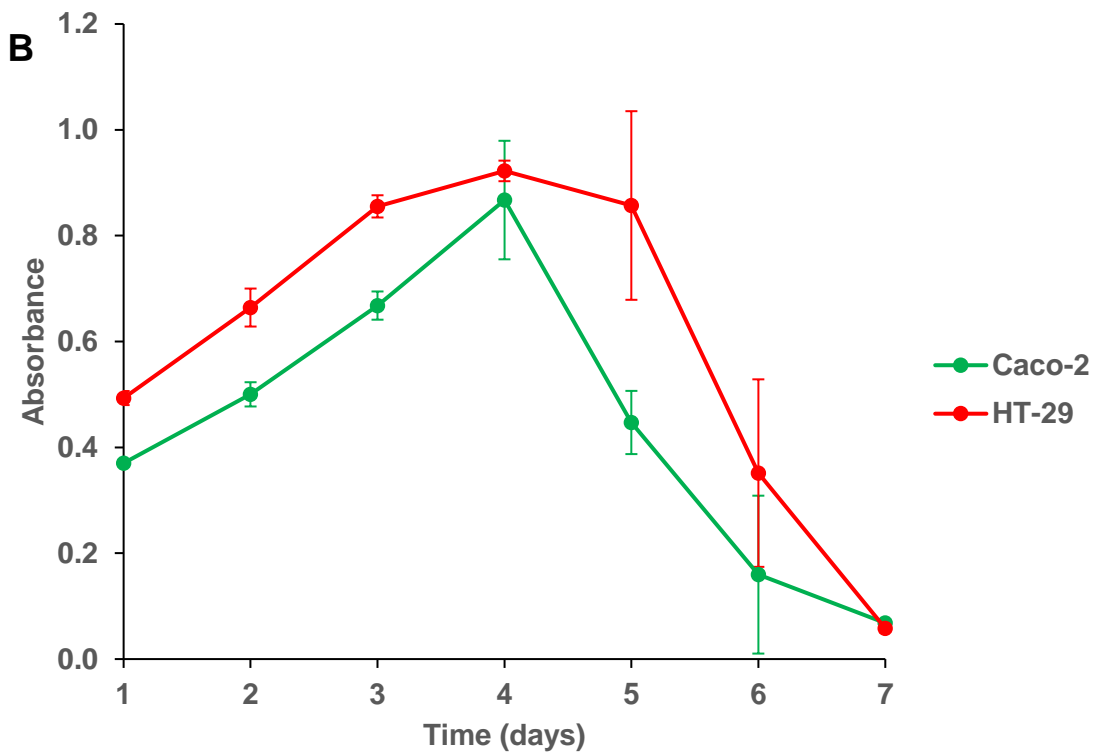
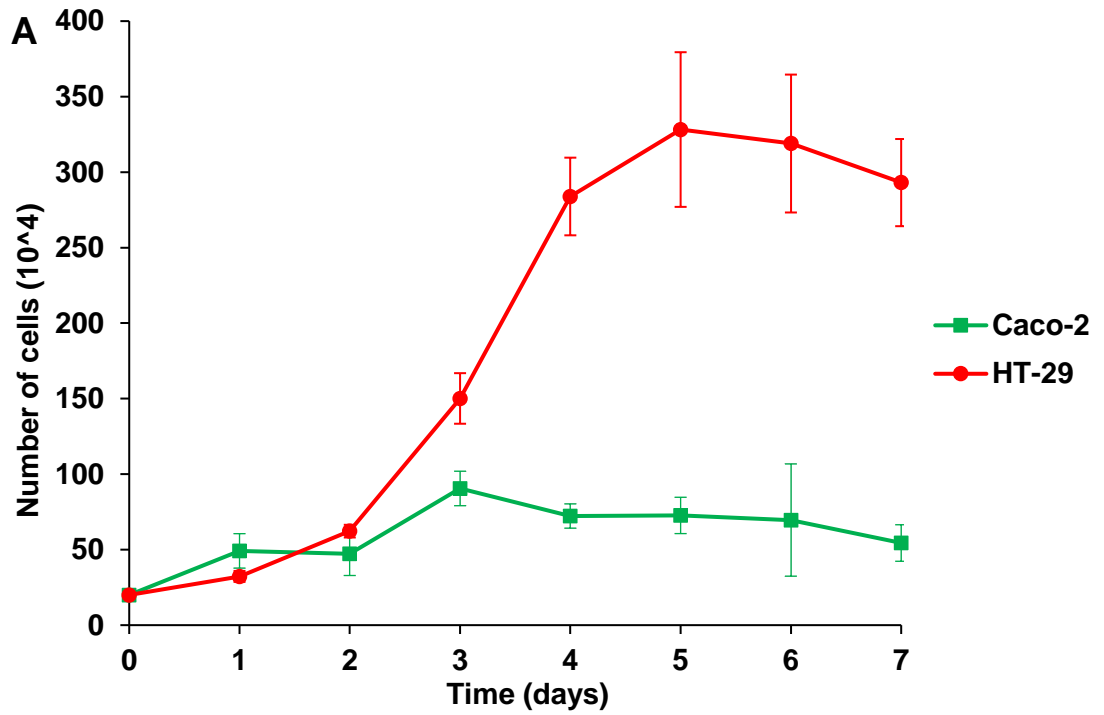


Figure 4.16. Growth curve of Caco-2 and HT-29 using trypan blue (A) and MTT assay (B).

AMPs have been shown to have a wide range of activities including anticancer properties (Rozek et al., 2000, Dennison et al., 2007) which was also investigated in this research. The anticancer activities of aurein 2.6 and LL-37 were investigated by treating the HT-29 and Caco-2 colon cancer cell lines with a range peptide concentration (1000 – 10 µg/mL). Cisplatin was used as the positive control as it is a well-established anticancer agent with the ability to induce cell death by interfering with DNA repair mechanism, thereby causing DNA damage in addition to inducing apoptosis in cancer cells (Dasari and Tchounwou, 2014).

The seeded cells were allowed 24 hrs to attach to the well plates before treatment. It was observed that the peptides and the positive control had a concentration dependent increase in activity against the cell lines used at the three points of evaluation (24, 48 and 72 hrs) (Figures 4.17 and 4.18), thereby demonstrating the anticancer properties of the AMPs. Aurein 1.2 which is one of the most active aurein family was suggested to demonstrate anticancer activities by invading the negatively charged cancer cell membrane due to their positive surface charge (Dennison et al., 2007). This could also be the mechanism of action of aurein 2.6. However further investigations are required to confirm this.

A study by Niemirowicz et al. (2015) showed minimal activity of LL-37 HT-29 colon cancer cell at concentrations ≤ 100 µg. This was also observed in this study with higher concentrations required to induce more cell death. Cell death by LL-37 could be due to a selective cancer cell wall invasion as a result of their surface charge. It has been demonstrated to also cause cell death by a caspase-independent apoptosis in colon cancer cells (Niemirowicz et al., 2015, Ren et al., 2013, Piktel et al., 2016, Ren et al., 2012).

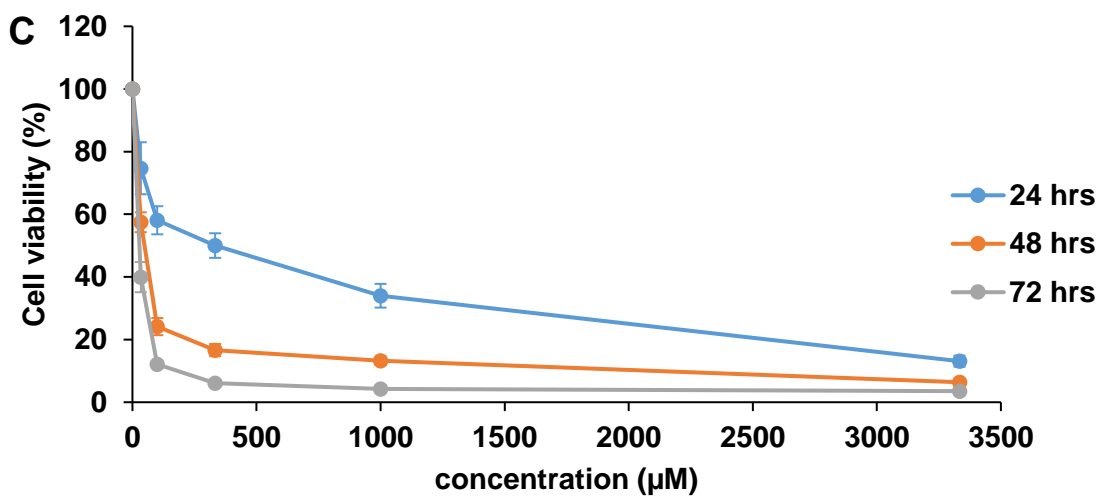
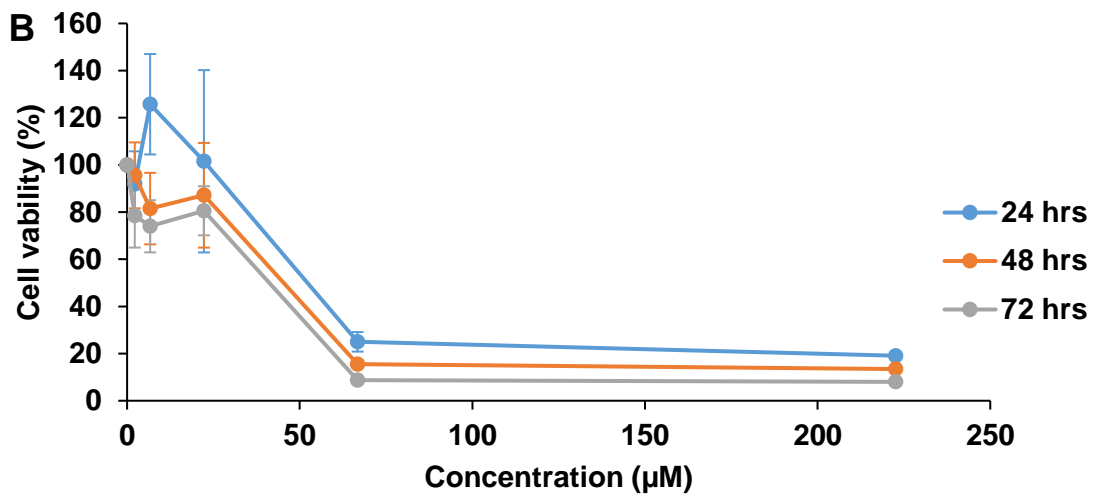
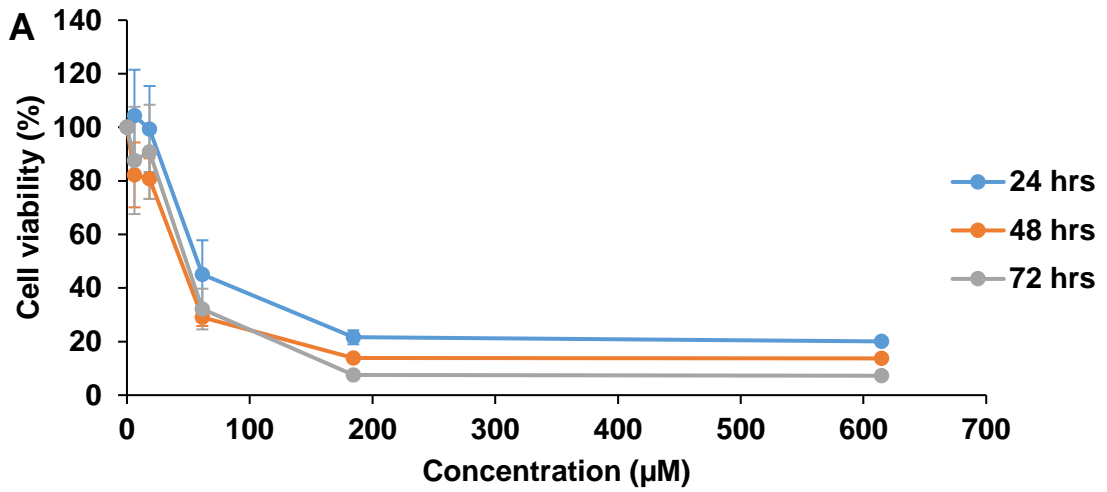


Figure 4.17. Cytotoxicity of aurein 2.6 (A), LL-37 (B) and cisplatin (C) on HT-29 colon cancer cell line.

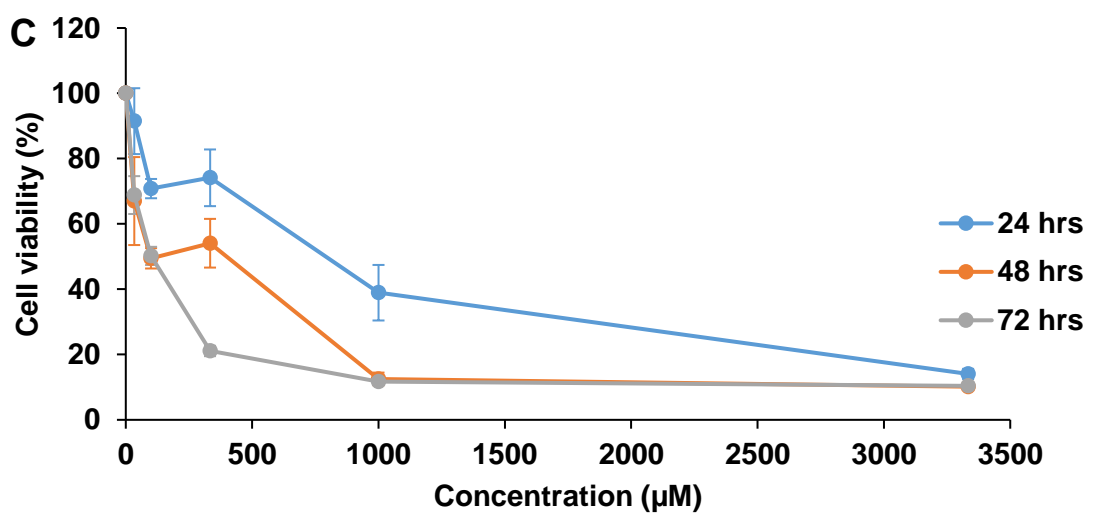
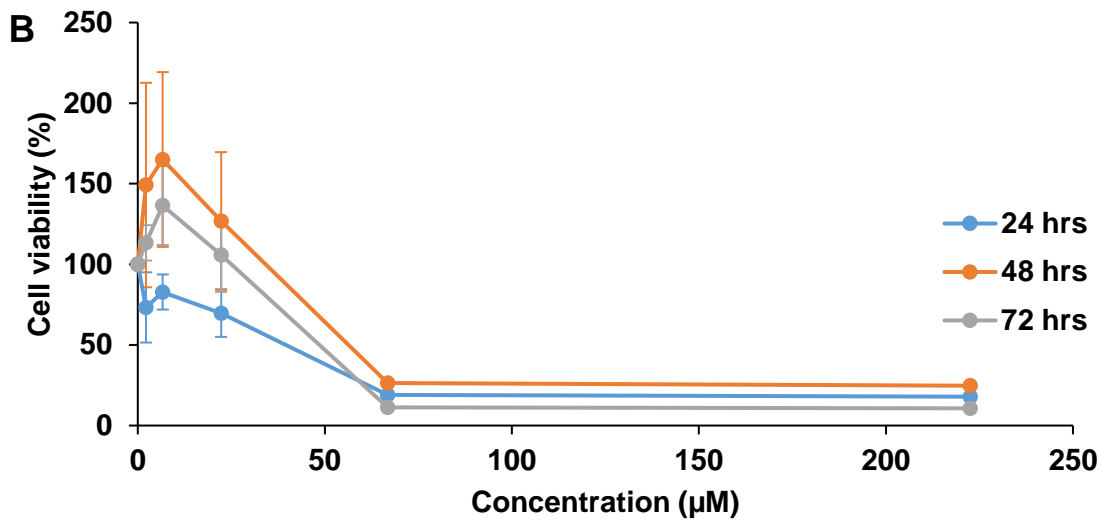
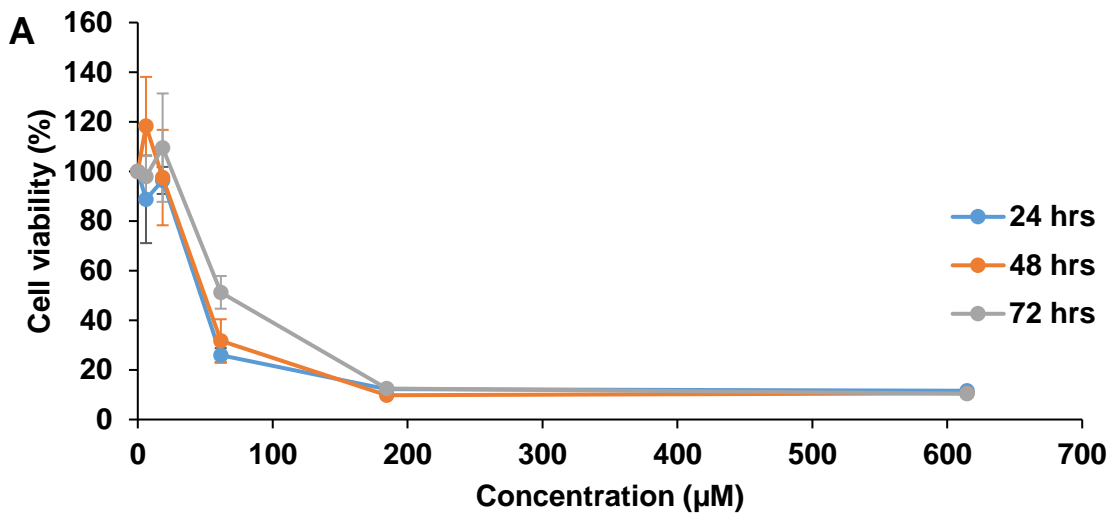


Figure 4.18. Cytotoxicity of aurein 2.6 (A), LL-37 (B) and cisplatin (C) on Caco-2 colon cancer cell line.

Results from the determination of the peptide concentration required to kill 50% of the cell population (IC_{50}) after 24, 48 and 72 hrs of treating the cell lines with aurein 2.6, LL-37 and cisplatin are shown in Table 4.3. The treatment of HT-29 cell line with the various actives demonstrated a time dependent increase in activity as seen from the decrease in IC_{50} value over time. However, this was not the case for the treatment of Caco-2 cell lines except for cisplatin, which maintained a time depended activity. This time dependent activity of cisplatin on both cell lines has also been reported in a study by Leong et al. (2016). However, an IC_{50} of 181.1 ± 6.1 , 104.5 ± 1.2 , 75.7 ± 4.7 and 120.9 ± 7.0 , 93.5 ± 3.0 , $62.3 \pm 1.2 \mu M$ were obtained for its use on HT-29 and Caco-2 respectively after 24, 48 and 72 hrs (Leong et al., 2016). Initial investigations into the activities of aurein 2.6 peptide on colon cancer cell lines also demonstrated similar range of IC_{50} (Rozek et al., 2000).

Table 4.3. IC_{50} of aurein 2.6, LL-37 and cisplatin on HT-29 and Caco-2 colon cancer cell lines.

| Time (hrs) | IC50 of aurein 2.6 (Mean \pm μM) | | IC50 of LL-37 (Mean \pm μM) | | IC50 of cisplatin (Mean \pm μM) | |
|------------|--|-------------|-------------------------------------|-------------|---|---------------|
| | HT-29 | Caco-2 | HT-29 | Caco-2 | HT-29 | Caco-2 |
| 24 | 93 \pm 11 | 73 \pm 6 | 51 \pm 9 | 34 \pm 6 | 500 \pm 41 | 746 \pm 144 |
| 48 | 69 \pm 4 | 80 \pm 11 | 38 \pm 5 | 57 \pm 10 | 146 \pm 9 | 332 \pm 36 |
| 72 | 71 \pm 1 | 90 \pm 9 | 32 \pm 4 | 45 \pm 5 | 19 \pm 20 | 254 \pm 13 |

To be able to localise the release of these AMPs in the colon, a Eudragit S100-based shell filament was adapted for FDM 3D printing based on previously used principles involving the use of a plasticiser and a non-melting component. This polymer was chosen as it is only soluble at $pH \geq 7$ which makes it a good candidate for colon targeting. This will potentially localise the activity of the AMPs in the colon and completely avoid the harsh conditions of the stomach which is one of the reasons for the poor oral bioavailability of peptides and proteins (Moroz et al., 2016). The optimised formulation of the polymer, TEC and talc was processed by HME and the resultant filament allowed 3D printing by FDM at 190 °C.

TGA of the filament demonstrated no significant weight loss at the HME and 3D printing processing temperatures indicating the stability of the filament. Weight loss from the filaments started occurring above 200 °C due to TEC degradation before the polymer degradation above 350 °C (Figure 4.19A). The DSC analysis of Eudragit S100 demonstrated a T_g of 174 °C which was in agreement with the findings of Parikh et al.

(2014). The Tg of Eudragit S100 has been also reported to be 188.5 Tg (Sharma et al., 2011) which could be as a result of the used experimental conditions. The addition of the plasticiser (TEC) and the non-melting component resulted in a shift in the Tg from 174 °C to 85.7 °C (Figure 4.19B).

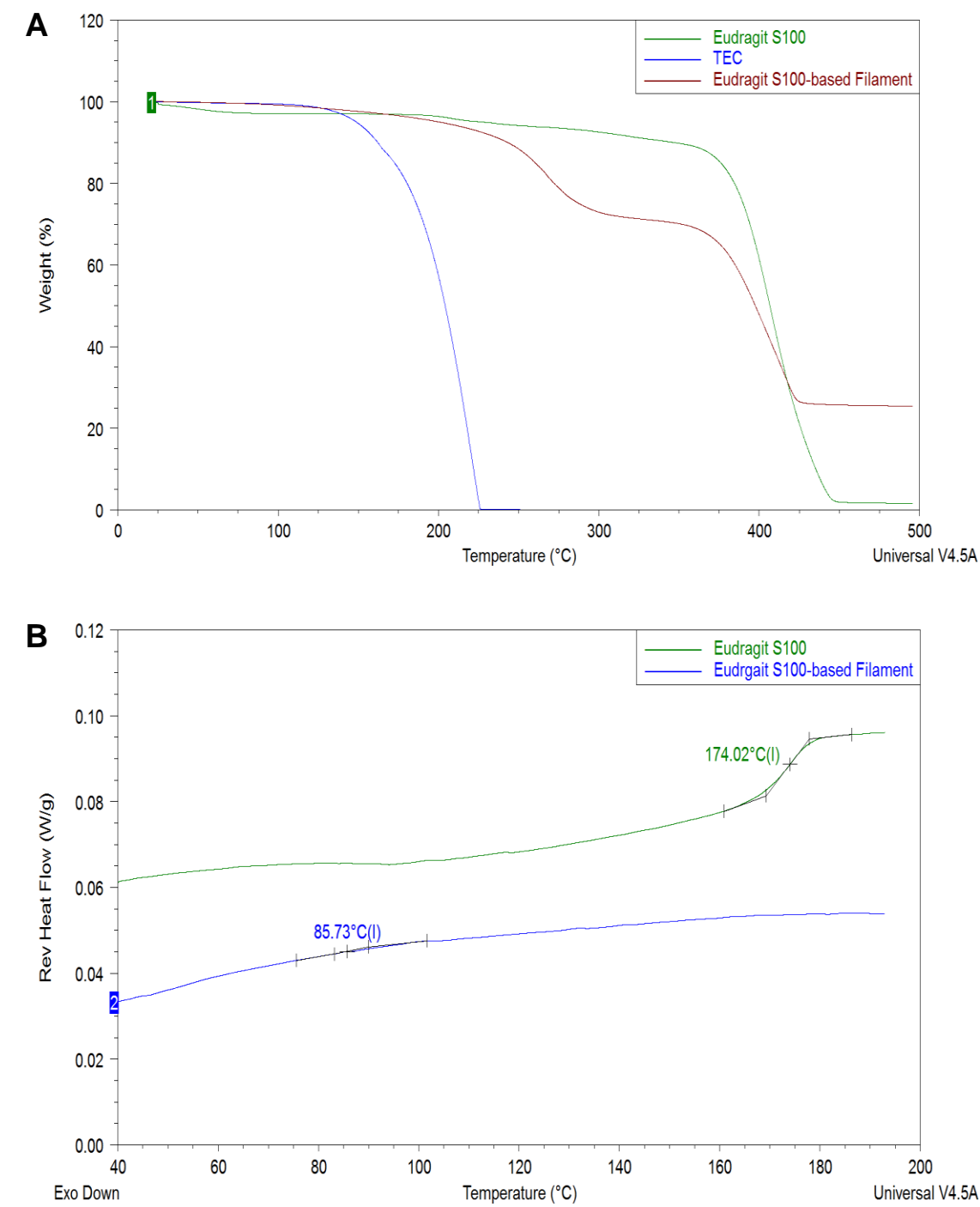


Figure 4.19. TGA (A) and DSC (B) thermographs of Eudragit S100 polymer and Eudragit S100-based filament.

The modified FDM head, which allows the coordination of an FDM head and a syringe-based liquid dispenser, was used in this study. This will allow the FDM printing of the Eudragit S100-base filament as the shell filament which could be subsequently filled with a peptide solution to form a liquid capsule. The multiphase printing mode was also chosen as the default approach for this experiment since this will reduce interchanging of the printing heads as explained earlier, therefore reducing the impact of the processes on the peptides. A shell thickness of 1.6 mm was chosen since this offered adequate protection to the core content (Okwuosa et al., 2018).

It was crucial to determine the temperature changes that occurs during FDM 3D printing using the multi-phase approach as peptides are sensitive to environmental conditions (Johansson et al., 1998, Xhindoli et al., 2014). These initial investigations were essential to ensure the integrity of the peptides are maintained since changes in secondary structure of a peptides could affect their biological activity (Thành, 2015). This was investigated using a thermal imaging camera, which demonstrated fluctuations in the temperature as determined from readings from particular areas during the shell printing (Figures 4.20 and 4.21). This however seems to be influenced by the position of the heated nozzle in relation to the spot being measured, therefore making this initial investigation inconclusive and unreliable. However, at the end of the initial 75 % shell printing step, the shell cools down to the temperature of the plate (20 °C) which was ideal for the peptides injection (Figures 4.20 and 4.21) before the final sealing stage. The cooling of the shell layers as printing progresses could also be seen from the colour coding of the layers from the thermal camera (Figure 4.21), which confirms the fast cooling and solidification of FDM 3D printed objects.

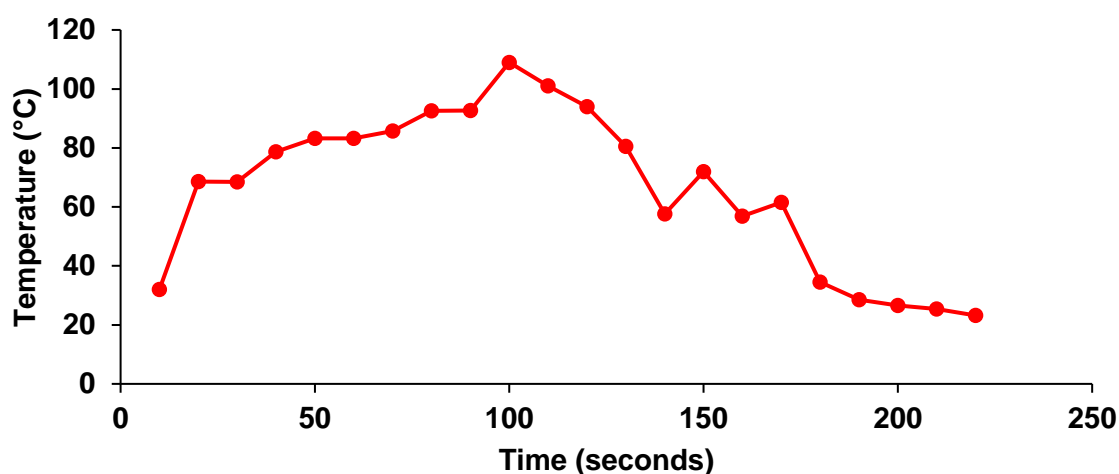
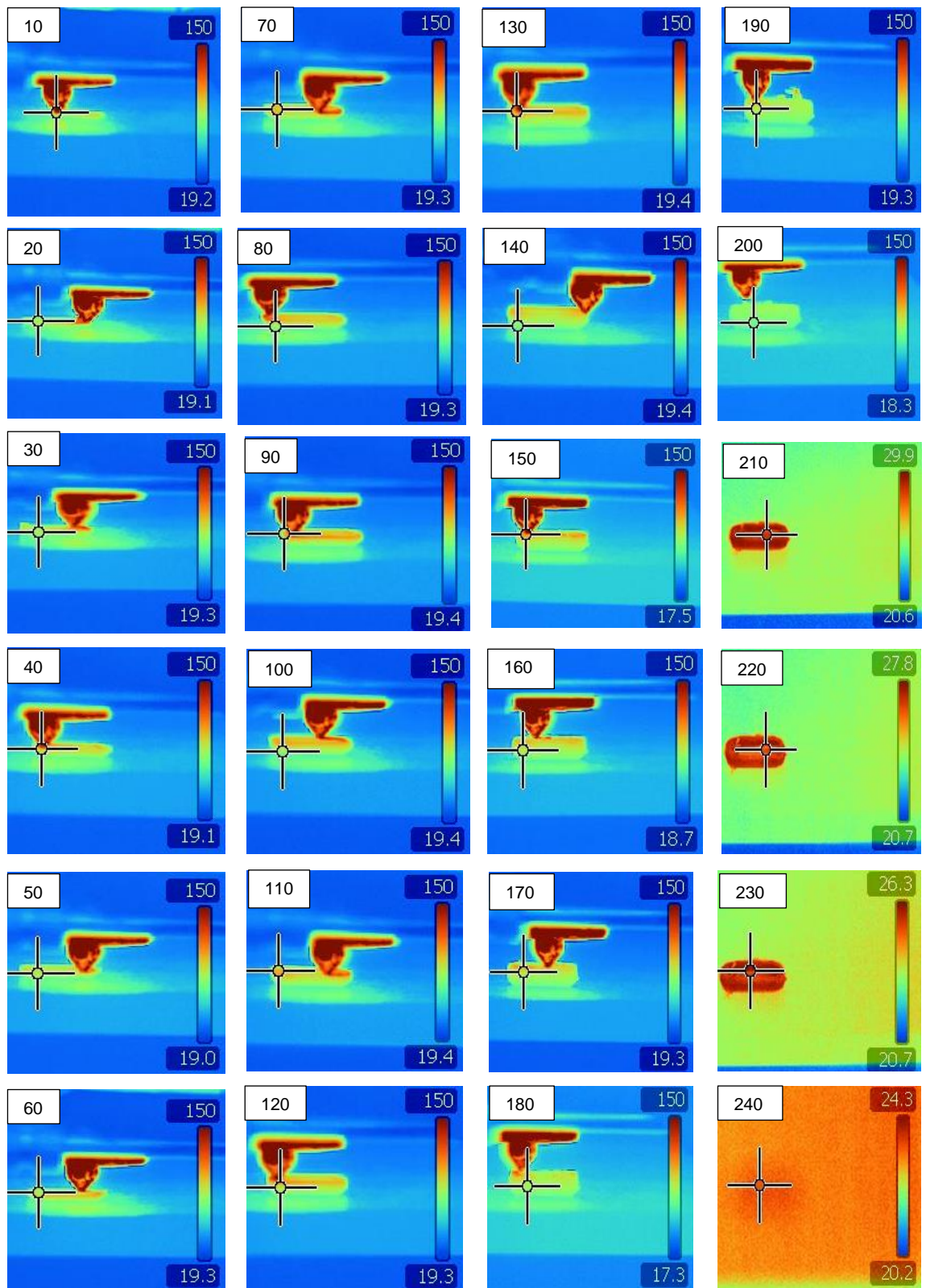


Figure 4.20. Temperature changes during FDM 3D printing of Eudragit S100.



Number = time (sec)

Figure 4.21. Temperature changes during FDM 3D printing of Eudragit S100.

Since 3D printing is a thermal process and is required to completely seal the capsule after the peptide filling, it was also necessary to determine the impact of temperature change on the solution structure of the AMPs. A temperature interval scan over the range 10 °C to 90 °C was undertaken on the peptides using circular dichroism.

At 20 °C Aurein 2.6 displayed a random coil secondary structure with a minimum around 205 nm and a negative shoulder around 228 nm (Figure 4.22A). Exposure to temperatures between 10 to 90 °C demonstrated a loss of negative ellipticity around 205 nm and a gain of negative ellipticity around 228 nm suggesting the possibility of a heating induced folding of the peptide into a helical structure (increase in helicity from 2.4 % \pm 0.006 to 6.8 % \pm 0.001). This therefore suggests a temperature induced partial folding into a more organised structure. Similar behaviour was also observed in a study on a peptide with a random coil structure (Kjaergaard et al., 2010). A comparison of its solution structure at 20 °C and 90 °C demonstrated a change in secondary structure as calculated from Dichroweb (Whitmore and Wallace, 2008, Whitmore and Wallace, 2004) ($p < 0.05$).

The solution structure of LL-37 in PBS 5.9 suggested an α -helical structure at 20 °C with broad negative minima around 208 and 223 nm (Figure 4.22B). This was in agreement with research undertaken by Thennarasu et al. (2010), which identified a broad minima at 206 and 222 nm in an aqueous buffer solution (pH 7.4), a characteristic of an α -helical conformation. Further analysis using Dichroweb (Whitmore and Wallace, 2008, Whitmore and Wallace, 2004) showed that although the CD spectra of LL-37 (Figure 4.22B) displayed an α -helical conformation, the calculated percentage helicity was < 10 %. The α -helical content conformation of LL-37 showed little variation over the temperature range studied [10 to 90 °C; ($p > 0.05$)] therefore indicating that the peptide was potentially stable (Figure 4.22B). In support of these data, it was observed that *Pyrularia pubera* thionin, an AMP displayed similar α -helical structure behaviour when exposed to high temperature (Vila-Perello et al., 2005). A random coil conformation at 20 °C has been identified for LL37 (Zhang et al., 2010, Turner et al., 1998). In pure water, it was also observed to demonstrate a temperature–dependent equilibrium between a left-handed PPII helix and a random coil secondary structure at an increased temperature (Zhang et al., 2010). The solution structure of LL37 has also been shown to be affected by the pH of the media, physiological ion composition as well as salt type and concentration (Johansson et al., 1998, Xhindoli et al., 2014).

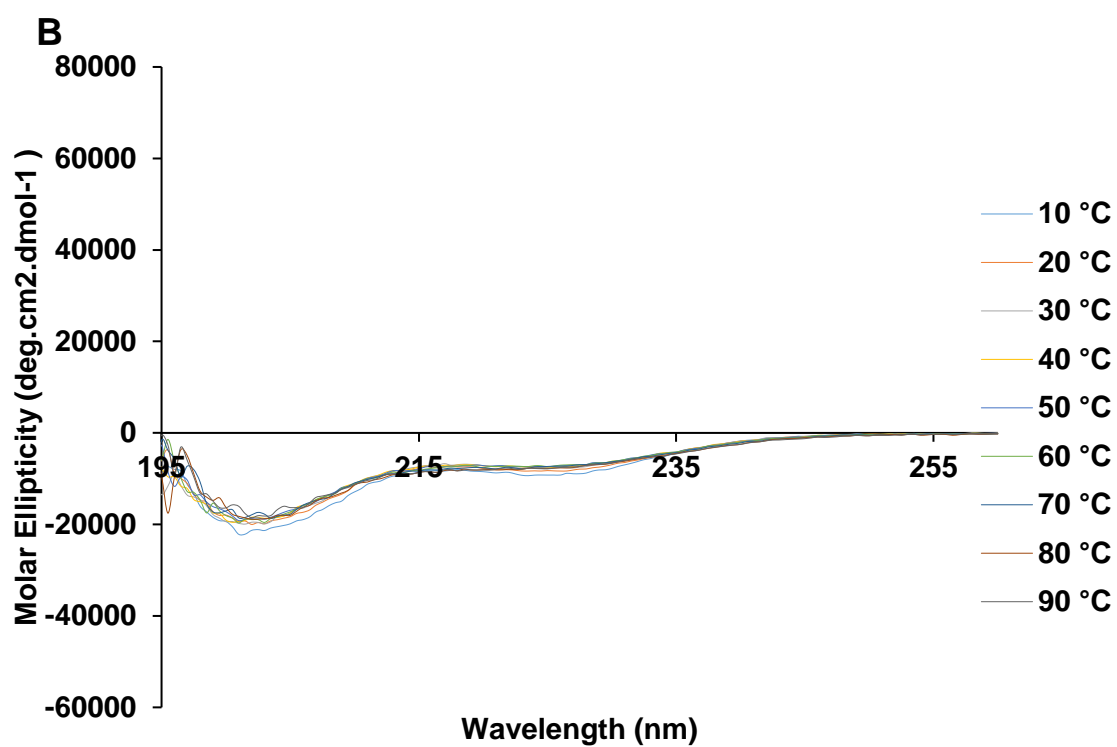
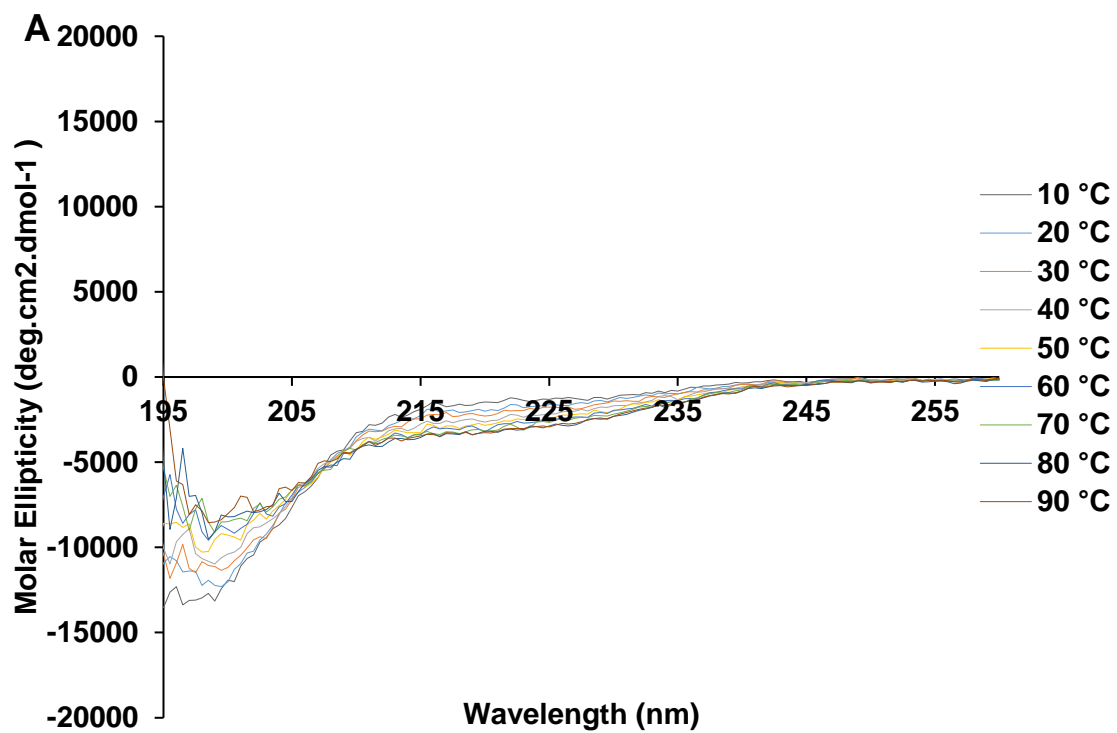


Figure 4.22. Impact of temperature on the secondary structure of aurein 2.6 (A) and LL-37 (B).

Using the modified dual FDM heads, a 3D printed liquid capsule was manufactured, with the core being a peptide solution (0.01 mg/mL) and the shell 3D printed from a Eudragit S100-based filament. The integrity of the peptides before and after 3D printing were investigated by circular dichroism to determine the impact of the 3D printing processes on the solution structure of the AMPs. It was observed that the secondary structure of the peptides remained the same after 3D printing ($p > 0.05$) (Figures 4.23A and B), which demonstrated the efficiency of the system in carrying thermolabile actives. This led to the conclusion that coordinated peptide dispensing and FDM 3D printing did not affect the AMPs used.

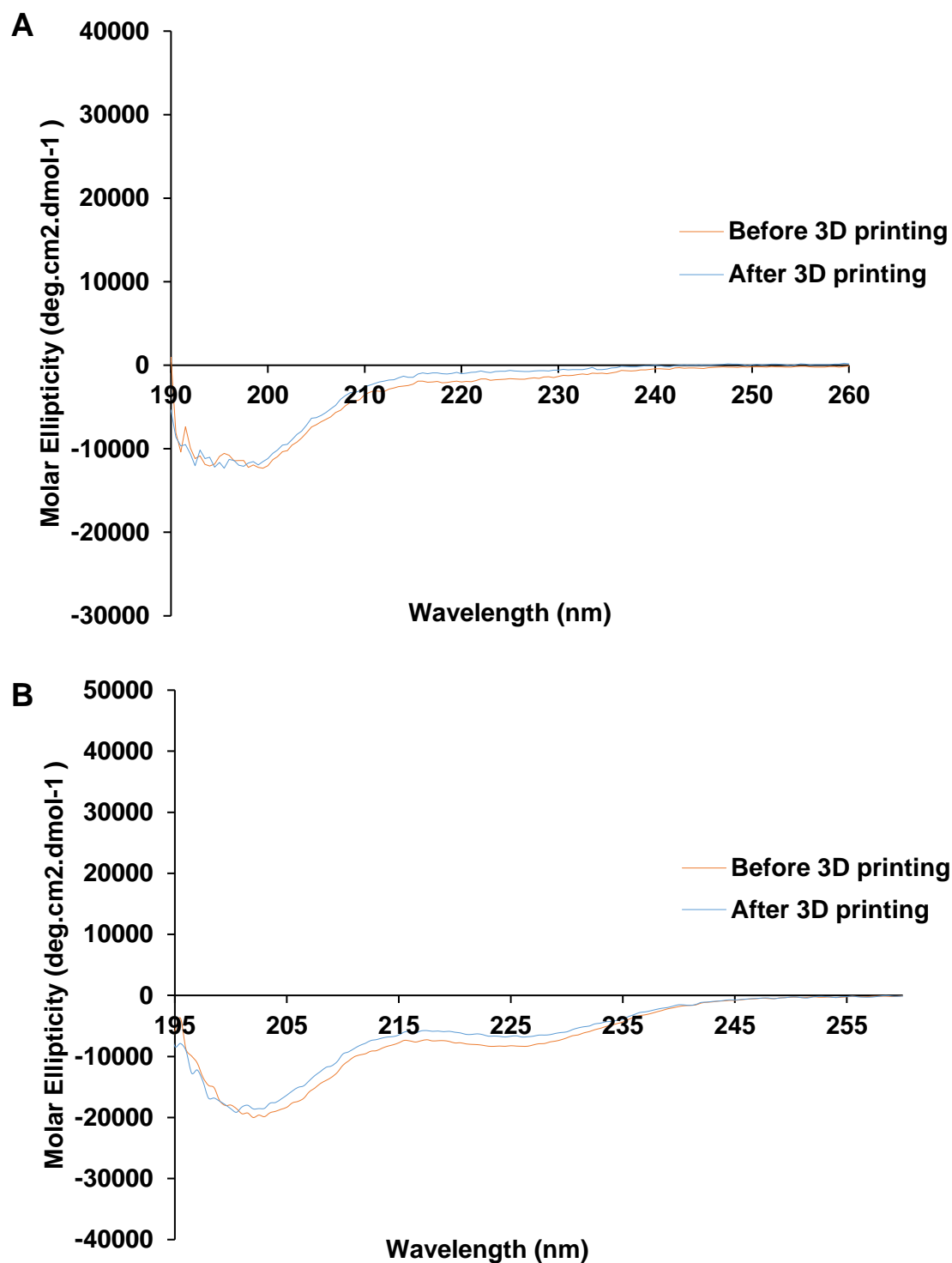


Figure 4.23. The impact of coordinated FDM 3D printing and syringe-based liquid dispenser on the secondary structure of aurein 2.6 (A) and LL-37 (B).

In order to demonstrate a proof of concept, colon targeting was demonstrated using a theophylline loaded liquid-filled capsule. *In vitro* drug release analysis demonstrated a delayed drug release with about 30 % drug release in the acid media followed by a controlled drug release at elevated pH of 7.4 (Figure 4.24). Optimisation of the shell thickness will potentially decrease this initial drug leakage since < 10 % drug release in the acid media is usually optimal.

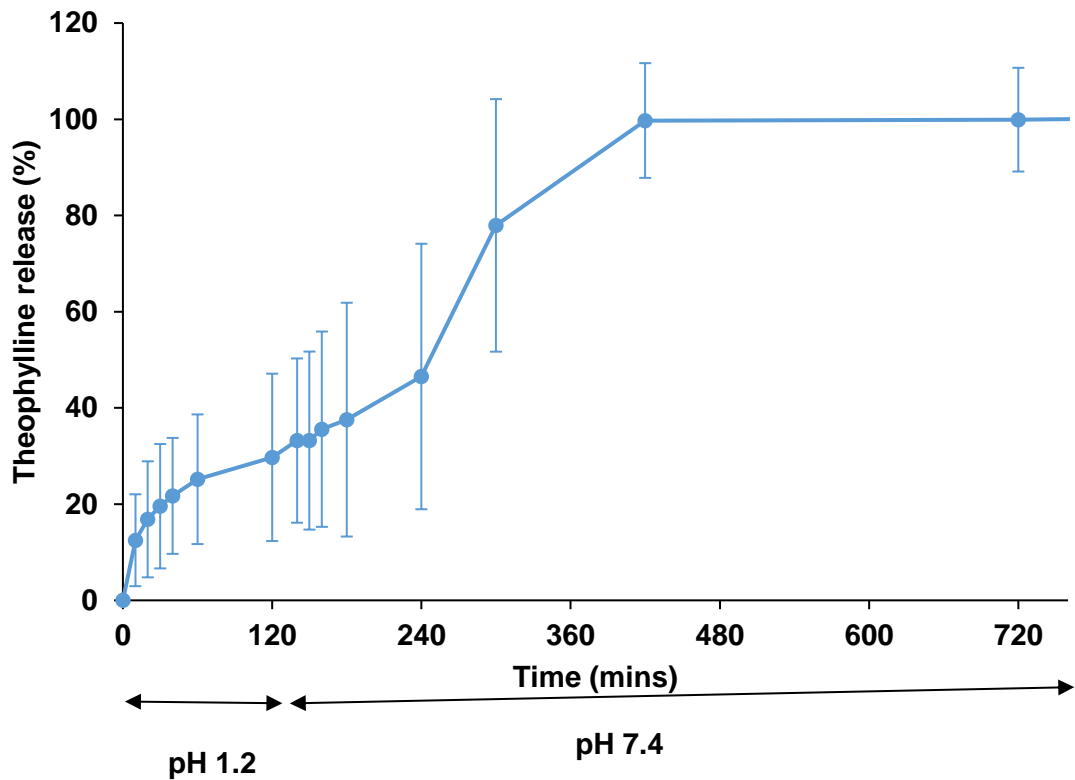


Figure 4.24. *In vitro* dissolution studies of the 3D printed colon targeting liquid capsule.

4.14 Conclusion

The anticancer activity of aurein 2.6 and LL-37 AMPs were demonstrated on the researched colon cancer cell lines where they both showed a concentration dependent increase in activity. The peptides also seemed to have a time dependent activity on HT-29 which does not seem to be the case when used on Caco-2 cell lines. The potential for colon targeting was demonstrated by adapting Eudragit S100 for FDM 3D printing, which was successfully used to fabricate liquid capsule to carry either large molecules (AMPs) or small molecules (theophylline). Drug release studies was carried out using the theophylline solution liquid-filled capsules, where more than 10 % of the active was released in the acid media after which a pH change to 7.4 produced a sustained release of theophylline over 5 hrs. The coordination of the FDM head and a liquid dispenser was able to preserve the secondary structure of the peptides by avoiding the thermal processing of the peptides which was confirmed by studies using circular dichroism.

This research presents a proof of concept for potential oral delivery of peptides for individualised drug therapy. It also demonstrates the potential of using Eudragit S100 to avoid peptides degradation due to the high acidity of the stomach, with drug release occurring in the lower part of the GIT with higher pH values and reduced enzymatic activity. Further research is required to achieve better control on drug release using this approach.

**Chapter 5 : Accelerated Stability
Studies for HME processed PVP and
Eudragit-based Filaments for FDM 3D
printing**

5.1 Introduction

Stability studies are an essential component in product development. They allow for the evaluation of the stability of pharmaceutical excipients, active ingredients and drug products in controlled conditions (ICH, 2003). Stability studies include testing those qualities of the product that might be susceptible to changes due to storage. They also include the study of the interaction of API and excipients, interaction between two or more APIs where applicable and the effect of container closure and packaging materials on the quality of the active ingredient or product. Data from such studies aid in recommending ideal storage conditions and shelf lives for the tested API or product before being introduced into the market. This ensures that safety, efficacy and quality is maintained during storage and use of pharmaceutical products.

The guidelines for stability studies are provided by the International Council for Harmonisation (ICH). Regional differences in environmental conditions were considered before setting these guidelines, which led to categorisation into four climatic zones and four different long-term stability-testing conditions were recommended (Table 5.1) (WHO, 2009). However, depending on the product development stage, stability studies could be carried out under different conditions and period.

One type of the initial stability tests usually carried out on products/potential products is the accelerated stability testing. They are used to estimate the effect of long term storage over a shorter period (ICH, 2003). The storage conditions are usually more extreme (Table 5.2 and Table 5.3) in comparison to the other stability testing routes which are designed to speed up or accelerate potential stability problems. This saves time during development since unstable products are fished out without much time and resource wastage. The storage condition during accelerated stability studies depend on the intended storage conditions for the drug / drug product (Table 5.2 and Table 5.3). Three points of stability testing are required during this study, which is usually carried out over 6 months (ICH, 2003). Physical, chemical or microbial changes as well changes due to light exposure could be investigated using adequate analytical equipment.

Intermediate stability studies are usually carried out when significant changes were observed during the accelerated studies. This requires a minimum of four testing points including the starting point (e.g. 0, 6, 9 and 12 months) and is usually carried out over 12 months (Table 5.2) (ICH, 2003). On the other hand, long term stability studies are usually carried out for over 12 months (Table 5.2, Table 5.3 and Table 5.4) with sampling done every three months for the first year, every six months for the second year and annually

afterwards depending on the proposed shelf life of the drug (ICH, 2003). Data from a minimum of 6 months could be submitted for substances with established stability.

Table 5.1. Stability testing conditions based on climatic zones (WHO, 2009).

| Climatic zone | Definition | Long-term testing conditions |
|-----------------|--|------------------------------|
| Zone I | Temperate | 21 °C / 45 % RH |
| Zone II | Subtropical, with possible high humidity | 25 °C / 60 % RH |
| Zone III | Hot and dry | 30 °C / 35 % RH |
| Zone IVA | Hot and humid | 30 °C / 65 % RH |
| Zone IVB | Hot and very humid | 30 °C / 75 % RH |

RH= Relative humidity

Table 5.2. General case of stability studies (ICH, 2003).

| Study type | Storage conditions | Minimum time period |
|---------------------|--|--------------------------|
| Long term | 25 °C ±2 °C / 60 % RH ±5 % RH Or 30 °C ±2 °C / 65 % RH ±5 % RH | 6 months or 12 months |
| Intermediate | 30 °C ±2 °C / 65 % RH ±5 % RH | 6 months |
| Accelerated | 40 °C ±2 °C / 75 % RH ±5 % RH | 6 months |

Table 5.3. APIs and products intended to be stored in the fridge (ICH, 2003).

| Study type | Storage conditions | Minimum time period |
|--------------------|---|---------------------|
| Long term | 5 °C ±3 °C | 12 months |
| Accelerated | 25 °C ±2 °C / 60 % RH ±5 % RH or 30 °C ±2 °C / 65 % RH ±5 % RH or 30 °C ±2 °C / 75 % RH ±5 % RH | 6 months |

Table 5.4. APIs and products intended for storage in freezer (ICH, 2003).

| Study type | Storage conditions | Minimum time period |
|------------------|--------------------|---------------------|
| Long term | -20 °C ±5 °C | 12 months |

Physical stability includes changes in the physical properties of the drug/drug product. This includes changes in organoleptic properties like appearance e.g. changes in shape or size, odour and taste which could affect drug use and compliance (Guo et al., 2013). Loss of weight, changes in pH and viscosity are looked out for when dealing with liquid dosage forms and mechanical resistance over time is usually examined for solid dosage forms. Changes in drug release pattern, which is possible with aging even with an already established and stable APIs are also investigated (Tingstad, 1964). During storage, APIs tends to transform into a more stable crystalline form. Therefore, APIs in their amorphous state might revert to their crystalline form, which might influence dissolution and drug release. Different analytical techniques are usually employed during physical stability testing (Table 5.5).

Table 5.5. Analytical equipment commonly used in physical characterisations and their applications (Guo et al., 2013).

| Analytical Method | Applications |
|--|---|
| Polarised light Microscopy (PLM) | Qualitative confirmation of presence of crystals |
| X-ray powder diffraction (XRPD) | Crystallinity quantification, miscibility, crystallisation kinetics |
| Fourier-transform infrared spectroscopy (FTIR) | Molecular level interaction, quantification |
| Fourier-transform Raman spectrometer (FT-Raman) | Molecular level interaction, quantification |
| Scanning electron microscopy (SEM) | Morphology of particles |
| Thermal gravimetric analysis (TGA) | Mass loss at elevated temperature |
| Inverse gas chromatography (IGC) | Surface energy and molecular mobility |
| Dissolution test | Changes in release pattern |

Chemical instability could occur during storage as impurities/degradation products could arise because of interaction with excipients and/or container closure or packaging materials. API/drug product chemical stability depends on the rate of oxidation or hydrolysis as a result of exposure to light/heat and humidity respectively (Waterman and Adami, 2005). This introduces changes in the chemical structure of the API which could affect its potency (Timothy J. Snape, 2010). The International Council of Harmonisation

controls the amount of degradants allowed during the shelf life of a product and this is based on the total daily intake of the drug (ICH, 2006).

Solid dispersions as a solid solution or suspension is one of the methods used to improve the solubility, dissolution rate and consequently the bioavailability of poorly soluble drugs (BCS class II drugs). Techniques used in the manufacturing of solid dispersions includes HME (Agrawal et al., 2016), spray drying (Paudel et al., 2013), supercritical carbon dioxide impregnation (Potter et al., 2015) or co-precipitation (Huang and Dai, 2014). These different techniques have been used to create a polymer-drug matrix where the drug may or may not be dispersed at the molecular level in the polymer. Several factors like the drug-polymer ratio, drug-polymer interaction (Sarode et al., 2013), the type of polymer used and the processing conditions plays a major role in the stability of the solid dispersion (Huang and Dai, 2014, Agrawal et al., 2013). Recrystallization could occur during storage and alter the release properties of the solid dispersion depending on the storage conditions (Agrawal et al., 2016), which emphasises the importance of stability studies during product development (Khougaz and Clas, 2000, Matsumoto and Zograf, 1999, Konno and Taylor, 2006).

The use of HME in the manufacturing of solid dispersion has been shown to be an efficient approach (Liu et al., 2012). In some cases, it was shown to offer a better physical stability in comparison to spray drying (Agrawal et al., 2013, Mahmah et al., 2014). Different polymers and APIs have been processed using HME for application to different pharmaceutical processes (Li et al., 2015, Andrews et al., 2010, Sarode et al., 2013, Zecevic et al., 2014).

PVP has been shown to be compatible with HME (Andrews et al., 2010, Yang et al., 2016, LaFontaine et al., 2016, Mahmah et al., 2014, Chan et al., 2015); either applied to improve solubility or the stability of an API. Amorphous solid dispersions are produced depending on the drug-polymer ratio. In an example, a micronised griseofulvin-PVP solid dispersion by HME was shown to remain amorphous at $\leq 20\%$ drug loading (LaFontaine et al., 2016). Solid dispersions with such polymers have been shown to remain stable over 3 months, maintaining similar release and physical properties (Guo et al., 2014). In another study, PVP was used in combination with another polymer which showed a slight reduction in drug release most likely due to aging after 2 months of storage (Jijun et al., 2011). The drug-polymers interaction as well as the polymer properties like the T_g in relation to the storage condition determines the ease of polymer rearrangement. A less hygroscopic PVP VA64 was more stable in comparison to PVP K12 which had a lower

T_g as a result of water uptake and therefore allows ease of polymer motility (Agrawal et al., 2016).

The use of Eudragits in the manufacturing of solid dispersions could also be achieved using HME (Sarode et al., 2013, Abu-Diak et al., 2011, Bennett et al., 2015, Feng et al., 2012, Zhang et al., 2014, Yang et al., 2014, Jijun et al., 2011). The interaction between lumefantrine (model basic compound) and Eudragit L100-55 (acidic compound) demonstrated the effect of the solid dispersion manufacturing process, polymer acid strength and drug loading on the acid-base interactions (Song et al., 2016). The ionic interactions between the polymer and the drug which depends on the drug-polymer miscibility also contributes to formation of solid dispersions (Maniruzzaman et al., 2013).

In a research where propranolol HCl and diphenhydramine HCl were used as model cationic APIs, it was discovered that the drug-polymer interactions between the amino groups of the drug molecule and the carbonyl groups of the methacrylate and ethyl acrylate copolymers played a key role in forming the amorphous solid dispersion (Maniruzzaman et al., 2013). This was demonstrated in a Eudragit S100-based solid dispersion which showed API precipitation inhibition as well as amorphous stabilisation (Chauhan et al., 2013). Eudragit S100 has also been utilised in a binary polymer system containing celecoxib, where the development of hydrogen bond with polyethylene oxide after HME contributed to the stability of the solid dispersion (Jones et al., 2016).

In this research and as shown in the previous chapters, 3D printing of the dosage forms were carried out using filaments. These filaments were manufactured as a solid dispersion of the drug, polymer and a non-melting component (talc) using HME before being inserted in the FDM 3D printing head to fabricate the tablets or capsule shells. The potential of 3D printing in pharmaceutical manufacturing and therefore personalised dosing is expected to revolve around these filaments, which could be easily scaled up, packaged appropriately and shipped to different hospitals and community pharmacies in a ready to use form. Since these filaments are potentially going to be the pre-product from which dosage forms of different sizes and doses could be manufactured from, it was important to investigate their stability at different storage conditions according to the ICH guideline.

5.2 Aims

This research aims to determine the long-term stability of PVP, Eudragit L100-55 and S100-based filaments manufactured by HME by accelerated 6 month stability studies. In order to achieve this, the research objectives includes:

- To carry out an accelerated stability studies on PVP, Eudragit L100-55 and S100-based filament based on ICH guideline.
- To determine the effect of storage conditions on the diameter and printability of the filaments.
- To determine the effect of storage on the physical properties of the filament through XRPD, TGA and DSC analysis.
- To determine the effect of storage on the integrity of the theophylline loaded PVP filament and on drug release.

5.3 Materials

Theophylline was purchased from ACROS Organics. Polyvinylpyrrolidone (PVP, MW 40,000) and triethyl citrate were purchased from Sigma-Aldrich (UK). Talc was ordered from Fluka Analytical (UK). Scotch blue painter's tape 50 mm was supplied by 3M (Bracknell, UK). Eudragit L100-55 and Eudragit S100 was donated by Evonik Industries (Darmstadt, Germany).

5.4 Methods

5.4.1 Preparation of filaments

The PVP and Eudragit based filaments were produced by Hot melt extrusion using the parameters in Table 5.6. The components were fed into the HME and allowed to evenly mix at 80 rpm for 5 mins before extrusion. The Eudragit-based filaments were drug free since they were used as shells for drug release modification.

5.4.2 Accelerated stability studies (storage conditions)

In order to determine the stability of the filaments over long-term storage, accelerated stability studies was carried out according to the ICH guideline. The PVP, Eudragit L100-55 and S100-based filaments were sealed in a PVC bag with or without a vacuum and stored in a fridge at 5 °C, in an incubator at 30 °C + 65 %RH or at 40 °C + 75 %RH. Vacuum was created using AndrewJames VS517 Dom Sealer. The filaments were characterised when freshly prepared and then after 1 month, 3 months and 6 months of storage to determine the effects of the storage conditions on the filaments.

5.4.3 Printability test using Makerbot 2X FDM 3D printer (Makerbot, US)

3D printing of the filaments stored in different conditions was attempted using the parameters in Table 5.6, to determine the effect of the storage conditions on 3D printing. Printing was carried out at a standard resolution (0.2 mm layer thickness) and a 100 % infill with rectilinear infill pattern. Other settings were left at default. A 10 mm caplet was designed and imported into the makerware software and used to test the printability of the filaments.

Table 5.6. Filament formulation, HME and 3D printing parameters.

| Polymer type | Polymer (%) | TEC (%) | Talc (%) | Drug (%) | Processing temp (°C) | Extrusion temp (°C) | Nozzle size (mm) | 3D printing temp (°C) | Platform temp (°C) |
|-------------------------|--------------------|----------------|-----------------|-----------------|-----------------------------|----------------------------|-------------------------|------------------------------|---------------------------|
| PVP | 50 | 12.5 | 27.5 | 10 | 100 | 90 | 1.25 | 110 | 40 |
| Eudragit L100-55 | 50 | 16.67 | 33.33 | | 135 | 125 | 1 | 185 | 40 |
| Eudragit S100 | 52.5 | 22.5 | 25 | | 130 | 120 | 1.5 | 190 | 20 |

5.4.4 Filament dimension

In order to determine the effect of the storage conditions on the diameter of the filaments, five points (10 cm apart) were marked with a pencil along the length of the filament. Changes in the diameter of those points were monitored at the points of characterisation using a Draper Electronic Digital Micrometre (0 – 25 mm) with a resolution of 0.001 mm.

5.4.5 X-ray powder diffractometry (XRPD)

X-ray powder diffraction was carried out on the filaments over 6 months to investigate changes in physical forms of the API or excipients. This was assessed using a powder X-ray diffractometer, D2 Phaser with Lynxeye (Bruker, Germany). Samples were scanned from $2\theta = 5^\circ$ to 50° . The divergence slit was 1 mm and the scatter slit 0.6 mm. The wavelength of the X-ray was 0.154 nm using Cu source and a voltage of 30 kV.

5.4.6 Differential scanning calorimetry (DSC)

For modulated temperature differential scanning calorimetry (MTDSC) analysis, a differential scanning calorimeter (DSC) Q2000 (TA Instruments, Elstree, Hertfordshire, UK) with a heating rate of $2^\circ\text{C}/\text{min}$ was employed. Each sample was subjected to a heat-cool-heat scan in order to measure and exclude the effect of moisture contents on filament plasticity with the exception of Eudragit S100-based filaments. A modulated scan was applied using an amplitude of 0.212°C and a period of 40 sec, scanning from -70 to 200°C . Analysis was carried out under a purge of nitrogen ($50\text{ mL}/\text{min}$). The data was analysed using a TA 2000 analysis software. TA pin-holed lid and $40\ \mu\text{L}$ aluminium pans were filled with approximately 5 mg sample. All measurements were carried out in triplicates.

5.4.7 Thermal gravimetric analysis (TGA)

TGA analysis for the extruded filaments were measured using a TGA Q5000 (TA Instruments, Hertfordshire, UK). Samples (10 mg) were added to an aluminium pan without lid. Samples were then heated from 25°C to 500°C at a heating rate of $10^\circ\text{C}/\text{min}$. All measurements were carried out in triplicates.

5.4.8 In vitro drug release studies (PVP-based filament)

In vitro drug release analysis from the filaments were carried out to determine the effect of the storage conditions on the release pattern of theophylline from the PVP-based filaments. Approximately 115 g of the filament was dissolved in 900 mL of 0.1M HCL at

a wavelength of 272 nm using an AT 7 Smart dissolution USP II apparatus (Sotax, Switzerland). Sampling was carried out automatically after every 5 min.

5.4.9 Determination of drug content (PVP-based filament)

To determine changes in the drug content of the filament after storage, the PVP-based filament containing theophylline was solubilised in 0.1 M HCl, which was allowed to sonicate for 2 hr. Assessment was carried out using an UV-HPLC system and an Xterra column (Waters, UK). A mobile phase of 10 mM solution of ammonium acetate buffer, methanol and acetonitrile (86:7:7) was used. Analysis was carried out at a wavelength of 272 nm, temperature of 40 °C, flow rate of 1 mL/min, injection volume was 5 µL and a run time of 7 min.

5.4.10 Statistical analysis

One-way ANOVA was employed using SPSS Software (22.0.0.2) to analyse the results. Differences in results above probability level ($p > 0.05$) was considered not significant whilst differences ($p < 0.05$) were considered significant

5.5 Results and discussions

The potential of FDM 3D printing in rapid drug manufacturing and dose personalisation requires the use of filaments. It is from these filaments that several doses could be printed on demand. This therefore is required to be stable during storage and therefore readily available for use. In this research, accelerated stability studies were carried out on a PVP-based filament loaded with theophylline as the model drug. Eudragit L100-55 and S100-based filament which were drug free and utilised as shell filaments were also investigated. The filaments were stored in a polyvinyl chloride (PVC) bag, sealed with or without vacuum and stored in a fridge at 5 °C, in an incubator at 30 °C + 65 %RH or at 40 °C + 75 %RH. The filaments were analysed before storage and these analyses were repeated after 1, 3 and 6 months to determine changes in the filament properties. The filaments in the vacuumed PVC bags were placed in a strong hollow PVC tube to avoid physical compression from the storage bag due to vacuuming.

The impact of the storage conditions of the diameter of the filaments were investigated since diameters greater than 2 mm will not pass through the 3D printer head and any deformation along the length of the filament could potentially affect 3D printing. An average of five different points of measurement on the filaments which was monitored during storage revealed no major changes in the filament diameter ($p \geq 0.05$) with the exception of the PVP-based filament (Table 5.7). It was observed that the storage of the filaments at 5 °C maintained the stability of the PVP-based filament which resulted in no changes in its diameter over time. However, storage at 30 °C + 65 % RH or 40 °C +75 % RH resulted in the deformation and flattening of the filament. This could be related to the hygroscopic nature of the PVP polymer leading to polymer relaxation (Fitzpatrick et al., 2002). Storage at 5 °C on the other hand, which is below the T_g of the polymer, resulted in the increase of its viscosity due to reduced polymer mobility and therefore providing a more stable condition by preventing polymer mobility (Fitzpatrick et al., 2002).

One of the major challenges from the use of filaments in drug manufacturing is ensuring compatibility with the 3D printer after storage. It was observed that the PVP, Eudragit L100-5 and S100-based filaments remained compatible with the 3D printer at the same temperature as the freshly prepared sample except for the PVP-based filament which deformed as a result of storage at 30 °C + 65 % RH or 40 °C +75 % RH. This early observation resulted in the termination of the stability studies for these failed conditions after the first month.

Table 5.7. Impact of storage conditions on filament diameter.

| Filament | Storage condition | Dimension (mm) | | |
|-------------------------|----------------------|----------------|----------------|----------------|
| | | Fresh | After 3 months | After 6 months |
| PVP | 5 °C | 1.50 ±0.04 | 1.47 ±0.04 | 1.53 ±0.03 |
| PVP | 5 °C + Vac | 1.50 ±0.01 | 1.51 ±0.02 | 1.48 ±0.02 |
| PVP | 30 °C + 65% RH | 1.37±0.09 | X | X |
| PVP | 30 °C + 65% RH + Vac | 1.49±0.01 | X | X |
| PVP | 40 °C + 75% RH | 1.51±0.02 | X | X |
| PVP | 40 °C + 75% RH + Vac | 1.54±0.09 | X | X |
| Eudragit L100-55 | 5 °C | 1.67 ±0.03 | 1.66 ±0.05 | 1.67 ±0.04 |
| Eudragit L100-55 | 5 °C + Vac | 1.67 ±0.14 | 1.72 ±0.16 | 1.65 ±0.14 |
| Eudragit L100-55 | 30 °C + 65% RH | 1.61 ±0.05 | 1.76 ±0.09 | 1.77 ±0.06 |
| Eudragit L100-55 | 30 °C + 65% RH + Vac | 1.73 ±0.06 | 1.72 ±0.03 | 1.75 ±0.04 |
| Eudragit L100-55 | 40 °C + 75% RH | 1.67 ±0.04 | 1.50 ±0.24 | 1.51 ±0.23 |
| Eudragit L100-55 | 40 °C + 75% RH + Vac | 1.68 ±0.04 | 1.73 ±0.05 | 1.64 ±0.08 |
| Eudragit S100 | 5 °C | 1.53 ±0.02 | 1.55 ±0.02 | 1.54 ±0.02 |
| Eudragit S100 | 5 °C + Vac | 1.61 ±0.08 | 1.61 ±0.05 | 1.62 ±0.05 |
| Eudragit S100 | 30 °C + 65% RH | 1.63 ±0.02 | 1.64 ±0.03 | 1.63 ±0.02 |
| Eudragit S100 | 30 °C + 65% RH + Vac | 1.62 ±0.03 | 1.61 ±0.02 | 1.62 ±0.03 |
| Eudragit S100 | 40 °C + 75% RH | 1.61 ±0.06 | 1.64 ±0.04 | 1.61 ±0.04 |
| Eudragit S100 | 40 °C + 75% RH + Vac | 1.64 ±0.03 | 1.65 ±0.05 | 1.58 ±0.04 |

XRPD was used to investigate changes in the physical forms of the API or the excipients because of the accelerated stability storage conditions used during the study. A fresh PVP-based filament loaded with theophylline as a model drug demonstrated sharp peaks from talc at $(2\theta) = 9.52, 19.54, 28.87^\circ$ and also peaks at $(2\theta) = 7$ and 12° due to theophylline, which remained in its crystalline form (Figures 5.1A and B) after HME. This was unlike some other drug models that were used previously with PVP (Okwuosa et al., 2016). These drug peaks were also observed to still appear after storage (Figures 5.1A and B) indicating that the excipient and the API remained in their crystalline forms throughout these conditions. Variations in peak intensities could be an early indication of stability problems. However, this was not investigated in this research.

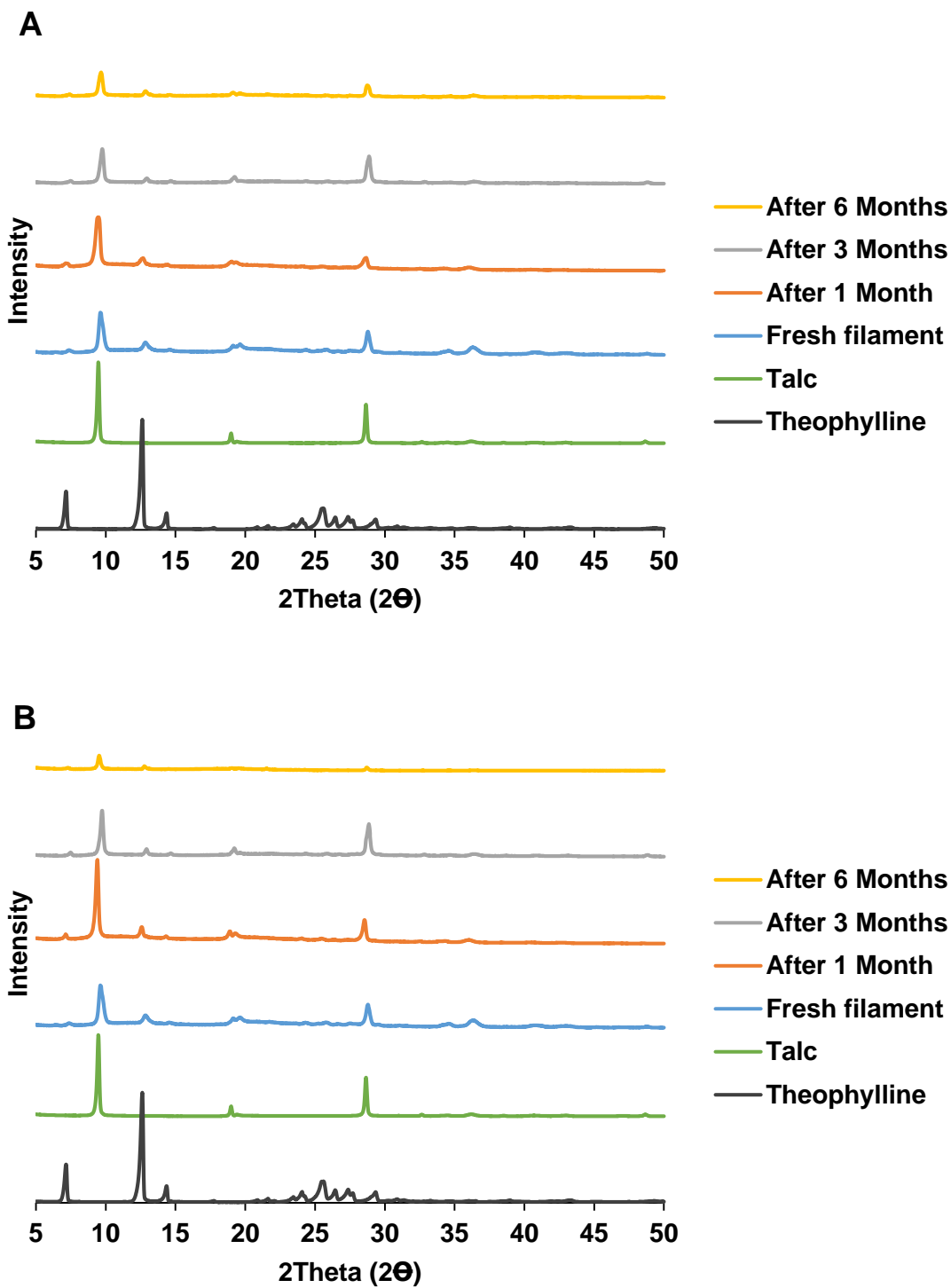


Figure 5.1. The impact of storage at 5 °C on the XRPD of PVP-based filament (A) no vacuum (B) vacuum.

Eudragit L100-55 and Eudragit S100 based filaments as used during this research were drug free since they were mostly used as shell filaments for engineering drug release patterns using the core-shell formulation strategy. A fresh Eudragit L100-55-based filament had peaks at $(2\theta) = 9.52, 19.54, 28.87^\circ$ due to talc as the polymers were amorphous in nature. Analysis after 1, 3 and 6 months revealed no changes as regards the physical forms of talc in any of the storage condition (Figures 5.2, 5.3 and 5.4). This indicated the stability of the excipients and consequently, the filaments. The Eudragit S100-based filament was also stable throughout the storage conditions with peaks at $(2\theta) = 9.52, 19.54, 28.87^\circ$ due to talc (Figures 5.5, 5.6 and 5.7) which remained the same throughout storage.

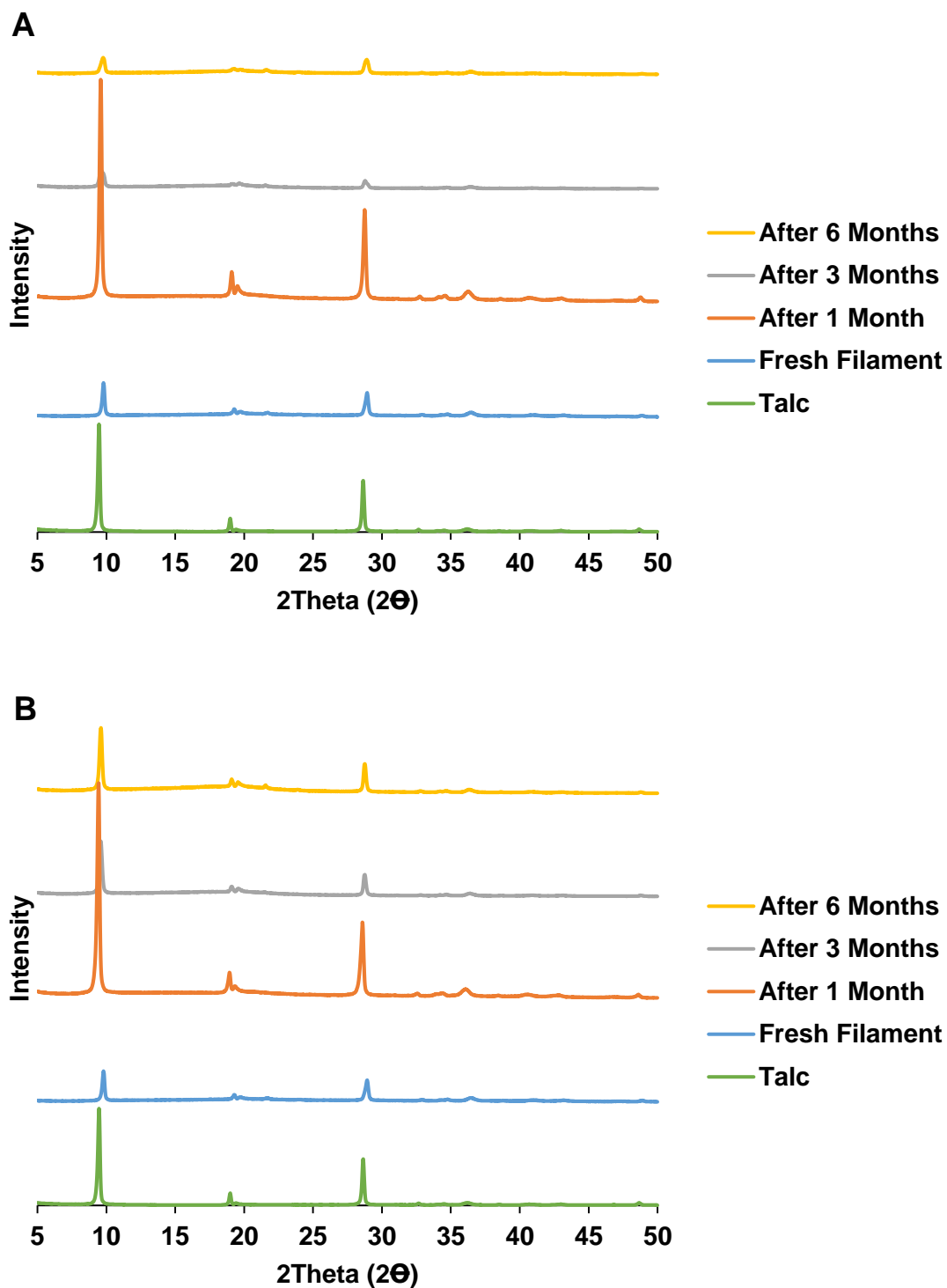


Figure 5.2. The impact of storage at 5 °C on the XRPD of Eudragit L 100-55-based filament (A) no vacuum (B) vacuum.

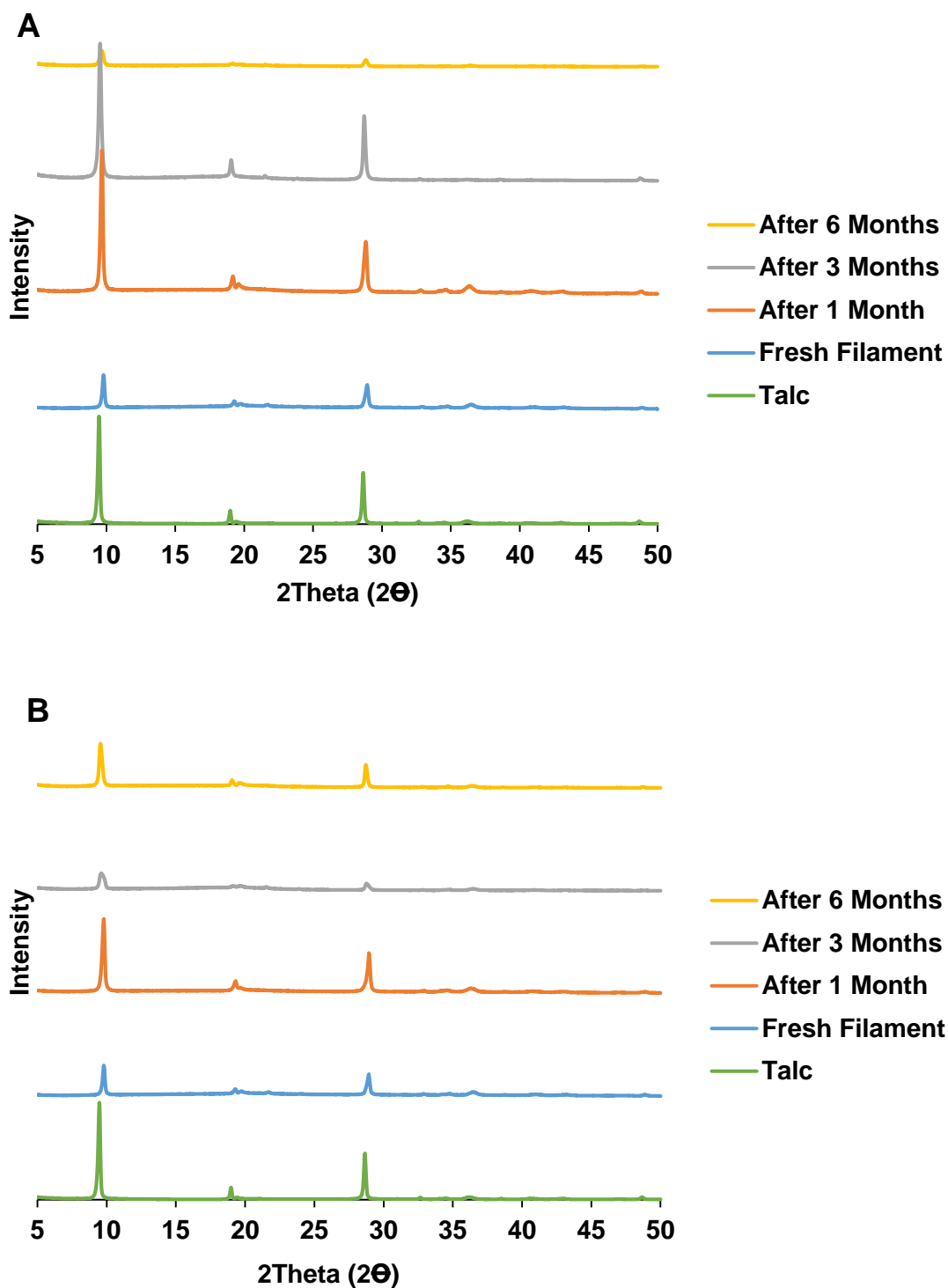


Figure 5.3. The impact of storage at 30 °C + 65 %RH on the XRPD of Eudragit L 100-55-based filament (A) no vacuum (B) vacuum.

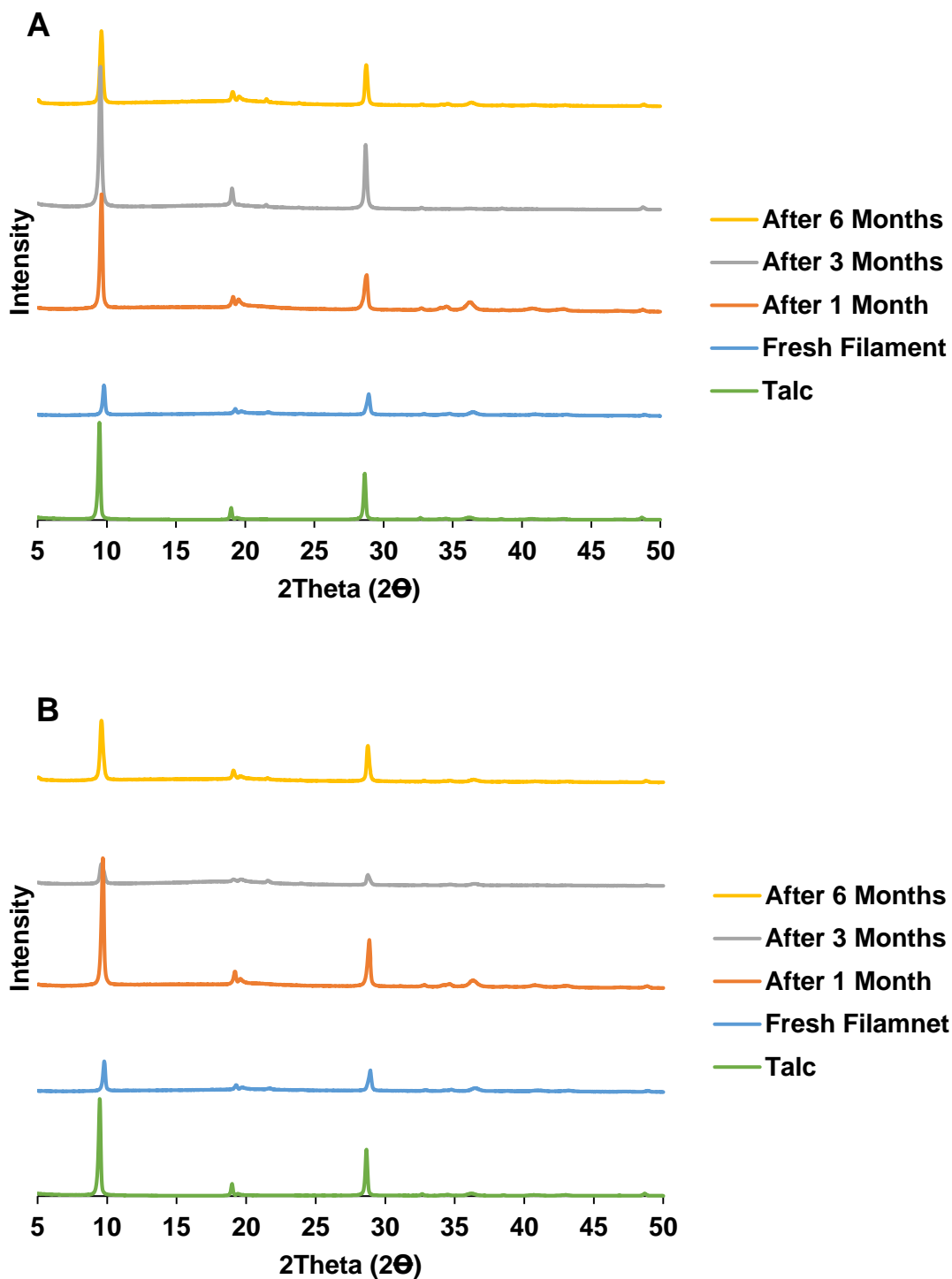


Figure 5.4. The impact of storage at 40 °C + 75 %RH on the XRPD of Eudragit L 100-55-based filament (A) no vacuum (B) vacuum.

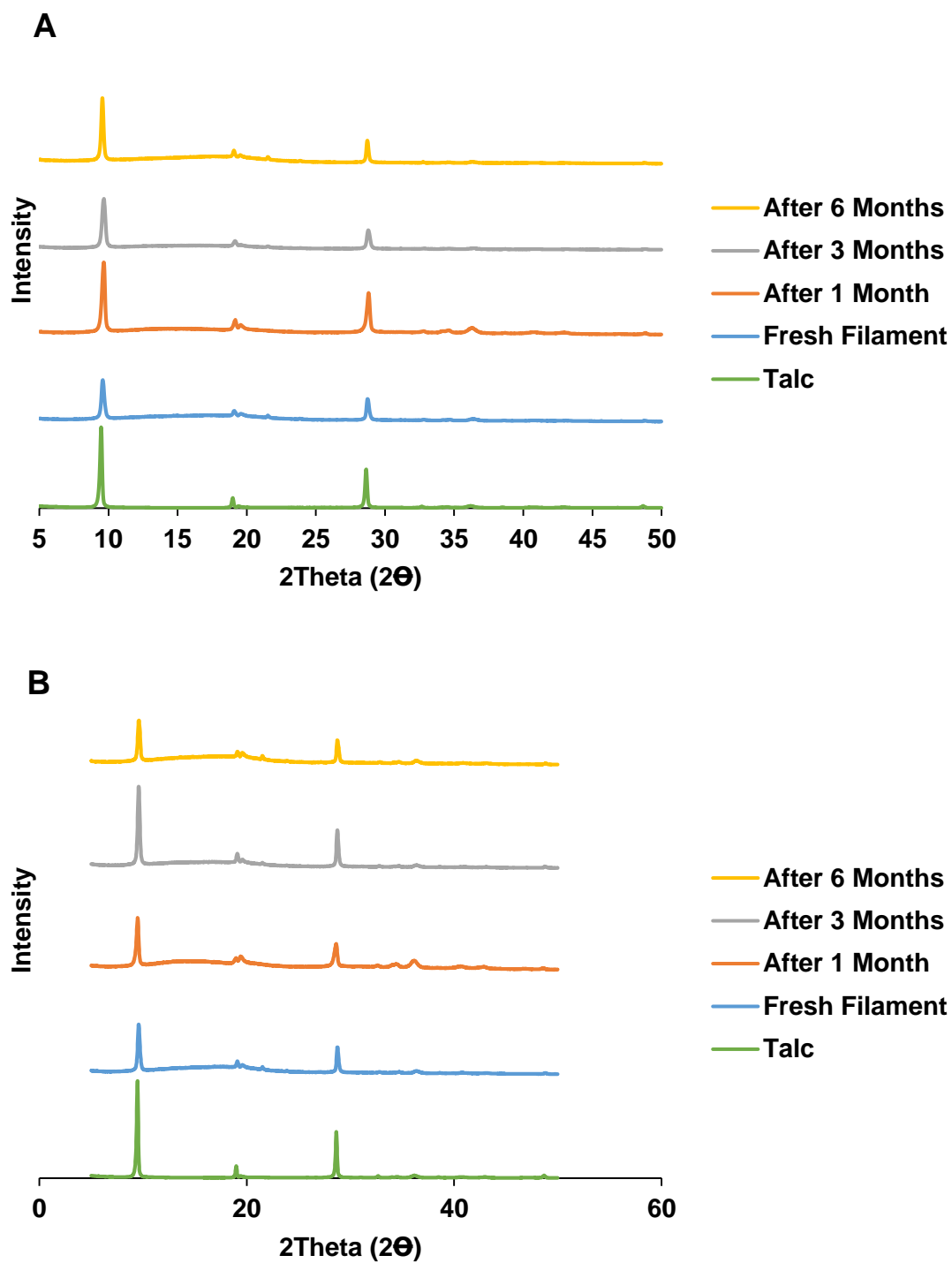


Figure 5.5. The impact of storage at 5 °C on the XRPD of Eudragit S100-filament (A) no vacuum (B) vacuum.

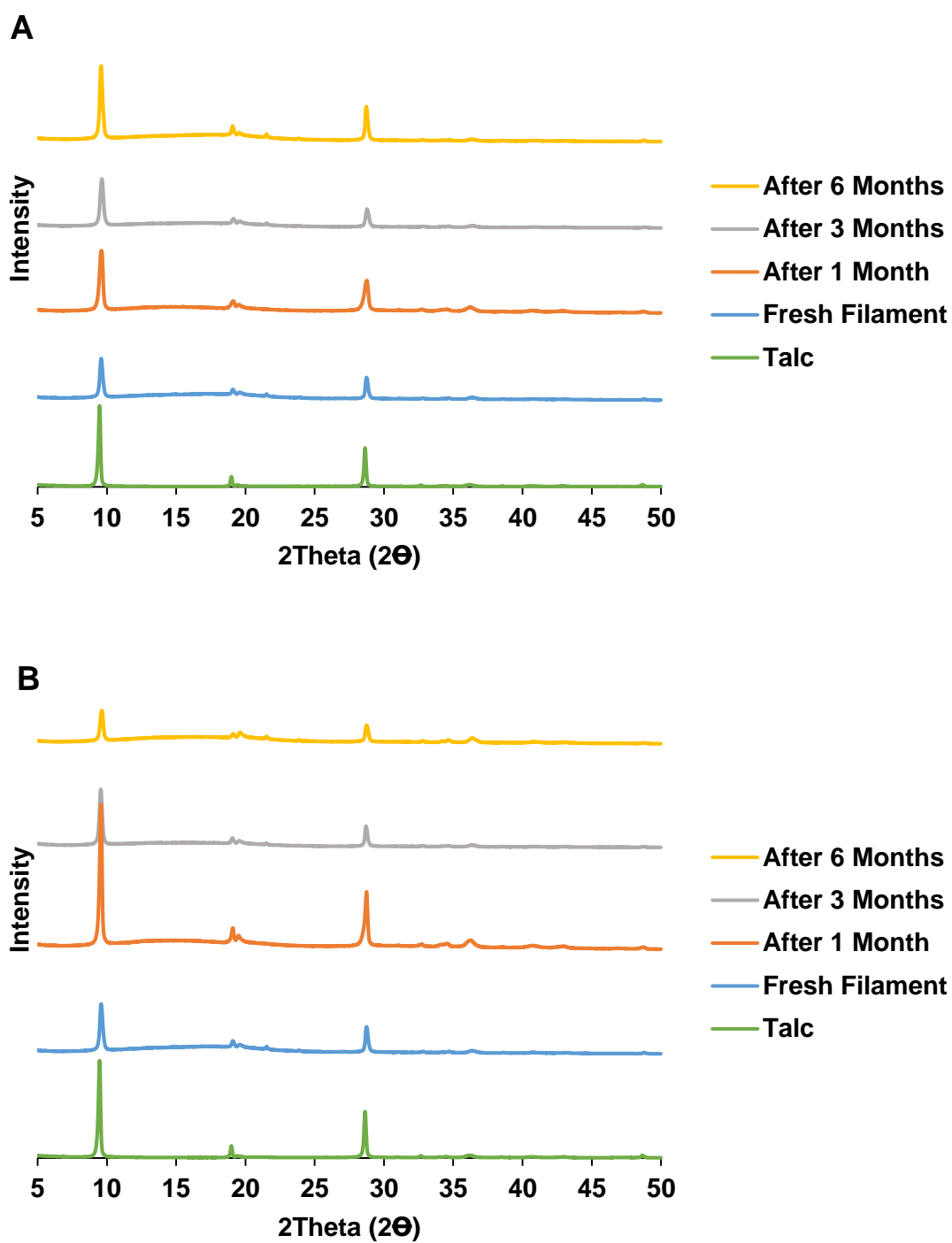


Figure 5.6. The impact of storage at 30 °C + 65 %RH on the XRPD of Eudragit S100-filament (A) no vacuum (B) vacuum.

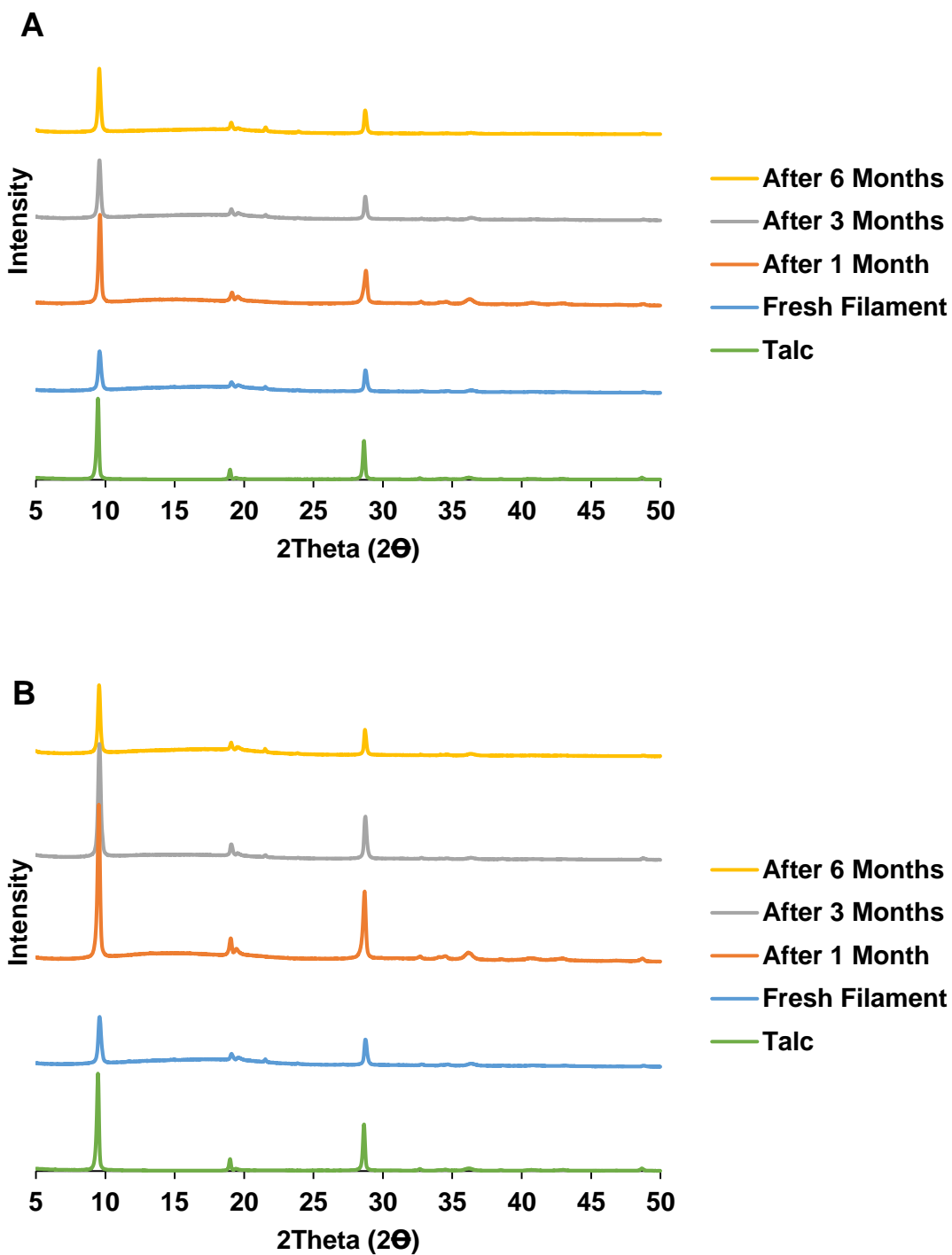


Figure 5.7. The impact of storage at 40 °C + 75 %RH on the XRPD of Eudragit S100-based filament (A) no vacuum (B) vacuum.

Thermogravimetric analysis provides information about the thermal stability of materials represented as a percentage weight loss, which might differ as samples age or due to excipient or API interactions. This analytical technique also provides information about the moisture content of the filament as demonstrated in this study (Table 5.8).

Table 5.8. Investigation of the moisture uptake of the stored filaments using TGA.

| Filament | Storage condition | Water loss (%) | | | |
|----------|----------------------|----------------|---------------|----------------|----------------|
| | | Fresh | After 1 month | After 3 months | After 6 months |
| PVP | 5 °C | 3.99 | 2.91 | 5.74 | 6.51 |
| PVP | 5 °C + Vac | 3.99 | 1.97 | 5 | 4.61 |
| PVP | 30 °C + 65 %RH | 3.99 | 4.44 | X | X |
| PVP | 30 °C + 65 %RH + Vac | 3.99 | 5 | X | X |
| PVP | 40 °C + 75 %RH | 3.99 | 5.1 | X | X |
| PVP | 40 °C + 75 %RH + Vac | 3.99 | 6.4 | X | X |
| L100-55 | 5 °C | 1.03 | 0.49 | 1.49 | 1.58 |
| L100-55 | 5 °C + Vac | 1.03 | 0.61 | 1.95 | 1.69 |
| L100-55 | 30 °C + 65 %RH | 1.03 | 0.68 | 2.1 | 2.1 |
| L100-55 | 30 °C + 65 %RH + Vac | 1.03 | 0.58 | 2.02 | 1.69 |
| L100-55 | 40 °C + 75 %RH | 1.03 | 0.57 | 1.75 | 2.75 |
| L100-55 | 40 °C + 75 %RH + Vac | 1.03 | 0.72 | 1.49 | 2.27 |
| S100 | 5 °C | 1.36 | 0.54 | 1.56 | 1.54 |
| S100 | 5 °C + Vac | 1.36 | 0.72 | 1.9 | 1.48 |
| S100 | 30 °C + 65 %RH | 1.36 | 0.69 | 1.56 | 2.23 |
| S100 | 30 °C + 65 %RH + Vac | 1.36 | 0.93 | 2.15 | 1.95 |
| S100 | 40 °C + 75 %RH | 1.36 | 0.65 | 2.19 | 2.21 |
| S100 | 40 °C + 75 %RH + Vac | 1.36 | 0.66 | 1.7 | 2.73 |

PVP – Polyvinyl pyrrolidone, L100-55 = Eudragit L100-55 and S100 = Eudragit S100

Fresh samples of PVP-based filament showed an initial weight loss of up to 3.99 % at 120 °C due to water loss, which was expected as PVP is hygroscopic. Up to 6 % water content has been reported (Gupta et al., 2014). The storage of this filament at 5 °C did not result in an increase in moisture uptake after the first month as indicated by the water loss % in Table 5.8 and Figure 5.8. However, its storage at the other condition resulted in an increase in moisture content with water loss of up to 6.4 % after the first month. PVP has been reported to be able to take moisture up to 40% of its weight (Ramineni et

al., 2013). This was believed to be the reason behind the deformation of the polymers at the storage conditions with the exception of its storage at 5 °C. The storage of these stable filament over 6 months resulted in water loss of approx. 6.51 and 4.61 % for the filament store without and with a vacuum respectively (Table 5.8 and Figure 5.9). However, this did not influence the diameter nor physical appearance of the filaments which could also be due to storage at temperature below the T_g of the polymer as explained earlier which reduces polymer mobility (Fitzpatrick et al., 2002).

Besides the moisture variations, this filament demonstrated no changes in the obtained TGA thermograph before and after storage with weight losses due to the degradation of the APIs and excipients occurring in a similar manner (Figures 5.8 and 5.9). The second weight loss occurs as a result of theophylline degradation, the third as a result of the polymers and TEC as discussed in Section 2.5 (Okwuosa et al., 2016) were the polymer improved the stability of TEC. As a result, degradation occurring at the same time. No further weight losses were observed since talc is stable above 500 °C.

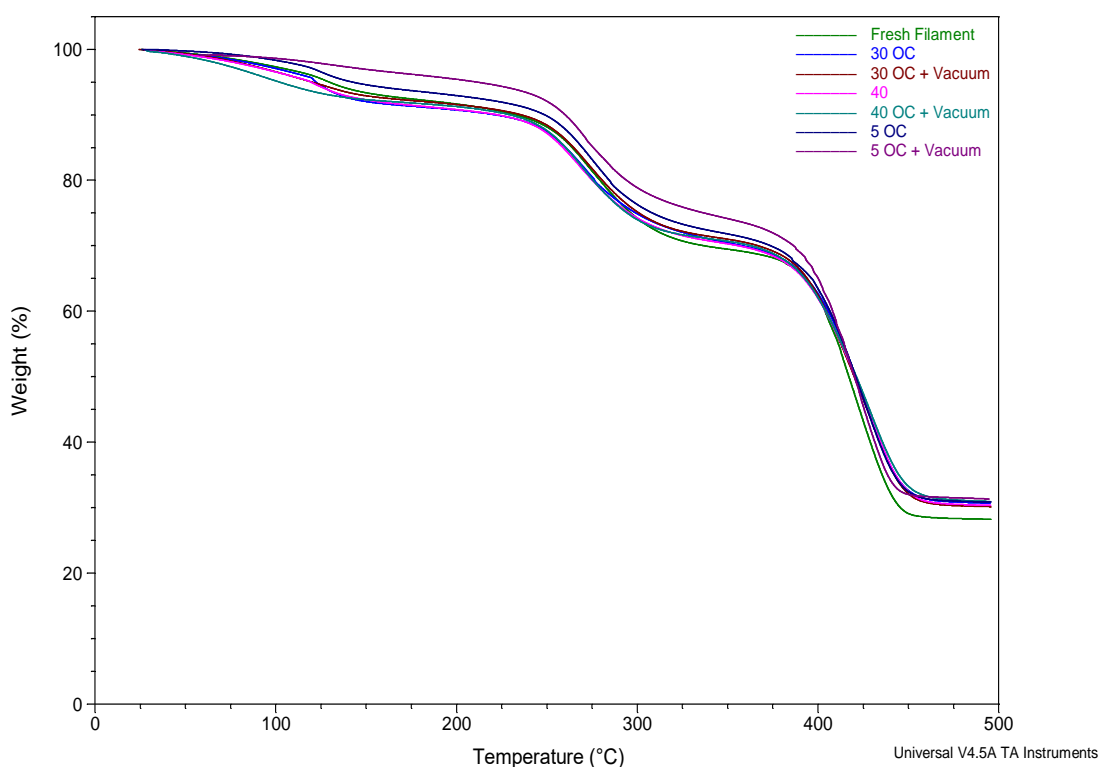


Figure 5.8. The impact of different storage condition on TGA of PVP-based filament after 1 month.

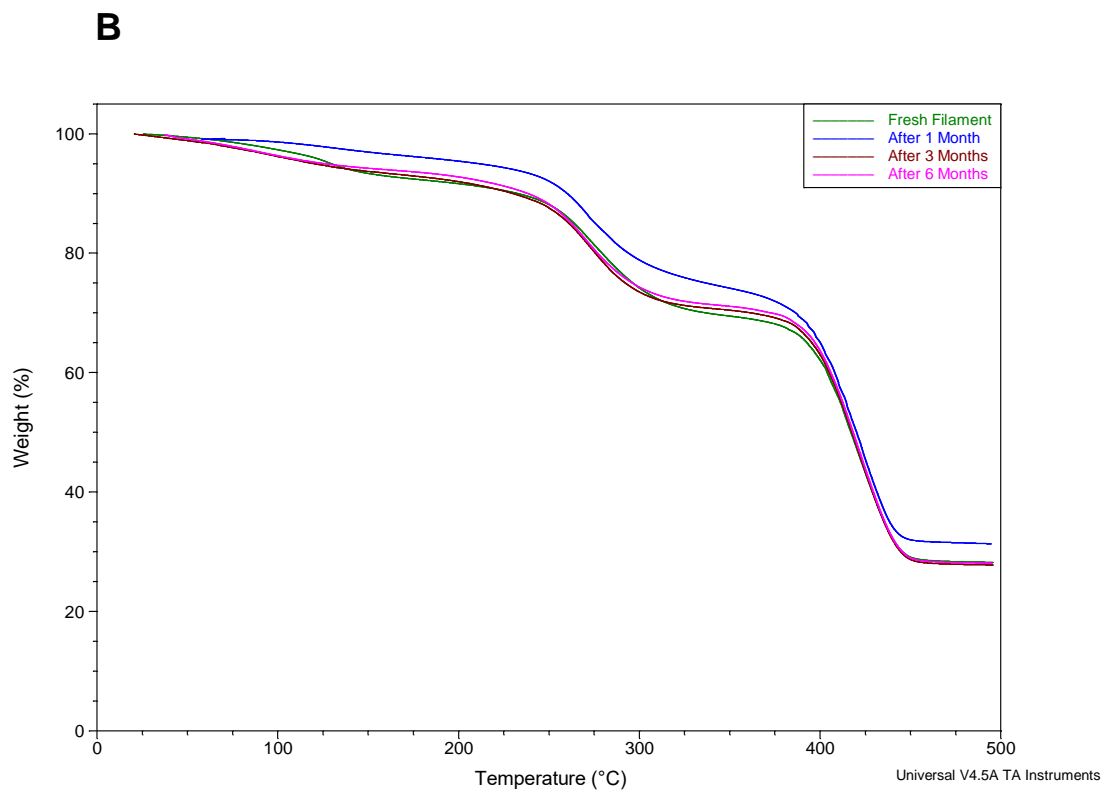
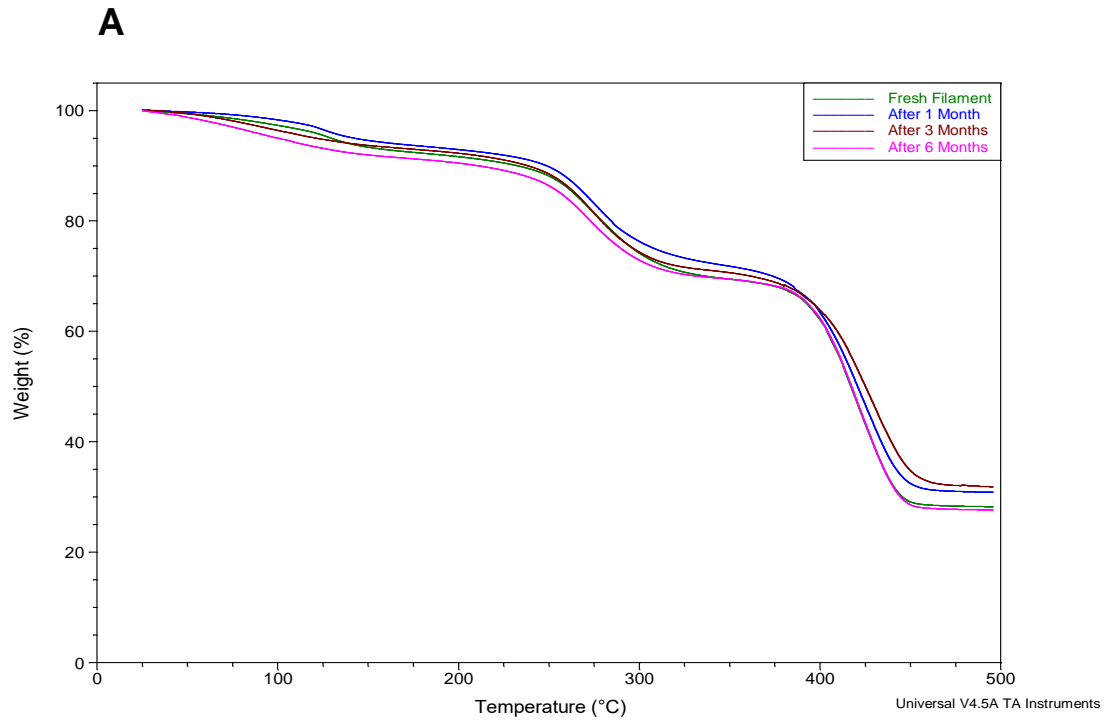


Figure 5.9. The impact of storage at 5 °C on the TGA of PVP-based filament (A) no vacuum (B) vacuum.

The TGA thermograph for Eudragit L100-55-based filament demonstrated an initial weight loss of 1.03 % due to water evaporation from the fresh sample, with a slight increase in moisture uptake as seen from its water loss after storage in the investigated conditions (Table 5.8, Figures 5.10, 5.11 and 5.12). This was expected since Eudragit L100-55 does not seem to be very hygroscopic. A 4 % moisture loss was observed in an earlier study in Chapter 3 although lower water contents have been reported (Parikh et al., 2014). The lower moisture content observed in the filaments in comparison to the polymer alone could be due to the HME processing technique involved in filament manufacturing which might lead to water loss. The storage of the filaments at 5 °C, 30 °C + 65 %RH or 45 °C + 75 %RH over 6 months did not seem to affect its weight loss pattern. A first major weight loss due to TEC from approx. 190 °C was observed in all the thermographs followed by another weight loss from approx. 315 °C due to the polymer degradation. This is in contrast with a study by (Parikh et al., 2014) where the degradation temperature of Eudragit L100-55 was reported to be 176 °C. As mentioned earlier, talc does not show any weight loss pattern since it is stable above the experimental temperature.

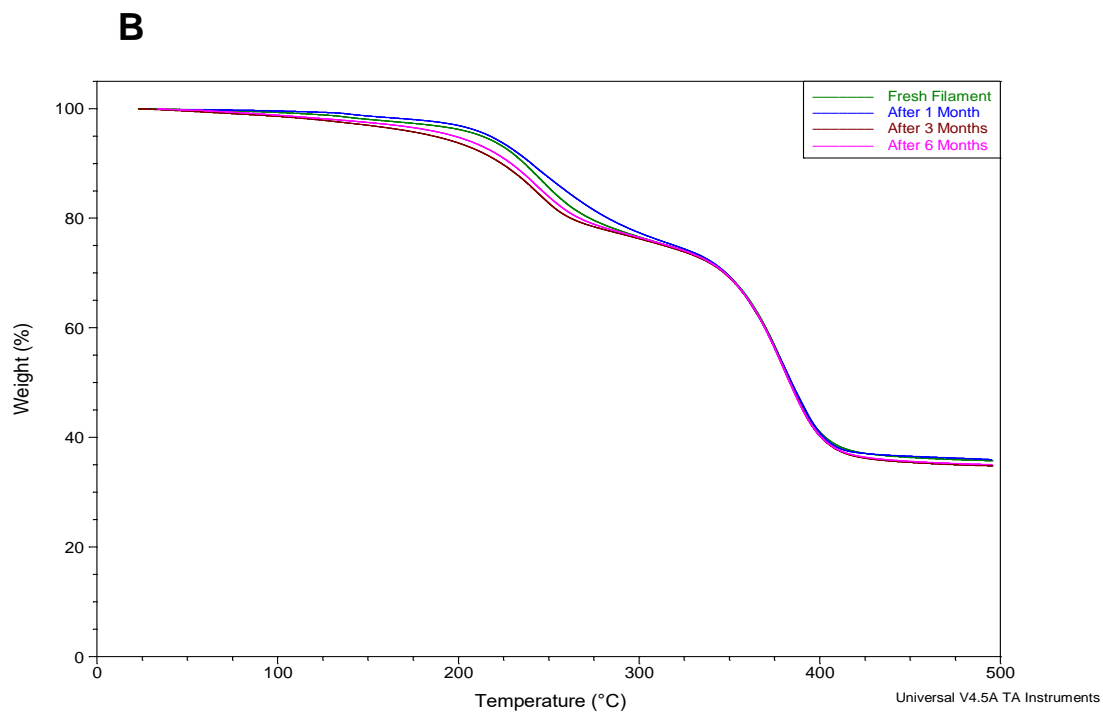
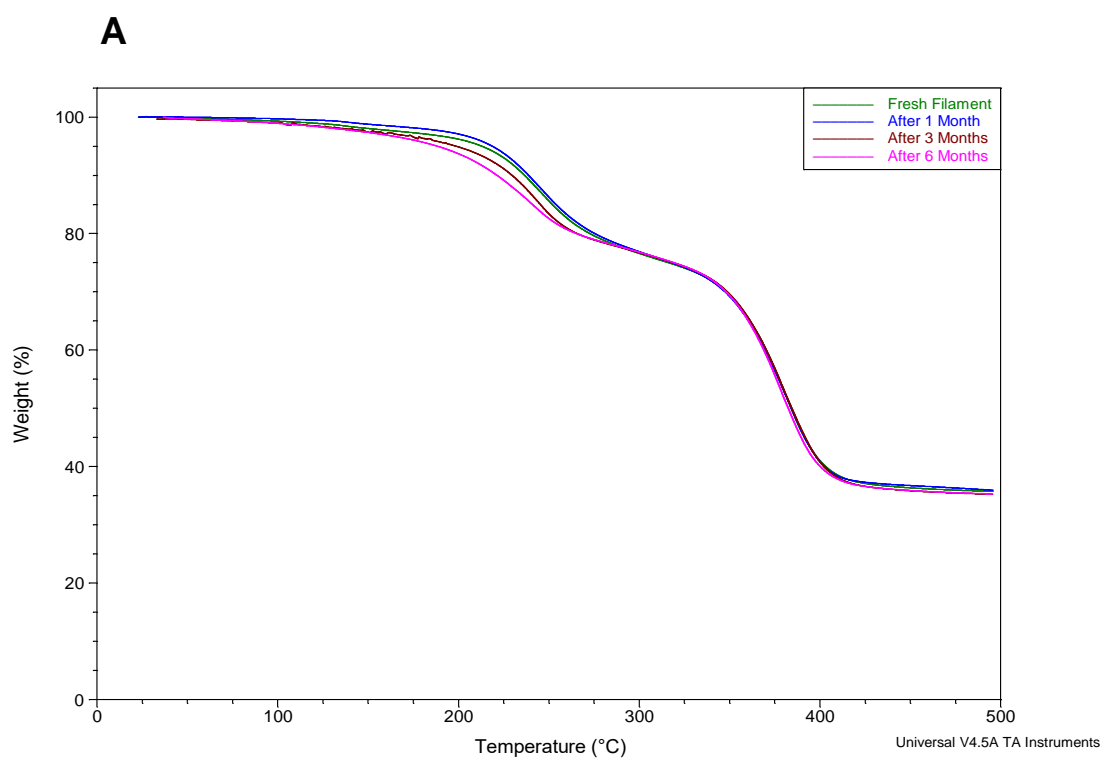


Figure 5.10. The impact of storage at 5 °C on the TGA of Eudragit L 100-55-based filament (A) no vacuum (B) vacuum.

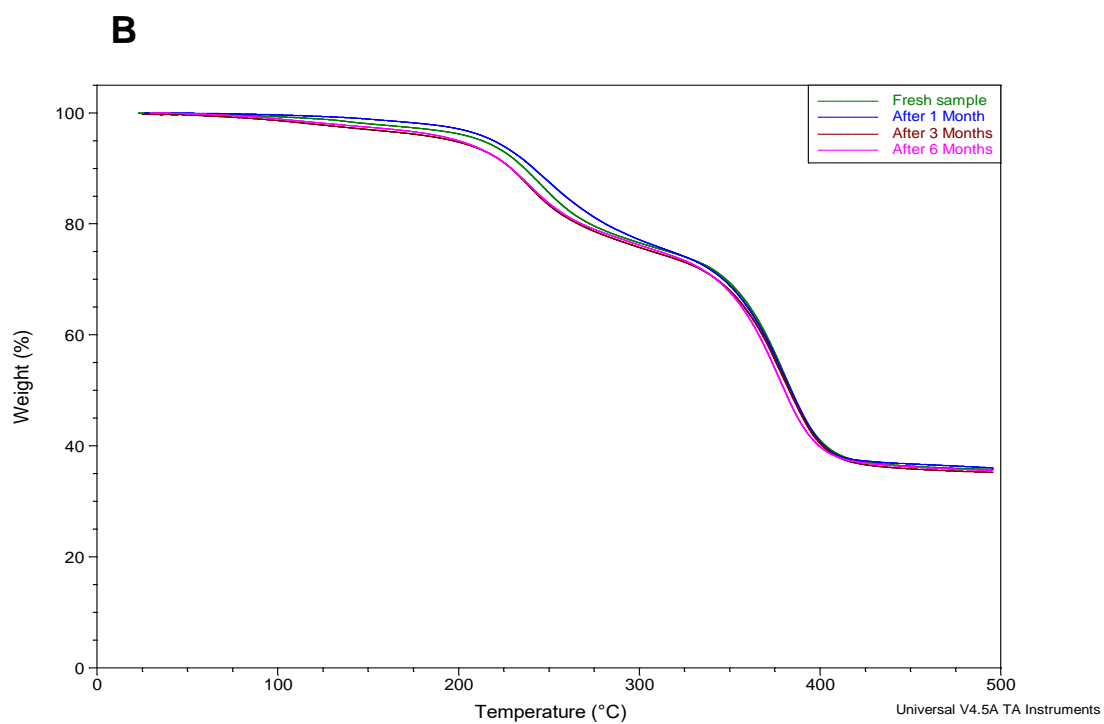
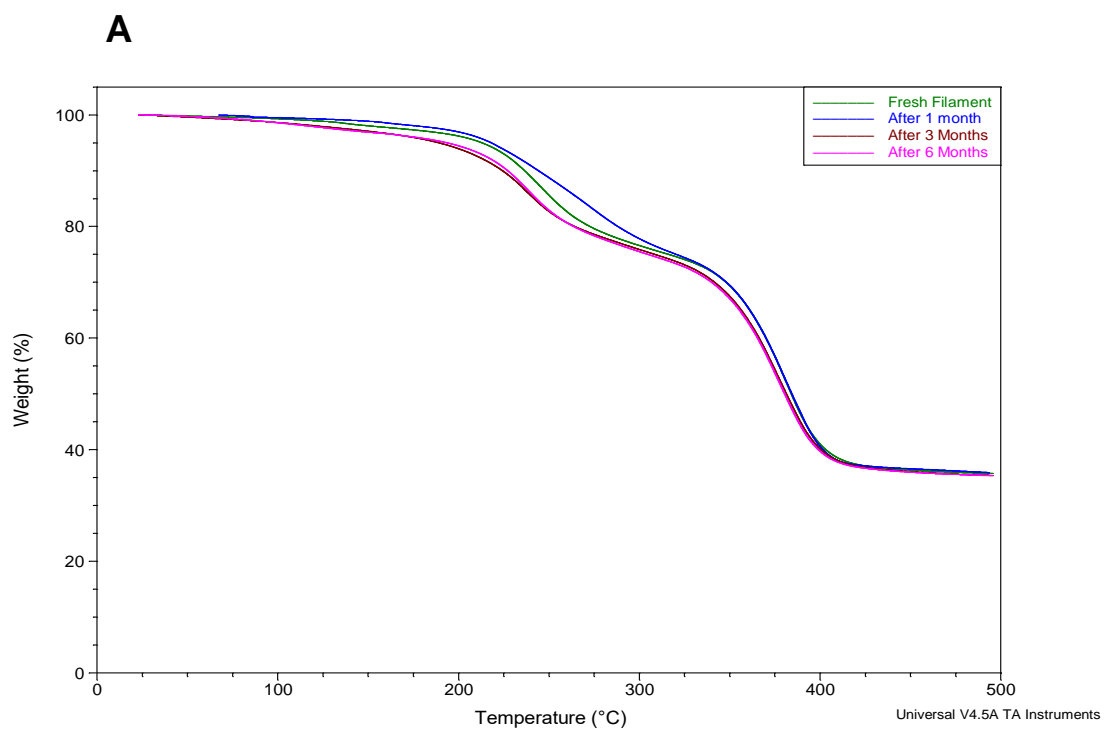


Figure 5.11. The impact of storage at 30 °C + 65 %RH on the TGA of Eudragit L 100-55-based filament (A) no vacuum (B) vacuum.

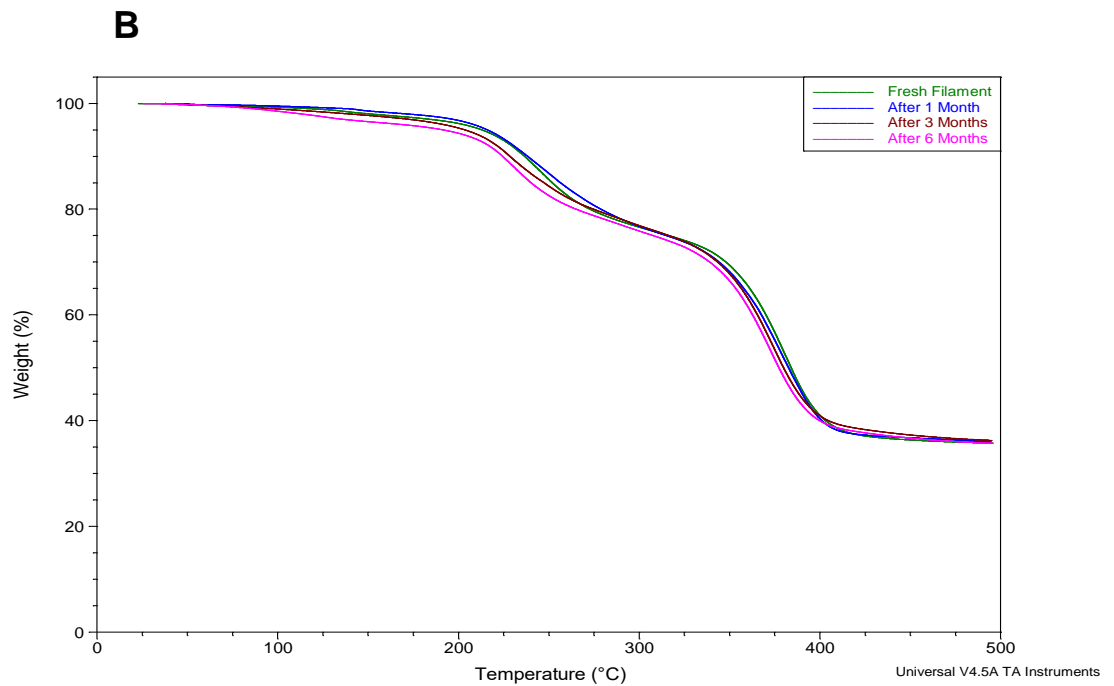
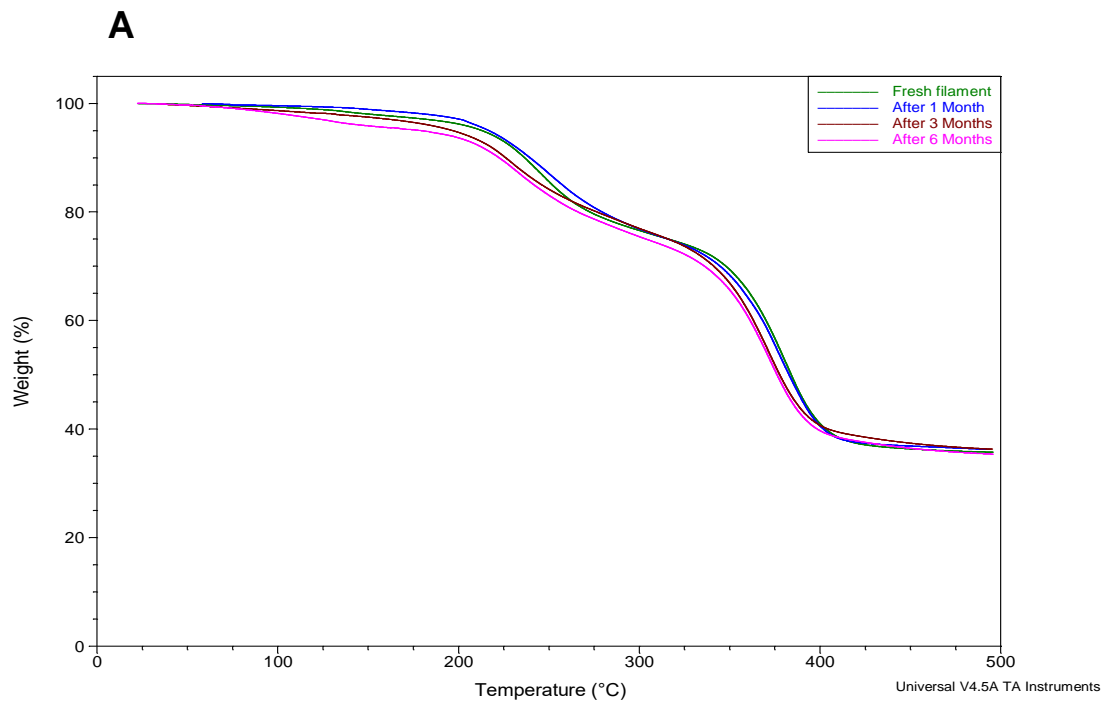


Figure 5.12. The impact of storage at 40 °C + 75 %RH on the TGA of Eudragit L 100-55-based filament (A) no vacuum (B) vacuum.

Eudragit S100 has been reported to have a moisture content as low as 0.2 % (Parikh et al., 2014). The Eudragit S100-based filaments demonstrated slight variations in their moisture content due to storage as observed from the water loss in Table 5.8. Figures 5.13, 5.14 and 5.15 showed the weight loss pattern from a freshly prepared Eudragit-based filament in comparison with their weight loss patterns after storage in the researched condition. These TGA results showed a similar pattern with the first major weight loss due to TEC above 200 °C and the second weight loss due to the Eudragit polymer starting from approx. 350 °C. which was also in contract to the study by Parikh et al. (2014). As also expected, talc remained unaltered during the thermal process due to in high degradation temperature.

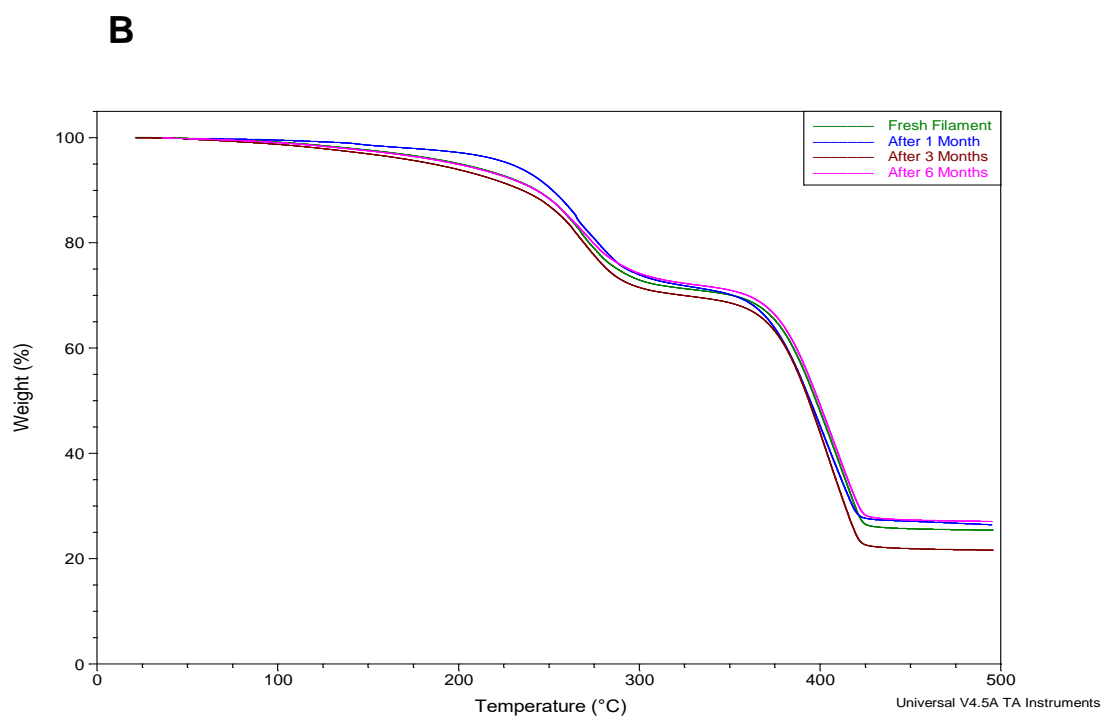
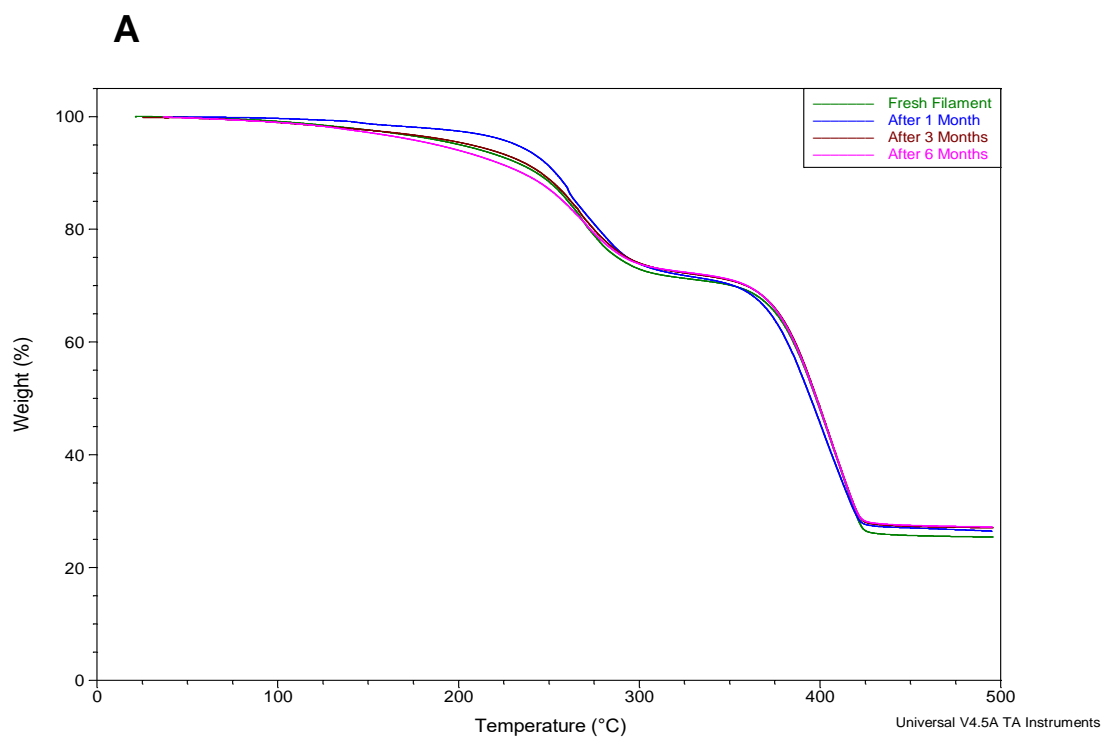


Figure 5.13. The impact of storage at 5 °C on the TGA of Eudragit S100-based filament (A) no vacuum (B) vacuum.

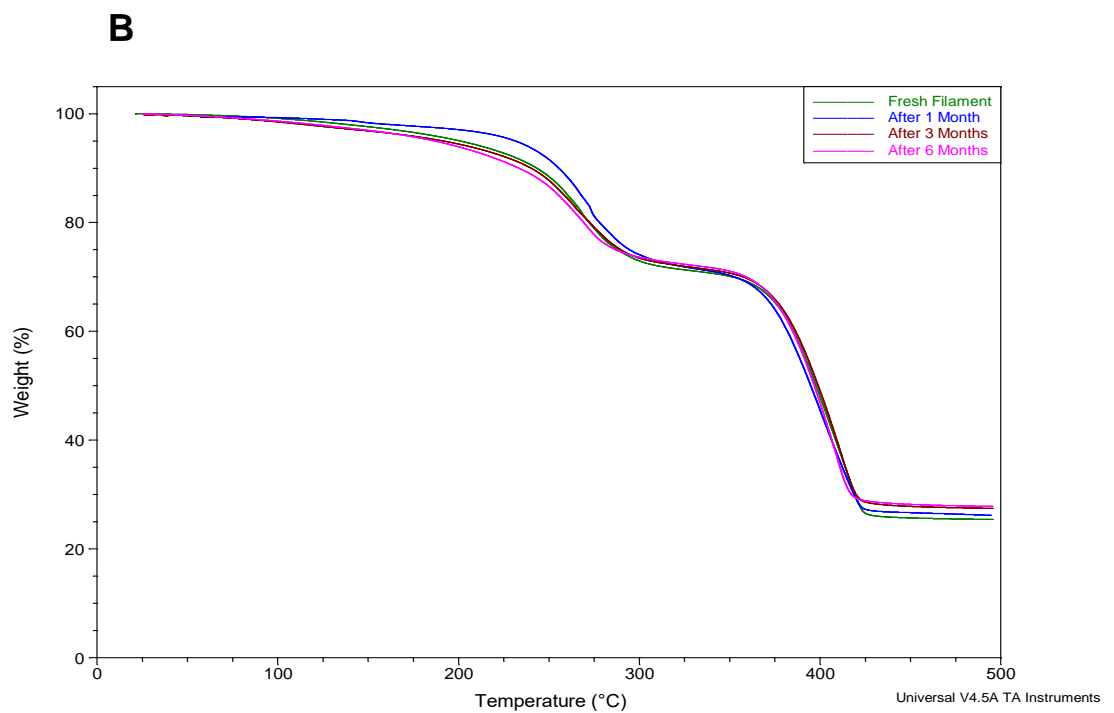
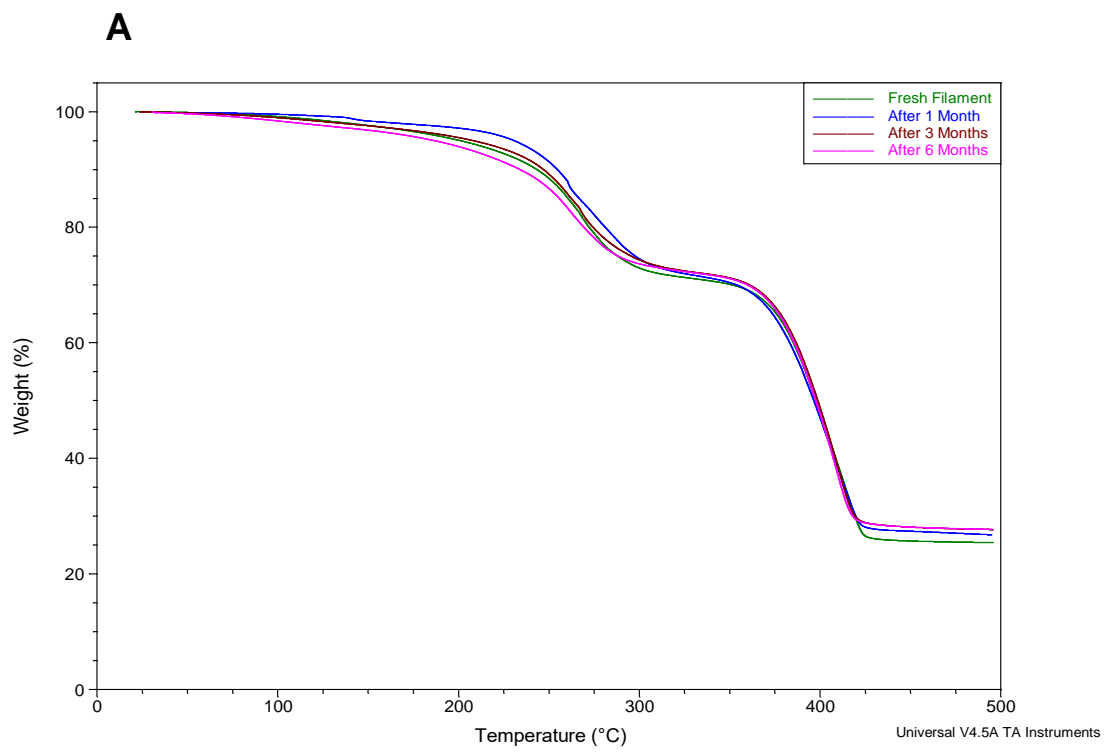


Figure 5.14. The impact of storage at 30 °C + 65 %RH on the TGA of Eudragit S100-based filament (A) no vacuum (B) vacuum.

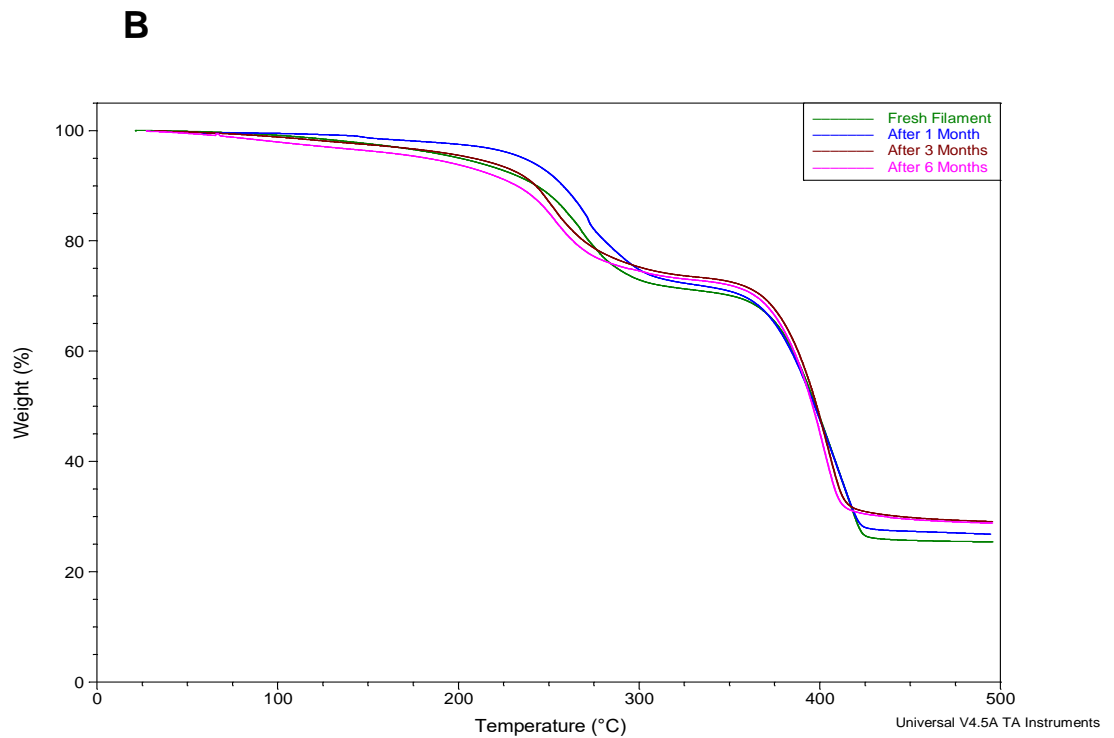
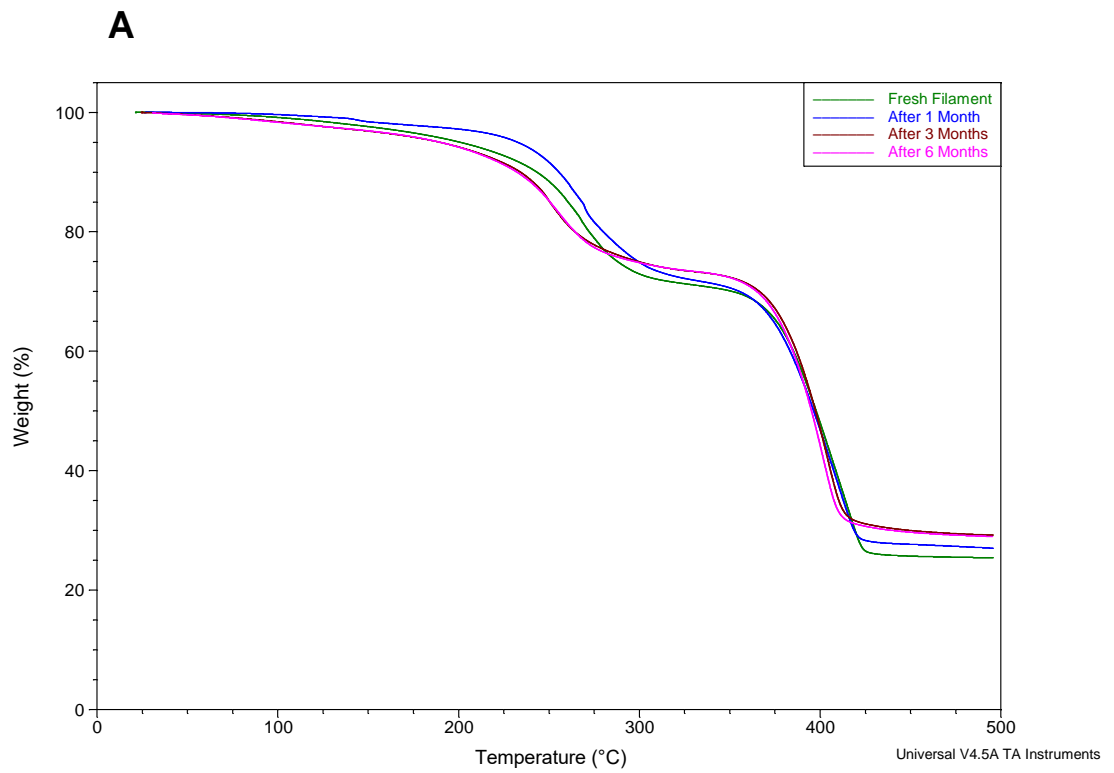


Figure 5.15. The impact of storage at 40 °C + 65 %RH on the TGA of Eudragit S100-based filament (A) no vacuum (B) vacuum.

MTDSC analysis was used to investigate the effect of the storage conditions on the glass transition temperature of the filaments. This allows for the separation of complex events into reversible and non-reversible heat flow especially since PVP, a hygroscopic polymer was used in this study. A previous report on the T_g of a PVP-based filament demonstrated a broad endothermic effect before 100 °C, suggesting the evaporation of water (Okwuosa et al., 2016). This occurs around the T_g of this filament and was observed to still interfere with the thermograph after separation of the events as seen from the reversible heat flow in (Chapter 7: Supplementary data, Figures 7.5A and 7.6A). This therefore made the determination of the actual T_g of the filament challenging using this approach. A heat-cool-heat method was used to exclude the effect of moisture on the T_g of the filaments. This demonstrated a T_g of the PVP-based filament before storage to be 70.2 °C which is similar to a previous report (Okwuosa et al., 2016) (Chapter 7: Supplementary data, Figures 7.5B and 7.6B). It was also observed that its storage at 5 °C (with or without vacuum) did not seem to produce a significant shift in the T_g of the polymer. However, it is believed that this might not be a clear representation of the effects of the storage conditions on the T_g of the filament. The heat-cool-heat approach completely dehydrates the filament into a state that is not a representation of the filaments after storage. Since the polymer used is hydroscopic, with water being a plasticiser, changes due to storage will be dependent on the extent of water intake which was observed to increase due to storage from the TGA analysis. This effect was excluded by the heat-cool-heat approach used in this study, resulting in a similar T_g before and after storage.

Interactions between the polymer and other excipients and API could also influence the T_g of a polymer matrix. For example, the recrystallisation of the API as a result of storage could increase the T_g of the polymer (Baik et al., 1997). Recrystallization has been shown to be influenced by the relationship between the T_g and the recrystallization temperature (Nojima et al., 1998). However, this was not the case in this study with the T_g of the polymer remaining within the same range as observed from the second heat scan (Chapter 7: Supplementary data, Figures 7.5B and 7.6B).

The MTDSC of Eudragit L100-55 showed the interference of water evaporation on the T_g of the polymer and therefore the need for a heat-cool-heat approach. The initial scan demonstrated a smaller endothermic event (Chapter 7: Supplementary data, Figures 7.7A, 7.8A, 7.9A, 7.10A, 7.11A and 7.12A) in comparison to that obtained from a PVP based polymer. The second scan revealed no major shift in the T_g of the filament after the first month of storage in the investigated condition. However a slight increase in the

T_g after the 3rd and 6th month across the investigated storage conditions were observed (Chapter 7: Supplementary data, Figures 7.7B, 7.8B, 7.9B, 7.10B, 7.11B and 7.12B).

A freshly prepared Eudragit S100-based filament demonstrated a T_g of approx. 85.89 °C. Its storage in the investigated conditions according to the ICH guidelines demonstrated no major shift in the T_g of the filament as a result of storage (Chapter 7: Supplementary data, Figures 7.13, 7.14, 7.15) demonstrating the stability of this filament irrespective of the storage condition. However, a slight increase in T_g was observed after 3 months of storage under vacuum at 40 °C + 75% RH (Chapter 7: Supplementary data, Figure 7.15B), a similar behaviour obtained when Eudragit L100-55-based filament was stored in all the experimented condition. Unlike PVP and Eudragit L100-55-based filaments, a heat-cool-head approach was not required, demonstrating its non-hygroscopic nature. This also demonstrates the stability of polymers with high T_g as proposed by Fridgeirsdottir et al. (2018).

It was important that the integrity of the API loaded on the PVP-based filaments stayed intact throughout the stability trial. As a result, samples were taken at the points of analysis and analysed using HPLC. It was observed that there was no degradation of the API due to storage at 5 °C over the 6 months stability studies. Drug contents obtained from the filaments stored without vacuum were 99.94 ±0.05 %, 99.90 ±0.07 %, 100.19 ±3.15 % and was 99.52 ±0.25 %, 99.39 ±1.91 %, 100.87 ±1.50 % when stored in a vacuum after 1, 3 and 6 Months respectively ($p > 0.05$).

Investigating into the effect of the storage condition on the *in vitro* release profile of theophylline from the filament was demonstrated using a USP II dissolution apparatus. An increase in drug release was observed once stored at 5 °C in comparison to a freshly prepared filament and storage in the other investigated conditions after 1 month (Figure 5.16A). Hundred percent of the APIs were released at approximately 15 min in comparison to 100 % release at 40 min from the other samples. This fast release properties of the PVP-based filament was maintained through the 6 months storage as seen in Figure 5.16B indicating no changes in the release properties of the filament due to storage.

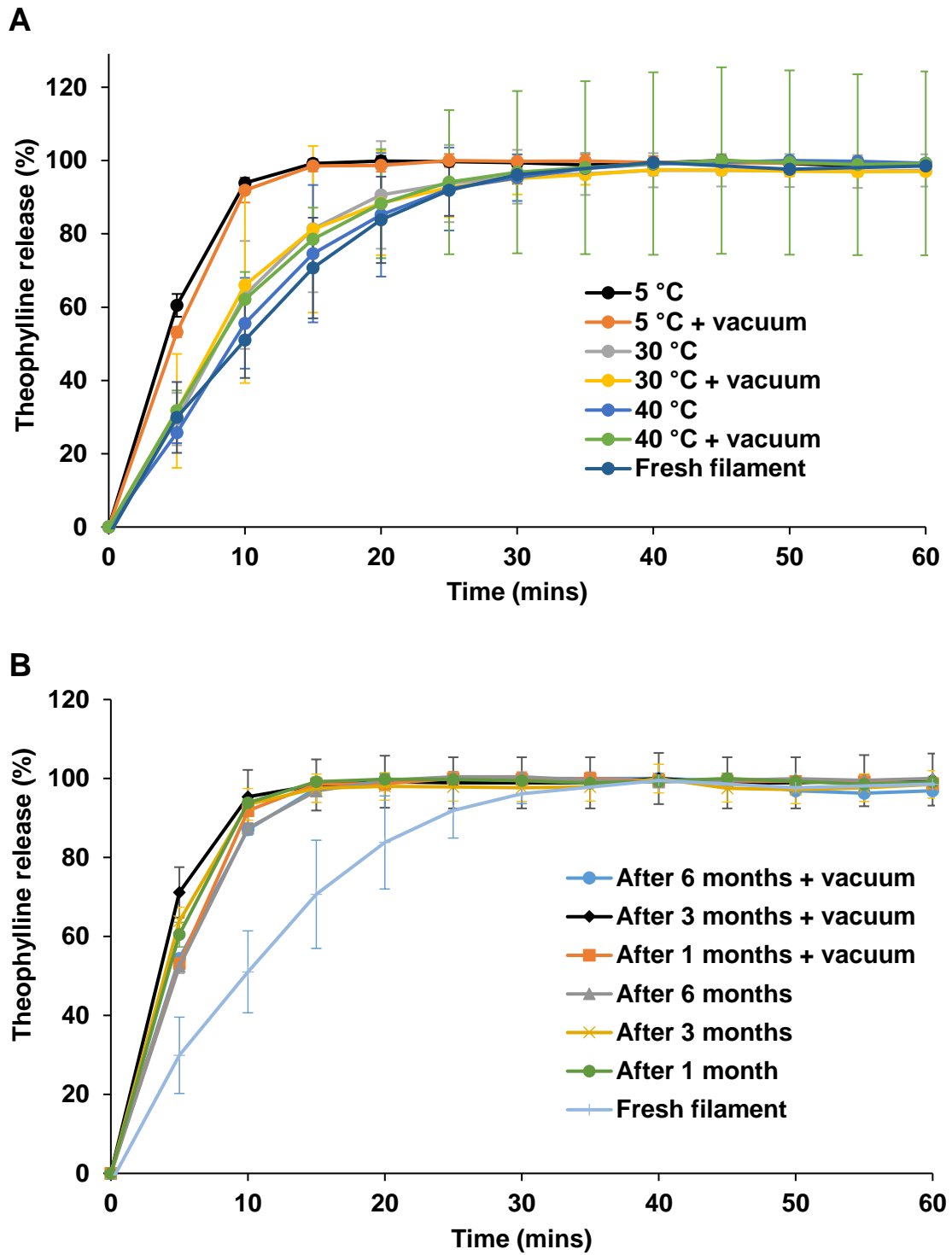


Figure 5.16. In-vitro drug release profile from PVP-based filament after storage in different condition for 1 month (A) and after storage at 5 °C alone for 6 months (B).

5.6 Conclusions

This research demonstrated the use of accelerated stability studies in the determination of the long-term stability of a PVP, Eudragit L100-55 and S100-based filament. These filaments were manufactured using HME extrusion which is well established in the preparation of solid dispersions. The PVP-based filament was only stable when stored at 5 °C. This could be due to storage below the T_g of polymer which increases polymer viscosity, therefore preventing polymer mobility. Storage at the other conditions lead to the flattening and deformation of the filaments, rendering them incompatible with FDM 3D printer head which lead to the discontinuation of this study in these storage conditions. The storage of the PVP-based filament at 5 °C demonstrated no changes in physical form of the loaded API, likewise its degradation pattern. However, increase in moisture content was observed after storage as seen from the TGA. An investigation into the changes in the T_g of the filament due to storage demonstrated the interference of water evaporating during analysis. However, the complete removal of water from the sample by a heat-cool-heat approach revealed no alterations in the T_g of the filament. This was believed not to be a good representation of the filament properties after storage since water content plays a role in T_g.

Eudragit L100-55 and S100-based filaments remained stable throughout the 6 months stability studies with no changes in their physical form and TGA thermograph. They also remained compatible with the 3D printer. The use of a heat-cool-heat approach was required to determine the T_g of the Eudragit L100-55 based filaments due to the effect of water evaporation on the MTDSC thermograph, which influences the actual T_g of the filament. However, an increase in T_g was observed after 3 months in all the storage conditions. A heat-cool-heat approach was not required during the MTDSC of Eudragit S100 which presented no variations in the T_g of the filament after storage with the exception of its storage under vacuum at 40 °C + 75 %RH which demonstrated an increase in T_g after 3 months.

The Eudragit L100-55 and 100-based filaments were also less hygroscopic and remained printable irrespective of the storage conditions, indicating the potential of having a high T_g and less hygroscopic polymers in a polymer matrix as a better alternative. The stability of these filaments will go a long way to encourage the large-scale manufacturing of filaments which could be transported and stored in different regions and used on demand for dose personalisation using a FDM 3D printer. This was believed to probably be the path of this technology as research strives to establish this technique in the pharmaceutical industries for dose personalisation.

Chapter 6 : General conclusions and future work

6.1 General conclusions

The use of the oral route for drug delivery remains one of the safest and commonly used routes for drug administrations (GBIResearch, 2012). Dosage forms are usually manufactured in large numbers using conventional manufacturing approaches resulting in dose personalisation limitations. The knowledge about pharmacogenomics created more awareness on the impact of genetic makeup of different patients on responses to the same medication, thus emphasising the need for a more personalised approach to drug dosing (Mooney, 2015). This has the potential of increasing positive outcomes from drug use and reducing adverse drug effects.

The use of FDM 3D printing amongst other 3D printing approaches showed great potential in drug manufacturing and dose personalisation with the ability to create 3D products on a small scale without requiring several processing steps and large and expensive equipment. Products are ready to use once printed with no further processing required. This benchtop and readily available equipment seemed to be the future of dose personalisation although with many limitations especially at this early stage of development. Mostly extended release dosage forms were manufactured due to the nature of the polymer used which also required high processing temperature, making it unsuitable for thermolabile actives. Limitations in loading drugs into these commercially available non-pharmaceutical grade polymers (PVA, PLA) were also a major drawback to the technique. There was also limited information in the application of the technique in the manufacturing of other oral solid dosage forms e.g. capsules. The ability to manufacture filaments for 3D printing using HME and employing pharmaceutical grade polymers seemed to be a breakthrough in the use of this technology. This provided a solution to some of the major limitations of FDM 3D printing.

By coordinating FDM with HME, it was possible to produce the first example of applying PVP, a well-used pharmaceutical grade polymer, for the FDM 3D printing of immediate release tablets. Since the majority of oral dosage forms demonstrate such release profiles, this was believed to be a positive contribution. Immediate drug release was proved using two model drugs, indicating potential compatibility with a wider variety of API, showing the versatility of the PVP-based filament. It also creates more opportunities for the use of thermolabile actives since 3D printing was achieved at a much lower temperature in comparison to the use of the commercially available PVA filament that requires temperatures up to 210 °C, due to the high T_g of the polymer. The manufactured tablets showed excellent mechanical properties when tested against the requirements of the BP. Although they were manufactured using an entirely different approach to powder

compression-based tablets, they demonstrated acceptable in-batch variations and presented qualities required for an immediate release dosage form. Weight variations were one of the main concerns during this study. However, this was attributed to the variations in the filament diameter, in addition to the possibilities of partial blockade of the printing nozzle during tablet 3D printing. This research improves the potentials of this technology in the dose personalisation of bespoke immediate release tablets and opened doors for the adaptation of other pharmaceutical grade polymers for FDM 3D printing.

The splitting of solid dosage form is a very common practise in the absence of an adequate dose personalisation techniques. This eliminates the barrier function of delayed release (DR) tablets thereby rendering such practises impractical for such dosage forms. The ability to use multiple heads in FDM 3D printing was used to an advantage in the fabrication of DR tablets based on a shell-core structure in a single process. This was unlike conventional approaches which requires a separate coating stage to achieve release modifications. To the author's knowledge, this is the first report of producing DR tablets based on FDM 3D printing technology which complied with BP criteria. Both filaments were processed by HME to form a matrix system using a plasticiser (TEC) and a non-melting component (talc). The replacement of talc with an alkalisng agent (TBP) created an enteric release tablet following the BP criteria for enteric dosage forms. This accelerates the drug release profiles obtainable using this technology. Delayed release tablets of theophylline, budesonide and diclofenac sodium were achieved using this approach, which further emphasises the flexibility of the PVP-based filament. This therefore demonstrates the potentials of this technology for a wider range of actives for delayed release oral products. These were only possible by applying a thin layer of oleic acid over the shell filament during 3D printing to reduce nozzle blockage. This seemed to do so by providing a lubricating effect which prevents the filaments from sticking to the walls of the heated nozzle, whilst maintaining the physical properties of the filament. In addition, the layer thickness of the delayed release filament needed to be ≥ 0.52 mm to achieve sufficient core protection in the acid medium which is thicker than the usual coating thickness used to modify the release of conventional dosage forms. One of the major implications of this approach in the manufacturing of delayed release dosage form is providing a single step solution to the conventional approach which required tablets compression and another coating step to achieve release modification. This therefore offers an approach in drug modification with reduced processing time in addition to the potentials of dose personalisation. The shell-core approach also opens doors to the manufacturing of other dosage forms such as capsules

by constructing a shell structure which could be either filled with solids, semisolids or liquids.

The manufacturing of capsules using FDM 3D printing proved to be challenging, resulting in few available researches in its application in the manufacturing of one of the most acceptable oral delivery forms. However, this research demonstrated the first report of a fully automated process for the 3D printing of liquid-filled capsules. This could only be possible by replacing one of the heads of a dual FDM printer with a syringe-based liquid dispenser which allows the coordination of FDM 3D printing and liquid dispensing using the same device. Both immediate and extended drug release profiles based on methacrylate polymer shells were fabricated and the suitability of the system for different APIs (dipyridamole and theophylline) as a suspension or solution was demonstrated. It was possible to construct a capsule shell structure that maintains its integrity and instantly contains the loaded liquid dose without any curing step. However, in contrast to the conventional capsules, 1.6 mm shell thickness was required to maintain the capsule integrity after loading with the liquids. This was due to the layer-by-layer fashion of 3D printing and therefore requiring the fusing of many layers of the extruded filament to prevent leakages. A concentric filling pattern and the use of a multi-phase 3D printing approach resulted in a tightly layered capsule shell with minimised interruptions during shell printing and liquid dispensing. Above all, this technique demonstrated the ability to control dosing, as well as drug release by manipulating the dispensed volume and shell thickness simply via software. In a clinical setting, this will empower healthcare staff with the capability to provide specific dosing and drug release patterns in individualised liquid-filled capsules without the need to change the capsule shell formulation. This advancement in the use of 3D printers in liquid capsules manufacturing and previous adaptations in the manufacturing of tablets indicates the potentials of this techniques in the manufacturing of the two most popular and widely accepted oral dosage forms. The modification of the dual FDM 3D printer completely minimised the impact of temperature, which encourages the use of a wider range of APIs including peptides and proteins.

The use of AMPs has been investigated to have a wide range of activities. In this regard, the anticancer activity of Aurein 2.6 and LL-37 AMPs were investigated which demonstrated a concentration dependent colon cancer cell line activity, a vital addition to the ongoing research on the potentials of AMPs in cancer management. The peptides demonstrated changes in their secondary structure when the effect of temperature was investigated. However, the use of the modified dual FDM 3D printer in the fabrication of a potential colon targeting liquid capsules loaded with AMPs did not alter the secondary structure of the peptides as confirmed by CD. Therefore, indicating the maintenance of

biological activity after the 3D printing process. *In vitro* colon targeting studies using a Eudragit S100-based shell filament was investigated using model liquid solution as a proof of concept to demonstrate colon targeting potentials. The produced liquid-filled capsule demonstrated acid resistance and a gradual release of theophylline after a change in pH to 7.4. Further optimisation is required to inhibit drug release in the gastric phase. This research further emphasises the possibility to adapt this technology in most aspects of oral drug delivery and provides a potential approach in peptide delivery using a similar approach investigated for the conventional delivery of peptides.

Stability studies are crucial in drug development and are routinely carried out on pharmaceutical products before being introduced into the market. Therefore, it was vital that some of the successfully adapted filaments are assessed for stability. Accelerated stability studies were carried out on the PVP, Eudragit L100 55 and S100-based filaments since they are the primary products from which several doses could be manufactured from depending on the patient's requirement at a particular time. It was crucial that these filaments remain stable during their shelf life and remain compatible with the 3D printer for application in dose personalisation. In a clinical setting, the manufactured and stored filaments must remain in a ready to use condition to tackle everyday challenges in drug dosing. This research was based on the ICH guideline and demonstrated the stability of PVP-based filament when stored at 5 °C in comparison to storage at 30 °C + 65 %RH and 40 °C + 75 %RH. This was attributed to storage below the T_g of PVP which increases polymer viscosity, thereby reducing motility. As a result, the physical properties of the filament were maintained. The Eudragit-based polymers were stable in all the storage conditions and maintained their physical properties with minimal shift in T_g. This was attributed to their less hygroscopic nature and potentially, the high T_g of the polymer, therefore indicating the possibility of polymers with similar characteristics being better candidates for FDM 3D printing.

In conclusion, this work demonstrated the potential of FDM 3D printing in the manufacturing of tablets or capsules for oral dose personalisation using pharmaceutical grade polymers and a bench top equipment (FDM 3D printer). The adaptation of this technology for pharmaceutical purposes is expected to continue evolving over the years and potentially bring an end to the "one size fits all" approach in conventional dosing.

6.2 Future works

3D printing of personalised pharmaceutical dosage forms is still at the early stages of research and development with our research group being one of the pioneers. As a result, more is yet to be accomplished in this research area with most of the setbacks centred on the limitations of the technology itself since they were not initially designed for pharmaceutical use.

Batch reproducibility problems were observed during the manufacturing of the filaments and dosage forms during this study. Therefore, the validation of the filament manufacturing process will benefit their use for FDM 3D printing. This could be carried out by identifying key processing parameters that affects quality during HME. The performance of the filament could also be investigated during FDM 3D printing processes to ensure that reproducible and validated production in good manufacturing practise (GMP) environment is maintained. This will transition to clinical trials and product introduction into the market.

It will be beneficial to attempt to improve the stability of the PVP-based filament since it is a well-established polymer for pharmaceutical purposes. Its hygroscopic nature was concluded to play a key role in its instability. This could be improved by modifying the filament formulation to minimise and control moisture uptake or the optimisation of its storage condition.

The coordination of FDM 3D printing and liquid dispensing produced a liquid-filled capsule which led to investigations on the colonic delivery of AMPs using this approach. Although anticancer activities were established with the AMPs, it will be beneficial to investigate further, their mechanism of action. Colonic drug release was demonstrated using theophylline solution as a model core, as a proof of concept. Therefore, it will be desirable to develop an adequate analytical method for the peptide drug release studies to be able to do so with the peptides themselves. Theophylline release from the colon targeted 3D printed liquid-filled capsule in the gastric phase fell outside the recommendations of the BP. The capsule shell optimisation will be beneficial in controlling this undesirable initial drug release. In addition, it will be beneficial to reduce the overall capsule shell thickness and size to encourage better patient acceptance and therefore, manufacture products with similar dimensions as the well accepted conventional hard shell liquid-filled capsules.

Chapter 7 : Supplementary Data

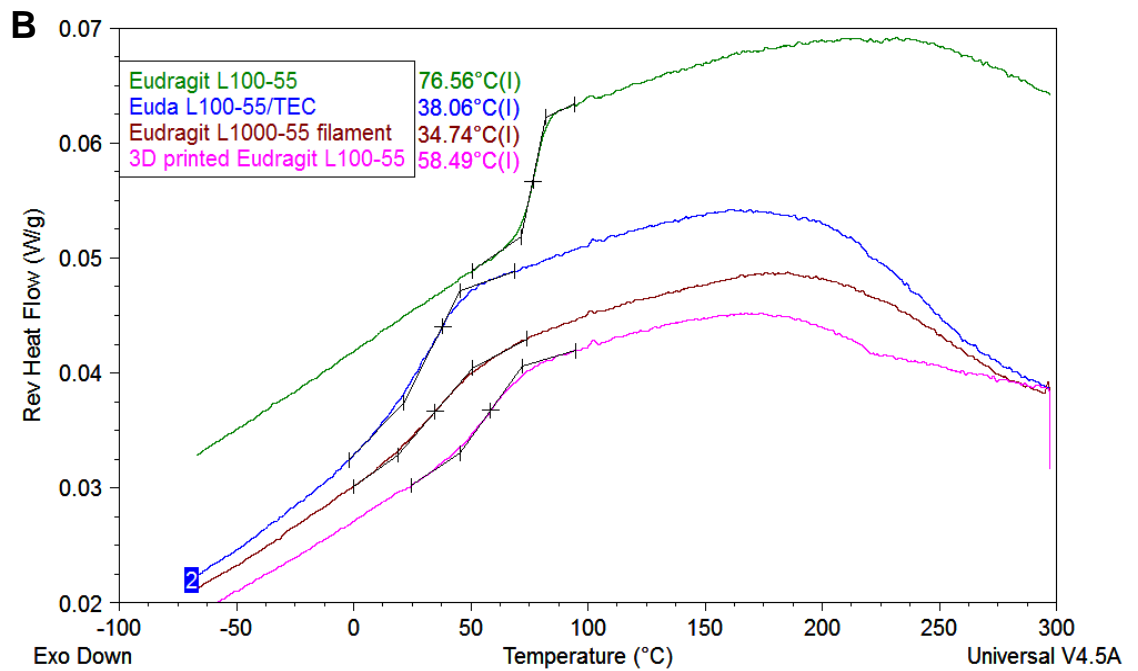
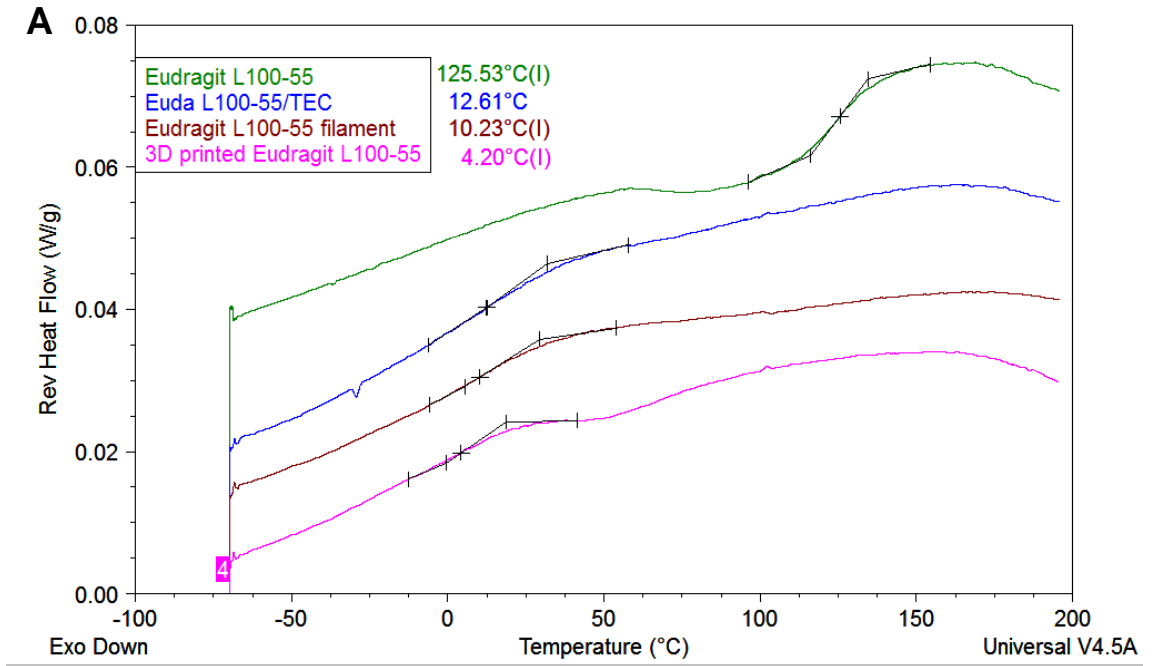


Figure 7.1. Reversing MTDSC thermographs of Eudragit L100-55, Eudragit L100-55:TEC filament, API-free filaments, and 3D printed shell (A) First heat-scan and (B) second heat-scan.

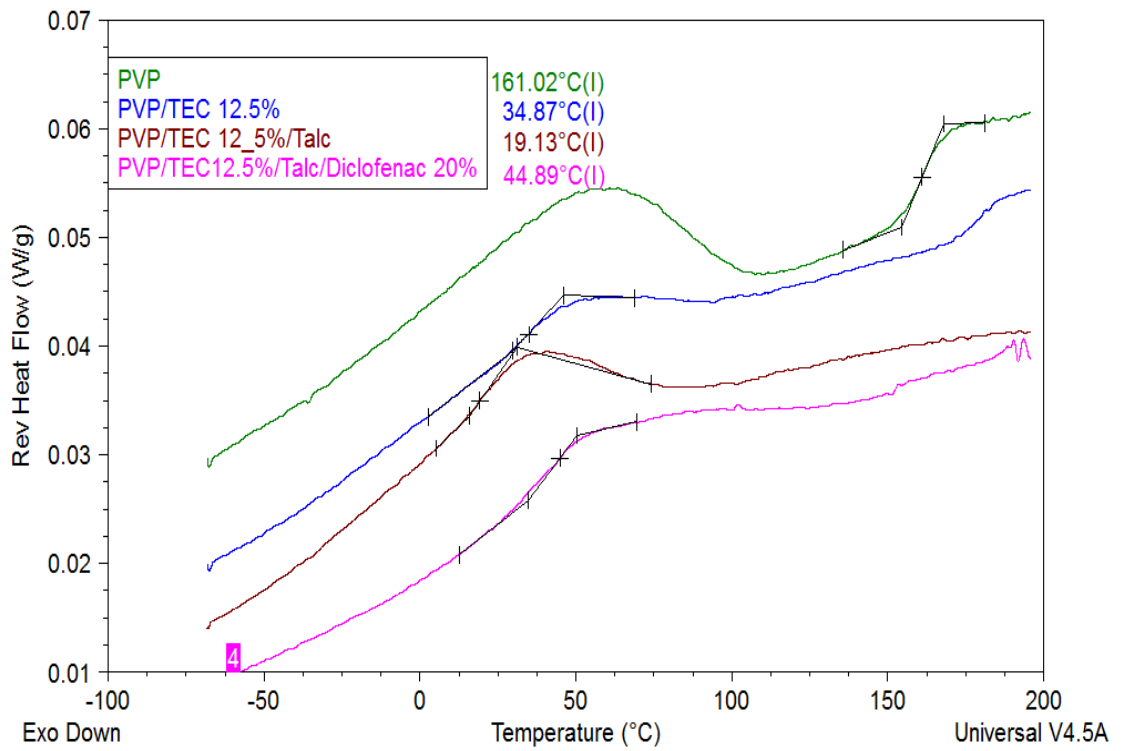


Figure 7.2 Reversing DSC thermographs of PVP, PVP: TEC (12.5%) filament, as well as diclofenac-loaded filaments (first heat-scan).

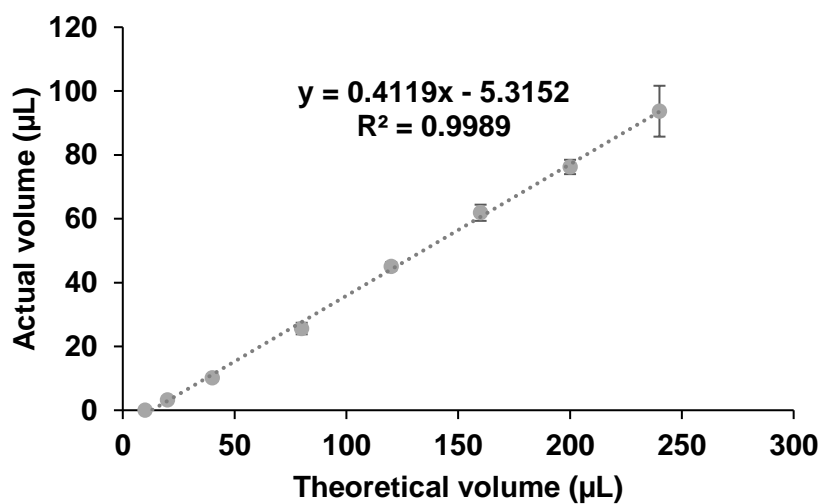
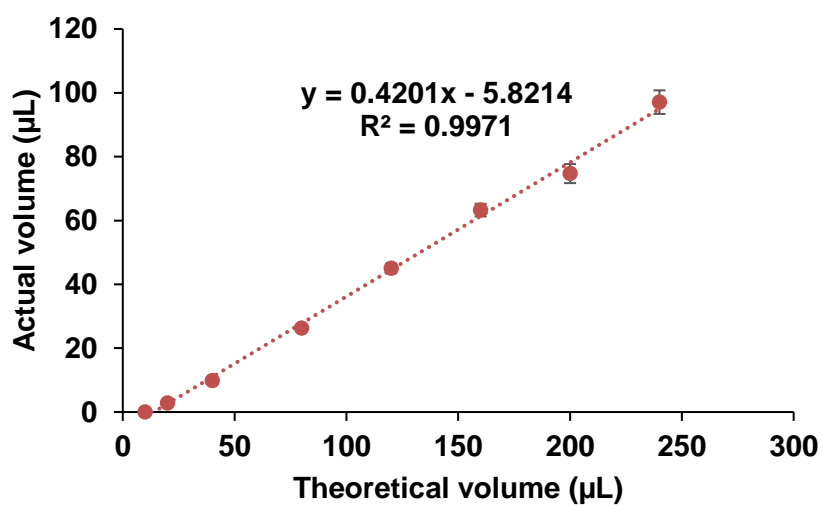
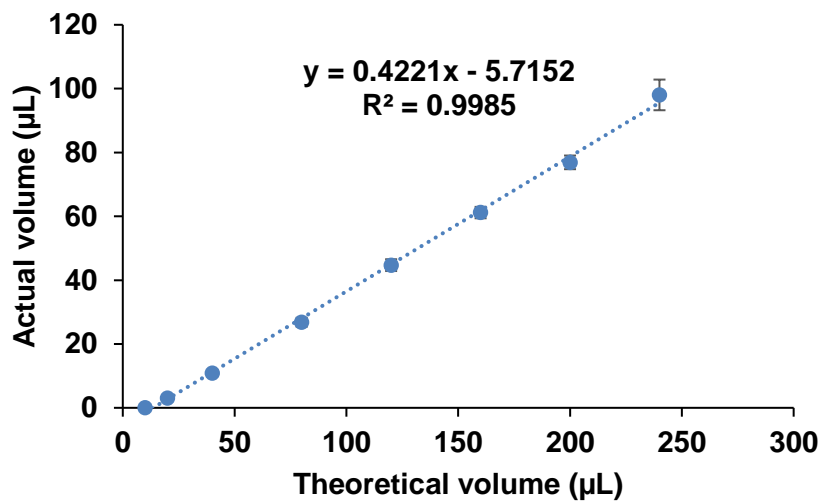


Figure 7.3. Linear relationship theoretical volume of the software and dispensed volume using single-phase printing mode and different nozzle aperture sizes (blue, orange and grey graphs for 0.25, 0.41 or 0.84 mm nozzles respectively).

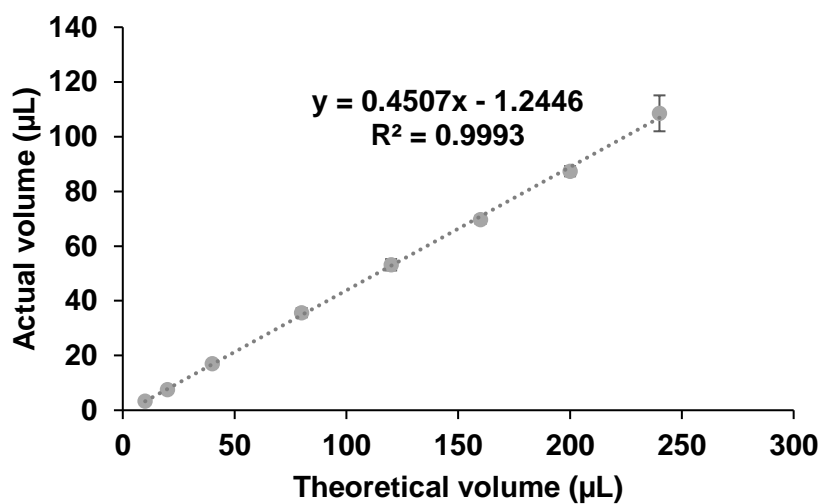
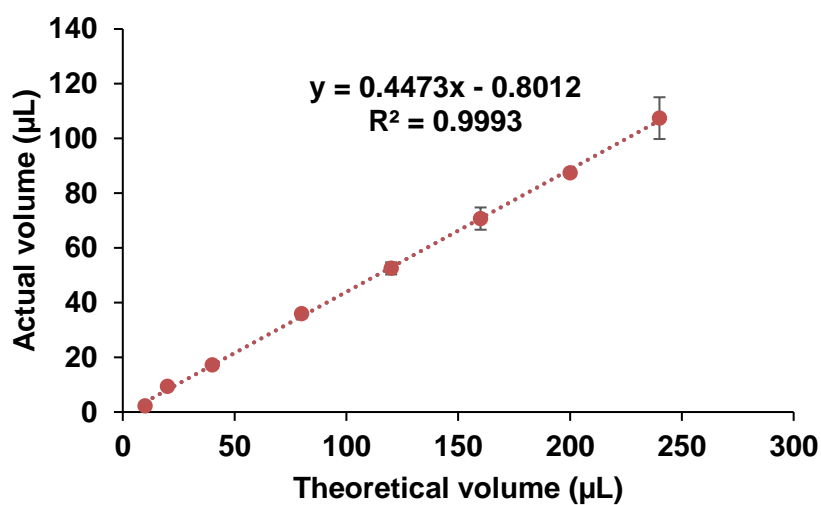
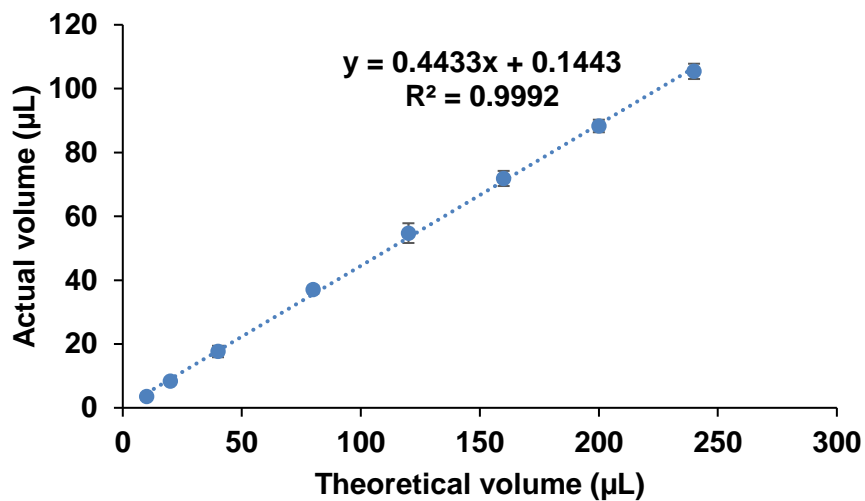


Figure 7.4. Linear relationship theoretical volume of the software and dispensed volume using multi-phase printing mode and different nozzle aperture sizes (blue, orange and grey graphs for 0.25, 0.41 or 0.84 mm nozzles respectively).

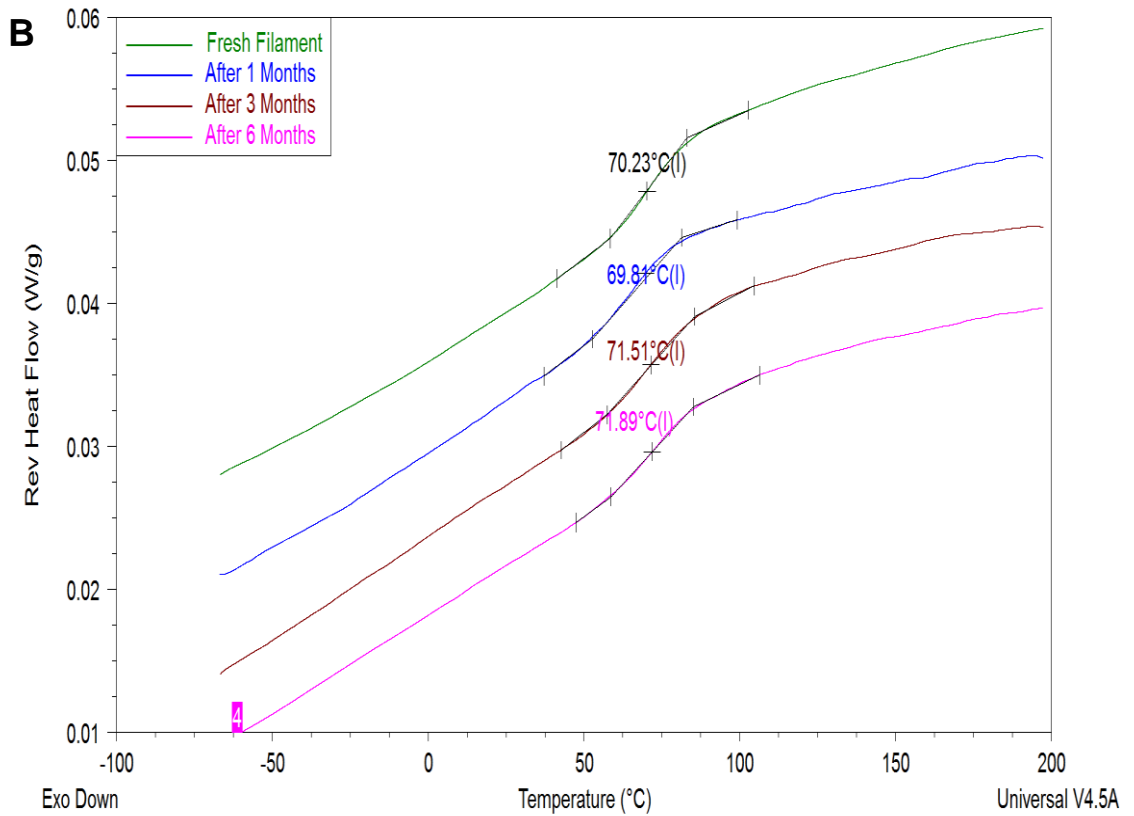
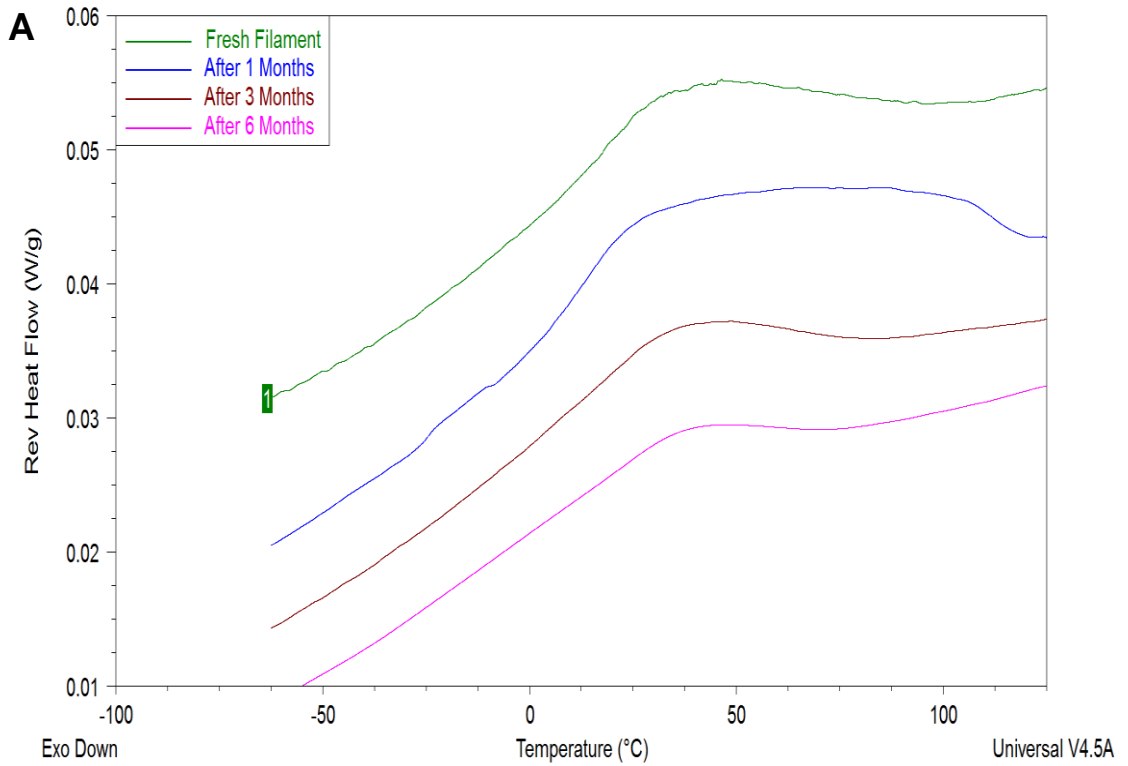


Figure 7.5. Reversible heat flow for the first (A) and second (B) MTDSC thermograph used to investigate the impact of storage at 5 oC without vacuum on the Tg of PVP-based filaments.

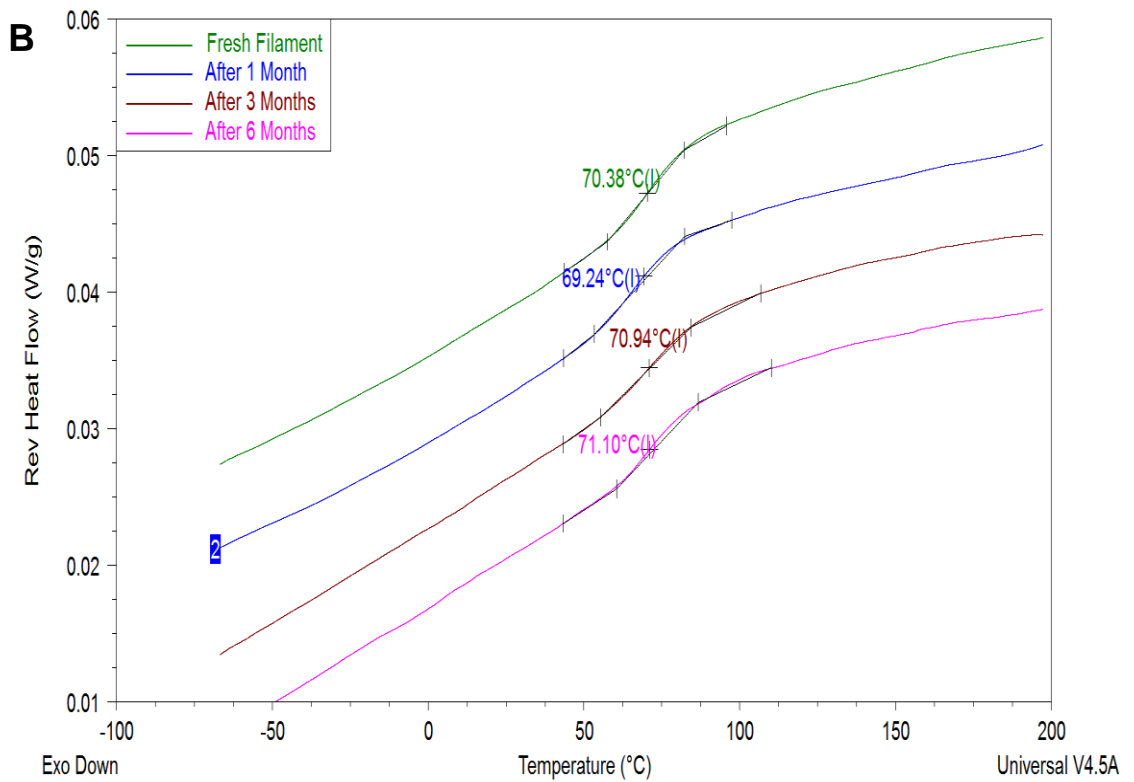
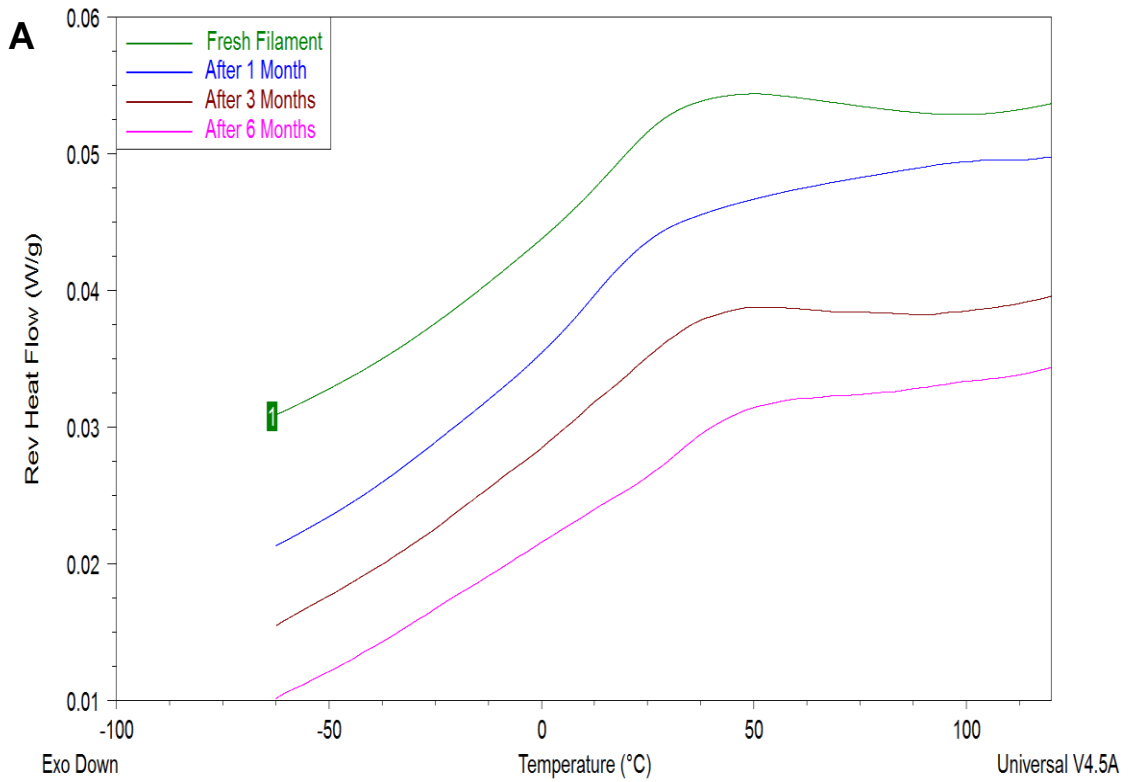


Figure 7.6. Reversible heat flow for the first (A) and second (B) MTDSC thermograph used to investigate the impact of storage at 5 oC + vacuum on the Tg of PVP-based filaments.

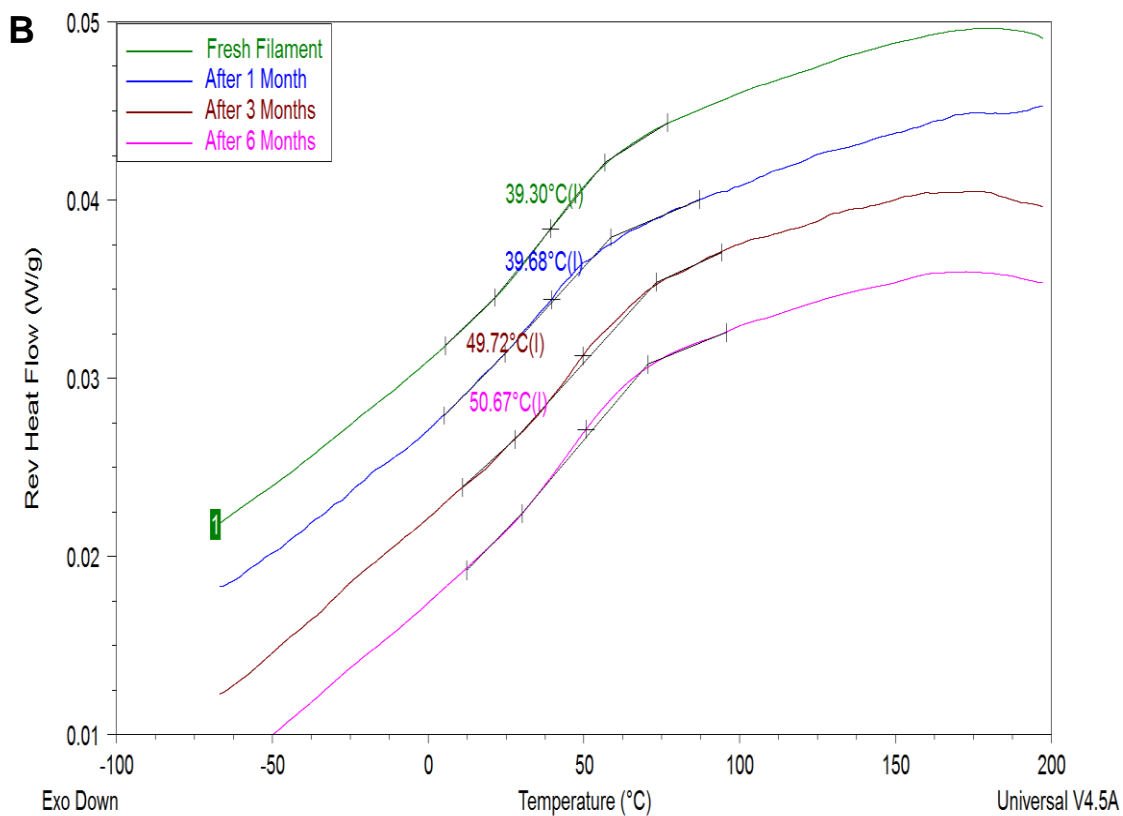
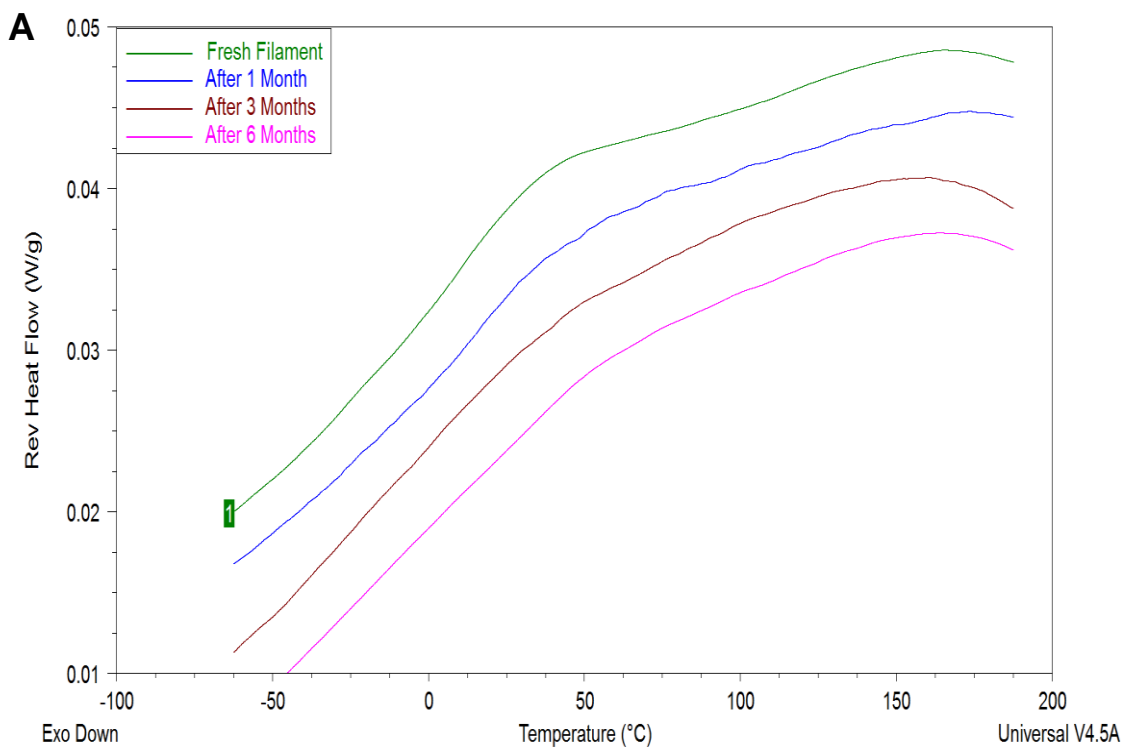


Figure 7.7. Reversible heat flow for the first (A) and second (B) MTDSC thermograph used to investigate the impact of storage at 5 °C without vacuum on the T_g of Eudragit L100-55-based filaments.

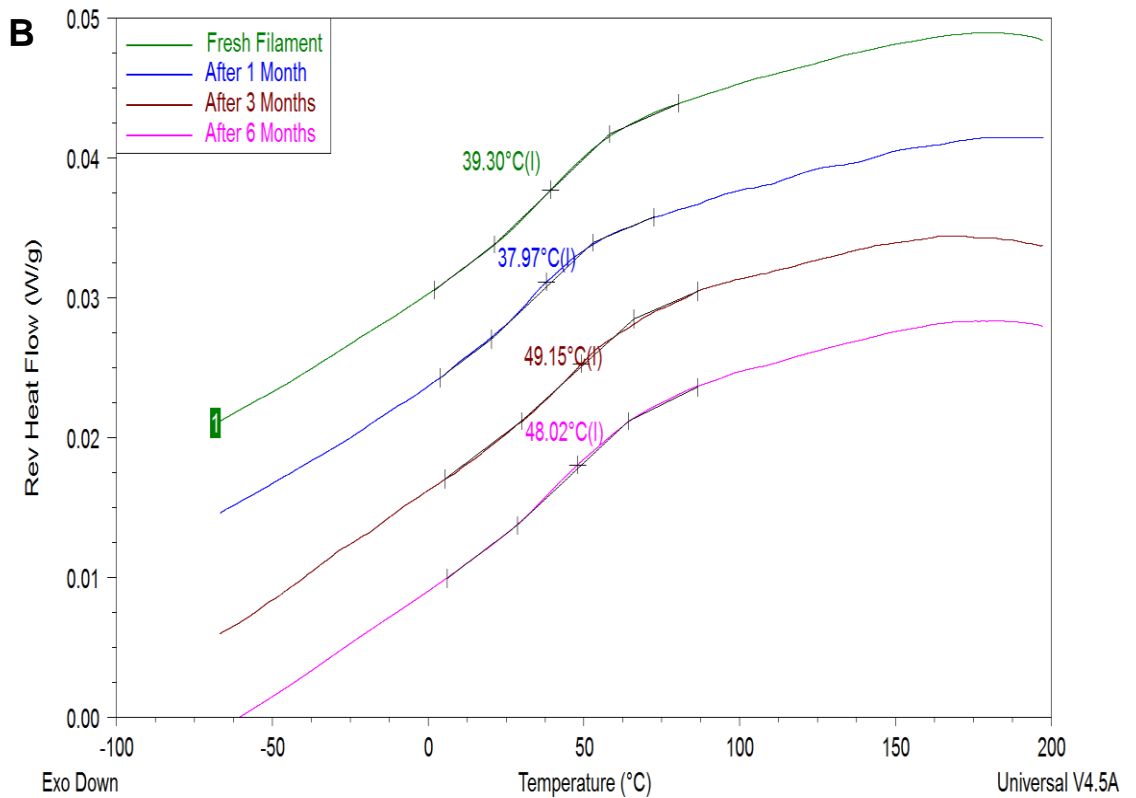
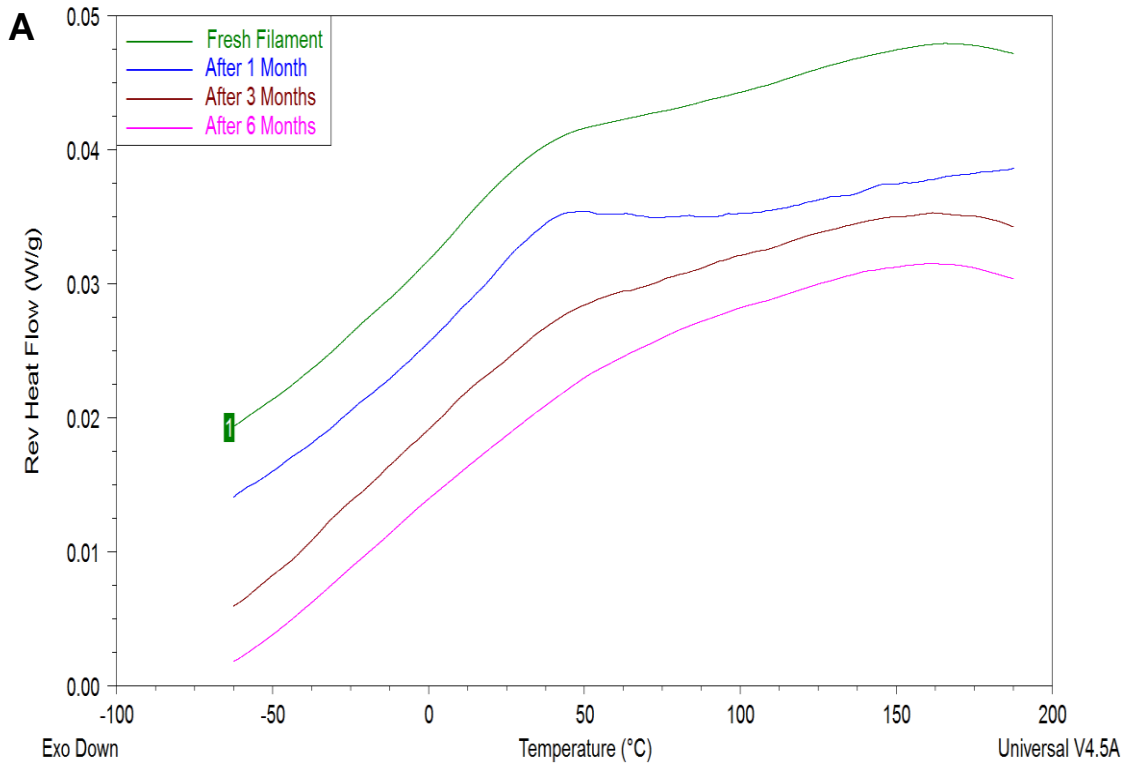


Figure 7.8. Reversible heat flow for the first (A) and second (B) MTDSC thermograph used to investigate the impact of storage at 5 °C + vacuum on the T_g of Eudragit L100-55-based filaments.

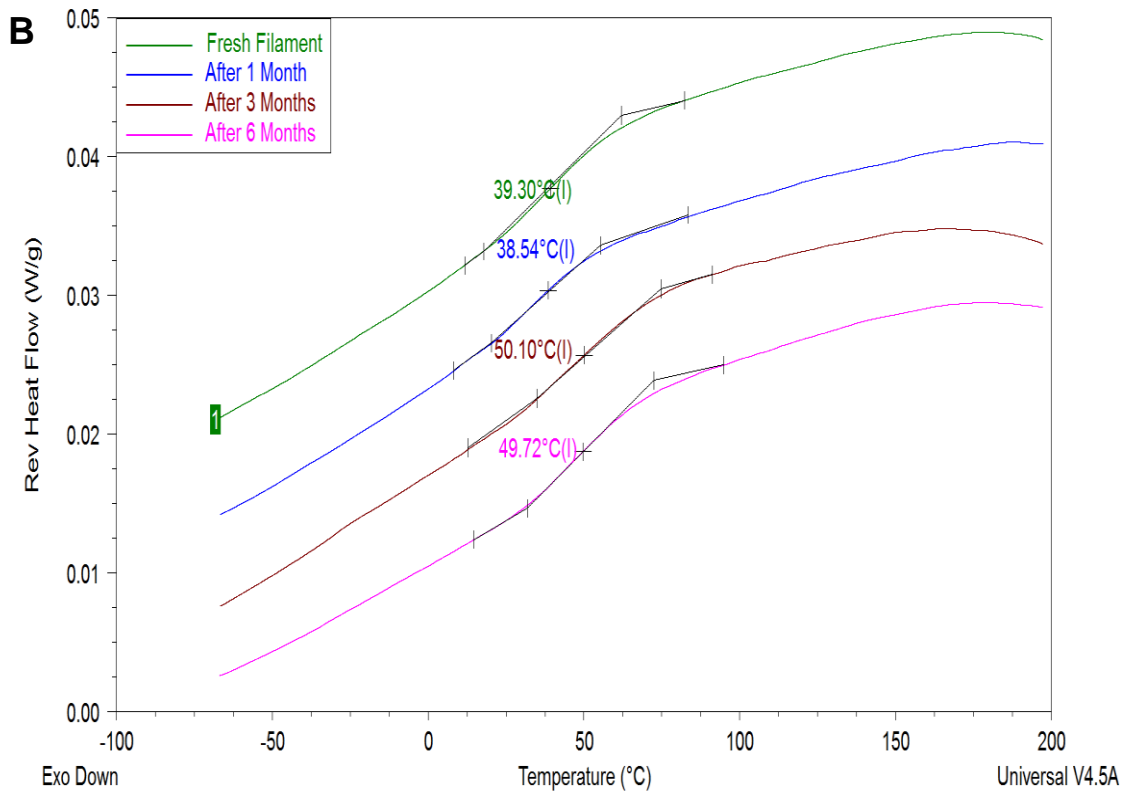
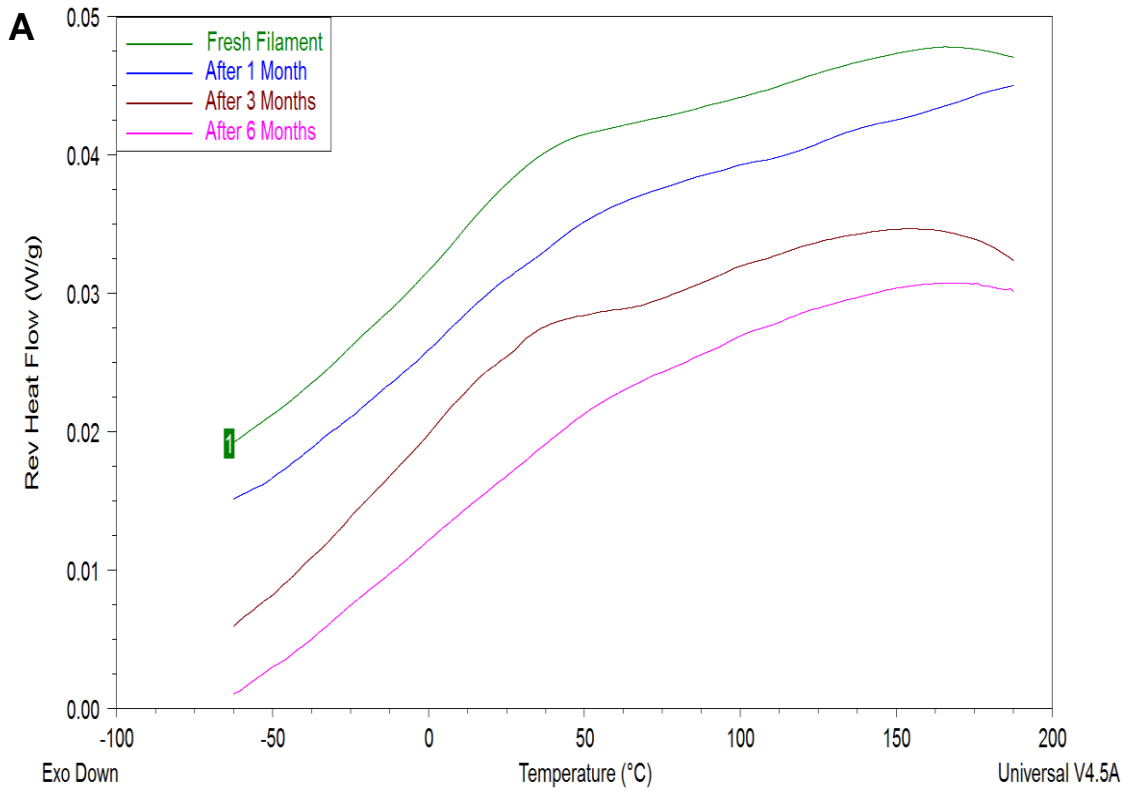


Figure 7.9. Reversible heat flow for the first (A) and second (B) MTDSC thermograph used to investigate the impact of storage at 30 °C and 65 %RH without vacuum on the Tg of Eudragit L100-55-based filaments.

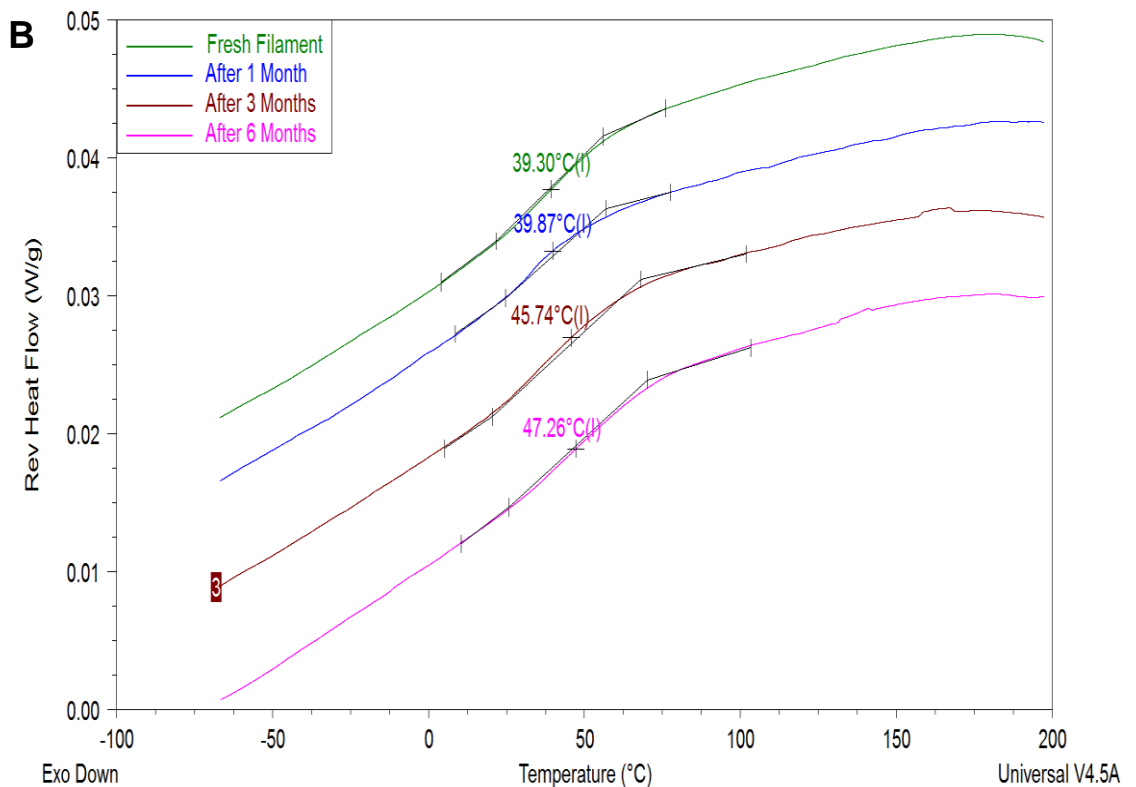
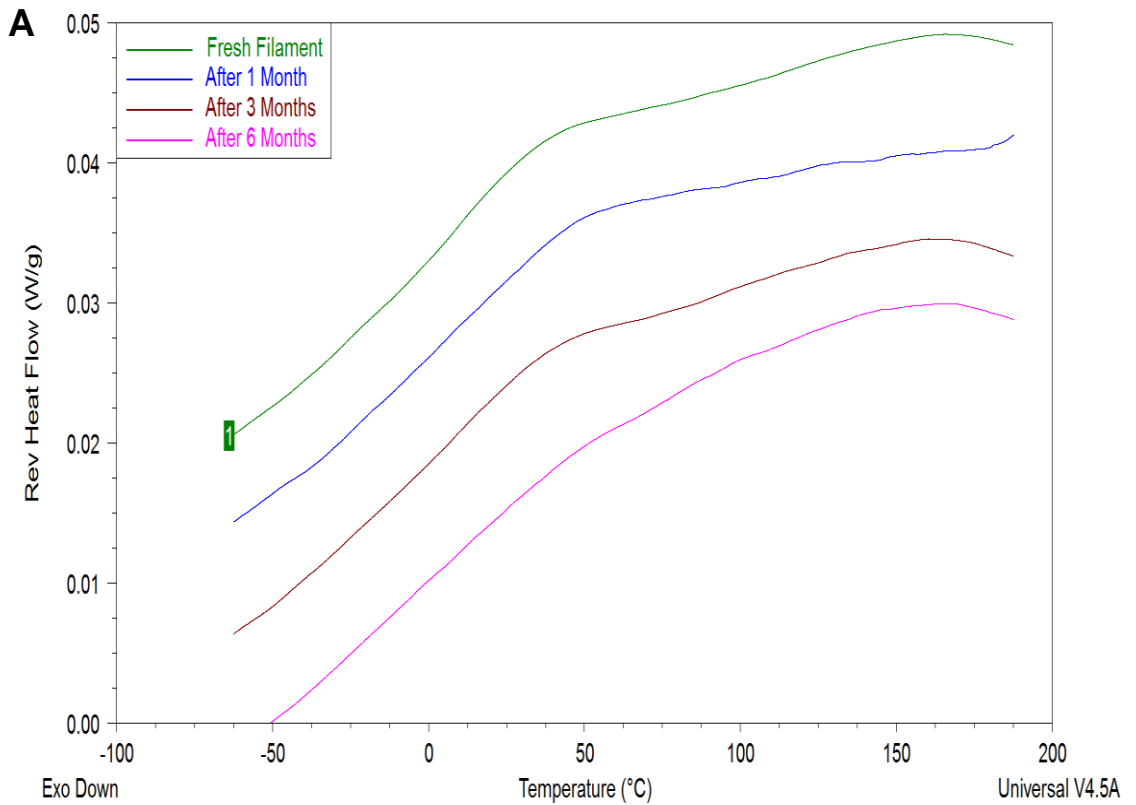


Figure 7.10. Reversible heat flow for the first (A) and second (B) MTDSC thermograph used to investigate the impact of storage at 30 °C and 65 %RH + vacuum on the Tg of Eudragit L100-55-based filaments.

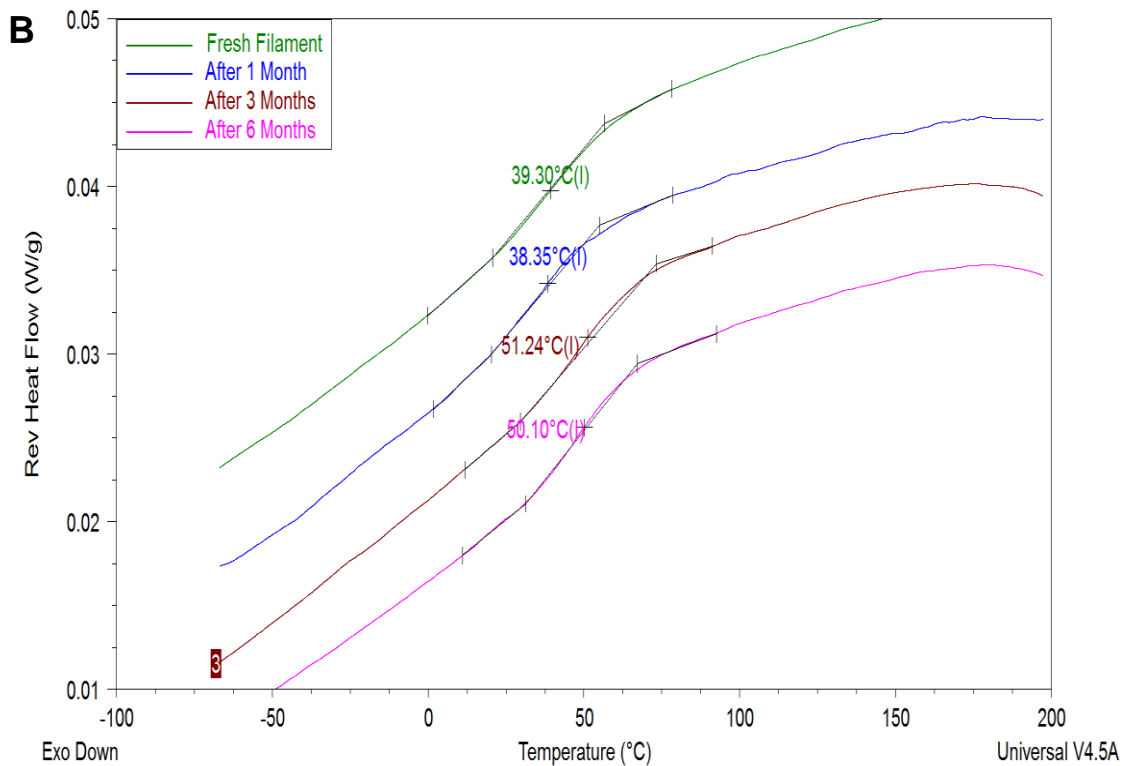
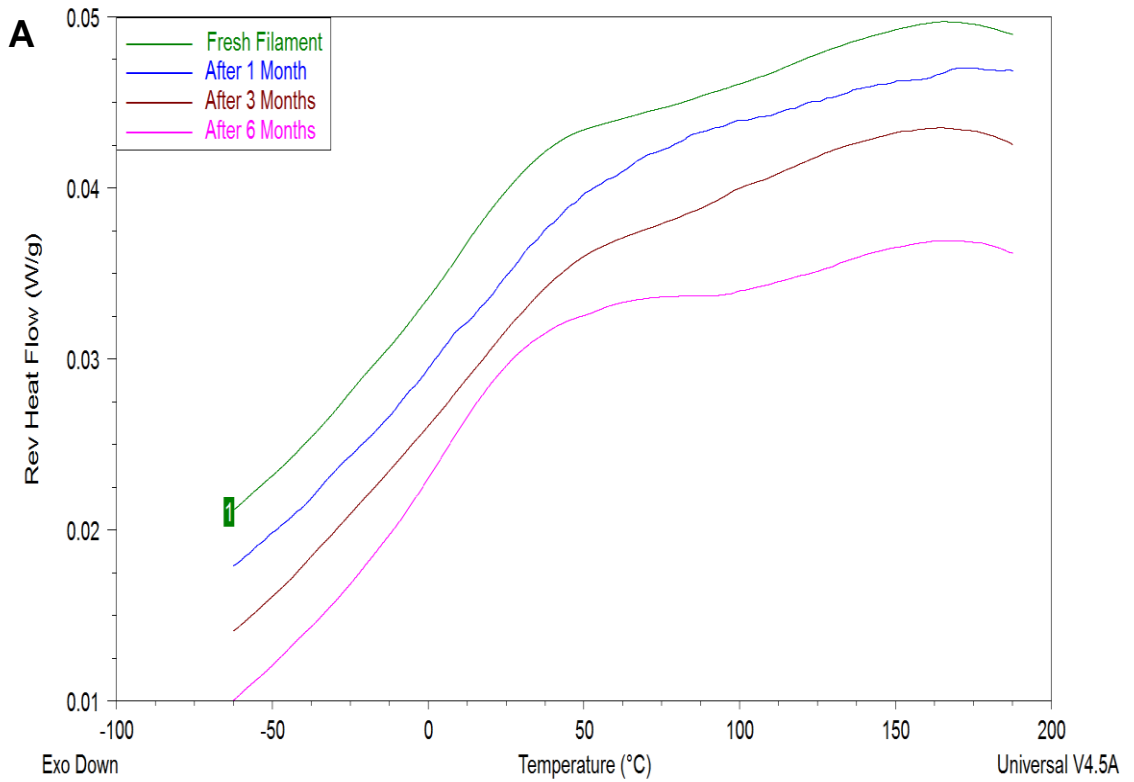


Figure 7.11. Reversible heat flow for the first (A) and second (B) MTDSC thermograph used to investigate the impact of storage at 40 °C and 75 %RH without vacuum on the Tg of Eudragit L100-55-based filaments.

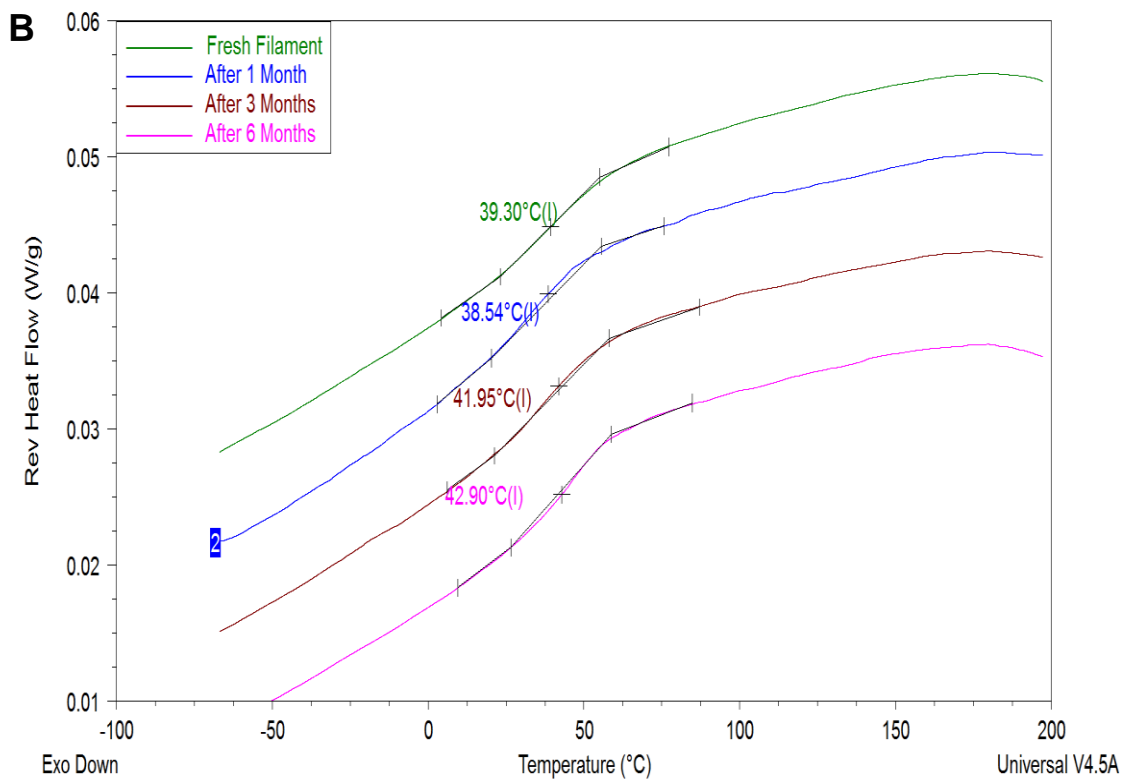
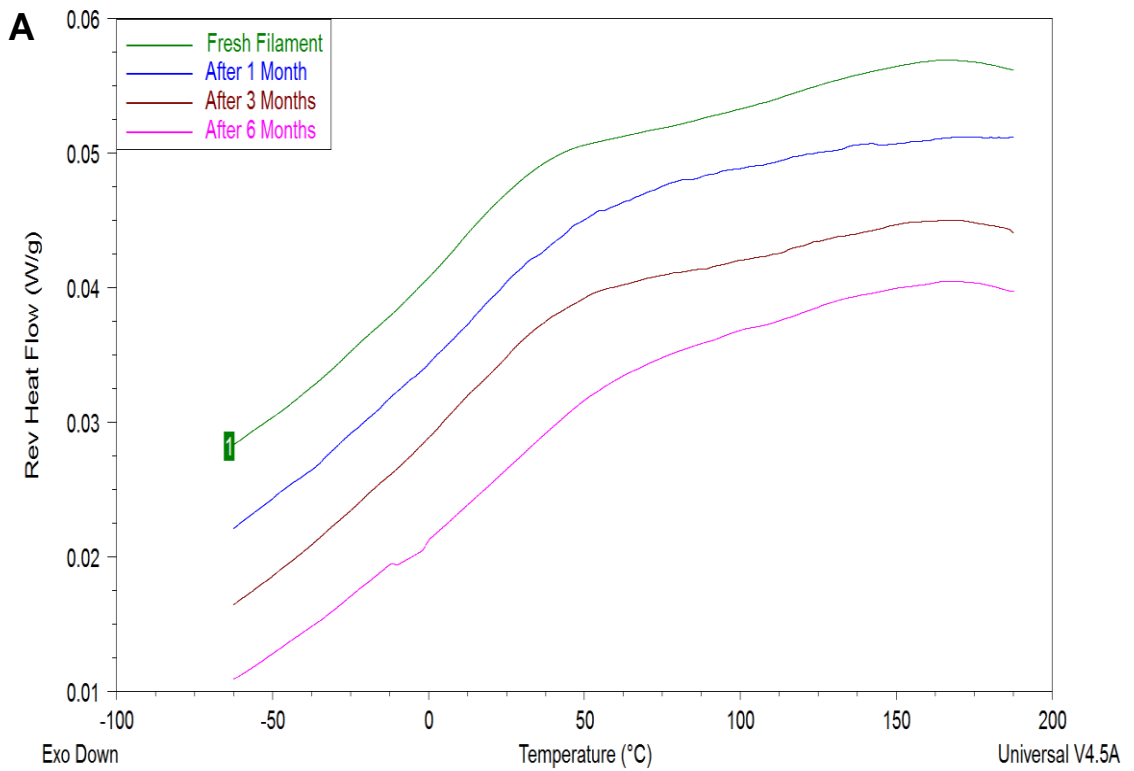


Figure 7.12. Reversible heat flow for the first (A) and second (B) MTDSC thermograph used to investigate the impact of storage at 40 °C and 75 %RH + vacuum on the Tg of Eudragit L100-55-based filaments.

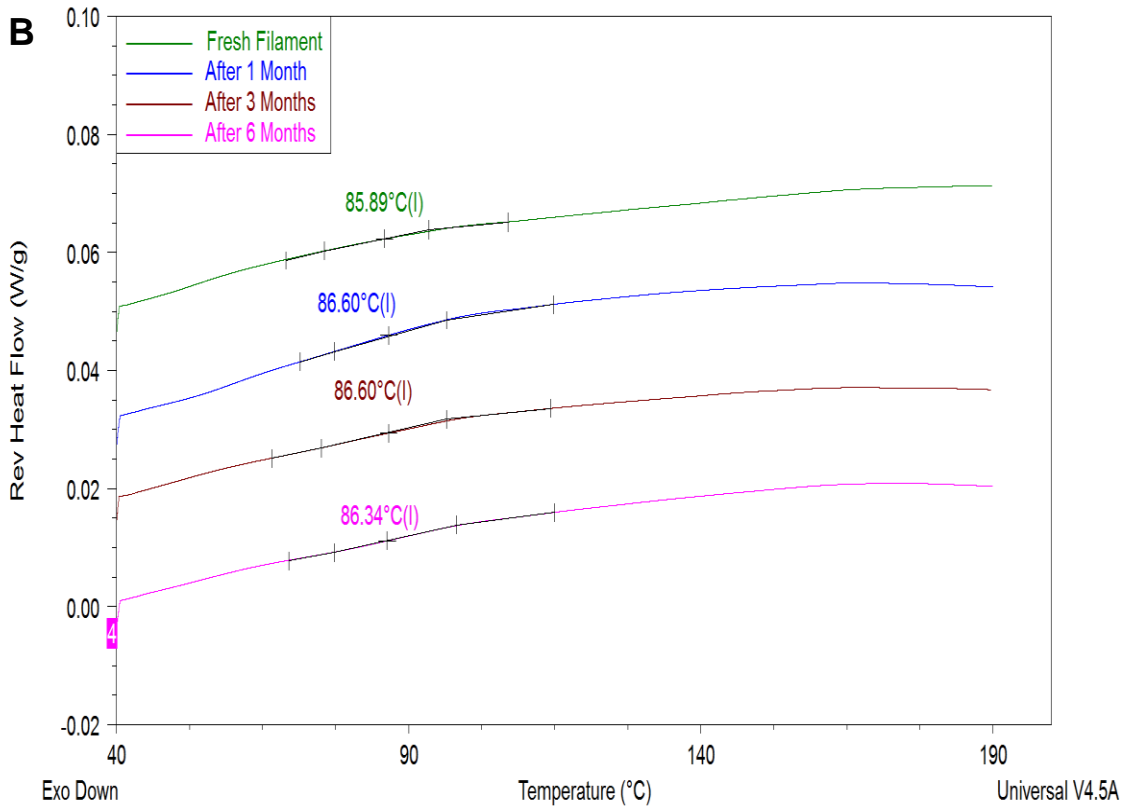
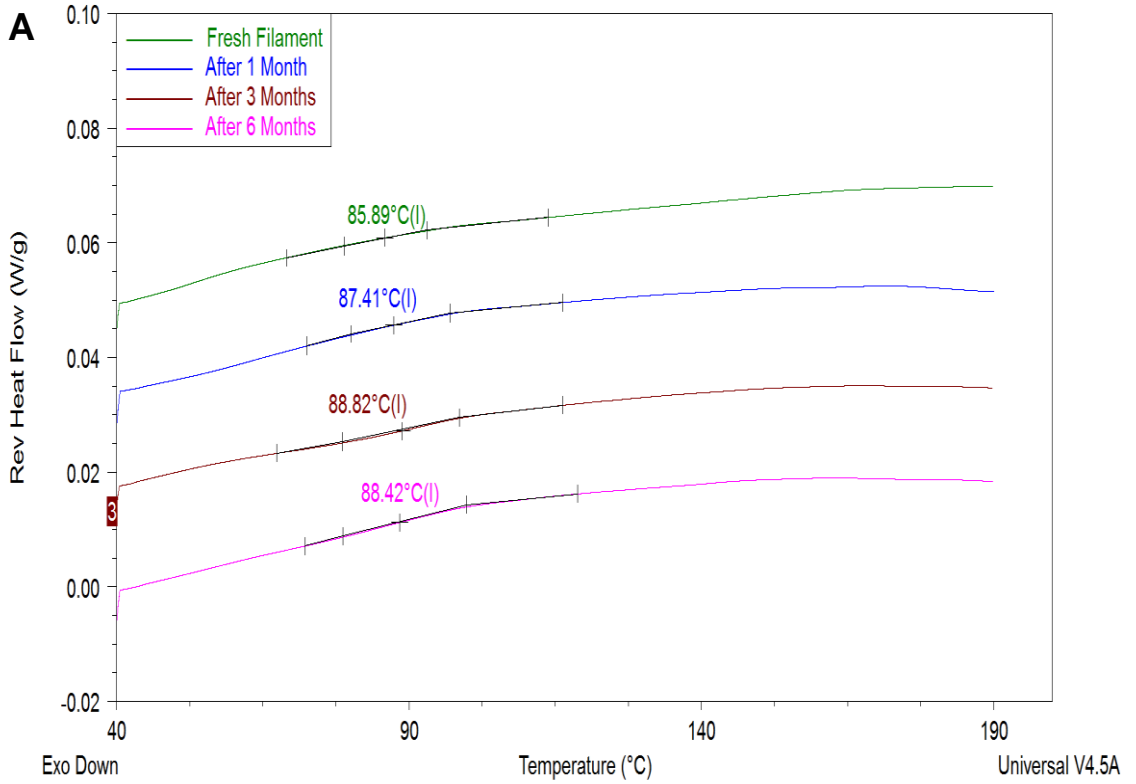


Figure 7.13. Reversible heat flow for the MTDSC thermograph used to investigate the impact of storage at 5 °C without vacuum (A) or with vacuum (B) on the T_g of Eudragit S100-based filaments.

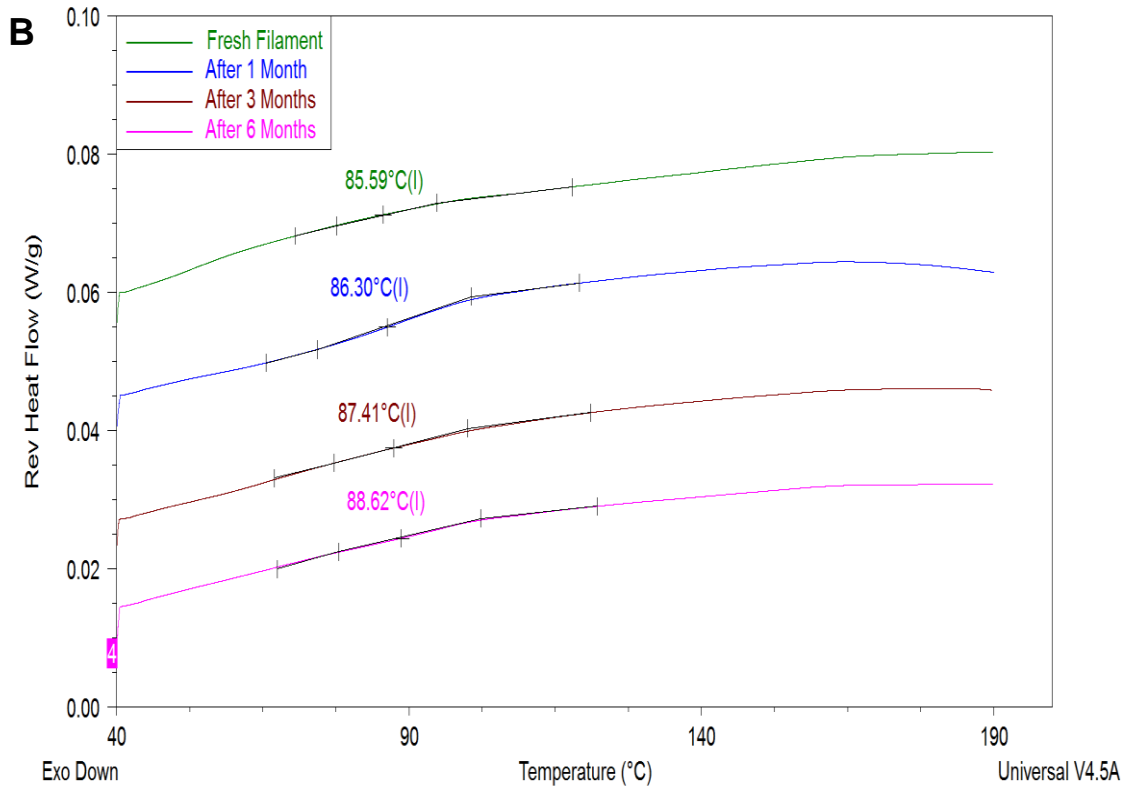
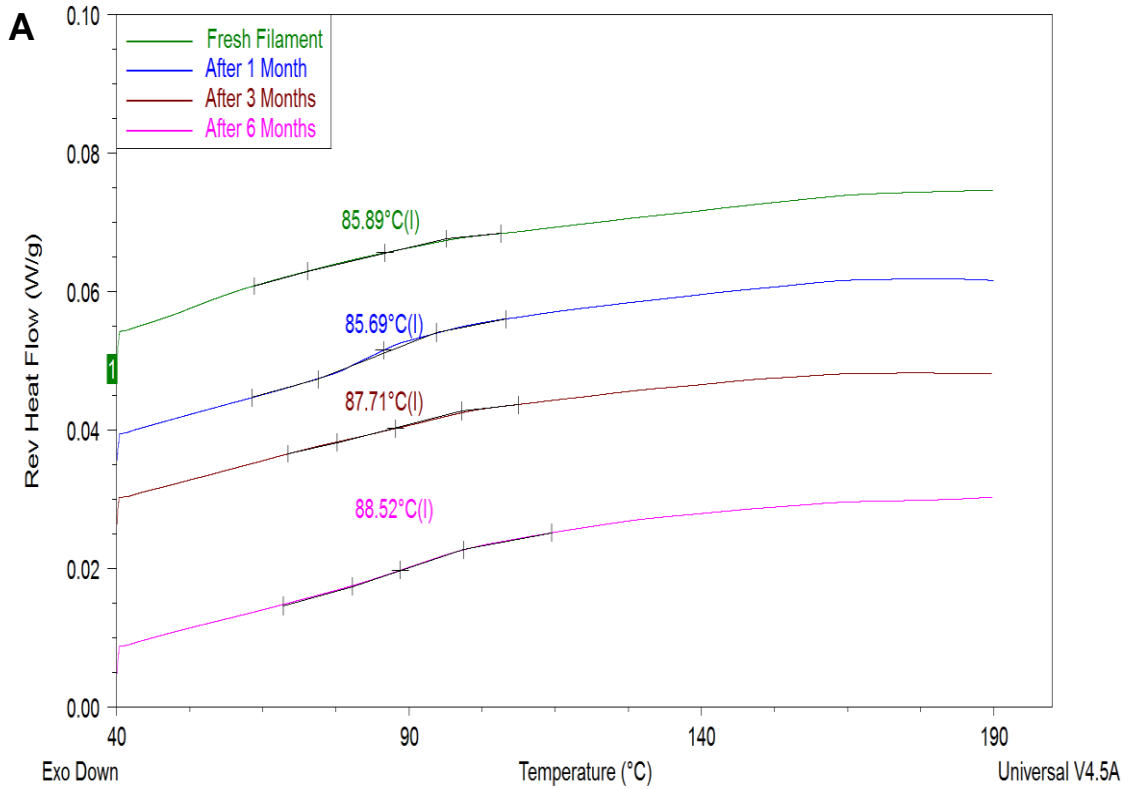


Figure 7.14. Reversible heat flow for the MTDSC thermograph used to investigate the impact of storage at 30 °C and 65 %RH without vacuum (A) or with vacuum (B) on the T_g of Eudragit S100-based filaments.

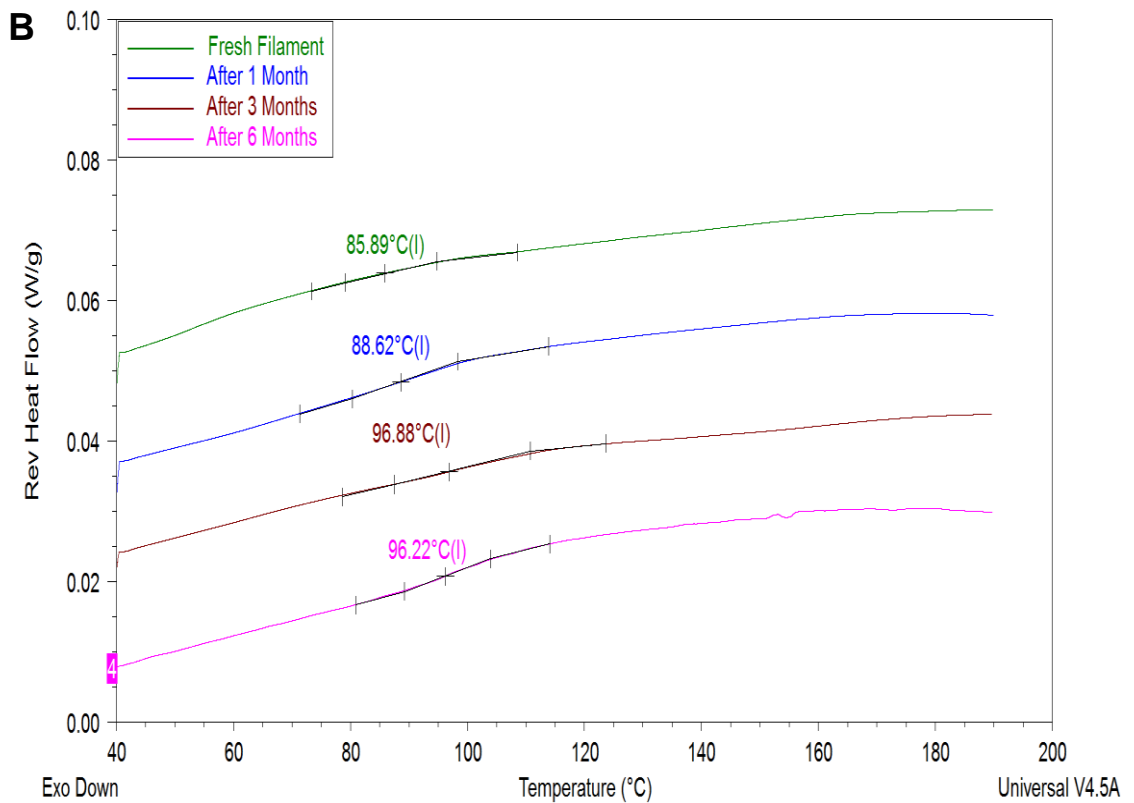
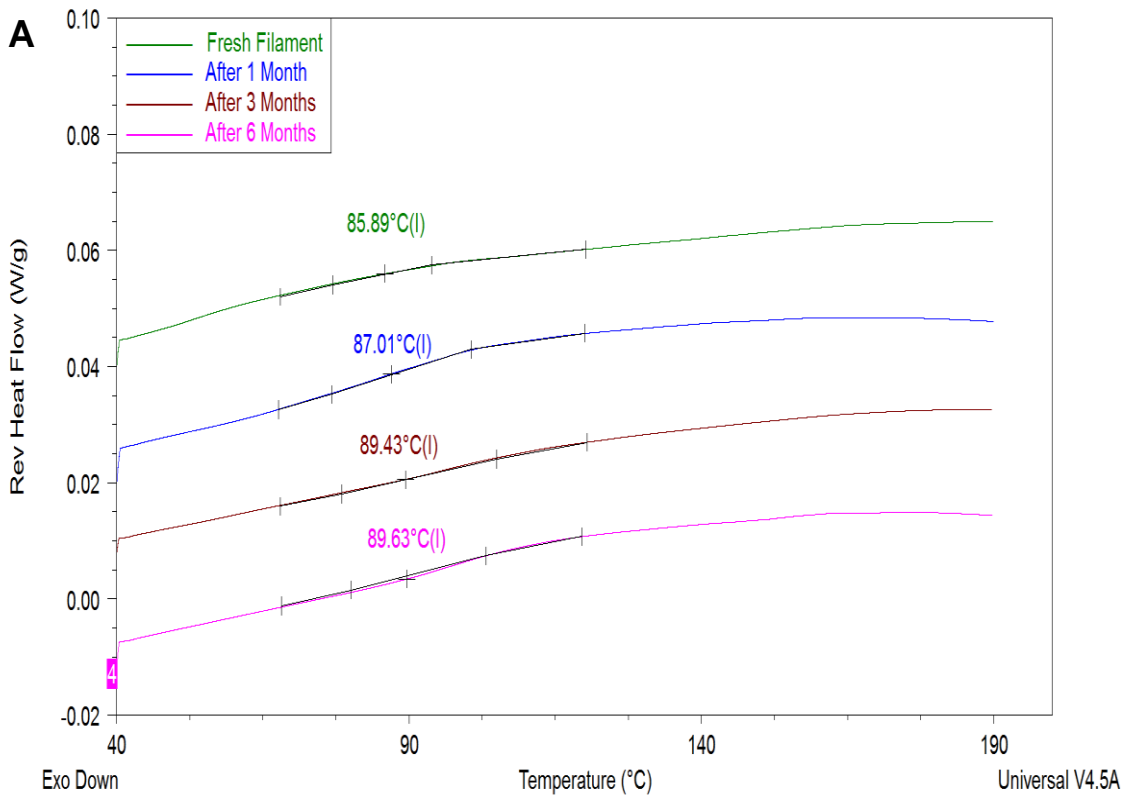


Figure 7.15. Reversible heat flow for the MTDSC thermograph used to investigate the impact of storage at 40 °C and 75 %RH without vacuum (A) or with vacuum (B) on the T_g of Eudragit S100-based filaments.

References

- A, G., Ren, L., Zhou, Z., Lu, D. & Wang, S. 2013. Design and evaluation of biodegradable enteric microcapsules of amifostine for oral delivery. *International Journal of Pharmaceutics*, 453, 441-447.
- Abrahamsson, B., Alpsten, M., Jonsson, U. E., Lundberg, P. J., Sandberg, A., Sundgren, M., Svenheden, A. & Tölli, J. 1996. Gastro-intestinal transit of a multiple-unit formulation (metoprolol CR/ZOK) and a non-disintegrating tablet with the emphasis on colon. *International Journal of Pharmaceutics*, 140, 229-235.
- Abu-Diak, O. A., Jones, D. S. & Andrews, G. P. 2011. An investigation into the dissolution properties of celecoxib melt extrudates: understanding the role of polymer type and concentration in stabilizing supersaturated drug concentrations. *Mol Pharm*, 8, 1362-71.
- Agrawal, A. M., Dudhedia, M. S., Patel, A. D. & Raikes, M. S. 2013. Characterization and performance assessment of solid dispersions prepared by hot melt extrusion and spray drying process. *Int J Pharm*, 457, 71-81.
- Agrawal, A. M., Dudhedia, M. S. & Zimny, E. 2016. Hot Melt Extrusion: Development of an Amorphous Solid Dispersion for an Insoluble Drug from Mini-scale to Clinical Scale. *AAPS PharmSciTech*, 17, 133-47.
- Ahmed, S. U. & Naini, V. 2010. Generic Oral Controlled Release Product Development: Formulation and Process Considerations. In: WEN, H. & PARK, K. (eds.) *Oral Controlled Release Formulation Design and Drug Delivery*. New Jersey: John Wiley & Sons, Inc.
- Ahuja, N., Katare, O. P. & Singh, B. 2007. Studies on dissolution enhancement and mathematical modeling of drug release of a poorly water-soluble drug using water-soluble carriers. *European Journal of Pharmaceutics and Biopharmaceutics*, 65, 26-38.
- Akhgari, A. & Tavakol, A. 2016. Prediction of Optimum Combination of Eudragit RS/Eudragit RL/Ethyl Cellulose Polymeric Free Films Based on Experimental Design for Using as a Coating System for Sustained Release Theophylline Pellets. *Adv Pharm Bull*, 6, 219-25.
- Al-Metwali, B. & Mulla, H. 2017. Personalised dosing of medicines for children. *J Pharm Pharmacol*, 69, 514-524.
- Alhnan, M. A., Cosi, D., Murdan, S. & Basit, A. W. 2010. Inhibiting the gastric burst release of drugs from enteric microparticles: the influence of drug molecular mass and solubility. *J Pharm Sci*, 99, 4576-83.
- Alhnan, M. A., Okwuosa, T. C., Sadia, M., Wan, K.-W., Ahmed, W. & Arafat, B. 2016. Emergence of 3D Printed Dosage Forms: Opportunities and Challenges. *Pharm Res*, 33, 1817-1832.

- Allen, T. M., Hansen, C., Martin, F., Redemann, C. & Yau-Young, A. 1991. Liposomes containing synthetic lipid derivatives of poly(ethylene glycol) show prolonged circulation half-lives in vivo. *Biochim Biophys Acta*, 1066, 29-36.
- Alomari, M., Mohamed, F. H., Basit, A. W. & Gaisford, S. 2014. Personalised dosing: Printing a dose of one's own medicine. *Int J Pharm*, 494, 568-577.
- Amaral, M. H., Lobo, J. M. & Ferreira, D. C. 2001. Effect of hydroxypropyl methylcellulose and hydrogenated castor oil on naproxen release from sustained-release tablets. *AAPS PharmSciTech*, 2, E6.
- An Nguyen, C., Niamien Konan-Kouakou, Y., Allémann, E., Doelker, E., Quintanar, D., Fessi, H. & Gurny, R. 2006. *Preparation of surfactant-free nanoparticles of methacrylic acid copolymers used for film coating*.
- Anatomy&Physiology. 2013. *Gigestive System: The Alimentary Canal and Accessory Gigestive Organs* [Online]. Available: <http://anatomyandphysiology.com/digestive-system-overview/> [Accessed 29/01 2018].
- Anatomy&Physiology. 2014. *Digestive System: Histology of the Alimentary Canal* [Online]. Available: <http://anatomyandphysiology.com/digestive-system-histology-alimentary-canal/> [Accessed 29/01 2018].
- Ando, M., Ito, R., Ozeki, Y., Nakayama, Y. & Nabeshima, T. 2007. Evaluation of a novel sugar coating method for moisture protective tablets. *Int J Pharm*, 336, 319-28.
- Andrews, G. P., AbuDiak, O. A. & Jones, D. S. 2010. Physicochemical characterization of hot melt extruded bicalutamide-polyvinylpyrrolidone solid dispersions. *J Pharm Sci*, 99, 1322-35.
- Andrews, G. P., Jones, D. S., Diak, O. A., McCoy, C. P., Watts, A. B. & McGinity, J. W. 2008. The manufacture and characterisation of hot-melt extruded enteric tablets. *European Journal of Pharmaceutics and Biopharmaceutics*, 69, 264-273.
- Aprecia. 2014. *Zipdose® technology* [Online]. Available: <https://aprecia.com/zipdose-platform/zipdose-technology.php> [Accessed 12/3/2015].
- Armstrong, N. A., James, K. C. & Pugh, W. K. 1984. Drug migration into soft gelatin capsule shells and its effect on in-vitro availability. *J Pharm Pharmacol*, 36, 361-5.
- Asada, M., Takahashi, H., Okamoto, H., Tanino, H. & Danjo, K. 2004. Theophylline particle design using chitosan by the spray drying. *International Journal of Pharmaceutics*, 270, 167-174.
- Ashour, E. A., Majumdar, S., Alsheteli, A., Alshehri, S., Alsulays, B., Feng, X., Gryczke, A., Kolter, K., Langley, N. & Repka, M. A. 2016. Hot melt extrusion as an approach to improve

- solubility, permeability and oral absorption of a psychoactive natural product, piperine. *J Pharm Pharmacol*, 68, 989-98.
- ATCC. 2016. Caco-2 [Online]. Available: https://www.lgcstandards-atcc.org/products/all/HTB-37.aspx?geo_country=gb#specifications [Accessed 24/04 2018].
- Aungst, B. J. 2012. Absorption enhancers: applications and advances. *Aaps j*, 14, 10-8.
- Baik, M.-Y., Kim, K.-J., Cheon, K.-C., Ha, Y.-C. & Kim, W.-S. 1997. Recrystallization Kinetics and Glass Transition of Rice Starch Gel System. *Journal of Agricultural and Food Chemistry*, 45, 4242-4248.
- Banerjee, R., Tyagi, P., Li, S. & Huang, L. 2004. Anisamide-targeted stealth liposomes: a potent carrier for targeting doxorubicin to human prostate cancer cells. *Int J Cancer*, 112, 693-700.
- Bayat, A., Dorkoosh, F. A., Dehpour, A. R., Moezi, L., Larijani, B., Junginger, H. E. & Rafiee-Tehrani, M. 2008. Nanoparticles of quaternized chitosan derivatives as a carrier for colon delivery of insulin: Ex vivo and in vivo studies. *International Journal of Pharmaceutics*, 356, 259-266.
- Bechgaard, H. & Nielsen, G. H. 1978. Controlled-Release Multiple-Units and Single-Unit Doses a Literature Review. *Drug Development and Industrial Pharmacy*, 4, 53-67.
- Bendas, E. R. & Abdelbary, A. A. 2014. Instantaneous enteric nano-encapsulation of omeprazole: Pharmaceutical and pharmacological evaluation. *International Journal of Pharmaceutics*, 468, 97-104.
- Bennett, R. C., Keen, J. M., Bi, Y. V., Porter, S., Durig, T. & McGinity, J. W. 2015. Investigation of the interactions of enteric and hydrophilic polymers to enhance dissolution of griseofulvin following hot melt extrusion processing. *J Pharm Pharmacol*, 67, 918-38.
- Beutler, E. 1969. Drug-induced hemolytic anemia. *Pharmacol Rev*, 21, 73-103.
- Bhatt, H., Naik, B. & Dharamsi, A. 2014. Solubility Enhancement of Budesonide and Statistical Optimization of Coating Variables for Targeted Drug Delivery. *Journal of Pharmaceutics*, 2014, 13.
- Blaesi, A. H. & Saka, N. 2015. Melt-processed polymeric cellular dosage forms for immediate drug release. *Journal of Controlled Release*, 220, 397-405.
- Boehm, R. D., Daniels, J., Stafslie, S., Nasir, A., Lefebvre, J. & Narayan, R. J. 2015. Polyglycolic acid microneedles modified with inkjet-deposited antifungal coatings. *Biointerphases*, 10, 011004.
- Boetker, J., Water, J. J., Aho, J., Arnfast, L., Bohr, A. & Rantanen, J. 2016. Modifying release characteristics from 3D printed drug-eluting products. *Eur J Pharm Sci*.

- Boland, T., Xu, T., Damon, B. & Cui, X. 2006. Application of inkjet printing to tissue engineering. *Biotechnol J*, 1, 910-7.
- Bose, S. & Bogner, R. H. 2007. Solventless pharmaceutical coating processes: a review. *Pharm Dev Technol*, 12, 115-31.
- Brøndsted, H. & Kopeček, J. i. 1991. Hydrogels for site-specific oral drug delivery: synthesis and characterization. *Biomaterials*, 12, 584-592.
- Brown, D., Ford, J. L., Nunn, A. J. & Rowe, P. H. 2004. An assessment of dose-uniformity of samples delivered from paediatric oral droppers. *J Clin Pharm Ther*, 29, 521-529.
- Buanz, A. B., Saunders, M. H., Basit, A. W. & Gaisford, S. 2011. Preparation of personalized-dose salbutamol sulphate oral films with thermal ink-jet printing. *Pharm Res*, 28, 2386-92.
- Bumrah, G. S. & Sharma, R. M. 2016. Raman spectroscopy – Basic principle, instrumentation and selected applications for the characterization of drugs of abuse. *Egyptian Journal of Forensic Sciences*, 6, 209-215.
- CancerResearchUK. 2015a. *Dukes's Staging System* [Online]. Available: <http://about-cancer.cancerresearchuk.org/about-cancer/bowel-cancer/stages-grades/dukes-staging> [Accessed 19/03 2018].
- CancerResearchUK. 2015b. *Number Stages* [Online]. Available: <http://about-cancer.cancerresearchuk.org/about-cancer/bowel-cancer/stages-grades/number-staging> [Accessed 19/03 2018].
- CancerResearchUK. 2015c. *TNM Staging* [Online]. Available: <http://about-cancer.cancerresearchuk.org/about-cancer/bowel-cancer/stages-grades/tnm-staging> [Accessed 19/03 2018].
- Capsugel. 2012. *A New HPMC Capsule for Optimum Formulation of Pharmaceutical Dosage Forms* [Online]. Available: http://www.capsugel.com/media/library/WP-VcapsPlus_30270_FIN_10-8-12.pdf [Accessed 23/08/2017 2017].
- Capsulesupplies. 2018. *Capsule Sizes* [Online]. Available: <http://www.capsulesupplies.com/capsule-sizes/> [Accessed 01/03 2018].
- Cerea, M., Zheng, W., Young, C. R. & McGinity, J. W. 2004. A novel powder coating process for attaining taste masking and moisture protective films applied to tablets. *International Journal of Pharmaceutics*, 279, 127-139.
- Chai, X., Chai, H., Wang, X., Yang, J., Li, J., Zhao, Y., Cai, W., Tao, T. & Xiang, X. 2017. Fused Deposition Modeling (FDM) 3D Printed Tablets for Intra-gastric Floating Delivery of Domperidone. *Sci Rep*, 7, 2829.

- Chan, S. Y., Qi, S. & Craig, D. Q. 2015. An investigation into the influence of drug-polymer interactions on the miscibility, processability and structure of polyvinylpyrrolidone-based hot melt extrusion formulations. *Int J Pharm*, 496, 95-106.
- Chauhan, H., Hui-Gu, C. & Atef, E. 2013. Correlating the Behavior of Polymers in Solution as Precipitation Inhibitor to its Amorphous Stabilization Ability in Solid Dispersions. *Journal of Pharmaceutical Sciences*, 102, 1924-1935.
- Cheng, K. & Lim, L. Y. 2004. Insulin-Loaded Calcium Pectinate Nanoparticles: Effects of Pectin Molecular Weight and Formulation pH. *Drug Development and Industrial Pharmacy*, 30, 359-367.
- Chiou, W. L. & Riegelman, S. 1969. Preparation and Dissolution Characteristics of Several Fast-Release Solid Dispersions of Griseofulvin. *Journal of Pharmaceutical Sciences*, 58, 1505-1510.
- Chiu, M. H. & Prenner, E. J. 2011. Differential scanning calorimetry: An invaluable tool for a detailed thermodynamic characterization of macromolecules and their interactions. *Journal of Pharmacy and Bioallied Sciences*, 3, 39-59.
- Chung, P., Heller, J. A., Etemadi, M., Ottoson, P. E., Liu, J. A., Rand, L. & Roy, S. 2014. Rapid and low-cost prototyping of medical devices using 3D printed molds for liquid injection molding. *J Vis Exp*, e51745.
- Ciavarella, A. B., Khan, M. A., Gupta, A. & Faustino, P. J. 2016. Dose Uniformity of Scored and Unscored Tablets: Application of the FDA Tablet Scoring Guidance for Industry. *PDA J Pharm Sci Technol*, 70, 523-532.
- Clark, E. A., Alexander, M. R., Irvine, D. J., Roberts, C. J., Wallace, M. J., Sharpe, S., Yoo, J., Hague, R. J. M., Tuck, C. J. & Wildman, R. D. 2017. 3D printing of tablets using inkjet with UV photoinitiation. *Int J Pharm*, 529, 523-530.
- Cole, E. T., Cadé, D. & Benameur, H. 2008. Challenges and opportunities in the encapsulation of liquid and semi-solid formulations into capsules for oral administration. *Adv Drug Deliv Rev*, 60, 747-756.
- Coleman, N. J. & Craig, D. Q. M. 1996. Modulated temperature differential scanning calorimetry: A novel approach to pharmaceutical thermal analysis. *International Journal of Pharmaceutics*, 135, 13-29.
- Colorcon. 2018. *Controlled Release Alliance* [Online]. Available: <https://www.colorcon.com/products-formulation/all-products/polymers-controlled-release> [Accessed 23/04 2018].

- Convention, U. S. P. 2007. *The United States Pharmacopeia : USP30 : the National Formulary : NF25*, Rockville, Md, United States Pharmacopeial Convention Inc.
- Cooke, M. N., Fisher, J. P., Dean, D., Rimnac, C. & Mikos, A. G. 2003. Use of stereolithography to manufacture critical-sized 3D biodegradable scaffolds for bone ingrowth. *J Biomed Mater Res B Appl Biomater*, 64, 65-9.
- Corrêa, A. L., Senna, J. P. M. & de Sousa, Á. P. B. 2016. Effects of passage number on growth and productivity of hybridoma secreting MRSA anti-PBP2a monoclonal antibodies. *Cytotechnology*, 68, 419-427.
- Cynthia S. Randall, W. L. R., Pierre Ricou 2010. XRD in Pharmaceutical Analysis: A versatile Tool for Problem-Solving. *American Pharmaceutical Review*.
- Dasari, S. & Tchounwou, P. B. 2014. Cisplatin in cancer therapy: molecular mechanisms of action. *European journal of pharmacology*, 0, 364-378.
- Dave, V. S., Fahmy, R. M. & Hoag, S. W. 2015. Near-infrared spectroscopic analysis of the breaking force of extended-release matrix tablets prepared by roller-compaction: influence of plasticizer levels and sintering temperature. *Drug Dev Ind Pharm*, 41, 898-905.
- Davies, E. C., Green, C. F., Taylor, S., Williamson, P. R., Mottram, D. R. & Pirmohamed, M. 2009. Adverse Drug Reactions in Hospital In-Patients: A Prospective Analysis of 3695 Patient-Episodes. *PLoS ONE*, 4, e4439.
- De Jaeghere, W., De Beer, T., Van Bocxlaer, J., Remon, J. P. & Vervaet, C. 2015. Hot-melt extrusion of polyvinyl alcohol for oral immediate release applications. *International Journal of Pharmaceutics*, 492, 1-9.
- Deepthi, Y. & Murthy, T. E. G. 2015. Design and development and evaluation of candesartan cilexetil liquid filling formulations. *Int J Pharm Investig*, 5, 81-86.
- Dennison, S. R., Harris, F. & Phoenix, D. A. 2007. The interactions of aurein 1.2 with cancer cell membranes. *Biophys Chem*, 127, 78-83.
- Desai, P. M., Liew, C. V. & Heng, P. W. S. 2016. Review of Disintegrants and the Disintegration Phenomena. *J Pharm Sci*, 105, 2545-2555.
- Dombroski, C. E., Balsdon, M. E. & Froats, A. 2014. The use of a low cost 3D scanning and printing tool in the manufacture of custom-made foot orthoses: a preliminary study. *BMC Res Notes*, 7, 443.
- Dressman, J. B. & Lennernas, H. 2000. *Oral Drug Absorption : Prediction and Assessment*, Baton Rouge, UNITED STATES, CRC Press.

- DrugBank. 2017. *Acetylsalicylic acid* [Online]. Available: <https://www.drugbank.ca/drugs/DB00945> [Accessed 22/11 2017].
- Drugs.com. 2017. *Aspirin* [Online]. Available: <https://www.drugs.com/aspirin.html> [Accessed 22/11 2017].
- Drugs.com. 2018a. *Dipyridamole* [Online]. Available: <https://www.drugs.com/mtm/dipyridamole.html> [Accessed 03/04 2018].
- Drugs.com. 2018b. *Magnesium Silicate* [Online]. Available: <https://www.drugs.com/inactive/magnesium-silicate-122.html#ref1> [Accessed 03/04 2018].
- Drugs.com. 2018c. *Theophylline* [Online]. Available: <https://www.drugs.com/mtm/theophylline.html> [Accessed 3/04 2018].
- Dubos, R. J. 1939a. STUDIES ON A BACTERICIDAL AGENT EXTRACTED FROM A SOIL BACILLUS : I. PREPARATION OF THE AGENT. ITS ACTIVITY IN VITRO. *J Exp Med*, 70, 1-10.
- Dubos, R. J. 1939b. STUDIES ON A BACTERICIDAL AGENT EXTRACTED FROM A SOIL BACILLUS : II. PROTECTIVE EFFECT OF THE BACTERICIDAL AGENT AGAINST EXPERIMENTAL PNEUMOCOCCUS INFECTIONS IN MICE. *J Exp Med*, 70, 11-7.
- Dudek, P. 2013. FDM 3D Printing Technology in Manufacturing Composite Elements. *Archives of Metallurgy and Materials*.
- Dürr, U. H. N., Sudheendra, U. S. & Ramamoorthy, A. 2006. LL-37, the only human member of the cathelicidin family of antimicrobial peptides. *Biochimica et Biophysica Acta (BBA) - Biomembranes*, 1758, 1408-1425.
- Eichelbaum, M., Ingelman-Sundberg, M. & Evans, W. E. 2006. Pharmacogenomics and Individualized Drug Therapy. *Annual Review of Medicine*, 57, 119-137.
- El Aidy, S., van den Bogert, B. & Kleerebezem, M. 2015. The small intestine microbiota, nutritional modulation and relevance for health. *Curr Opin Biotechnol*, 32, 14-20.
- Elzayat, E. M., Abdel-Rahman, A. A., Ahmed, S. M., Alanazi, F. K., Habib, W. A., Abou-Auda, H. S. & Sakr, A. 2017. Formulation and pharmacokinetics of multi-layered matrix tablets: Biphasic delivery of diclofenac. *Saudi Pharm J*, 25, 688-695.
- Emami, J. & Kazemali, M. R. 2016. Design and in vitro evaluation of a novel controlled onset extended-release delivery system of metoprolol tartrate. *Res Pharm Sci*, 11, 81-92.
- Enright, E. F., Gahan, C. G. M., Joyce, S. A. & Griffin, B. T. 2016. The Impact of the Gut Microbiota on Drug Metabolism and Clinical Outcome. *The Yale Journal of Biology and Medicine*, 89, 375-382.

- Erramouspe, J. & Jarvi, E. J. 1997. Effect on dissolution from halving methylphenidate extended-release tablets. *Ann Pharmacother*, 31, 1123-6.
- Ervasti, T., Simonaho, S. P., Ketolainen, J., Forsberg, P., Fransson, M., Wikstrom, H., Folestad, S., Lakio, S., Tajarobi, P. & Abrahmsen-Alami, S. 2015. Continuous manufacturing of extended release tablets via powder mixing and direct compression. *Int J Pharm*, 495, 290-301.
- Evans, D. F., Pye, G., Bramley, R., Clark, A. G., Dyson, T. J. & Hardcastle, J. D. 1988. Measurement of gastrointestinal pH profiles in normal ambulant human subjects. *Gut*, 29, 1035-1041.
- Evonik. 2010. *Methacrylate Polymers for Oral Drug Delivery* [Online]. Available: <http://healthcare.evonik.com/product/health-care/en/products/pharmaceutical-excipients/pages/default.aspx> [Accessed 23/08 2017].
- Evonik. 2018. *EUDRAGIT® Application Guidelines (12th edition)* [Online]. Available: http://otomed.co.kr/english/sub12_evonik_eng_04-02.php [Accessed 22/06 2018].
- Fadda, H. M. & Basit, A. W. 2005. Dissolution of pH responsive formulations in media resembling intestinal fluids: bicarbonate versus phosphate buffers. *Journal of Drug Delivery Science and Technology*, 15, 273-279.
- Faiz, O., Blackburn, S. & Moffat, D. 2011. *Anatomy at a Glance*, Hoboken, UNITED KINGDOM, John Wiley & Sons, Incorporated.
- Fang, Y., Wang, G., Zhang, R., Liu, Z., Liu, Z., Wu, X. & Cao, D. 2014. Eudragit L/HPMCAS blend enteric-coated lansoprazole pellets: enhanced drug stability and oral bioavailability. *AAPS PharmSciTech*, 15, 513-21.
- FDA. 1979. *SCOGS Database* [Online]. Available: <https://www.accessdata.fda.gov/scripts/fdcc/?set=SCOGS> [Accessed 03/04 2018].
- FDA. 2013. *Paving the Way to Personalized Medicine: FDA's Role in a New Era of Medical Product Development* [Online]. Available: <http://www.fda.gov/downloads/ScienceResearch/SpecialTopics/PersonalizedMedicine/UCM372421.pdf> [Accessed 20/04/2016 2016].
- FDA. 2017a. *CDER Researchers Explore the Promise and Potential of 3D Printed Pharmaceuticals* [Online]. Available: <https://www.fda.gov/Drugs/NewsEvents/ucm588136.htm> [Accessed 16/02 2018].
- FDA. 2017b. *Statement by FDA Commissioner Scott Gottlieb, M.D., on FDA ushering in new era of 3D printing of medical products; provides guidance to manufacturers of medical devices* [Online]. Available:

<https://www.fda.gov/NewsEvents/Newsroom/PressAnnouncements/ucm587547.htm>

[Accessed 16/02 2017].

FDA. 2018. *Emerging Technology Program* [Online]. Available:

<https://www.fda.gov/AboutFDA/CentersOffices/OfficeofMedicalProductsandTobacco/CDER/ucm523228.htm> [Accessed 16/02 2018].

Feng, J., Xu, L., Gao, R., Luo, Y. & Tang, X. 2012. Evaluation of polymer carriers with regard to the bioavailability enhancement of bifendate solid dispersions prepared by hot-melt extrusion. *Drug Dev Ind Pharm*, 38, 735-43.

Fenoglio-Preiser, C. M. & Ovid Technologies, I. 2008. *Gastrointestinal pathology an atlas and text*, Philadelphia, Philadelphia : Wolters Kluwer/Lippincott Williams & Wilkins.

Fini, A., Cavallari, C., Ospitali, F. & Gonzalez-Rodriguez, M. L. 2011. Theophylline-loaded Compritol microspheres prepared by ultrasound-assisted atomization. *J Pharm Sci*, 100, 743-57.

Fitzpatrick, S., McCabe, J. F., Petts, C. R. & Booth, S. W. 2002. Effect of moisture on polyvinylpyrrolidone in accelerated stability testing. *International Journal of Pharmaceutics*, 246, 143-151.

Forbes. 2016. *FDA Approved 3D Printed Drug Available In The US* [Online]. Available:

<https://www.forbes.com/sites/jenniferhicks/2016/03/22/fda-approved-3d-printed-drug-available-in-the-us/#3e3d6d89666b> [Accessed 16/02 2018].

Formlabs. 2015. *Form 1+ high-resolution 3D printer* [Online]. Available:

<http://formlabs.com/products/form-1-plus/> [Accessed 12/3/2015].

Frejberg, A. 2013. *Confocal Raman Principle* [Online]. Available:

http://www.kemi.dtu.dk/english/research/physicalchemistry/raman_spektroskopi/raman_spectrometer [Accessed 30/03 2018].

Fridgeirdottir, G. A., Harris, R. J., Dryden, I. L., Fischer, P. M. & Roberts, C. J. 2018. Multiple Linear Regression Modeling To Predict the Stability of Polymer-Drug Solid Dispersions: Comparison of the Effects of Polymers and Manufacturing Methods on Solid Dispersion Stability. *Mol Pharm*, 15, 1826-1841.

Fujimori, J., Yonemochi, E., Fukuoka, E. & Terada, K. 2002. Application of eudragit RS to thermo-sensitive drug delivery systems. I. Thermo-sensitive drug release from acetaminophen matrix tablets consisting of eudragit RS/PEG 400 blend polymers. *Chem Pharm Bull (Tokyo)*, 50, 408-12.

Gabizon, A., Catane, R., Uziely, B., Kaufman, B., Safra, T., Cohen, R., Martin, F., Huang, A. & Barenholz, Y. 1994. Prolonged circulation time and enhanced accumulation in

- malignant exudates of doxorubicin encapsulated in polyethylene-glycol coated liposomes. *Cancer Res*, 54, 987-92.
- Gabizon, A. & Papahadjopoulos, D. 1988. Liposome formulations with prolonged circulation time in blood and enhanced uptake by tumors. *Proc Natl Acad Sci U S A*, 85, 6949-53.
- GBIResearch. 2012. *Oral drug delivery market report* [Online]. Available: http://www.contractpharma.com/issues/2012-06/view_features/oral-drug-delivery-market-report/ [Accessed 12/3/2015].
- Ginsburg, G. S. & Willard, H. F. 2009. Genomic and personalized medicine: foundations and applications. *Transl Res*, 154, 277-87.
- Giunchedi, P., Ltorre, M., Maggi, L., Conti, B. & Conte, U. 1995. Cellulose Acetate Trimellitate Microspheres Containing NSAIDS. *Drug Development and Industrial Pharmacy*, 21, 315-330.
- Goyanes, A., Buanz, A. B., Hatton, G. B., Gaisford, S. & Basit, A. W. 2015a. 3D printing of modified-release aminosalicylate (4-ASA and 5-ASA) tablets. *Eur J Pharm Biopharm*, 89, 157-62.
- Goyanes, A., Buanz, A. B. M., Basit, A. W. & Gaisford, S. 2014. Fused-filament 3D printing (3DP) for fabrication of tablets. *International Journal of Pharmaceutics*, 476, 88-92.
- Goyanes, A., Chang, H., Sedough, D., Hatton, G. B., Wang, J., Buanz, A., Gaisford, S. & Basit, A. W. 2015b. Fabrication of controlled-release budesonide tablets via desktop (FDM) 3D printing. *Int J Pharm*, 496, 414-20.
- Goyanes, A., Fina, F., Martorana, A., Sedough, D., Gaisford, S. & Basit, A. W. 2017. Development of modified release 3D printed tablets (printlets) with pharmaceutical excipients using additive manufacturing. *Int J Pharm*, 527, 21-30.
- Goyanes, A., Robles Martinez, P., Buanz, A., Basit, A. W. & Gaisford, S. 2015c. Effect of geometry on drug release from 3D printed tablets. *International Journal of Pharmaceutics*, 494, 657-663.
- Goyanes, A., Wang, J., Buanz, A., Martinez-Pacheco, R., Telford, R., Gaisford, S. & Basit, A. W. 2015d. 3D Printing of Medicines: Engineering Novel Oral Devices with Unique Design and Drug Release Characteristics. *Molecular Pharmaceutics*, 12, 4077-4084.
- Grießmann, K., Breitzkreutz, J., Schubert-Zsilavec, M. & Abdel-Tawab, M. 2007. Dosing accuracy of measuring devices provided with antibiotic oral suspensions. *Paediatr Perinat Drug Ther*, 8, 61-70.

- Griffin, E. N. & Niebergall, P. J. 1999. Release kinetics of a controlled-release multiparticulate dosage form prepared using a hot-melt fluid bed coating method. *Pharm Dev Technol*, 4, 117-24.
- Gross, B. C., Erkal, J. L., Lockwood, S. Y., Chen, C. & Spence, D. M. 2014. Evaluation of 3D Printing and Its Potential Impact on Biotechnology and the Chemical Sciences. *Anal Chem*, 86, 3240-3253.
- Guo, Y., Shalaev, E. & Smith, S. 2013. Physical stability of pharmaceutical formulations: solid-state characterization of amorphous dispersions. *TrAC Trends in Analytical Chemistry*, 49, 137-144.
- Guo, Z., Lu, M., Li, Y., Pang, H., Lin, L., Liu, X. & Wu, C. 2014. The utilization of drug-polymer interactions for improving the chemical stability of hot-melt extruded solid dispersions. *J Pharm Pharmacol*, 66, 285-96.
- Gupta, S. S., Meena, A., Parikh, T. & T.M. Serajuddin, A. 2014. *Investigation of thermal and viscoelastic properties of polymers relevant to hot melt extrusion - I: Polyvinylpyrrolidone and related polymers.*
- Gwinup, G., Elias, A. N. & Domurat, E. S. 1991. Insulin and C-peptide levels following oral administration of insulin in intestinal-enzyme protected capsules. *General Pharmacology: The Vascular System*, 22, 243-246.
- Haastrup, P. F., Gronlykke, T. & Jarbol, D. E. 2015. Enteric coating can lead to reduced antiplatelet effect of low-dose acetylsalicylic acid. *Basic Clin Pharmacol Toxicol*, 116, 212-5.
- Habib, W. A., Alanizi, A. S., Abdelhamid, M. M. & Alanizi, F. K. 2014. Accuracy of tablet splitting: Comparison study between hand splitting and tablet cutter. *Saudi Pharm J*, 22, 454-9.
- Hamman, J. 2010. *Chitosan Based Polyelectrolyte Complexes as Potential Carrier Materials in Drug Delivery Systems.*
- Hao, S., Wang, B., Wang, Y., Zhu, L., Wang, B. & Guo, T. 2013. Preparation of Eudragit L 100-55 enteric nanoparticles by a novel emulsion diffusion method. *Colloids and Surfaces B: Biointerfaces*, 108, 127-133.
- Hergel, J. & Lefebvre, S. 2014. Clean color: Improving multi-filament 3D prints. *Comput. Graph. Forum*, 33, 469-478.
- Higashi, K., Seo, A., Egami, K., Otsuka, N., Limwikrant, W., Yamamoto, K. & Moribe, K. 2016. Mechanistic insight into the dramatic improvement of probucol dissolution in neutral solutions by solid dispersion in Eudragit E PO with saccharin. *J Pharm Pharmacol*, 68, 655-64.

- Hill, S. W., Varker, A. S., Karlage, K. & Myrdal, P. B. 2009. Analysis of drug content and weight uniformity for half-tablets of 6 commonly split medications. *J Manag Care Pharm*, 15, 253-61.
- Hilton, A. K. & Deasy, P. B. 1993. Use of hydroxypropyl methylcellulose acetate succinate in an enteric polymer matrix to design controlled-release tablets of amoxicillin trihydrate. *J Pharm Sci*, 82, 737-43.
- Hom, F. S., Veresh, S. A. & Ebert, W. R. 1975. Soft gelatin capsules II: Oxygen permeability study of capsule shells. *J Pharm Sci*, 64, 851-7.
- Hong, M., Zhu, S., Jiang, Y., Tang, G. & Pei, Y. 2009. Efficient tumor targeting of hydroxycamptothecin loaded PEGylated niosomes modified with transferrin. *J Control Release*, 133, 96-102.
- Hoskin, D. W. & Ramamoorthy, A. 2008. Studies on anticancer activities of antimicrobial peptides. *Biochimica et Biophysica Acta (BBA) - Biomembranes*, 1778, 357-375.
- Huang, H., Wu, Z., Qi, X., Zhang, H., Chen, Q., Xing, J., Chen, H. & Rui, Y. 2013. Compression-coated tablets of glipizide using hydroxypropylcellulose for zero-order release: In vitro and in vivo evaluation. *International Journal of Pharmaceutics*, 446, 211-218.
- Huang, W., Zheng, Q., Sun, W., Xu, H. & Yang, X. 2007. Levofloxacin implants with predefined microstructure fabricated by three-dimensional printing technique. *Int J Pharm*, 339, 33-8.
- Huang, Y. & Dai, W.-G. 2014. Fundamental aspects of solid dispersion technology for poorly soluble drugs. *Acta Pharmaceutica Sinica B*, 4, 18-25.
- Hussein, A., El-Menshawe, S. & Afouna, M. 2012. Enhancement of the in-vitro dissolution and in-vivo oral bioavailability of silymarin from liquid-filled hard gelatin capsules of semisolid dispersion using Gelucire 44/14 as a carrier. *Die Pharmazie*, 67, 209-14.
- Huyghebaert, N., Vermeire, A. & Remon, J. P. 2004. Alternative method for enteric coating of HPMC capsules resulting in ready-to-use enteric-coated capsules. *Eur J Pharm Sci*, 21, 617-23.
- ICH. 2003. *Stability Testing of New Drug Substances and Product* [Online]. Available: http://www.ich.org/fileadmin/Public_Web_Site/ICH_Products/Guidelines/Quality/Q1A_R2/Step4/Q1A_R2_Guideline.pdf [Accessed 02/05 2018].
- ICH. 2006. *Impurities in New Drug Product* [Online]. Available: http://www.ich.org/fileadmin/Public_Web_Site/ICH_Products/Guidelines/Quality/Q3B_R2/Step4/Q3B_R2_Guideline.pdf [Accessed 28/11 2017].

- Ijaz, H., Qureshi, J., Danish, Z., Zaman, M., Abdel-Daim, M., Hanif, M., Waheed, I. & Mohammad, I. S. 2015. Formulation and in-vitro evaluation of floating bilayer tablet of lisinopril maleate and metoprolol tartrate. *Pak J Pharm Sci*, 28, 2019-25.
- Innerbody. 2018. *Digestive System* [Online]. Available: <http://www.innerbody.com/image/digeov.html> [Accessed 29/01 2018].
- Jannin, V. & Cuppok, Y. 2013. Hot-melt coating with lipid excipients. *International Journal of Pharmaceutics*, 457, 480-487.
- Jansen, P. J., Oren, P. L., Kemp, C. A., Maple, S. R. & Baertschi, S. W. 1998. Characterization of impurities formed by interaction of duloxetine HCl with enteric polymers hydroxypropyl methylcellulose acetate succinate and hydroxypropyl methylcellulose phthalate. *J Pharm Sci*, 87, 81-5.
- Jijun, F., Lishuang, X., Xiaoli, W., Shu, Z., Xiaoguang, T., Xingna, Z., Haibing, H. & Xing, T. 2011. Nimodipine (NM) tablets with high dissolution containing NM solid dispersions prepared by hot-melt extrusion. *Drug Dev Ind Pharm*, 37, 934-44.
- Johansson, J., Gudmundsson, G. H., Rottenberg, M. E., Berndt, K. D. & Agerberth, B. 1998. Conformation-dependent antibacterial activity of the naturally occurring human peptide LL-37. *J Biol Chem*, 273, 3718-24.
- Jones, D. S., Tian, Y., Li, S., Yu, T., Abu-Diak, O. A. & Andrews, G. P. 2016. The Use of Binary Polymeric Networks in Stabilizing Polyethylene Oxide Solid Dispersions. *Journal of Pharmaceutical Sciences*, 105, 3064-3072.
- Kablitz, C. D. & Urbanetz, N. A. 2007. Characterization of the film formation of the dry coating process. *European Journal of Pharmaceutics and Biopharmaceutics*, 67, 449-457.
- Kamaly, N., Yameen, B., Wu, J. & Farokhzad, O. C. 2016. Degradable Controlled-Release Polymers and Polymeric Nanoparticles: Mechanisms of Controlling Drug Release. *Chemical reviews*, 116, 2602-2663.
- Kapoor, V. K. 2016. *Colon Anatomy* [Online]. Available: <https://emedicine.medscape.com/article/1949039-overview#showall> [Accessed 16/03 2018].
- Katstra, W. E., Palazzolo, R. D., Rowe, C. W., Giritlioglu, B., Teung, P. & Cima, M. J. 2000. Oral dosage forms fabricated by Three Dimensional Printing™. *Journal of Controlled Release*, 66, 1-9.
- Khaled, S. A., Alexander, M. R., Wildman, R. D., Wallace, M. J., Sharpe, S., Yoo, J. & Roberts, C. J. 2018. 3D extrusion printing of high drug loading immediate release paracetamol tablets. *Int J Pharm*, 538, 223-230.

- Khaled, S. A., Burley, J. C., Alexander, M. R. & Roberts, C. J. 2014. Desktop 3D printing of controlled release pharmaceutical bilayer tablets. *Int J Pharm*, 461, 105-11.
- Khaled, S. A., Burley, J. C., Alexander, M. R., Yang, J. & Roberts, C. J. 2015a. 3D printing of five-in-one dose combination polypill with defined immediate and sustained release profiles. *Journal of Controlled Release*, 217, 308-314.
- Khaled, S. A., Burley, J. C., Alexander, M. R., Yang, J. & Roberts, C. J. 2015b. 3D printing of tablets containing multiple drugs with defined release profiles. *International Journal of Pharmaceutics*, 494, 643-650.
- Khan, S., Boateng, J. S., Mitchell, J. & Trivedi, V. 2015. Formulation, characterisation and stabilisation of buccal films for paediatric drug delivery of omeprazole. *AAPS PharmSciTech*, 16, 800-10.
- Khogaz, K. & Clas, S. D. 2000. Crystallization inhibition in solid dispersions of MK-0591 and poly(vinylpyrrolidone) polymers. *J Pharm Sci*, 89, 1325-34.
- Kim, D. S., Kim, D. W., Kim, K. S., Choi, J. S., Seo, Y. G., Youn, Y. S., Oh, K. T., Yong, C. S., Kim, J. O., Jin, S. G. & Choi, H.-G. 2016. Development of a novel l-sulpiride-loaded quaternary microcapsule: Effect of TPGS as an absorption enhancer on physicochemical characterization and oral bioavailability. *Colloids and Surfaces B: Biointerfaces*, 147, 250-257.
- Kim, J. E., Cho, H. J. & Kim, D. D. 2014. Budesonide/cyclodextrin complex-loaded lyophilized microparticles for intranasal application. *Drug Dev Ind Pharm*, 40, 743-8.
- Kjaergaard, M., Nørholm, A.-B., Hendus-Altenburger, R., Pedersen, S. F., Poulsen, F. M. & Kragelund, B. B. 2010. Temperature-dependent structural changes in intrinsically disordered proteins: Formation of α -helices or loss of polyproline II? *Protein Science : A Publication of the Protein Society*, 19, 1555-1564.
- Kneidl, B., Peller, M., Winter, G., Lindner, L. H. & Hossann, M. 2014. Thermosensitive liposomal drug delivery systems: state of the art review. *Int J Nanomedicine*, 9, 4387-98.
- Knopp, M. M., Nguyen, J. H., Becker, C., Francke, N. M., Jørgensen, E. B., Holm, P., Holm, R., Mu, H., Rades, T. & Langguth, P. 2016. Influence of polymer molecular weight on in vitro dissolution behavior and in vivo performance of celecoxib:PVP amorphous solid dispersions. *European Journal of Pharmaceutics and Biopharmaceutics*, 101, 145-151.
- Knopp, M. M., Olesen, N. E., Holm, P., Langguth, P., Holm, R. & Rades, T. 2015. Influence of Polymer Molecular Weight on Drug-polymer Solubility: A Comparison between Experimentally Determined Solubility in PVP and Prediction Derived from Solubility in Monomer. *Journal of Pharmaceutical Sciences*, 104, 2905-2912.

- Kong, J. L., Du, X. B., Fan, C. X., Xu, J. F. & Zheng, X. J. 2004. [Determination of primary structure of a novel peptide from mistletoe and its antitumor activity]. *Yao Xue Xue Bao*, 39, 813-7.
- Konno, H. & Taylor, L. S. 2006. Influence of different polymers on the crystallization tendency of molecularly dispersed amorphous felodipine. *J Pharm Sci*, 95, 2692-705.
- Kopoor, V. K. 2016. *Anatomy* [Online]. Medscape. Available: <https://emedicine.medscape.com/article/1899389-overview#showall> [Accessed 29/01 2018].
- Korkiatithaweechai, S., Umsarika, P., Praphairaksit, N. & Muangsin, N. 2011. Controlled release of diclofenac from matrix polymer of chitosan and oxidized konjac glucomannan. *Mar Drugs*, 9, 1649-63.
- Kotagale, N., Maniyar, M., Somvanshi, S., Umekar, M. & Patel, C. J. 2010. Eudragit-S, Eudragit-L and cellulose acetate phthalate coated polysaccharide tablets for colonic targeted delivery of azathioprine. *Pharm Dev Technol*, 15, 431-7.
- Koziolek, M., Grimm, M., Becker, D., Iordanov, V., Zou, H., Shimizu, J., Wanke, C., Garbacz, G. & Weitschies, W. 2015. Investigation of pH and Temperature Profiles in the GI Tract of Fasted Human Subjects Using the Intellicap® System. *Journal of Pharmaceutical Sciences*, 104, 2855-2863.
- Kyobula, M., Adedeji, A., Alexander, M. R., Saleh, E., Wildman, R., Ashcroft, I., Gellert, P. R. & Roberts, C. J. 2017. 3D inkjet printing of tablets exploiting bespoke complex geometries for controlled and tuneable drug release. *J Control Release*, 261, 207-215.
- LaboratoryInfo.com. 2015. *High Performance Liquid Chromatography (HPLC) : Principle, Types, Instrumentation and Applications* [Online]. Available: <https://laboratoryinfo.com/hplc/> [Accessed 03/04 2018].
- LaFontaine, J. S., Prasad, L. K., Brough, C., Miller, D. A., McGinity, J. W. & Williams, R. O., 3rd 2016. Thermal Processing of PVP- and HPMC-Based Amorphous Solid Dispersions. *AAPS PharmSciTech*, 17, 120-32.
- Lai, M. C., Hageman, M. J., Schowen, R. L., Borchardt, R. T., Laird, B. B. & Topp, E. M. 1999. Chemical stability of peptides in polymers. 2. Discriminating between solvent and plasticizing effects of water on peptide deamidation in poly(vinylpyrrolidone). *Journal of Pharmaceutical Sciences*, 88, 1081-1089.
- Lan, P. X., Lee, J. W., Seol, Y. J. & Cho, D. W. 2009. Development of 3D PPF/DEF scaffolds using micro-stereolithography and surface modification. *J Mater Sci Mater Med*, 20, 271-9.

- Lazarou, J., Pomeranz, B. H. & Corey, P. N. 1998. Incidence of adverse drug reactions in hospitalized patients: a meta-analysis of prospective studies. *Jama*, 279, 1200-5.
- Leapfrog. 2018. *Benefits of 3D Printing for Engineers with the BOIt Pro* [Online]. Available: <https://www.lpfrg.com/en/professionals/benefits-of-3d-printing-for-engineers/> [Accessed 11/06 2018].
- Lee, B. K., Yun, Y. H., Choi, J. S., Choi, Y. C., Kim, J. D. & Cho, Y. W. 2012. Fabrication of drug-loaded polymer microparticles with arbitrary geometries using a piezoelectric inkjet printing system. *Int J Pharm*, 427, 305-10.
- Leong, K. H., Looi, C. Y., Loong, X.-M., Cheah, F. K., Supratman, U., Litaudon, M., Mustafa, M. R. & Awang, K. 2016. Cycloart-24-ene-26-ol-3-one, a New Cycloartane Isolated from Leaves of *Aglaia exima* Triggers Tumour Necrosis Factor-Receptor 1-Mediated Caspase-Dependent Apoptosis in Colon Cancer Cell Line. *PLoS ONE*, 11, e0152652.
- Leuner, C. & Dressman, J. 2000. Improving drug solubility for oral delivery using solid dispersions. *European Journal of Pharmaceutics and Biopharmaceutics*, 50, 47-60.
- Li, L., Wang, L., Li, J., Jiang, S., Wang, Y., Zhang, X., Ding, J., Yu, T. & Mao, S. 2014. Insights into the mechanisms of chitosan-anionic polymers-based matrix tablets for extended drug release. *Int J Pharm*, 476, 253-65.
- Li, S., Tian, Y., Jones, D. S. & Andrews, G. P. 2016a. Optimising Drug Solubilisation in Amorphous Polymer Dispersions: Rational Selection of Hot-melt Extrusion Processing Parameters. *AAPS PharmSciTech*, 17, 200-13.
- Li, S., Yu, T., Tian, Y., McCoy, C. P., Jones, D. S. & Andrews, G. P. 2016b. Mechanochemical Synthesis of Pharmaceutical Cocrystal Suspensions via Hot Melt Extrusion: Feasibility Studies and Physicochemical Characterization. *Mol Pharm*, 13, 3054-68.
- Li, S. A., Lee, W. H. & Zhang, Y. 2012. Efficacy of OH-CATH30 and its analogs against drug-resistant bacteria in vitro and in mouse models. *Antimicrob Agents Chemother*, 56, 3309-17.
- Li, S. S., Gullbo, J., Lindholm, P., Larsson, R., Thunberg, E., Samuelsson, G., Bohlin, L. & Claesson, P. 2002. Ligatoxin B, a new cytotoxic protein with a novel helix-turn-helix DNA-binding domain from the mistletoe *Phoradendron liga*. *Biochem J*, 366, 405-13.
- Li, X., Ding, L., Xu, Y., Wang, Y. & Ping, Q. 2009. Targeted delivery of doxorubicin using stealth liposomes modified with transferrin. *Int J Pharm*, 373, 116-23.
- Li, X., Peng, H., Tian, B., Gou, J., Yao, Q., Tao, X., He, H., Zhang, Y., Tang, X. & Cai, C. 2015. Preparation and characterization of azithromycin – Aerosil 200 solid dispersions with enhanced physical stability. *International Journal of Pharmaceutics*, 486, 175-184.

- Libretexts. 2017. *Powder X-ray Diffraction* [Online]. Available: https://chem.libretexts.org/Core/Analytical_Chemistry/Instrumental_Analysis/Diffraction_on_Scattering_Techniques/Powder_X-ray_Diffraction [Accessed 12/12 2017].
- Limited, E. P. 2014. *Specifications For Empty Hard Gelatin Capsules* [Online]. Available: <http://www.erawat.com/technical-details.html> [Accessed 23/08/2017 2014].
- Lin, H., May, R. K., Evans, M. J., Zhong, S., Gladden, L. F., Shen, Y. & Zeitler, J. A. 2015. Impact of Processing Conditions on Inter-tablet Coating Thickness Variations Measured by Terahertz In-Line Sensing. *J Pharm Sci*, 104, 2513-22.
- Liska, R., Schuster, M., Inführ, R., Turecek, C., Fritscher, C., Seidl, B., Schmidt, V., Kuna, L., Haase, A., Varga, F., Lichtenegger, H. & Stampfl, J. 2007. Photopolymers for rapid prototyping. *Journal of Coatings Technology and Research*, 4, 505-510.
- Liu, F., Lizio, R., Meier, C., Petereit, H. U., Blakey, P. & Basit, A. W. 2009. A novel concept in enteric coating: a double-coating system providing rapid drug release in the proximal small intestine. *J Control Release*, 133, 119-24.
- Liu, F., Merchant, H. A., Kulkarni, R. P., Alkademi, M. & Basit, A. W. 2011. Evolution of a physiological pH6.8 bicarbonate buffer system: Application to the dissolution testing of enteric coated products. *European Journal of Pharmaceutics and Biopharmaceutics*, 78, 151-157.
- Liu, F., Moreno, P. & Basit, A. W. 2010. A novel double-coating approach for improved pH-triggered delivery to the ileo-colonic region of the gastrointestinal tract. *European Journal of Pharmaceutics and Biopharmaceutics*, 74, 311-315.
- Liu, S., Fan, L., Sun, J., Lao, X. & Zheng, H. 2017. Computational resources and tools for antimicrobial peptides. *J Pept Sci*, 23, 4-12.
- Liu, X., Lu, M., Guo, Z., Huang, L., Feng, X. & Wu, C. 2012. Improving the chemical stability of amorphous solid dispersion with cocrystal technique by hot melt extrusion. *Pharm Res*, 29, 806-17.
- Lorber, B., Hsiao, W. K., Hutchings, I. M. & Martin, K. R. 2014. Adult rat retinal ganglion cells and glia can be printed by piezoelectric inkjet printing. *Biofabrication*, 6, 015001.
- Lu, Y. & Chen, S. 2012. Projection printing of 3-dimensional tissue scaffolds. *Methods Mol Biol*, 868, 289-302.
- Lucas, R. A., Bowtle, W. J. & Ryden, R. 1987. Disposition of vancomycin in healthy volunteers from oral solution and semi-solid matrix capsules. *J Clin Pharm Ther*, 12, 27-31.
- Luo, Y., Zhu, J., Ma, Y. & Zhang, H. 2008. Dry coating, a novel coating technology for solid pharmaceutical dosage forms. *International Journal of Pharmaceutics*, 358, 16-22.

- Macchi, E., Zema, L., Maroni, A., Gazzaniga, A. & Felton, L. A. 2015. Enteric-coating of pulsatile-release HPC capsules prepared by injection molding. *European Journal of Pharmaceutical Sciences*, 70, 1-11.
- Mahadevan, V. 2017. Anatomy of the stomach. *Surgery (Oxford)*, 35, 608-611.
- Mahmah, O., Tabbakh, R., Kelly, A. & Paradkar, A. 2014. A comparative study of the effect of spray drying and hot-melt extrusion on the properties of amorphous solid dispersions containing felodipine. *J Pharm Pharmacol*, 66, 275-84.
- Maniruzzaman, M., Morgan, D. J., Mendham, A. P., Pang, J., Snowden, M. J. & Douroumis, D. 2013. Drug-polymer intermolecular interactions in hot-melt extruded solid dispersions. *International Journal of Pharmaceutics*, 443, 199-208.
- Mansing G. Patil, S. M. K. a. S. G. P. 2011. Formulation and evaluation of orally disintegrating tablet containing tramadol hydrochloride by mass extrusion technique. *Journal of Applied Pharmaceutical Science*, 178-181.
- Marketsandmarkets. 2013. *Drug delivery technology market* [Online]. Available: <http://www.marketsandmarkets.com/Market-Reports/drug-delivery-technologies-market-1085.html?gclid=CIXRuMT5osQCF6WtAodmiUAZg> [Accessed 12/3/2015].
- Markl, D., Zeitler, J. A., Rasch, C., Michaelsen, M. H., Müllertz, A., Rantanen, J., Rades, T. & Bøtker, J. 2017. Analysis of 3D Prints by X-ray Computed Microtomography and Terahertz Pulsed Imaging. *Pharm Res*, 34, 1037-1052.
- Maroni, A., Curto, M. D. D., Serraton, M., Zema, L., Foppoli, A., Gazzaniga, A. & Sangalli, M. E. 2009. Feasibility, stability and release performance of a time-dependent insulin delivery system intended for oral colon release. *European Journal of Pharmaceutics and Biopharmaceutics*, 72, 246-251.
- Maroni, A., Zema, L., Curto, M. D. D., Loreti, G. & Gazzaniga, A. 2010. Oral pulsatile delivery: Rationale and chronopharmaceutical formulations. *International Journal of Pharmaceutics*, 398, 1-8.
- Maroni, A., Zema, L., Del Curto, M. D., Foppoli, A. & Gazzaniga, A. 2012. Oral colon delivery of insulin with the aid of functional adjuvants. *Advanced Drug Delivery Reviews*, 64, 540-556.
- Mathiowitz, E., Jacob, J. S., Jong, Y. S., Carino, G. P., Chickering, D. E., Chaturvedi, P., Santos, C. A., Vijayaraghavan, K., Montgomery, S., Bassett, M. & Morrell, C. 1997. Biologically erodable microspheres as potential oral drug delivery systems. *Nature*, 386, 410-4.

- Matsumoto, T. & Zografi, G. 1999. Physical properties of solid molecular dispersions of indomethacin with poly(vinylpyrrolidone) and poly(vinylpyrrolidone-co-vinyl-acetate) in relation to indomethacin crystallization. *Pharm Res*, 16, 1722-8.
- Matuskova, Z., Anzenbacherova, E., Vecera, R., Tlaskalova-Hogenova, H., Kolar, M. & Anzenbacher, P. 2014. Administration of a probiotic can change drug pharmacokinetics: effect of *E. coli* Nissle 1917 on amidarone absorption in rats. *PLoS One*, 9, e87150.
- Mayersohn, M. & Gibaldi, M. 1966. New method of solid-state dispersion for increasing dissolution rates. *Journal of Pharmaceutical Sciences*, 55, 1323-1324.
- McDougall, D. A. J., Martin, J., Playford, E. G. & Green, B. 2016. Determination of a suitable voriconazole pharmacokinetic model for personalised dosing. *Journal of Pharmacokinetics and Pharmacodynamics*, 43, 165-177.
- McLean, S., Sheikh, A., Cresswell, K., Nurmatov, U., Mukherjee, M., Hemmi, A. & Pagliari, C. 2013. The Impact of Telehealthcare on the Quality and Safety of Care: A Systematic Overview. *Plos One*, 8.
- McMahon, S. R., Rimsza, M. E. & Bay, R. C. 1997. Parents can dose liquid medication accurately. *Pediatrics*, 100, 330-3.
- McMains, S. 2005. Layered manufacturing technologies. *Commun. ACM*, 48, 50-56.
- MedlinePlus. 2018. *Colonic Diseases* [Online]. Available: <https://medlineplus.gov/colonicdiseases.html> [Accessed 16/03 2018].
- Melchels, F. P., Feijen, J. & Grijpma, D. W. 2009. A poly(D,L-lactide) resin for the preparation of tissue engineering scaffolds by stereolithography. *Biomaterials*, 30, 3801-9.
- Melchels, F. P. W., Feijen, J. & Grijpma, D. W. 2010. A review on stereolithography and its applications in biomedical engineering. *Biomaterials*, 31, 6121-6130.
- Meléndez, P. A., Kane, K. M., Ashvar, C. S., Albrecht, M. & Smith, P. A. 2008. Thermal inkjet application in the preparation of oral dosage forms: Dispensing of prednisolone solutions and polymorphic characterization by solid-state spectroscopic techniques. *Journal of Pharmaceutical Sciences*, 97, 2619-2636.
- Melocchi, A., Parietti, F., Loreti, G., Maroni, A., Gazzaniga, A. & Zema, L. 2015. 3D printing by fused deposition modeling (FDM) of a swellable/erodible capsular device for oral pulsatile release of drugs. *J Drug Deliv Sci Technol*.
- Melocchi, A., Parietti, F., Maroni, A., Foppoli, A., Gazzaniga, A. & Zema, L. 2016. Hot-melt extruded filaments based on pharmaceutical grade polymers for 3D printing by fused deposition modeling. *Int J Pharm*, 509, 255-63.

- Microencapsulation.net. 2018. *Fluid Bed Coating* [Online]. Available: <http://microencapsulation.net/fluidBed.html> [Accessed 19/03 2018].
- Miller, K. D., Siegel, R. L., Lin, C. C., Mariotto, A. B., Kramer, J. L., Rowland, J. H., Stein, K. D., Alteri, R. & Jemal, A. 2016. Cancer treatment and survivorship statistics, 2016. *CA Cancer J Clin*, 66, 271-89.
- Ming-Thau, S., Huei-Lan, C., Ching-Cheng, K., Cheng-Hsiung, L. & Sokoloski, T. D. 1992. Dissolution of diclofenac sodium from matrix tablets. *International Journal of Pharmaceutics*, 85, 57-63.
- Mohammed, N. N., Majumdar, S., Singh, A., Deng, W., Murthy, N. S., Pinto, E., Tewari, D., Durig, T. & Repka, M. A. 2012. Klucel EF and ELF polymers for immediate-release oral dosage forms prepared by melt extrusion technology. *AAPS PharmSciTech*, 13, 1158-69.
- Mohomed, K. 2016. *Thermogravimetric Analysis (TGA): Theory and Applications* [Online]. Available: file:///ha-023/pers-H/00069750/Downloads/CA-2016-TGA.pdf [Accessed 12/12 2017].
- Mooney, S. D. 2015. Progress Towards the Integration of Pharmacogenomics in Practice. *Human genetics*, 134, 459-465.
- Moroz, E., Matoori, S. & Leroux, J.-C. 2016. Oral delivery of macromolecular drugs: Where we are after almost 100years of attempts. *Advanced Drug Delivery Reviews*, 101, 108-121.
- Muheem, A., Shakeel, F., Jahangir, M. A., Anwar, M., Mallick, N., Jain, G. K., Warsi, M. H. & Ahmad, F. J. 2016. A review on the strategies for oral delivery of proteins and peptides and their clinical perspectives. *Saudi Pharmaceutical Journal*, 24, 413-428.
- Mura, M., Wang, J., Zhou, Y., Pinna, M., Zvelindovsky, A. V., Dennison, S. R. & Phoenix, D. A. 2016. The effect of amidation on the behaviour of antimicrobial peptides. *European Biophysics Journal*, 45, 195-207.
- Nair, A. B., Gupta, R., Kumria, R., Jacob, S. & Attimarad, M. 2010. Formulation and evaluation of enteric coated tablets of proton pump inhibitor. *J Basic Clin Pharm*, 1, 215-21.
- Nair, R., Nyamweya, N., Gonen, S., Martinez-Miranda, L. J. & Hoag, S. W. 2001. Influence of various drugs on the glass transition temperature of poly(vinylpyrrolidone): a thermodynamic and spectroscopic investigation. *Int J Pharm*, 225, 83-96.
- Niemirowicz, K., Prokop, I., Wilczewska, A. Z., Wnorowska, U., Piktel, E., Watek, M., Savage, P. B. & Bucki, R. 2015. Magnetic nanoparticles enhance the anticancer activity of cathelicidin LL-37 peptide against colon cancer cells. *Int J Nanomedicine*, 10, 3843-53.

- Nojima, S., Tanaka, H., Rohadi, A. & Sasaki, S. 1998. The effect of glass transition temperature on the crystallization of ϵ -caprolactone-styrene diblock copolymers. *Polymer*, 39, 1727-1734.
- Nollenberger, K. & Albers, J. 2013. Poly(meth)acrylate-based coatings. *Int J Pharm*, 457, 461-9.
- Noviasky, J., Lo, V., Luft, D. D. & Saseen, J. 2006. Clinical inquiries. Which medications can be split without compromising efficacy and safety? *J Fam Pract*, 55, 707-8.
- O'Driscoll, N. H., Labovitiadi, O., Cushnie, T. P. T., Matthews, K. H., Mercer, D. K. & Lamb, A. J. 2013. Production and Evaluation of an Antimicrobial Peptide-Containing Wafer Formulation for Topical Application. *Current Microbiology*, 66, 271-278.
- Obara, S., Maruyama, N., Nishiyama, Y. & Kokubo, H. 1999. Dry coating: an innovative enteric coating method using a cellulose derivative. *European Journal of Pharmaceutics and Biopharmaceutics*, 47, 51-59.
- Ochi, M., Kimura, K., Kanda, A., Kawachi, T., Matsuda, A., Yuminoki, K. & Hashimoto, N. 2016. Physicochemical and Pharmacokinetic Characterization of Amorphous Solid Dispersion of Meloxicam with Enhanced Dissolution Property and Storage Stability. *AAPS PharmSciTech*, 17, 932-939.
- Ohmori, S., Ohno, Y., Makino, T. & Kashihara, T. 2004. Effect of moisture on impact toughness of sugar-coated tablets manufactured by the dusting method. *Chem Pharm Bull (Tokyo)*, 52, 329-34.
- Okwuosa, T. C., Pereira, B. C., Arafat, B., Cieszyńska, M., Isreb, A. & Alhnan, M. A. 2017. Fabricating a Shell-Core Delayed Release Tablet Using Dual FDM 3D Printing for Patient-Centred Therapy. *Pharmaceutical Research*, 34, 427-437.
- Okwuosa, T. C., Soares, C., Gollwitzer, V., Habashy, R., Timmins, P. & Alhnan, M. A. 2018. On demand manufacturing of patient-specific liquid capsules via co-ordinated 3D printing and liquid dispensing. *Eur J Pharm Sci*, 118, 134-143.
- Okwuosa, T. C., Stefaniak, D., Arafat, B., Isreb, A., Wan, K.-W. & Alhnan, M. A. 2016. A Lower Temperature FDM 3D Printing for the Manufacture of Patient-Specific Immediate Release Tablets. *Pharmaceutical Research*, 33, 2704-2712.
- Oliveira, P. R., Mendes, C., Klein, L., Sangoi Mda, S., Bernardi, L. S. & Silva, M. A. 2013. Formulation development and stability studies of norfloxacin extended-release matrix tablets. *Biomed Res Int*, 2013, 716736.
- Ozguney, I., Ozcan, I., Ertan, G. & Guneri, T. 2007. The preparation and evaluation of sustained release suppositories containing ketoprofen and Eudragit RL 100 by using factorial design. *Pharm Dev Technol*, 12, 97-107.

- Pachua, L. & Mazumder, B. 2013. Evaluation of Albizia procera gum as compression coating material for colonic delivery of budesonide. *Int J Biol Macromol*, 61, 333-9.
- Paliwal, S. R., Paliwal, R., Mishra, N., Mehta, A. & Vyas, S. P. 2010. A novel cancer targeting approach based on estrone anchored stealth liposome for site-specific breast cancer therapy. *Curr Cancer Drug Targets*, 10, 343-53.
- Pamudji, J. S., Mauludin, R. & Nurhabibah 2014. Influence of β -cyclodextrin on Cefixime Stability in Liquid Suspension Dosage Form. *Procedia Chem*, 13, 119-127.
- Paprskarova, A., Mozna, P., Oga, E. F., Elhissi, A. & Alhnan, M. A. 2016. Instrumentation of Flow-Through USP IV Dissolution Apparatus to Assess Poorly Soluble Basic Drug Products: a Technical Note. *AAPS PharmSciTech*, 17, 1261-6.
- Parikh, T., Gupta, S. S., Meena, A. & T.M. Serajuddin, A. 2014. *Investigation of thermal and viscoelastic properties of polymers relevant to hot melt extrusion - III: Polymethacrylates and polymethacrylic acid based polymers.*
- Park, K. 2015. 3D printing of 5-drug polypill. *J Control Release*, 217, 352.
- ParticleScience. 2011. *Hot Melt Extrusion* [Online]. Available: <http://www.particlesciences.com/news/technical-briefs/2011/hot-melt-extrusion.html> [Accessed 13/05 2016].
- Patel, M. M. 2011. Cutting-edge technologies in colon-targeted drug delivery systems. *Expert Opinion on Drug Delivery*, 8, 1247-1258.
- Pati, F., Shim, J.-H., Lee, J.-S. & Cho, D.-W. 2013. 3D printing of cell-laden constructs for heterogeneous tissue regeneration. *Manufacturing Letters*, 1, 49-53.
- Patil Arun, C. S., Khobragade Deepak, Umathe Sudhir, Avari Jasmine 2011. Evaluation of Hot Melt Coating as Taste Masking Tool. *International Research Journal of Pharmacy*.
- Patil, H., Tiwari, R. V. & Repka, M. A. 2016. Hot-Melt Extrusion: from Theory to Application in Pharmaceutical Formulation. *AAPS PharmSciTech*, 17, 20-42.
- Paudel, A., Worku, Z. A., Meeus, J., Guns, S. & Van den Mooter, G. 2013. Manufacturing of solid dispersions of poorly water soluble drugs by spray drying: Formulation and process considerations. *International Journal of Pharmaceutics*, 453, 253-284.
- Peate, I. 2018. Anatomy and physiology, 9. The gastrointestinal system. *British Journal of Healthcare Assistants*, 12, 110-115.
- Peek, B. T., Al-Achi, A. & Coombs, S. J. 2002. Accuracy of tablet splitting by elderly patients. *JAMA*, 288, 451-2.

- PharmTech. 2016. *FDA and the Emerging Technology of 3D Printing* [Online]. Available: <http://www.pharmtech.com/fda-and-emerging-technology-3d-printing> [Accessed 16/02 2018].
- Pietrzak, K., Isreb, A. & Alhnan, M. A. 2015. A flexible-dose dispenser for immediate and extended release 3D printed tablets. *Eur J Pharm Biopharm.*
- Piktel, E., Niemirowicz, K., Wnorowska, U., Wątek, M., Wollny, T., Głuszek, K., Góźdz, S., Levental, I. & Bucki, R. 2016. The Role of Cathelicidin LL-37 in Cancer Development. *Archivum Immunologiae et Therapiae Experimentalis*, 64, 33-46.
- Popov, V. K., Evseev, A. V., Ivanov, A. L., Roginski, V. V., Volozhin, A. I. & Howdle, S. M. 2004. Laser stereolithography and supercritical fluid processing for custom-designed implant fabrication. *J Mater Sci Mater Med*, 15, 123-8.
- Potter, C., Tian, Y., Walker, G., McCoy, C., Hornsby, P., Donnelly, C., Jones, D. S. & Andrews, G. P. 2015. Novel supercritical carbon dioxide impregnation technique for the production of amorphous solid drug dispersions: a comparison to hot melt extrusion. *Mol Pharm*, 12, 1377-90.
- Qi, X., Chen, H., Rui, Y., Yang, F., Ma, N. & Wu, Z. 2015. Floating tablets for controlled release of ofloxacin via compression coating of hydroxypropyl cellulose combined with effervescent agent. *Int J Pharm*, 489, 210-7.
- Qiao, M., Luo, Y., Zhang, L., Ma, Y., Stephenson, T. S. & Zhu, J. 2010a. Sustained release coating of tablets with Eudragit((R)) RS/RL using a novel electrostatic dry powder coating process. *Int J Pharm*, 399, 37-43.
- Qiao, M., Zhang, L., Ma, Y., Zhu, J. & Chow, K. 2010b. A novel electrostatic dry powder coating process for pharmaceutical dosage forms: immediate release coatings for tablets. *Eur J Pharm Biopharm*, 76, 304-10.
- Qiao, M., Zhang, L., Ma, Y., Zhu, J. & Xiao, W. 2013. A novel electrostatic dry coating process for enteric coating of tablets with Eudragit(R) L 100-55. *Eur J Pharm Biopharm*, 83, 293-300.
- Radwan, M. A., Abou El Ela Ael, S., Hassan, M. A. & El-Maraghy, D. A. 2015. Pharmacokinetics and analgesic effect of ketorolac floating delivery system. *Drug Deliv*, 22, 320-7.
- Raijada, D., Genina, N., Fors, D., Wisaeus, E., Peltonen, J., Rantanen, J. & Sandler, N. 2013. A step toward development of printable dosage forms for poorly soluble drugs. *J Pharm Sci*, 102, 3694-704.
- Raman, C. V. & Krishnan, K. S. 1928. A New Type of Secondary Radiation. *Nature*, 121, 501.

- Ramineneni, S. K., Cunningham, L. L., Dziubla, T. D. & Puleo, D. A. 2013. COMPETING PROPERTIES OF MUCOADHESIVE FILMS DESIGNED FOR LOCALIZED DELIVERY OF IMIQUIMOD. *Biomaterials science*, 1, 753-762.
- Räsänen, E., Rantanen, J., Jørgensen, A., Karjalainen, M., Paakkari, T. & Yliruusi, J. 2001. Novel identification of pseudopolymorphic changes of theophylline during wet granulation using near infrared spectroscopy. *Journal of Pharmaceutical Sciences*, 90, 389-396.
- Rattanakit, P., Moulton, S. E., Santiago, K. S., Liawruangrath, S. & Wallace, G. G. 2012. Extrusion printed polymer structures: a facile and versatile approach to tailored drug delivery platforms. *Int J Pharm*, 422, 254-63.
- Reiner, T., Carr, N., Radom, #237, M, r., #283, ch, Ond, #345, ej, #352, t'ava, Dachsbacher, C. & Miller, G. 2014. Dual-color mixing for fused deposition modeling printers. *Comput. Graph. Forum*, 33, 479-486.
- Reinus, J. F. & Simon, D. 2014. *Gastrointestinal Anatomy and Physiology : The Essentials*, Hoboken, UNITED KINGDOM, John Wiley & Sons, Incorporated.
- Ren, S. X., Cheng, A. S. L., To, K. F., Tong, J. H. M., Li, M. S., Shen, J., Wong, C. C. M., Zhang, L., Chan, R. L. Y., Wang, X. J., Ng, S. S. M., Chiu, L. C. M., Marquez, V. E., Gallo, R. L., Chan, F. K. L., Yu, J., Sung, J. J. Y., Wu, W. K. K. & Cho, C. H. 2012. Host Immune Defense Peptide LL-37 Activates Caspase-Independent Apoptosis and Suppresses Colon Cancer. *Cancer research*, 72, 6512-6523.
- Ren, S. X., Shen, J., Cheng, A. S. L., Lu, L., Chan, R. L. Y., Li, Z. J., Wang, X. J., Wong, C. C. M., Zhang, L., Ng, S. S. M., Chan, F. L., Chan, F. K. L., Yu, J., Sung, J. J. Y., Wu, W. K. K. & Cho, C. H. 2013. FK-16 Derived from the Anticancer Peptide LL-37 Induces Caspase-Independent Apoptosis and Autophagic Cell Death in Colon Cancer Cells. *PLoS ONE*, 8, e63641.
- Renukuntla, J., Vadlapudi, A. D., Patel, A., Boddu, S. H. S. & Mitra, A. K. 2013. Approaches for Enhancing Oral Bioavailability of Peptides and Proteins. *International journal of pharmaceutics*, 447, 75-93.
- Revision, U. S. P. C. C. o. 2007. *U.S. pharmacopeia & national formulary*, United States Pharmacopeial Convention, Inc.
- Ribeiro, Y. A., Caires, A. C. F., Boralle, N. & Ionashiro, M. 1996. Thermal decomposition of acetylsalicylic acid (aspirin). *Thermochimica Acta*, 279, 177-181.
- Romero-Torres, S., Perez-Ramos, J. D., Morris, K. R. & Grant, E. R. 2005. Raman spectroscopic measurement of tablet-to-tablet coating variability. *J Pharm Biomed Anal*, 38, 270-4.

- Roni, M. A., Kibria, G. & Jalil, R. 2009. Formulation and in vitro Evaluation of Alfuzosin Extended Release Tablets Using Directly Compressible Eudragit. *Indian J Pharm Sci*, 71, 252-8.
- Rosemond. 2015. *Medicine management for patients with trouble swallowing pills* [Online]. Available: <http://www.rosemontpharma.com/health-professionals> [Accessed 12/3/2015].
- Rosenzweig, D. H., Carelli, E., Steffen, T., Jarzem, P. & Haglund, L. 2015. 3D-Printed ABS and PLA Scaffolds for Cartilage and Nucleus Pulposus Tissue Regeneration. *Int J Mol Sci*, 16, 15118-35.
- Rowe, C. W., Katstra, W. E., Palazzolo, R. D., Giritlioglu, B., Teung, P. & Cima, M. J. 2000. Multimechanism oral dosage forms fabricated by three dimensional printing™. *Journal of Controlled Release*, 66, 11-17.
- Roy, H., Brahma, C. K., Nandi, S. & Parida, K. R. 2013. Formulation and design of sustained release matrix tablets of metformin hydrochloride: Influence of hypromellose and polyacrylate polymers. *Int J Appl Basic Med Res*, 3, 55-63.
- Rozek, T., Wegener, K. L., Bowie, J. H., Olver, I. N., Carver, J. A., Wallace, J. C. & Tyler, M. J. 2000. The antibiotic and anticancer active aurein peptides from the Australian Bell Frogs *Litoria aurea* and *Litoria raniformis* the solution structure of aurein 1.2. *Eur J Biochem*, 267, 5330-41.
- Rujivipat, S. & Bodmeier, R. 2010. Improved drug delivery to the lower intestinal tract with tablets compression-coated with enteric/nonenteric polymer powder blends. *European Journal of Pharmaceutics and Biopharmaceutics*, 76, 486-492.
- Ryu, G. S. & Lee, Y. J. 2012. Analysis of liquid medication dose errors made by patients and caregivers using alternative measuring devices. *J Manag Care Pharm*, 18, 439-45.
- Saal, W., Ross, A., Wyttenbach, N., Alsenz, J. & Kuentz, M. 2017. A Systematic Study of Molecular Interactions of Anionic Drugs with a Dimethylaminoethyl Methacrylate Copolymer Regarding Solubility Enhancement. *Mol Pharm*, 14, 1243-1250.
- Saal, W., Ross, A., Wyttenbach, N., Alsenz, J. & Kuentz, M. 2018. Unexpected Solubility Enhancement of Drug Bases in the Presence of a Dimethylaminoethyl Methacrylate Copolymer. *Mol Pharm*, 15, 186-192.
- Sadia, M., Arafat, B., Ahmed, W., Forbes, R. T. & Alhnan, M. A. 2018. Channelled tablets: An innovative approach to accelerating drug release from 3D printed tablets. *Journal of Controlled Release*, 269, 355-363.

- Sadia, M., Sosnicka, A., Arafat, B., Isreb, A., Ahmed, W., Kelarakis, A. & Alhnan, M. A. 2016. Adaptation of pharmaceutical excipients to FDM 3D printing for the fabrication of patient-tailored immediate release tablets. *Int J Pharm*, 513, 659-668.
- Saffran, M., Kumar, G. S., Savariar, C., Burnham, J. C., Williams, F. & Neckers, D. C. 1986. A new approach to the oral administration of insulin and other peptide drugs. *Science*, 233, 1081-4.
- Sahoo, J., Murthy, P. N., Biswal, S. & Manik 2009. Formulation of sustained-release dosage form of verapamil hydrochloride by solid dispersion technique using Eudragit RLPO or Kollidon SR. *AAPS PharmSciTech*, 10, 27-33.
- Sakae, O. & Hiroyasu, K. 2008. Application of HPMC and HPMCAS to Aqueous Film Coating of Pharmaceutical Dosage Forms. In: MCGINITY, J. W. & FELTON, L. A. (eds.) *Aqueous Film Coating of Pharmaceutical Dosage Forms*. Boca Raton, FL.: CRC Press.
- Sakarkar, D. M., Dorle, A. K., Mahajan, N. M. & Sudke, S. G. 2013. Design of sustained release pellets of ferrous fumarate using cow ghee as hot-melt coating agent. *Int J Pharm Investig*, 3, 151-6.
- Sanderson, K. 2015. 3D printing: the future of manufacturing medicine? *Pharm. J.*, 7865.
- Sandler, N., Kassamakov, I., Ehlers, H., Genina, N., Ylitalo, T. & Haeggstrom, E. 2014a. Rapid interferometric imaging of printed drug laden multilayer structures. *Sci. Rep.*, 4.
- Sandler, N., Määttänen, A., Ihalainen, P., Kronberg, L., Meierjohann, A., Viitala, T. & Peltonen, J. 2011. Inkjet printing of drug substances and use of porous substrates-towards individualized dosing. *J Pharm Sci*, 100, 3386-3395.
- Sandler, N., Salmela, I., Fallarero, A., Rosling, A., Khajeheian, M., Kolakovic, R., Genina, N., Nyman, J. & Vuorela, P. 2014b. Towards fabrication of 3D printed medical devices to prevent biofilm formation. *International Journal of Pharmaceutics*, 459, 62-64.
- Sarode, A. L., Sandhu, H., Shah, N., Malick, W. & Zia, H. 2013. Hot melt extrusion (HME) for amorphous solid dispersions: predictive tools for processing and impact of drug-polymer interactions on supersaturation. *Eur J Pharm Sci*, 48, 371-84.
- Sauer, D. & McGinity, J. 2009. Properties of theophylline tablets dry powder coated with Eudragit E PO and Eudragit L 100-55. *Pharm Dev Technol*, 14, 632-41.
- Schiele, J. T., Quinzler, R., Klimm, H. D., Pruszydlo, M. G. & Haefeli, W. E. 2013. Difficulties swallowing solid oral dosage forms in a general practice population: prevalence, causes, and relationship to dosage forms. *Eur J Clin Pharmacol*, 69, 937-48.
- Scoutaris, N., Alexander, M. R., Gellert, P. R. & Roberts, C. J. 2011. Inkjet printing as a novel medicine formulation technique. *J Control Release*, 156, 179-185.

- Sebaugh, J. L. 2011. Guidelines for accurate EC50/IC50 estimation. *Pharm Stat*, 10, 128-34.
- Senatov, F. S., Niaza, K. V., Zadorozhnyy, M. Y., Maksimkin, A. V., Kaloshkin, S. D. & Estrin, Y. Z. 2016. Mechanical properties and shape memory effect of 3D-printed PLA-based porous scaffolds. *J Mech Behav Biomed Mater*, 57, 139-48.
- Shah, J., Vasanti, S., Anroop, B. & Vyas, H. 2008. Enhancement of dissolution rate of valdecoxib by solid dispersions technique with PVP K 30 & PEG 4000: preparation and in vitro evaluation. *Journal of Inclusion Phenomena and Macrocyclic Chemistry*, 63, 69-75.
- Shah, V. P., Yamamoto, L. A., Schuirman, D., Elkins, J. & Skelly, J. P. 1987. Analysis of in vitro dissolution of whole vs. half controlled-release theophylline tablets. *Pharm Res*, 4, 416-9.
- Sharma, A. & Jain, C. P. 2010. Preparation and characterization of solid dispersions of carvedilol with PVP K30. *Research in Pharmaceutical Sciences*, 5, 49-56.
- Sharma, M., Sharma, V., Panda, A. & Majumdar, D. K. 2011. *Development of enteric submicron particle formulation of papain for oral delivery.*
- Sharma, M., Sharma, V., Panda, A. K. & Majumdar, D. K. 2013. Development of enteric submicron particles formulation of alpha-amylase for oral delivery. *Pharm Dev Technol*, 18, 560-9.
- Siddique, S., Khanam, J. & Bigoniya, P. 2010. Development of sustained release capsules containing "coated matrix granules of metoprolol tartrate". *AAPS PharmSciTech*, 11, 1306-14.
- SIGMA-ALDRICH. 2016a. *Dipyridamole* [Online]. Available: <http://www.sigmaaldrich.com/catalog/product/sigma/d9766?lang=en®ion=GB> [Accessed 16/06 2016].
- SIGMA-ALDRICH. 2016b. *Polyvinylpyrrolidone* [Online]. Available: <http://www.sigmaaldrich.com/catalog/product/sial/pvp40?lang=en®ion=GB&gclid=C1zz7LauOswCFYidGwodgMAM0A> [Accessed 11/05 2016].
- SIGMA-ALDRICH. 2016c. *Theophylline melting point standard* [Online]. Available: <http://www.sigmaaldrich.com/catalog/product/sial/phr1151?lang=en®ion=GB> [Accessed 16/06 2016].
- SIGMA-ALDRICH. 2018a. *Aspirin* [Online]. Available: <https://www.sigmaaldrich.com/catalog/product/sigma/a2093?lang=en®ion=GB> [Accessed 03/04 2018].

- SIGMA-ALDRICH. 2018b. *Theophylline* [Online]. Available: <https://www.sigmaaldrich.com/catalog/product/sigma/t1633?lang=en®ion=GB> [Accessed 03/04 2018].
- Silva Oliveira, M., Miguel Agostinho, S. C., Guzzi Plepis, A. M. d. & Tabak, M. 2006. On the Thermal Decomposition of Dipyridamole: Thermogravimetric, Differential Scanning Calorimetric and Spectroscopic Studies. *Spectroscopy Letters*, 39, 145-161.
- Sinha, V., Singh, A., Kumar, R. V., Singh, S., Kumria, R. & Bhinge, J. 2007a. Oral colon-specific drug delivery of protein and peptide drugs. *Crit Rev Ther Drug Carrier Syst*, 24, 63-92.
- Sinha, V. R., Singh, A., Singh, S. & Bhinge, J. R. 2007b. Compression coated systems for colonic delivery of 5-fluorouracil. *J Pharm Pharmacol*, 59, 359-65.
- Skoog, S. A., Goering, P. L. & Narayan, R. J. 2014. Stereolithography in tissue engineering. *J Mater Sci Mater Med*, 25, 845-56.
- Skowyra, J., Pietrzak, K. & Alhnan, M. A. 2015. Fabrication of extended-release patient-tailored prednisolone tablets via fused deposition modelling (FDM) 3D printing. *Eur J Pharm Sci*, 68, 11-7.
- Sobhani, P., Christopherson, J., Ambrose, P. J. & Corelli, R. L. 2008. Accuracy of oral liquid measuring devices: comparison of dosing cup and oral dosing syringe. *Ann Pharmacother*, 42, 46-52.
- Song, Y., Zemlyanov, D., Chen, X., Su, Z., Nie, H., Lubach, J. W., Smith, D., Byrn, S. & Pinal, R. 2016. Acid-base interactions in amorphous solid dispersions of lumefantrine prepared by spray-drying and hot-melt extrusion using X-ray photoelectron spectroscopy. *International Journal of Pharmaceutics*, 514, 456-464.
- Songa, A. S., Meka, V. S., Nali, S. R. & Kolapalli, V. R. 2013. An in vitro and in vivo investigation into the suitability of compression coated tablets of indomethacin for the treatment of rheumatoid arthritis which follow circadian rhythms. *Drug Dev Ind Pharm*, 39, 447-56.
- Stevens, R. E., Limsakun, T., Evans, G. & Mason, D. H., Jr. 1998. Controlled, multidose, pharmacokinetic evaluation of two extended-release carbamazepine formulations (Carbatrol and Tegretol-XR). *J Pharm Sci*, 87, 1531-4.
- Sun, H., Liu, D., Li, Y., Tang, X. & Cong, Y. 2014. Preparation and in vitro/in vivo characterization of enteric-coated nanoparticles loaded with the antihypertensive peptide VLPVPR. *Int J Nanomedicine*, 9, 1709-16.
- Svangard, E., Burman, R., Gunasekera, S., Lovborg, H., Gullbo, J. & Goransson, U. 2007. Mechanism of action of cytotoxic cyclotides: cycloviolacin O2 disrupts lipid membranes. *J Nat Prod*, 70, 643-7.

- Szakonyi, G. & Zelkó, R. 2012. The effect of water on the solid state characteristics of pharmaceutical excipients: Molecular mechanisms, measurement techniques, and quality aspects of final dosage form. *International Journal of Pharmaceutical Investigation*, 2, 18-25.
- Taki, M., Tagami, T. & Ozeki, T. 2017. Preparation of polymer-blended quinine nanocomposite particles by spray drying and assessment of their instrumental bitterness-masking effect using a taste sensor. *Drug Dev Ind Pharm*, 43, 715-722.
- Technoorg-Linda. 2018. *High-Resolution Scanning Electron Microscopy* [Online]. Available: <http://www.technoorg.hu/news-and-events/articles/high-resolution-scanning-electron-microscopy-1/> [Accessed 03/04 2018].
- Thành, M. X. 2015. Effect of Secondary Structure on Biological Activities of Antimicrobial Peptides. *VNU Journal of Science: Natural Sciences and Technology*, 44-53.
- Thennarasu, S., Tan, A., Penumatchu, R., Shelburne, C. E., Heyl, D. L. & Ramamoorthy, A. 2010. Antimicrobial and Membrane Disrupting Activities of a Peptide Derived from the Human Cathelicidin Antimicrobial Peptide LL37. *Biophysical Journal*, 98, 248-257.
- Thermofisher. 2017. *HAAKE MiniCTW Micro-conical Twin Screw Computer* [Online]. Available: <https://www.thermofisher.com/order/catalog/product/567-2090> [Accessed 11/12 2017].
- Thingiverse 2017. Thingiverse website (<https://www.thingiverse.com/thing:20733>) last accessed 23/6/2017.
- Thoma, K. & Bechtold, K. 1999. Influence of aqueous coatings on the stability of enteric coated pellets and tablets. *European Journal of Pharmaceutics and Biopharmaceutics*, 47, 39-50.
- Timothy J. Snape, A. M. A. a. J. D. 2010. Understanding the chemical basis of drug stability and degradation. *The Pharmaceutical Journal*.
- Tingstad, J. E. 1964. Physical Stability Testing of Pharmaceuticals. *Journal of Pharmaceutical Sciences*, 53, 955-962.
- Tiwari, R., Gupta, A., Joshi, M. & Tiwari, G. 2014. Bilayer Tablet Formulation of Metformin HCl and Acarbose: A Novel Approach To Control Diabetes. *PDA J Pharm Sci Technol*, 68, 138-52.
- Tokudome, Y., Nakamura, K., Itaya, Y. & Hashimoto, F. 2015. Enhancement of Skin Penetration of Hydrophilic and Lipophilic Compounds by pH-sensitive Liposomes. *J Pharm Pharm Sci*, 18, 249-57.
- Torchilin, V. P. 2000. Drug targeting. *European Journal of Pharmaceutical Sciences*, 11, S81-S91.

- Toropainen, T., Velaga, S., Heikkila, T., Matilainen, L., Jarho, P., Carlfors, J., Lehto, V. P., Jarvinen, T. & Jarvinen, K. 2006. Preparation of budesonide/gamma-cyclodextrin complexes in supercritical fluids with a novel SEDS method. *J Pharm Sci*, 95, 2235-45.
- Touitou, E. & Rubinstein, A. 1986. Targeted enteral delivery of insulin to rats. *International Journal of Pharmaceutics*, 30, 95-99.
- Tsuda, S., Jaffery, H., Doran, D., Hezwani, M., Robbins, P. J., Yoshida, M. & Cronin, L. 2015. Customizable 3D Printed 'Plug and Play' Millifluidic Devices for Programmable Fluidics. *Plos One*, 10.
- Tudja, P., Khan, M. Z., Mestrovic, E., Horvat, M. & Golja, P. 2001. Thermal behaviour of diclofenac sodium: decomposition and melting characteristics. *Chem Pharm Bull (Tokyo)*, 49, 1245-50.
- Turner, J., Cho, Y., Dinh, N.-N., Waring, A. J. & Lehrer, R. I. 1998. Activities of LL-37, a Cathelin-Associated Antimicrobial Peptide of Human Neutrophils. *Antimicrobial Agents and Chemotherapy*, 42, 2206-2214.
- Uddin, M. J., Scoutaris, N., Klepetsanis, P., Chowdhry, B., Prausnitz, M. R. & Douroumis, D. 2015. Inkjet printing of transdermal microneedles for the delivery of anticancer agents. *Int J Pharm*, 494, 593-602.
- UNMC. 2018. *The Antimicrobial Peptide Database* [Online]. Available: <http://aps.unmc.edu/AP/main.php> [Accessed 25/04 2018].
- Van Epps, H. L. 2006. Rene Dubos: unearthing antibiotics. *J Exp Med*, 203, 259.
- Varum, F. J., Merchant, H. A., Goyanes, A., Assi, P., Zboranova, V. & Basit, A. W. 2014. Accelerating the dissolution of enteric coatings in the upper small intestine: evolution of a novel pH 5.6 bicarbonate buffer system to assess drug release. *Int J Pharm*, 468, 172-7.
- Vemula, S. K. 2015a. Formulation and pharmacokinetics of colon-specific double-compression coated mini-tablets: Chronopharmaceutical delivery of ketorolac tromethamine. *Int J Pharm*, 491, 35-41.
- Vemula, S. K. 2015b. A Novel Approach to Flurbiprofen Pulsatile Colonic Release: Formulation and Pharmacokinetics of Double-Compression-Coated Mini-Tablets. *AAPS PharmSciTech*, 16, 1465-73.
- Verdonck, E., Schaap, K. & Thomas, L. C. 1999. A discussion of the principles and applications of Modulated Temperature DSC (MTDSC). *International Journal of Pharmaceutics*, 192, 3-20.

- Vila-Perello, M., Sanchez-Vallet, A., Garcia-Olmedo, F., Molina, A. & Andreu, D. 2005. Structural dissection of a highly knotted peptide reveals minimal motif with antimicrobial activity. *J Biol Chem*, 280, 1661-8.
- Vinner, G. K., Vladislavljević, G. T., Clokie, M. R. J. & Malik, D. J. 2017. Microencapsulation of *Clostridium difficile* specific bacteriophages using microfluidic glass capillary devices for colon delivery using pH triggered release. *PLoS ONE*, 12, e0186239.
- Vogenberg, F. R., Isaacson Barash, C. & Pursel, M. 2010. Personalized Medicine: Part 1: Evolution and Development into Theranostics. *Pharmacy and Therapeutics*, 35, 560-576.
- Water, J. J., Bohr, A., Boetker, J., Aho, J., Sandler, N., Nielsen, H. M. & Rantanen, J. 2015. Three-Dimensional Printing of Drug-Eluting Implants: Preparation of an Antimicrobial Polylactide Feedstock Material. *Journal of Pharmaceutical Sciences*, 104, 1099-1107.
- Waterman, K. C. & Adami, R. C. 2005. Accelerated aging: Prediction of chemical stability of pharmaceuticals. *International Journal of Pharmaceutics*, 293, 101-125.
- WeillCornellMedicalCollege. 2014. *Study Shows Inconsistent dosages of widely used eye disease drug* [Online]. Available: <http://weill.cornell.edu/news/pr/2014/09/study-shows-inconsistent-dosages-of-widely-used-eye-disease-drug-szilard-kiss-donald-damico.html> [Accessed 12/3/2015].
- Weitschies, W., Blume, H. & Mönnikes, H. 2010. Magnetic Marker Monitoring: High resolution real-time tracking of oral solid dosage forms in the gastrointestinal tract. *European Journal of Pharmaceutics and Biopharmaceutics*, 74, 93-101.
- Wendel, B., Rietzel, D., Kühnlein, F., Feulner, R., Hülder, G. & Schmachtenberg, E. 2008. Additive Processing of Polymers. *Macromolecular Materials and Engineering*, 293, 799-809.
- Whitmore, L. & Wallace, B. A. 2004. DICHROWEB, an online server for protein secondary structure analyses from circular dichroism spectroscopic data. *Nucleic Acids Res*, 32, W668-73.
- Whitmore, L. & Wallace, B. A. 2008. Protein secondary structure analyses from circular dichroism spectroscopy: methods and reference databases. *Biopolymers*, 89, 392-400.
- WHO. 2009. *Stability Testing of Active Pharmaceutical Ingredients and Finished Pharmaceutical Products* [Online]. Available: <http://apps.who.int/medicinedocs/documents/s19133en/s19133en.pdf> [Accessed 02/05 2018].

- Wilding, I. R., Coupe, A. J. & Davis, S. S. 2001. The role of γ -scintigraphy in oral drug delivery. *Advanced Drug Delivery Reviews*, 46, 103-124.
- Wilson, B., Babubhai, P. P., Sajeev, M. S., Jenita, J. L. & Priyadarshini, S. R. 2013. Sustained release enteric coated tablets of pantoprazole: formulation, in vitro and in vivo evaluation. *Acta Pharm*, 63, 131-40.
- Winick, E. 2017. *Additive Manufacturing in the Aerospace Industry* [Online]. Available: <https://www.engineering.com/AdvancedManufacturing/ArticleID/14218/Additive-Manufacturing-in-the-Aerospace-Industry.aspx> [Accessed 17/04 2017].
- Wong, J. H. & Ng, T. B. 2005. Sesquin, a potent defensin-like antimicrobial peptide from ground beans with inhibitory activities toward tumor cells and HIV-1 reverse transcriptase. *Peptides*, 26, 1120-6.
- Wonnemann, M., Schug, B., Anschütz, M., Brendel, E., Nucci, G. D. & Blume, H. 2008. Comparison of two marketed nifedipine modified-release formulations: An exploratory clinical food interaction study. *Clinical Therapeutics*, 30, 48-58.
- Wu, D., Gao, Y., Qi, Y., Chen, L., Ma, Y. & Li, Y. 2014. Peptide-based cancer therapy: Opportunity and challenge. *Cancer Letters*, 351, 13-22.
- Xhindoli, D., Pacor, S., Guida, F., Antcheva, N. & Tossi, A. 2014. Native oligomerization determines the mode of action and biological activities of human cathelicidin LL-37. *Biochemical Journal*, 457, 263-275.
- Xia, X., Cheng, L., Zhang, S., Wang, L. & Hu, J. 2017. The role of natural antimicrobial peptides during infection and chronic inflammation. *Antonie van Leeuwenhoek*.
- Xie, D., Zhang, H., Shu, X., Xiao, J. & Cao, S. 2010. Multi-materials drop-on-demand inkjet technology based on pneumatic diaphragm actuator. *Sci China Tech Sci*, 53, 1605-1611.
- Yamamoto, A., Taniguchi, T., Rikyuu, K., Tsuji, T., Fujita, T., Murakami, M. & Muranishi, S. 1994. Effects of various protease inhibitors on the intestinal absorption and degradation of insulin in rats. *Pharm Res*, 11, 1496-500.
- Yang, F., Su, Y., Zhang, J., DiNunzio, J., Leone, A., Huang, C. & Brown, C. D. 2016. Rheology Guided Rational Selection of Processing Temperature To Prepare Copovidone-Nifedipine Amorphous Solid Dispersions via Hot Melt Extrusion (HME). *Mol Pharm*, 13, 3494-3505.
- Yang, Q., Ma, Y. & Zhu, J. 2015. Applying a novel electrostatic dry powder coating technology to pellets. *Eur J Pharm Biopharm*, 97, 118-24.

- Yang, Z., Nollenberger, K., Albers, J., Moffat, J., Craig, D. & Qi, S. 2014. The effect of processing on the surface physical stability of amorphous solid dispersions. *Eur J Pharm Biopharm*, 88, 897-908.
- Yang, Z. Y., Lu, Y. & Tang, X. 2008. Pseudoephedrine hydrochloride sustained-release pellets prepared by a combination of hot-melt subcoating and polymer coating. *Drug Dev Ind Pharm*, 34, 1323-30.
- Yeshak, M. Y., Burman, R., Asres, K. & Goransson, U. 2011. Cyclotides from an extreme habitat: characterization of cyclic peptides from *Viola abyssinica* of the Ethiopian highlands. *J Nat Prod*, 74, 727-31.
- Yin, H. S., Mendelsohn, A. L., Wolf, M. S., Parker, R. M., Fierman, A., Van Schaick, L., Bazan, I. S., Kline, M. D. & Dreyer, B. P. 2010. Parents' medication administration errors: Role of dosing instruments and health literacy. *Arch Pediatr Adolesc Med* 164, 181-186.
- Yoo, J.-W., Giri, N. & Lee, C. H. 2011. pH-sensitive Eudragit nanoparticles for mucosal drug delivery. *International Journal of Pharmaceutics*, 403, 262-267.
- Yu, D. G., Branford-White, C., Ma, Z. H., Zhu, L. M., Li, X. Y. & Yang, X. L. 2009a. Novel drug delivery devices for providing linear release profiles fabricated by 3DP. *Int J Pharm*, 370, 160-6.
- Yu, D. G., Branford-White, C., Yang, Y. C., Zhu, L. M., Welbeck, E. W. & Yang, X. L. 2009b. A novel fast disintegrating tablet fabricated by three-dimensional printing. *Drug Dev Ind Pharm*, 35, 1530-6.
- Yu, D. G., Yang, X. L., Huang, W. D., Liu, J., Wang, Y. G. & Xu, H. 2007. Tablets with material gradients fabricated by three-dimensional printing. *J Pharm Sci*, 96, 2446-56.
- Zaid, A. N. 2012. Development and stability evaluation of enteric coated Diclofenac sodium tablets using Sureteric. *Pak J Pharm Sci*, 25, 59-64.
- Zecevic, D. E., Meier, R., Daniels, R. & Wagner, K. G. 2014. Site specific solubility improvement using solid dispersions of HPMC-AS/HPC SSL--mixtures. *Eur J Pharm Biopharm*, 87, 264-70.
- Zhang, X., Oglęcka, K., Sandgren, S., Belting, M., Esbjörner, E. K., Nordén, B. & Gräslund, A. 2010. Dual functions of the human antimicrobial peptide LL-37—Target membrane perturbation and host cell cargo delivery. *Biochimica et Biophysica Acta (BBA) - Biomembranes*, 1798, 2201-2208.
- Zhang, Y., Luo, R., Chen, Y., Ke, X., Hu, D. & Han, M. 2014. Application of carrier and plasticizer to improve the dissolution and bioavailability of poorly water-soluble baicalein by hot melt extrusion. *AAPS PharmSciTech*, 15, 560-8.